SYNTHESIS AND CHARACTERIZATION OF SOME HYDROPHILIC POLYSULFONE BASED MEMBRANES AND THEIR APPLICATION FOR SUSTAINABLE WATER PURIFICATION

Thesis

Submitted in partial fulfilment of the requirements for the degree of

DOCTOR OF PHILOSOPHY

by

G P SYED IBRAHIM

DEPARTMENT OF CHEMISTRY

NATIONAL INSTITUTE OF TECHNOLOGY KARNATAKA,

SURATHKAL, MANGALORE – 575025

August, 2020

DECLARATION

I hereby declare that the Research Thesis entitled **"SYNTHESIS AND CHARACTERIZATION OF SOME HYDROPHILIC POLYSULFONE BASED MEMBRANES AND THEIR APPLICATION FOR SUSTAINABLE WATER PURIFICATION"** which is being submitted to the National Institute of Technology Karnataka, Surathkal in partial fulfillment of the requirements for the award of the Degree of **Doctor of Philosophy** in Chemistry is a bonafide report of the research work carried out by me. The material contained in this Research Thesis has not been submitted to any University or Institution for the award of any degree.

G P Syed Ibrahim
Reg. No. 158025CY15F08,
Department of Chemistry

Place: NITK, Surathkal
Date:

CERTIFICATE

This is to *certify* that the Research Thesis entitled **"SYNTHESIS AND CHARACTERIZATION OF SOME HYDROPHILIC POLYSULFONE BASED MEMBRANES AND THEIR APPLICATION FOR SUSTAINABLE WATER PURIFICATION"** submitted by **G P Syed Ibrahim (Register Number: 158025CY15F08)** as the record of the research work carried out by him is *accepted as the Research Thesis submission* in partial fulfilment of the requirements for the award of degree of **Doctor of Philosophy**.

Dr. Arun M. Isloor
Research Guide

Chairman- DRPC

ACKNOWLEDGEMENTS

I would like to express my deep sense of gratitude to my research supervisor, Dr. Arun M. Isloor, Professor, Department of Chemistry, NITK, Surathkal for giving me an opportunity to pursue my research work under his valuable guidance. Without his supervision and persistence, this thesis would not have been possible.

I acknowledge NITK, Surathkal for providing the fellowship and financial support necessary for the completion of my doctoral work.

My sincere gratitude is due towards my RPAC members, Prof M. B Saidutta of Chemical Engineering and Dr. Udaya Kumar Dalimba, Department of Chemistry, for their timely assessment and evaluation of my research progress. Their valuable inputs at various stages of my work have contributed immensely in giving the final shape to my research work.

I am very grateful to the present Head of the Department, Prof. Arun M. Isloor and former Heads of the Department, Prof. Krishna Bhat and Prof. B. Ramachandra Bhat for providing the administrative facilities and infrastructure. I am also thankful to Prof. A. Nithyananda Shetty, Prof. A. Chitharanjan Hegde, Prof. A. Vasudeva Adhikari, Prof. D. Krishna Bhat, Dr. D. Udayakumar, Dr. Darshak R. Trivedi, Dr. Sib Sankar Mal, Dr. Beneesh P.B., Dr. Debashree Chakraborthy, Dr. Saikat Dutta, Dr. Vijayendra S. Shetti and Dr. Lakshmi Vellanki for their assistance and moral support.

I would like to convey my appreciation to Prof. K. Narayan Prabhu, Prof. Udupa and Prof. Uday Bhat of Department of Metallurgical and Materials Engineering, NITK for allowing me to avail the instrumentation facility whenever required. I am thankful to the Department of Chemical Engineering and Physics for extending the instrumental facilities. I am very thankful to Prof. Ahmed Fauzi Ismail, Advanced Membrane Technology Centre (AMTEC), Universiti Teknologi Malaysia for providing me an opportunity to conduct a part of my research work in the AMTEC.

I would like to extend my appreciation to Prof. Ramin Farnood, Department of Chemical Engineering and Applied Chemistry, University of Toronto, Canada and Prof. Siamak Nejati, Department of Chemical and Biomolecular Engineering, University of Nebraska, USA for allowing me to conduct part of my research work in their lab. I am also very thankful to Prof. Mona Bavarian, Department of Chemical and Biomolecular Engineering, University of Nebraska for her kind help and suggestions.

I truly appreciate the support extended by my research group at NITK, including Dr. Harikrishna Nandam, Dr. Raghavendra Hebbar, Dr. Irfana Moideen K., Dr. Chandrashekar Nayak, Miss Panchami, Mr. Sathyanarayan, Mr. Sivaraman, Miss. Pallavi and Mr. Shivaprakash. I am thankful to all my friends at NITK, for making my stay fun-filled and cherished one.

I am grateful to the non-teaching staff, Mrs. Shamila, Mrs. Deepa, Mrs. Sharmila, Mr. Pradeep, Mr. Prashanth, Mr. Harish, Mr. Santosh, Mrs. Rashmi for their timely cooperation with laboratory and analysis work.

My sincere thanks to Captain Dr. S. Abideen, Department of Zoology, Dr. Zakir Husain College, Ilayangudi for his constant support and help provided during my bachelor's and master's study. I also thank all my professors from Dr. Zakir Husain College, Ilayangudi and Jamal Mohamed College, Trichy for educating me to achieve this level.

I am thankful to the Department of Science and Technology (DST), India, Water for Food Daugherty Global Institute, Indo-US Science and Technology Forum (IUSSTF) and the University of Nebraska for giving financial support for doing six months internship at University of Nebraska, Lincoln.

I am highly indebted to my parents for their everlasting faith in me which has been the backbone of my hard work and patience. This acknowledgment would be incomplete without the mention of my wife M. Anisha Begam for her endless love and support. I am very thankful to all my teachers who helped me to achieve this place. I also thank my family members and friends for their constant encouragement during my Ph.D. tenure. Finally, I extend my gratitude to all those who have contributed directly or indirectly towards the completion of this work.

Thank you.

G P Syed Ibrahim

ABSTRACT

The intensifying obligation to clean, freshwater and declining obtainability from natural resources, water need to be conserved effectually to come across future requirements. This deteriorating condition fascinated the attention of global researchers towards nonconventional sources, such as ocean water, treated water and groundwater. Membrane separation processes have been established briskly in the past decade into the leading technology for effective water treatment. Among the commercially available polymeric membranes, polysulfone based membranes play an important role as it exhibits improved chemical, thermal and mechanical stability. However, the trade-off between permeability and solute rejection, reduced surface hydrophilicity and higher propensity towards fouling of polysulfone membranes urge further development.

In this research work, polysulfone membrane performance was improved by incorporating hydrophilic polymeric nanoparticles and blending with hydrophilic polymers. The as-prepared composite or nanocomposite membranes were thoroughly characterized using analytical techniques.

The nanocomposite hollow fiber ultrafiltration membranes were prepared with surface modified halloysite nanotubes, zwitterionic polymer nanoparticles and zwitterionically modified Fe_3O_4 demonstrated improved antifouling ability and dye rejection with higher permeability compared to the pristine membrane. The as-added nanoparticles not only increased the membrane surface porosity but also altered the surface hydrophilicity and charge. The polysulfone blend ultrafiltration membrane was fabricated, which exhibited enhanced heavy metal ions such as Pb^{2+} (91.5 %) and Cd^{2+} (72.3 %) rejection. To further improve the heavy metal rejection, thin-film composite/nanocomposite membranes were prepared. The as-prepared nanofiltration membranes demonstrated higher rejection of heavy metal ions such as Pb^{2+} (>98%) and Cd^{2+} (>95 %) and improved antifouling property.

Keywords: Polysulfone, zwitterionic polymer nanoparticles, antifouling, water purification, heavy metal removal, hollow fiber membrane

CONTENTS

NOMENCLATURES

A) List of Abbreviations

AAS	Atomic absorption spectroscopy
AFM	Atomic force microscopy
AHM	Ammonium heptamolybdate tetrahydrate
ATR-FTIR	Attenuated total reflectance Fourier transform infrared
BER	Bore extrusion rate
BSA	Bovine serum albumin
CA	Cellulose acetate
CDH	Central Drug House
CNP	Chitosan nanoparticles
DER	Dope extrusion rate
DI	Deionized
DS	Degree of sulfonation
DSC	Differential scanning calorimeter
EDX	Energy-dispersive X-ray
FDR	Flux decline ratio
FRR	Flux recovery ratio
FS	Flat sheet
FTIR	Fourier transform infrared
GAA	Glacial acetic acid
GB	Glycine betaine
HA	Humic acid
HAc	Acetic acid
HP	Homopiperazine

HF	Hollow fiber
IPA	Isopropyl alcohol
MB	Methylene blue
MF	Microfiltration
MWCO	Molecular weight cut-off
MPD	m-Phenylenediamine
NF	Nanofiltration
NIPS	Non-solvent induced phase separation
NMP	N-methyl-2-pyrolidone
NMR	Nuclear magnetic resonance
NP	Nanoparticle
PA	Polyamide
PAN	Poly(acrylonitrile)
PANI	Polyaniline
PEG	Polyethylene glycol
PEI	Polyethyleneimine
PES	Polyethersulfone
PEUF	Polymer enhanced ultrafiltration
PIP	Piperazine
PMMA	Poly (methyl methacrylate)
PPSU	Polyphenylsulfone
PSF	Polysulfone
PU	Polyurethane
PVA	Polyvinyl alcohol
PVDF	Polyvinylidene difluoride
PVP	Poly(1-vinylpyrrolidone)

PWF	Pure water flux
RB 5	Reactive black 5
RO	Reverse osmosis
RO 16	Reactive orange 16
RT	Room temperature
SEM	Scanning electron microscopy
TEA	Triethylamine
TEM	Transmission electron microscopy
TFC	Thin-film composite
TGA	Thermal gravimetric analysis
TMC	Trimesoyl chloride
TMP	Transmembrane pressure
TPP	Sodium tripolyphosphate
UF	Ultrafiltration
UV	Ultraviolet
UV-Vis	Ultraviolet-Visible
WCA	Water contact angle
XRD	X-ray diffraction
ZP	Zeta potential

B) List of Symbols

Aq.	Aqueous
T_g	Glass transition temperature
ΔC	Concentration gradient
ΔP	Pressure gradient
ΔT	Temperature gradient

ΔE	Electric potential gradient
J_w	Water flux
Q	Amount of water passing through the membrane
Δt	Change in time
A	Area of the membrane sample
R	Rejection
C_p	Concentration of the solute in permeate
C_f	Concentration of the solute in feed
Wt.	Weight
W_w	Wet weights (g) of membrane samples
W_d	Dry weights (g) of membrane samples
E	Porosity
L	Thickness of the membrane sample
P	Density of water
Mw	Average molecular weight
R_a	Average roughness
R_q	Root mean square roughness
R_{irr}	Irreversible fouling ratio
R_{rev}	Reversible fouling ratio
r_p	Mean pore radius

CHAPTER 1

INTRODUCTION

Abstract: *This introductory chapter presents the significance of present research work on the use of membranes for water purification. It includes a general introduction, history and classification. It also gives brief details on the membrane materials, preparation methods and applications of membranes, along with a concise literature survey.*

1.1 GENERAL INTRODUCTION

Among the natural elements, water is one of the prime elements for humans, plants, and animals. The scarcity of potable water has been severe global anxiety for a long time (Kim *et al.* 2016). With the increased development of modern society and rapid population growth, the consumption of energy increases every year, which causes severe environmental pollution problems, especially air and water pollution. The discharge of contaminants into natural water resources leads to a shortage of clean water at the global level (Shannon *et al.* 2008). In many of the countries, groundwater resources are already dwindling. As stated by the World Health Organization, 1 billion people do not have access to clean water. It is predicted that, by the year 2025, approximately 3.5 million people will live in water-stressed countries (Elimelech *et al.* 2011). Figure 1.1 depicts the water scarcity across the globe.

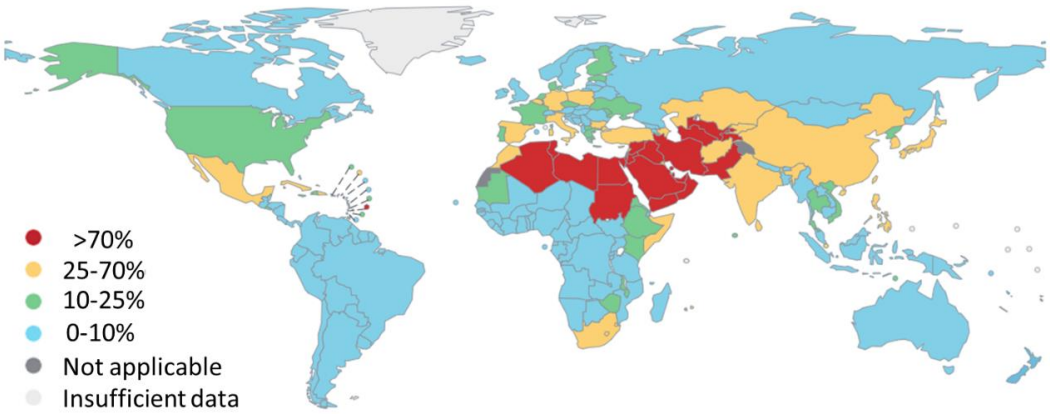

Figure 1.1 Schematic representation of water scarcity across the globe (Source: The United Nations, 2019, "World Water Development Report 2019")

The ocean contains about 97 % of water, which is having a high salt content of around 35,000 mg/L which makes it useless without any treatment. An additional 2 % of earth's water is present as ice at the polar caps and as glaciers. From the remaining 1 %, which is freshwater, 0.3 percent is present in the atmosphere and only 0.1 percent in rivers and lakes. The remaining 0.6 percent as groundwater and about half of the groundwater occurs at the

depth of 800 m (Elimelech *et al.* 2011). Since the freshwater and rainfall are unevenly distributed over the landmasses, many areas of the world today are subject to severe drought. In many of the places, the groundwater contains high salt concentration as a result of both natural and anthropogenic processes.

One encouraging and widely accepted method to use polymeric membranes for the purification of water. Due to the energy-efficient and less pollution of membranes, using polymeric membranes for clean water regeneration has attracted significant attention, and tremendous progress has been reported recently (Van der Bruggen *et al*. 2003, Sirshendu de *et al*. 2009, Dumée *et al*. 2010**,** Kang *et al.* 2012**,** Purkait *et al.* 2018). In addition, membrane devices and systems are almost always compact and modular.

1.2 HISTORICAL DEVELOPMENT OF MEMBRANE

The membrane technology is a relatively young branch of chemical research, and it began just 40 years ago. Nollet was the first person to study the membrane phenomena and discovered osmosis in the middle of the 18^{th} century. He has discovered that using a pig's bladder, the water-ethanol mixture can be separated when it was brought in contact on one side with pure water and another side with the water-ethanol mixture (Nollet 1752). Furthermore, he was the first person to propose the relation between a semipermeable membrane and the osmotic pressure. Later on, Graham studied the mass transport in the semipermeable membrane in a systematic manner. He also studied the diffusion of gasses through rubber and reported that rubber has different permeability for different gasses (Graham 1866).

Initial studies on membrane permeation were performed with natural materials like animal bladder or gum elastics. The first artificially prepared semipermeable membrane was reported by Traube. He had prepared by precipitating cupric ferrocyanide in a thin layer of porous porcelain (Traube 1867). In a while, Fick interpreted diffusion in liquid as a function of the concentration gradient, and Van't Hoff provided the explanation for the osmotic pressure of dilute solutions (Fick 1855, Cohen 1899). In a short time, the flux equation for electrolytes under the driving force of a concentration gradient was proposed by Nernst and Planck (Nernst 1888). Donnan proposed the theory of membrane potentials and membrane equilibrium (Donnan 1911).

Further advancement in science and polymer chemistry, membrane science and technology had entered the new phase at the beginning of the twentieth century. The first

synthetic membrane was made by impregnating filter paper with a solution of nitrocellulose in glacial acetic acid (Bechhold 1908). These nitrocellulose membranes were used as ultrafilters for the removal of fine particles and macromolecules (Zsigmondy *et al.* 1918, Joseph Elford 1931, McBain *et al.* 1931). The membranes for biomedical applications was developed and implemented in the large scale production by Kolff *et al.* (1944).

In the initial days of development, membrane science and technology had been only a subject of scientific interest with only a few practical applications. However, in early 1950, membrane science became a focus of interest, since it had many versatile applications in the field of biomedical and water treatment. The sudden boom in the advances of polymer chemistry attributed to the development of many novel polymeric membrane materials with extraordinary mechanical and chemical strength. Membrane transport properties had been defined by an inclusive theory, based on the thermodynamics of irreversible processes (Staverman 1952, Kedem *et al.* 1961). Spiegler studied the properties and extensive usage of ion-exchange membranes (Spiegler 1958).

The major advancement in the field of membrane science and technology could be the development of reverse osmosis membranes (Reid *et al.* 1959). The reverse osmosis membrane could separate the salt from the seawater. The initial studies were carried out with cellulose acetate membranes. The membranes exhibited a high rejection of salt with moderate flux to produce the drinking water.

In the development of reverse osmosis membranes, the first asymmetric cellulose acetate as the polymeric material was developed by Loeb and Sourirajan (Figure 1.2) (Loeb *et al.* 1962, Sourirajan *et al.* 1973). The newly developed membrane had a dense layer at the top which was responsible for the selectivity and flux. The membranes were prepared by the phase inversion method. Later, other membrane materials such as polysulfone, polyamide and polyacrylonitrile were employed for the preparation of asymmetric reverse osmosis membranes. These polymers exhibited greater mechanical, thermal and chemical stability than the cellulose acetate membranes. However, the cellulose acetate membranes were a dominant candidate until the development of interfacial-polymerized composite membranes (Riley *et al.* 1967, Cadotte *et al.* 1981). The as-prepared membranes were showed higher rejection of salt, better chemical and mechanical properties than cellulose ester membrane. Bray demonstrated the preparation of the spiral wound module for flat sheet membranes towards the reverse osmosis membrane application.

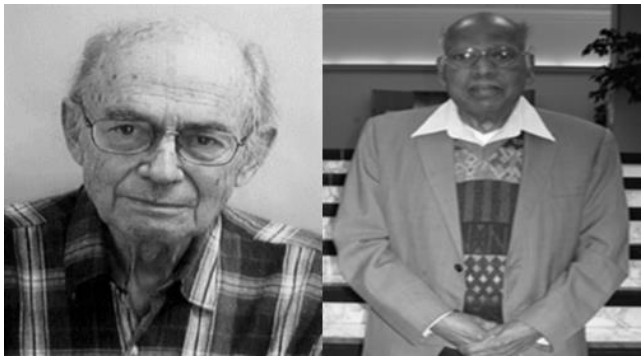

Figure 1. 2 Prof. Loeb (left) and Sourirajan (right) (Source: Internet)

A diverse methodology to membrane geometry was the preparation of asymmetric hollow fiber membranes with the aim of desalination of sea and brackish water by Du Pont Corporation. The as-made hollow fiber membrane had a wall thickness of only 6-7 microns. Nowadays the hollow fiber membranes are playing an important role in the preparation of reverses osmosis membrane since it is having many advantages like easy preparation, handling, low cost, high surface area, low maintenance, less fouling and easy cleaning. It also has importance in the field of gas separation and pervaporation. Additionally, there are many advancements in the arena of hemodialysis membranes under progress.

1.3 DEFINITION AND CLASSIFICATION OF MEMBRANE

It is rather difficult to furnish the precise and comprehensive definition of synthetic membranes. Nevertheless, the membrane can be defined as an "interface between two adjacent phases acting as a selective barrier, regulating the transport of substances between the two compartments"(Ulbricht 2006). The schematic representation of the membrane operation is presented in Figure 1.3.

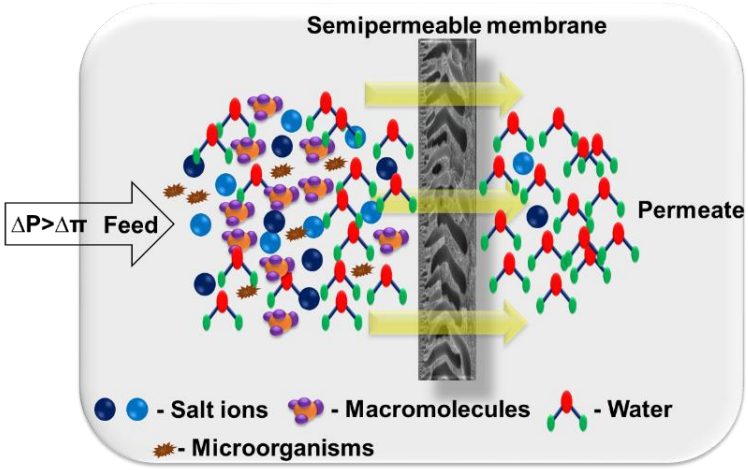

Figure 1. 3 Schematic representation of membrane operation

Synthetic membranes exhibit a broad range of classification based on their structure and pore size as shown in Figures 1.4 and 1.5. On the basis of membrane structure, the membrane can be classified as symmetric and asymmetric membranes and based on pore size it can be classified as microfiltration (MF), ultrafiltration (UF), nanofiltration (NF) and reverse osmosis membrane (RO). The classification based on the morphology and pore size of the membrane as follows.

1.3.1 Symmetric membrane

This type of membranes are referred to as isotropic membranes and denotes the uniform structure throughout the membrane thickness (Buonomenna *et al.* 2011). They are mainly used in dialysis, electrodialysis and microfiltration (Vardon *et al.* 2011) and has a thickness of 30 to 500 µm. Generally, mass transfer depends on the thickness of the membrane. Since it is having less thickness the permeation would be high.

1.3.2 Asymmetric membrane

These types of membranes contain both thin skin (0.1-5 µm) and a highly porous sub-layer (100-300 µm) (Vardon *et al.* 2011). The top skin layer acts as a selective barrier to the sub-layer and improves the selectivity. Thus, the skin layer pore size and nature of the material determine the asymmetric membrane separation performances (Hu *et al.* 2013). Consequently, the designing of skin layer structure has become a serious concern (Zhenxin *et al.* 1991) as the mass transfer is mainly depending on the top layer (Nunes *et al.* 2001). These membranes are mainly used in reverse osmosis, ultrafiltration and gas separation and occasionally in microfiltration. The schematic representation of the symmetric and asymmetric membranes is shown in Figure 1.4.

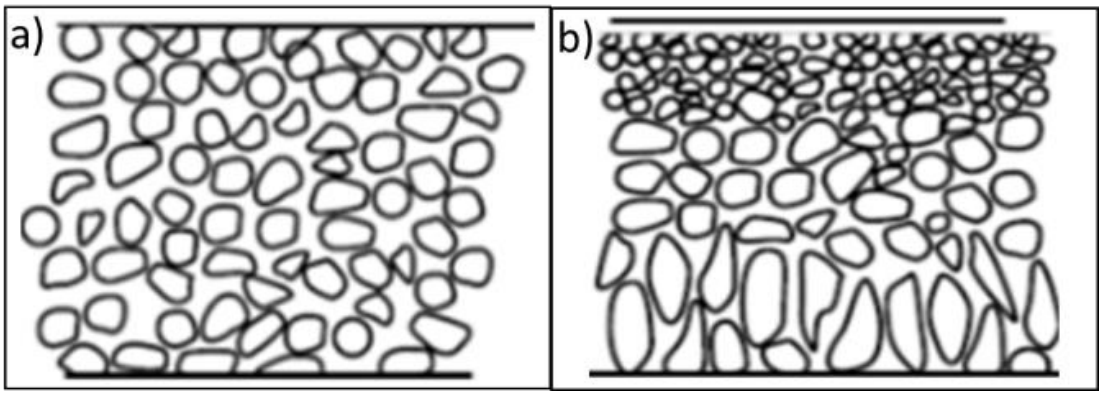

Figure 1. 4 a) Symmetric b) asymmetric membrane structure (Baker 2000)

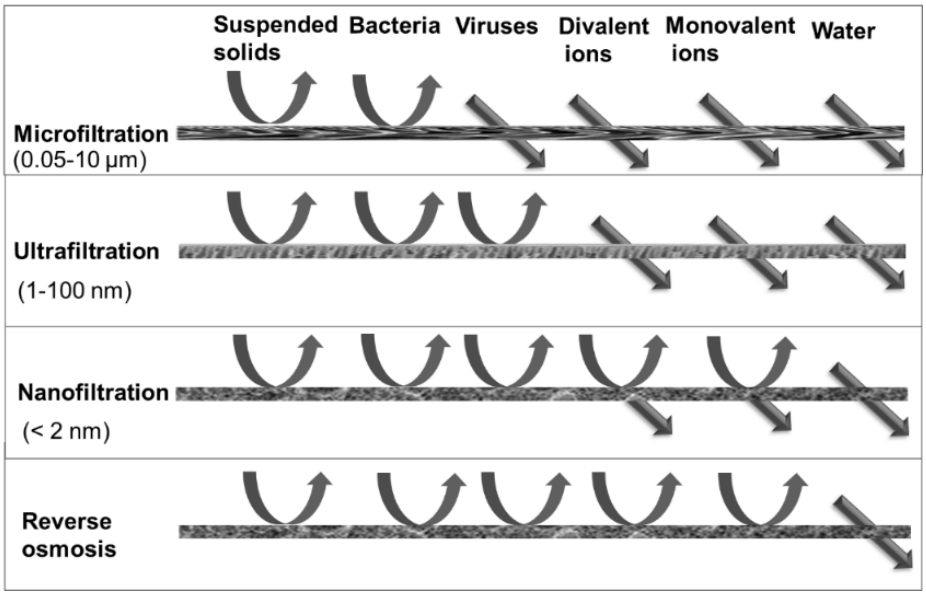

Figure 1. 5 Classification of membranes based on pore size (Mulder 2012)

1.3.3 Microfiltration (MF) membranes

These membranes are highly porous and have a pore size of 0.05-10 µm. It is used for the removal of suspension and emulsion. Since this type is pressure dependent, the maximum applied pressure is less than 2 bar. In addition to this, it is necessary to ensure the porosity (surface) is as high as possible with pore size distribution as constricted as possible. The separation principle is a sieving mechanism.

1.3.4 Ultrafiltration (UF) membranes

It has a pore size of 1-100 nm. These membranes are intermediate between microfiltration and nanofiltration. It is one of the excellent pre-treatment methods for the NF membranes. It can be used to filter the macromolecules and colloids from the solution. Since these membranes are porous, the rejection depends on the size and shape of the solutes with respect to the pore size of the membrane. Additionally, the UF membranes differ from the MF membranes by their asymmetric structure, in which the top dense skin layer increases the hydrodynamic resistance. The optimum range of applied pressure for UF is 1-5 bar.

1.3.5 Nanofiltration (NF) membranes

In general, the NF membranes would be used for the removal of lower molecular weight inorganic salts and small organic molecules from the solvent. It is one of the pretreatment methods for the RO membranes. As these membranes are capable of removing the small

size inorganic salt, the pore size of less than 2 nm must be engineered in the proper manner to increase the hydrodynamic resistance. However, in the case of UF, the low molecular solutes can be permeated easily. NF membranes are intermediate between the porous and dense nonporous membranes. Consequently, the higher pressure of 10-15 bar is required for the NF membranes.

1.3.6 Reverse osmosis (RO) membranes

These are all special types of membranes for the removal of inorganic salts. Both NF and RO hold the same principles. Subsequently, RO membranes need to remove both the monovalent and divalent inorganic salt to a greater extent. So, high pressure would be applied to overcome the hydrodynamic resistance. Figure 1.6 represents the RO operation. To allow water to pass through the membrane, the applied pressure should be higher than the osmotic pressure. For example, seawater has an osmotic pressure of 25 bar (Mulder 2012). As represented in Figure 1.6, if the applied pressure is greater than the osmotic pressure the water would move from high solute concentration to low solute concentration. However, if the applied pressure is less than the osmotic pressure, water would migrate from low solute concentration to high solute concentration. Therefore, the operating pressure range for RO is 15-100 bar.

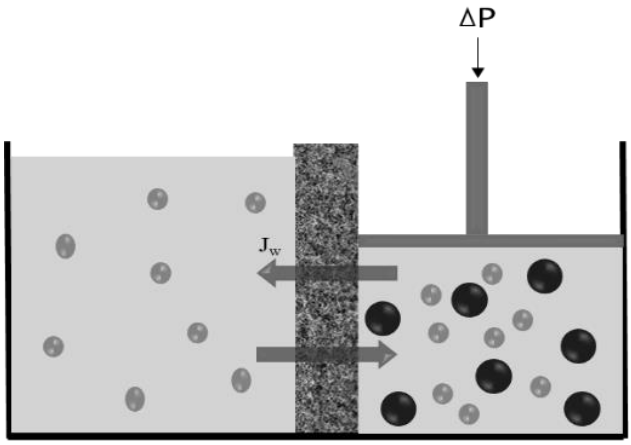

Figure 1. 6 Schematic representation of water flow (Jw) as a function of pressure (ΔP) in RO membrane

1.3.7 Forward osmosis (FO) membranes

Forward osmosis is one of the developing membrane technology that employs an osmotic pressure difference to drive the water transport through a semi-permeable membrane from low osmotic pressure side (feed) to the higher osmotic pressure side (draw)

(Cath *et al.* 2006). Compared to RO and NF, FO needs very less pressure and has a high rejection of an extensive choice of solutes (Phillip *et al.* 2010, Jin *et al.* 2012, Xie *et al.* 2012). In addition, FO is an attractive alternative to the conventional pressure-driven membrane process to overcome the high energy consumption as the high osmotic pressure draw solutions are naturally available (seawater and RO brine) (Achilli *et al.* 2009). The schematic representation of the FO system is presented in Figure 1.7.

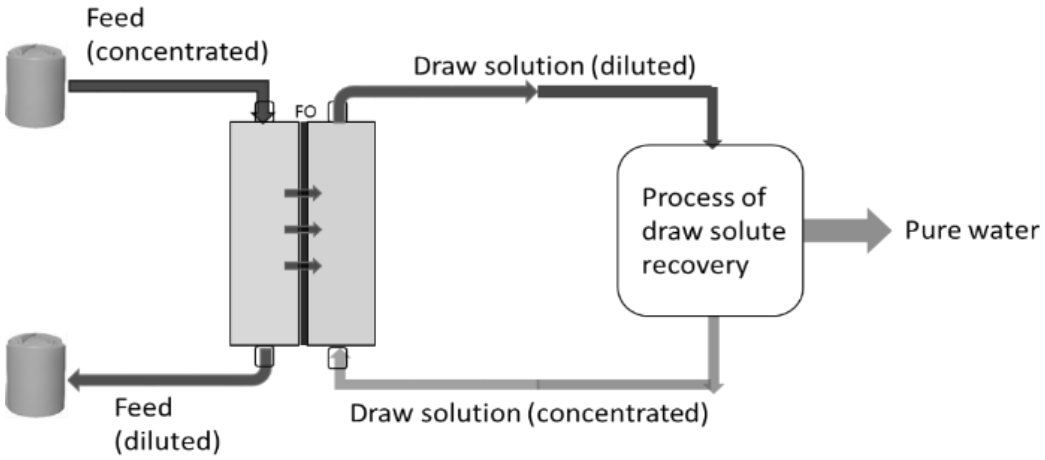

Figure 1. 7 Schematic representation of FO system

1.4 BASIC TERMINOLOGIES IN MEMBRANE SCIENCE

Certain rudimentary terminologies that are used in membrane science are as follows.

Flux: The pure water flux data determine the membrane porosity. It can be defined as "the amount of water passing through the unit area of the membrane per unit time". It is calculated by the following equation.

$$J = \frac{Q}{\Delta t \times A}$$

Where 'J' is water flux expressed in L/m^2 h, 'Q' is the amount of water passing through the membrane in litre, 'Δt' is the time in hour and 'A' is the effective membrane area which is expressed in m^2.

Solute rejection: The membrane rejection capacity is determined by the top skin layer of the membrane. The percentage of rejection can be elucidated by the following equation.

$$\text{Percentage of rejection} = \left(1 - \frac{C_p}{C_f}\right) \times 100$$

Where 'C_p' is the concentration of solute in permeate and 'C_f' is the concentration of solute in feed respectively.

Water uptake: The water uptake capacity is controlled by the surface hydrophilicity and porosity of the membrane. The water uptake is expressed as follows.

$$\text{Water uptake (\%)} = \left(\frac{W_w - W_d}{W_w}\right) \times 100$$

Where 'W_w' is the weight of the wet membrane and 'W_d' is the weight of the dry membrane correspondingly.

1.4.1 Membrane fouling and control

The membrane fouling is one of the crucial processes, as it is directly affecting the separation processes. It can be defined as the reversible or irreversible accumulation of retained particles, colloids, emulsions, suspensions, macromolecules and salts on or in the membrane. As a result, pore blocking and cake formation would be taken place. Additionally, the porous membranes like MF and UF are more vulnerable to fouling. There are three types of foulants that can be discriminated against.

- Organic precipitates (macromolecules, biological substances and so on)
- Inorganic precipitates (metal hydroxides, calcium salts etc.)
- Particulates

The fouling can be comprehended by plotting flux as a function of time as depicted in Figure 1.8. The decline in flux owing to the fouling process.

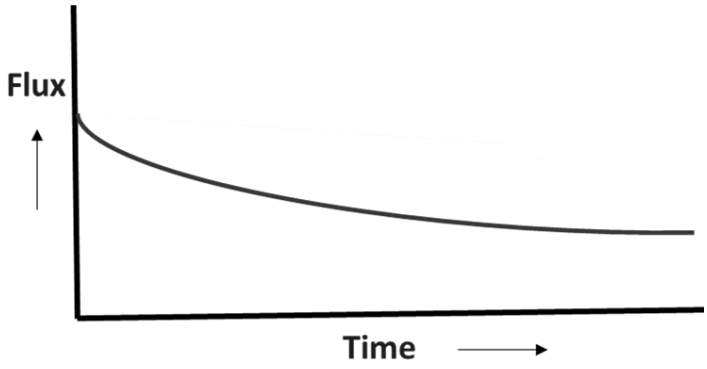

Figure 1. 8 Flux as a function of time

The membrane fouling can be controlled in the following ways.

- **Pre-treatment of the feed solution**

The feed solution should be treated with a complexing agent (like PEI, EDTA) before filtration is one of the methods to reduce the fouling. Moreover, other methods like pH adjustment, chlorination, charcoal treatment, heat treatment and pre-MF and UF can also benefit effectively.

- **Membrane properties**

The modification in the membrane properties can lead to a reduction of fouling. Likewise, engineering of pore size could control the fouling in an effective manner. Since proteins adsorb more strongly at the hydrophobic surfaces than the hydrophilic surfaces, the use of hydrophilic surfaces would be a decent choice. Besides, negatively charged membrane surfaces are chosen in the presence of negatively charged colloids in the feed. Thereby the protein adsorption can be reduced by electrostatic repulsion. However, surface zwitterionization can reduce both the positive and negative charged protein adsorption. The reduced surface roughness can prevent the fouling to some extent.

- **Cleaning**

In practice, cleaning methods would always be employed rather than the above-mentioned methods as they are able to perform to a minimum extent. The frequency of cleaning cycle can be assessed from the process optimization. There are three types of methods are available.

i. Hydraulic cleaning

It is meant only for the MF and UF membrane via back-flushing. The principle of back-flushing is that, changing of permeate direction from the permeate side to the feed side after releasing the pressure. So that, the adsorbed foulants on the membrane surface or in the membrane would be removed to a greater extent.

ii. Mechanical cleaning

It is applicable only to the tubular systems using oversized sponge balls.

iii. Chemical cleaning

The choice of chemical for cleaning depends on the module configuration, type of membrane, chemical resistance of the membrane and sort of foulant to be removed. This method is essential for reducing fouling. The amount of chemical and cleaning time is very important compared to the chemical resistance of the membrane. Here, a few of the chemicals are listed for chemical cleaning.

- Acids
- Alkali
- Detergents
- Enzymes
- Complexing agents (EDTA, PEI)
- Steam and gas sterilization

1.5 MEMBRANE MATERIALS

There are many polymeric materials available in the market. However, all the materials cannot be used for the membrane preparation application. The physical and chemical properties of the polymeric material determine the suitability to use as a membrane material. Further, hydrophilicity and hydrophobicity also important parameters for the good membrane material (Baker 2012).

In the preparation of MF and UF membranes, the same kind of polymeric material could be used. Nevertheless, the method of preparation is different from each other. The preparation methods for the MF membrane are sintering, stretching and track-etching. In which these techniques provide highly porous membranes.

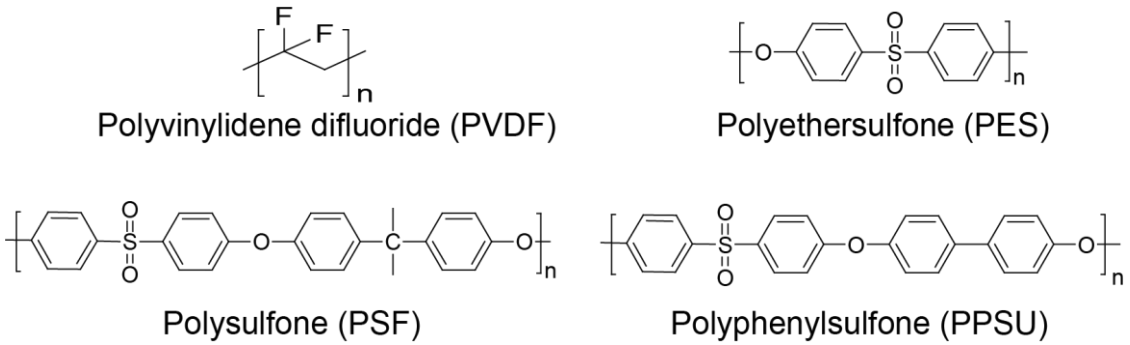

Figure 1. 9 Structures of few of the synthetic polymer

In the case of UF membranes, phase inversion technique is preferred. The polymers such as poly(vinylidene fluoride) (PVDF), polysulfone (PSF), polycarbonate, polyethersulfone (PES), polyamide, poly(ether-imide), polytetrafluoroethylene (PTFE) and isotactic polypropylene (PP) are desired polymers (Figure 1.9) for the preparation of MF and UF membranes.

1.5.1 Polysulfone (PSF) as membrane material

Among the polymer used for the preparation of UF membranes, PSF (Figure 1.10) is one of the main classes of a polymer. It has extraordinary chemical and thermal stability. It

exhibits the T_g value of 190 ^oC. These polymers are used widely for the preparation of UF and support material for composite membranes. PSF is insoluble in water and less hydrophilic in nature. However, it is soluble in polar aprotic solvents like DMF, NMP and DMSO. Since it has very good film-forming properties, the membrane preparation is so easy. Resistance to a wide range of pH and chlorine. Conversely, PSF is less hydrophilic (Mulder 2012). This drawback of PSF calls for the improvement to increase the surface wettability and fouling resistance character.

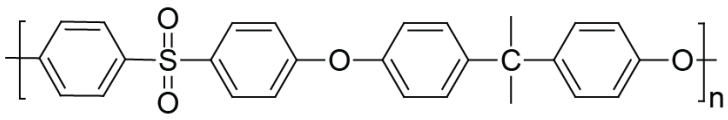

Figure 1. 10 Chemical structure of polysulfone (PSF)

1.6 FABRICATION OF MEMBRANES

As mentioned in chapter 1.5, there are many polymeric materials available for the preparation of the membrane. The number of the technique is also existing for the preparation of the membrane. Conversely, the kind of technique utilized depends mainly on the nature of the material and the desired structure of the membrane. For instance, in the preparation of MF and UF porous membrane structure is preferred. In the case of pervaporation and gas separation, nonporous membrane morphology is highly desirable.

1.6.1 Phase inversion method

The phase inversion technique is employed for the preparation of most of the commercially available membranes. It is a simple and adaptable technique that allows the preparation of all kinds of morphologies. Moreover, it is a process in which a polymer is transformed from a liquid state to a solid-state. During demixing, one of the liquid phases (high polymer concentration phase) will solidify to form the solid matrix. The concept of phase inversion comprises the following different techniques (Mulder 2012).

- **Precipitation by solvent evaporation**

This is one of the simplest techniques. In this method, the polymer is dissolved in a suitable solvent and cast over the suitable support. The support can be either porous nonwoven polyester or the nonporous glass if not metal plate. The solvent can evaporate under the inert atmosphere (N_2 atm), with the purpose of eliminating the water vapor. It provides a dense homogeneous membrane.

- **Precipitation from the vapor phase**

In this method, the polymer dope solution is placed in a vapor atmosphere where the vapor phase consists of a nonsolvent saturated with the same solvent. The membrane formation occurs due to the diffusion of nonsolvent into the film. This leads to the porous membrane without a top layer.

- **Precipitation by controlled evaporation**

In this case, the polymer is dissolved in the mixture of solvent and nonsolvent. As the solvent is more volatile than the nonsolvent, the composition moves during evaporation to a higher nonsolvent and polymer content. It leads to the formation of the skinned membrane.

- **Thermal precipitation**

This method is useful for the preparation of MF membranes. The polymer solution is prepared in a mixed or single solvent and cooled to assist phase separation is taking place.

- **Immersion precipitation**

Most of the commercially available polymeric membranes are prepared by phase inversion via immersion precipitation technique. In this method, the dope solution is prepared by dissolving the polymer in a single or mixture of solvent to obtain the homogenous solution. Then the polymer solution is cast on the appropriate support and immersed in a coagulation bath having nonsolvent. Precipitation occurs because of the exchanging of solvent and nonsolvent. The schematic representation of the immersion precipitation method is presented in Figure 1.11.

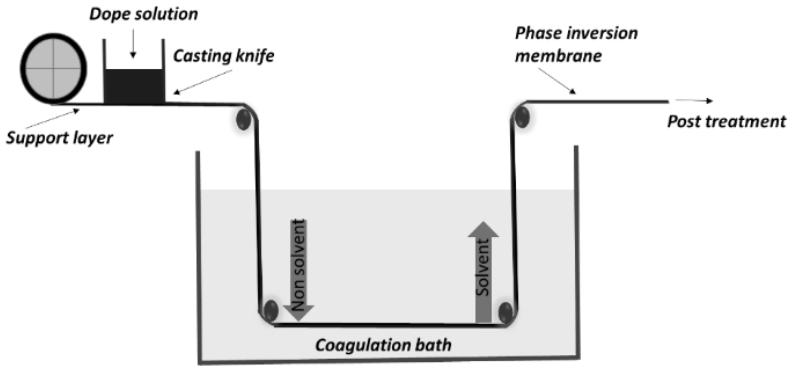

Figure 1. 11 Schematic representation of phase inversion method

1.7 APPLICATIONS OF MEMBRANE TECHNOLOGY

In the last two decades, membrane science and technology have attained significant growth. Based on the application, different forms and sizes are now available. It has the following advantages (Baker 2012).

- Energy efficient
- Low-temperature operation
- Recovery
- Water reuse
- Compact operation
- Easy scale-up

The membrane technology has the following applications.

1. Reverse osmosis (RO) membrane technology has been successfully used since the 1970s for brackish and seawater desalination. It is also employed for the removal of inorganic contaminants such as radionuclides, nitrates, arsenic and other contaminants such as pesticides.

2. A non- pressure, electric potential driven membrane called Electro Dialysis Reversal (EDR) has also been widely used for the removal of dissolved substances and contaminants.

3. Low-pressure microfiltration (MF) and ultrafiltration (UF) membrane filtration technologies have emerged as viable options for addressing the current and future drinking water regulations related to the treatment of surface water, groundwater under the influence and water reuse applications for microbial and turbidity removal. MF membranes are capable of removing particles with sizes down to 0.1- 0.2 microns. Some UF processes have a lower cutoff rating of 0.005-0.01 microns. Pressure or vacuum may be used as the driving force to transport water across the membrane surface.

4. Membrane Bioreactor (MBR) and tertiary treatment systems are the best available technologies for communities that are concerned about protecting the environment and preserving potable water supplies. Whether a community needs to improve the effluent quality from its existing conventional wastewater treatment plant or construct a new compact and highly efficient wastewater treatment system, MBRs provide cost-effective solutions that will meet or exceed discharge standards for years to come. Effluent from these systems is of such high quality that it can be safely discharged into the

most sensitive aquatic environments or reused in irrigation, industrial processes, or groundwater recharge.

5. The membrane gas separation industry is still growing and changing. Most of the large industrial gas companies started utilizing membrane technology now. Nowadays, some of the research group members are focusing on vapor separation, air dehydration and oxygen enrichment. It is also used for the separation of CO_2 from natural gas, hydrogen gas separation and oxygen/nitrogen separation. By fine-tuning the solubility of CO_2, the selectivity and permeability can be improved.

6. Pervaporation systems are now commercially available for two applications. The first and most important is the removal of water from concentrated alcohol solutions. The ethanol feed to the membrane contains about 10 % water. The pervaporation process removes the water as the permeate, producing a residue of pure ethanol containing less than 1 % water. The second commercial application of pervaporation is the removal of small amounts of volatile organic compounds (VOCs) from contaminated water.

7. The main purpose of dialysis is to remove urea, creatinine and other waste products directly from impure blood. Flat cellophane (cellulose) tube forms the dialysis membrane; the hollow fiber membrane was wound around a rotating drum immersed in a bath of saline. As blood was pumped through the tube, urea and other low molecular weight metabolites diffused across the membrane to the dialysate down a concentration gradient. The cellophane tubing does not allow diffusion of larger components in the blood such as proteins or blood cells. By maintaining the salt, potassium and calcium levels in the dialysate solution at the same levels as in the blood, the loss of these components from the blood will be prevented.

1.8 LITERATURE REVIEW

In this chapter, a brief review of the literature on existing methods of water treatment has been discussed. Membrane technology has attained an apex of success in the field of water treatment for the past two decades. Amid the polymeric materials, polysulfone (PSF) has attracted a remarkable consideration as a material of choice for the preparation of membranes.

Morosoff *et al*. (1978) reported the preparation of polymer hollow fiber reverse osmosis membranes. Where they used polysulfone as a substrate for the preparation of the

membrane. The results exhibited that the composite membrane has enhanced the rejection capacity.

The hydrophilic modification of the PSF membrane with polyvinylpyrrolidone (PVP) as an additive was reported (Munari *et al*. 1988). The author has studied the effect of adding PVP and its molecular weight on the viscosity of the casting solution. It has been reported that the addition of PVP can increase the PSF membrane permeation rate, porosity and water uptake compared to the neat PSF membrane.

Tremblay and group members studied the changes affecting carboxylated polysulfone (CPS) membranes in relation to membrane porosity. The pore size of CPS membranes containing COOH substituents was measured after exposure to acidic and basic environments. Membrane pore size was found to be dependent on the type of the carboxyl group. Pore size decreased by 10-25 % on exposure to acid. The conversion from the COOH form to the ionic COO^-Na^+ form, by exposure to a base, increased the pore size of the membrane by 30-100 %. These changes were fully reversible on conversion to the COOH form. Membranes were exposed to aqueous ethanol and chlorine to determine their resistance to these environments. Aqueous ethanol had no measurable effect on membrane pore size. For membranes in the -COOH form, 24-h exposure to chlorine resulted in a small increase in membrane pore size, while no significant change was observed for membranes in the COO^-Na^+ form (Tremblay *et al*. 1992).

Novel and general method of modifying hydrophobic polysulfone (PSF) to produce highly hydrophilic surfaces was reported by Song *et al*. (2000) (Scheme 1.1). This method is the low-temperature plasma technique. Graft polymer-modified surfaces were characterized with the help of FTIR-ATR and XPS. Study results demonstrated that poly(ethylene glycol) (PEG) could be grafted onto the PSF membrane surface by low-temperature plasma. The hydrophilic character of the modified surfaces was increased in comparison with that of the neat membrane. The contact angle for a modified PSF membrane was reduced apparently.

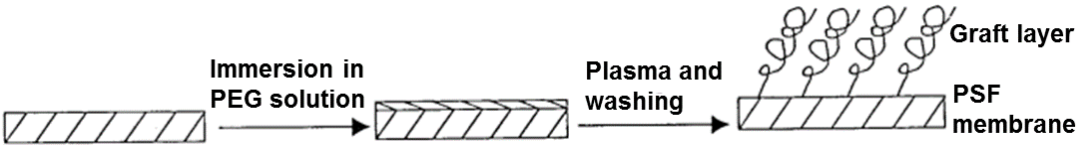

Scheme 1. 1 Grafting of PEG on polysulfone membrane by low-temperature plasma (Song et al. 2000)

Ribau *et al*. (2002) studied the effect of the pH on the ultrafiltration performance of natural surface waters with moderate natural organic matter (NOM) content using a plate-and-frame PSF membrane of 47 kDa MWCO. The results at three different pH values (acid, neutral and basic) demonstrated the important role of the pH on the ultrafiltration (UF) performance controlling the membrane fouling matter interactions. The higher fluxes and lower NOM rejections obtained, at basic pH when compared to acidic pH, are explained in terms of the variation of membrane and NOM charge, due to electrostatic repulsion and adsorption effects.

Hydrophilic polysulfone ultrafiltration (UF) membranes from blends of cellulose acetate with carboxylated polysulfone of 0.14 degree of carboxylation were prepared (Sajitha *et al*. 2002). The effects of polymer blend composition on compaction, pure water flux, water content and membrane hydraulic resistance have been investigated to evaluate the performance of the membranes. The performance of the blend membranes of various polymer blend compositions was compared with that of membranes prepared from pure cellulose acetate and blends of cellulose acetate and pure polysulfone. The hydrophilic cellulose acetate-carboxylated polysulfone blend UF membranes showed better performance compared to membranes prepared from pure cellulose acetate and blends of cellulose acetate and pure polysulfone.

Sundarrajan *et al*. (2007) synthesized the nanoparticles of MgO by the Aerogel method. These MgO nanoparticles were then mixed with polysulfone and then subjected to electrospinning to produce nanocomposite membranes. The hydrolysis of paraoxon, a nerve agent stimulant, in presence of these membranes was studied using UV. The amount of hydrolysis of the PSF-MgO composite membrane was 60 % less when compared to MgO nanoparticles as such usage. The loading percentage of MgO into nanofiber is 35 %. The fabricated composite membrane (containing 5 % MgO) was tested for chemical warfare agent stimulant, paraoxon and found to be about 2 times more reactive than currently used charcoal.

Liu and group membranes prepared multiwalled carbon nanotubes functionalized with poly(sulfone) (PSF) and poly(sulfobetaine methacrylate) (PSBMA) (MWCNT-PSF/PSBMA) through sequential atom transfer radical polymerization (Liu *et al*. 2010). The structure of MWCNT-PSF/PSBMA hybrid has been characterized by FTIR, Raman spectroscopy and high-resolution transmission electron microscopy. Incorporation of PSBMA chains to MWCNTs introduces amphiphilic and protein-resistant properties to MWCNT-PSF/PSBMA. The addition of 1 wt % MWCNT-PSF/PSBMA to PSF films significantly improves their protein-resistant characteristic, as the composite films show a 4.4 % of protein adsorption compared to poly(styrene) Petri dishes. The PSF/MWCNT-PSF/PSBMA composite has been applied to prepare antifouling ultrafiltration membranes for protein separation. This work validates an effective and convenient approach to prepare low-protein-adsorption surfaces and antifouling membranes.

Anadão *et al*. (2010) developed the composite nanofiltration (NF) membrane polyacrylic acid (PAA) in situ UV graft polymerization process using ultrafiltration (UF) polysulfone (PSF) membrane as porous support. FT-IR spectra indicated that grafting was performed. AFM microscopy showed the roughness of the surface was reduced by the increase of UV irradiation times. The salts rejection increase was accompanied by the grafting of polysulfone (PSF) ultrafiltration (UF) membrane. The rejection of Na_2SO_4, $MgSO_4$, NaCl and $CaCl_2$ salts by PSF-grafted-PAA nanofiltration (NF) membrane was in the range of 98, 60, 52 and 30 % respectively, under 0.3 MPa.

Yi *et al*. (2010) developed electro-ultrafiltration membranes is an attractive target. Electrically conducting ultrafiltration membranes by blending single-walled carbon nanotube/polyaniline (SWCNT/PANi) nanofibers into a polysulfone (PSF) matrix was reported. It is reported that, by selecting a number of nanofibers and applying a flash welding technique, the chemical structure, porosity, thermal stability, conductivity, hydrophilicity, permeability and Bovine Serum Albumin (BSA) rejection of these composite ultrafiltration membranes can be controlled. The addition of SWCNT/PANi nanofibers to the composites enhances the initial water permeability by 2.5-7.3 times and increases the hydrophilicity and maintains considerable rejection of BSA from 39.8-73.7 %. Electrical conductivity between 0.1 and 3.4×10^{-6} S cm-1 can be maintained over a broad pH range from 0.52-10.2. By regulating the flash welding intensity, the conductivity, permeability and BSA rejection can be enhanced up to 600, 2 and ~1.5 times, respectively.

A mixed matrix membrane consisting of a polysulfone and nano-ZnO particles by a combination of solution dispersion blending and phase-inversion method was prepared by Alhoshan *et al*. (2013). The study is focused on the influence of ZnO on membrane morphology, surface roughness and hydrophilicity, which were investigated through the methods of scanning electron microscopy, atomic force microscopy and contact angle meter, respectively. In addition, the changes in membrane characteristics with the addition of nano-ZnO particles were examined by pure water flux, water content and porosity and salts rejection including NaCl and $MgSO_4$. From the results, it was revealed that nano-ZnO particles constructed a membrane having a more hydrophilic, smooth and tightly packed surface, which offered a high flux and an effective permeability barrier. Moreover, it was observed that nano-ZnO particles produced a spongy membrane with uniform and well-interconnecting pores.

Our previous group member reported the preparation of PSF-CS blend membranes. Two different compositions of polysulfone in N-methylpyrrolidone (NMP) and chitosan in 1 % acetic acid were blended to prepare PSF–CS ultrafiltration membranes by the diffusion induced phase separation (DIPS) method. The proper blending of polysulfone and chitosan in PSF–CS membranes was confirmed by ATR-IR analysis. The surface and cross-sectional morphology of the membranes was studied by scanning electron microscopy (SEM). The membrane hydrophilicity was determined by water uptake and contact angle measurements. The PSF–CS membrane showed enhanced hydrophilicity compared to a PSF ultrafiltration membrane. An improved antifouling property was observed for PSF–CS blend membranes as compared to pristine PSF ultrafiltration membranes. Both the permeation and antifouling properties of PSF–CS membranes increased with an increase in chitosan composition (Rajesh *et al*. 2013).

Chai *et al*. (2016) prepared novel polysulfone-Fe_3O_4/GO mixed-matrix membrane by embedding the iron-decorated graphene oxide (Fe_3O_4/GO) into PSF polymer. Fe_3O_4/GO was then prepared by mixing both GO and Fe_3O_4 in the presence of ammonia hydroxide (NH_4OH) according to the co-precipitation method. A series of tests, such as X-ray diffraction (XRD) and Transmission Electron Microscopy (TEM) were performed to characterize the produced Fe_3O_4/GO nano-hybrid. The mixed-matrix membrane was fabricated by casting the pre-mix PSF- Fe_3O_4/GO polymer solution mixture using the phase inversion method. The performance of both neat PSF membrane and novel polysulfone-

Fe_3O_4/GO mixed-matrix membrane was evaluated by measuring the membrane permeate flux and humic acid rejection. The experiment demonstrated that the novel polysulfone-Fe_3O_4/GO mixed-matrix membrane was having 3 times higher permeate flux than the neat PSF membrane despite the drop in humic acid rejection from 89±2 % to 84±2 %. However, polysulfone-Fe_3O_4/GO mixed-matrix membrane permeability was increased with the compensation of decreasing retention capacity due to pore size enlargement, higher porosity as well as higher hydrophilicity.

Ding and co-workers prepared the composite nanofiltration membrane by coating the covalent crosslinked sulfonated polysulfone on a porous substrate (Scheme 1.2) (Ding *et al*. 2016). Polyethylene glycol (PEG), dopamine (DA) and m-phenylenediamine (MPD) were used as crosslinkers, respectively. The polyethersulfone/sulfonated polysulfone substrate was prepared by phase inversion. The membrane surface chemistry, hydrophilicity, morphology, PWF and rejections of PEG, methyl red and Na_2SO_4 were characterized. The effect of the sulfonated polysulfone concentration on the membrane characteristic was also investigated. The PEG-crosslinked membrane showed the lowest contact angle of 9.0°, the highest PEG-600 rejection of 99.8 %, the highest methyl red rejection of 99.8 % and the rejection of Na_2SO_4 was 93.4 % and the PWF was 3.1 L/m^2h. The DA crosslinked membrane had the highest PWF of 51.5 L m^{-2} h^{-1} and the rejections of PEG-600, methyl red and Na_2SO_4 were 46.0, 44.0 and 34.0 %, respectively.

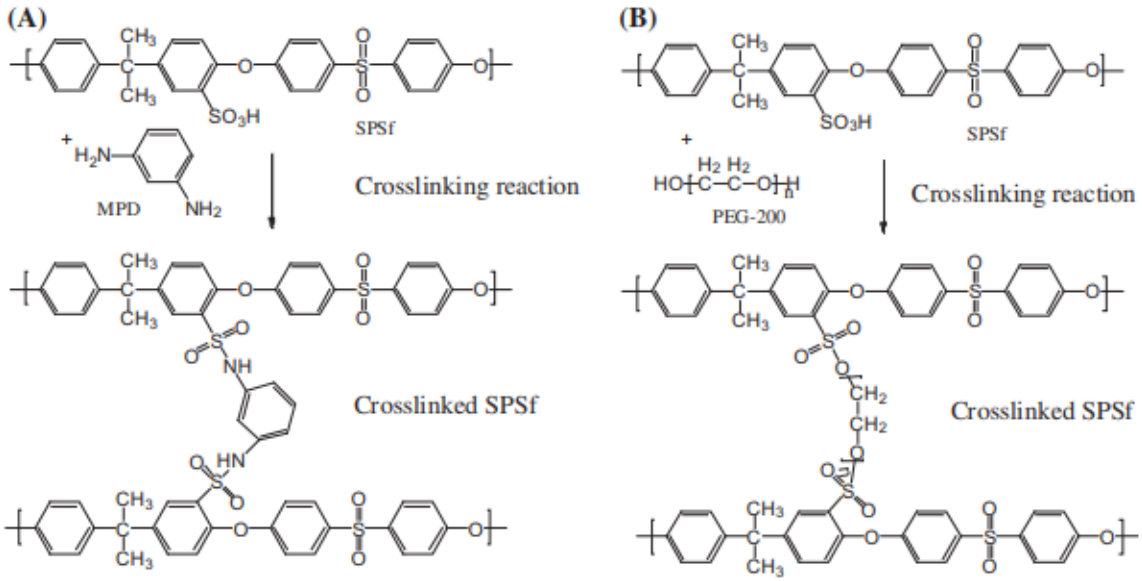

Scheme 1. 2 Crosslinking reaction of sulfonated polysulfone (SPSf) with A) meta phenylenediamine (MPD) and B) PEG-200 (Ding et al. 2016)

Basu *et al*. (2017) demonstrated the removal of pharmaceutical wastes through electrostatic repulsion and size sieving in NF and RO from the aqueous feed. It is reported that the incorporation of metal-organic frameworks (MOF) into the polymeric membrane exhibited the 55 % retention of paracetamol.

An antifouling hybrid ultrafiltration membranes using polysulfone (PSF) and sulfonic acid functionalized TiO_2 nanotubes (TNTs-SO_3H) prepared by Alsohaimi *et al*. (2017) (Scheme 1.3). Hybrid membranes containing TNTs-SO_3H up to 5 wt% were then prepared from the blend solutions of PSF/TNTs-SO_3H via a non-solvent induced phase separation (NIPS) method. The hybrid membranes were characterized using contact angle, Fourier transforms infrared spectroscopy, scanning electron microscopy and surface zeta potential studies. The antifouling capability of hybrid membranes with bovine serum albumin and humic acid (HA) as model foulants were investigated in detail. Hybrid membranes exhibited better water permeability and antifouling performance during the filtration of foulant solutions. The ultrafiltration of HA solutions of different concentrations was carried out at pH = 7 and 1 bar feed pressure, with the removal of HA from the aqueous solution being controlled through the charged behavior, porosity and exclusion of HA by hybrid membranes. The maximum removal of HA from 20 ppm aqueous solution was achieved using the hybrid membrane MTS-5 containing 5 wt% TNTs-SO_3H.

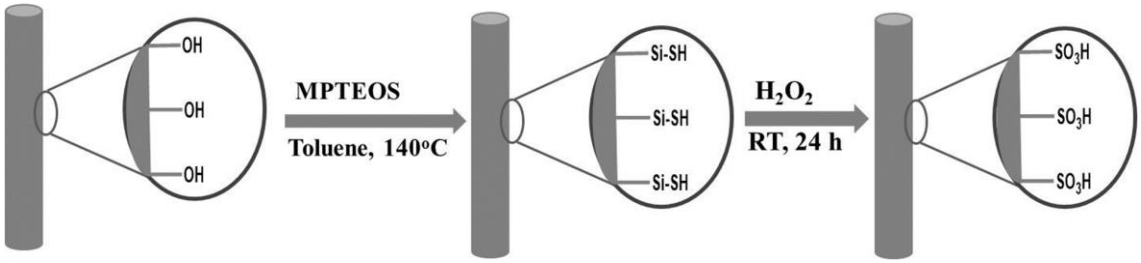

Scheme 1. 3 Synthesis of sulfonic acid functionalized TiO_2 nanotubes (Alsohaimi *et al*. 2017)

Polyamide (PA) thin-film nanocomposite (TFN) membrane incorporated with multiwalled carbon nanotubes-titania nanotube (MWCNT-TNT) hybrid was fabricated (Wan Azelee *et al*. 2017). The hybrid was introduced to the PA selective layer during the interfacial polymerization (IP) of trimesoyl chloride (TMC) and m-phenylenediamine (MPD) monomers over porous commercial polysulfone (PS) ultrafiltration support. The resultant TFN was characterized and applied for desalination. The results revealed that the acid-treated MWCNT-TNT, which act as filler in the PA membrane, improved the surface

properties of the membrane in term of surface charge, surface roughness and contact angle. Consequently, the water permeability increased significantly without compromising the salt rejection performance. The highest water permeability of 0.74 L/m^2 h bar was achieved for the TFN membrane containing 0.05 wt% acid-treated MWCNT-TNT, which is approximately 57.45 % than that of the neat PA membrane. The NaCl and Na_2SO_4 rejection of this membrane was 97.97 % and 98.07 %, respectively that is almost like the neat membrane.

Zambare and co-workers synthesized polyamine functionalized graphene oxide (fGO) based polysulfone mixed matrix membranes with enhanced hydrophilicity, permeability and antifouling properties (Zambare *et al*. 2017). The effect of chain length of the amine in fGO on the performance of the mixed matrix polysulfone membranes was studied using three different polyamines, such as ethylenediamine, diethylenetriamine and triethylenetetramine. Synthesized membranes were characterized by the water contact angle, tensile strength, SEM, AFM, EDS, overall porosity, water permeability, fouling resistance, etc. fGO based polysulfone membranes showed higher porosity and permeability, improved structural and mechanical properties and better anti-fouling potential with high flux recovery after bovine serum albumin (BSA) filtration with little change in BSA rejection. Polysulfone membranes containing 1 wt% of ethylenediamine functionalized graphene oxide and 5 wt% of polyethylene glycol (PEG-600) additives, displayed remarkably high pure water flux of 170.5 L/m^2h bar, a 3-fold increase over corresponding control membrane, in addition to substantially higher BSA rejection and higher normalized recovered flux after fouling.

Zhang *et al*. (2019) fabricated high flux TFC NF membranes with novel acyl chloride such as trimellitic anhydride chloride (TAC) and trimesoyl chloride (TMC) using PSF UF membrane as support (Scheme 1.4). The chemical composition and structure of the PA layer was tailored by using different concentration of TAC. It was reported that the as-added TAC led to the formation of a looser PA layer structure during the interfacial polymerization (IP) reaction. The added TAC also increased the surface hydrophilicity, roughness, pore size and surface charge. With 0.04 wt% of TAC, the TFC membrane demonstrated pure water permeability (PWP) of 13.2 L/m^2h bar and Na_2SO_4 rejection of 97.6 %.

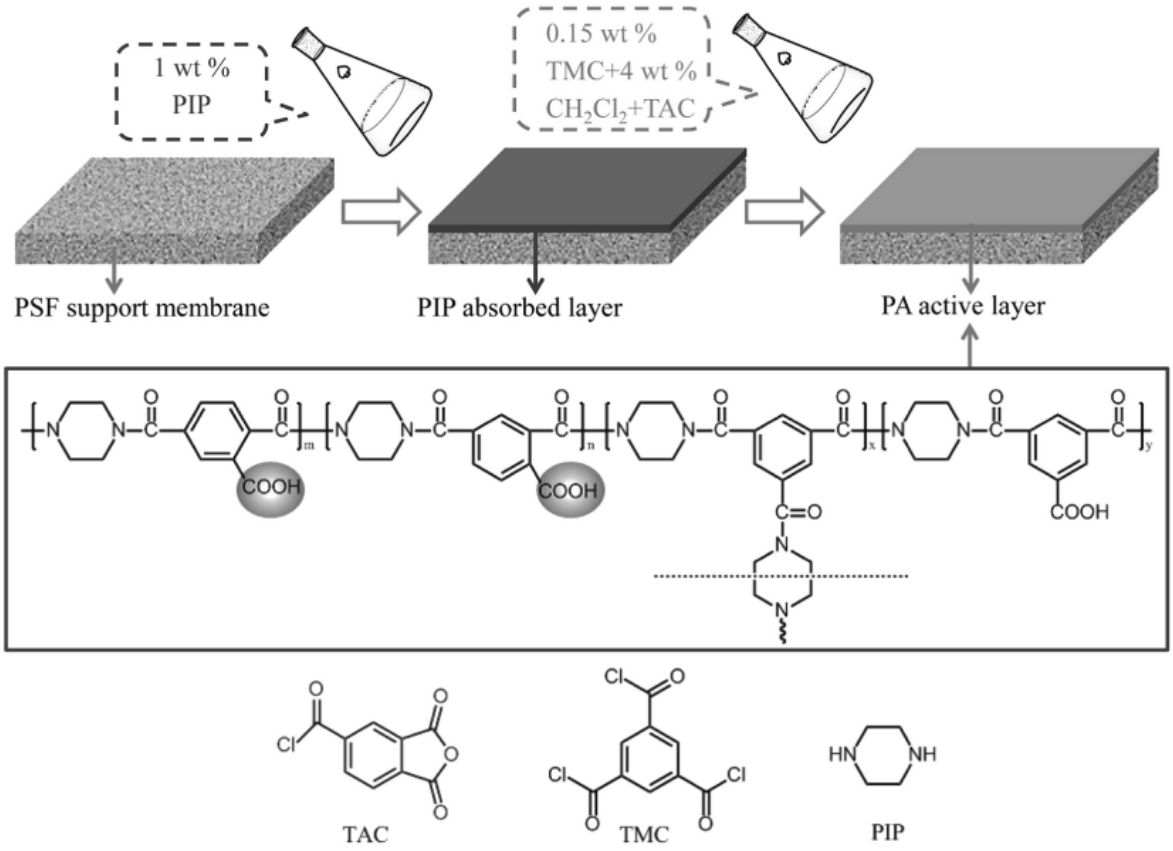

Scheme 1. 4 Synthesis of thin film composite (TFC) nanofiltration (NF) membranes (Zhang et al. 2019)

Xue and group members reported the preparation of chlorine resistant TFC NF membranes incorporated with β-cyclodextrin (β-CD) (Xue *et al*. 2019). The TFC membrane prepared with 1.8 wt% of β-CD bestowed improved permeability and chlorine resistant property for 96 h. The improved permeability of the TFC membrane was attributed to the synergistic effect of the intrinsic cavity and the inactive hydroxyl group formed the loose PA layer and water channel.

The cellulose nanocrystals (CNCs) incorporated TFN NF membranes were reported by Rahimi *et al*. The CNCs were dispersed in TMC solution with varying concentrations and reacted with PIP. It was observed that with an increase in the concentration of CNCs increased the PWP of the TFN NF membrane. However, the higher concentration of CNCs (above 0.1 wt%) resulted in deterioration of NF membrane performance. It was also mentioned that CNCs concentration of 0.05 wt% exhibited water flux of 22.47 L/m^2h and Na_2SO_4 rejection of 93.44 %. In addition, the modified TFN membrane presented improved antifouling property (Rahimi *et al*. 2020).

TFN hollow fiber NF membrane was fabricated by incorporating ZIF-93 metal-organic framework (MOF) (Echaide-Górriz *et al*. 2020). In the typical process, continuous MOF layers were prepared by liquid-phase crystallization followed by IP reaction on the MOF layer. The TFN membranes exhibited increased PWP and dye rejection compared to the pristine membrane. Nevertheless, Zinc ions released during the degradation of MOF was also attributed to the increase of PWP.

In another report, Zhu *et al*. (2020) reported the fabrication of the TFC membrane with a supramolecular based protective layer. The prepared TFC membranes exhibited improved chlorine resistance. The modified membranes demonstrated increased removal of dyes, salts and micropollutants with only ~10 % reduction in water permeability. The increased chlorine resistance was ascribed to the presence of a supramolecular coating layer, which avoided the degradation of the PA layer by acting as a radical scavenger.

From the above literature survey, it is evident that PSF can be employed as an excellent membrane material. However, limited research has been done on PSF as membrane material due to its lower hydrophilicity and flux. Hence more research is needed to overcome its drawbacks, as PSF being cheaper as compared to other commonly used polymers would make an economical membrane material. The following work has been proposed by taking these arguments into account.

1.9 SCOPE OF THE WORK

It is evident from the literature survey that the use of polysulfone (PSF) as membrane material has attracted many researchers worldwide for its expanding utility in the field of membrane separation technology. Keeping in view the advantages offered by this material, research is in progress to overcome their existing drawbacks (such as hydrophobicity and fouling) by some suitable modifications in order to make them an ideal membrane material. The possibility of enhancing the membrane properties in terms of their hydrophilicity, antifouling nature, chemical resistance, mechanical strength and thermal stability may help in large scale utilization of this material in the near future.

1.10 OBJECTIVES

1. To prepare neat and modified polysulfone-based ultrafiltration and nanofiltration membranes for water purification.
2. To synthesize the hydrophilic polymer and to fabricate the polysulfone blend membrane with improved performance.
3. To study the effect of both organic and inorganic hydrophilic additives on property and performance of the composite membranes.
4. To study the morphological features of all the prepared polysulfone membranes by SEM and to characterize the polymer, nanoparticles and membranes by FT-IR, UV-Vis, NMR, AFM, DSC, TGA, TEM, EDX and zeta potential analysis.
5. To study the permeation and rejection behavior of the newly prepared membranes.
6. To study heavy metal, salt and dye removal capacity of pristine polysulfone and modified polysulfone membranes.
7. To determine pristine polysulfone and modified polysulfone membrane properties in terms of water uptake, porosity and contact angle measurement and to study the antifouling property and reusability of the prepared membranes.

CHAPTER 2

BIO-INSPIRED, FOULING RESISTANT, TANNIC ACID FUNCTIONALIZED HALLOYSITE NANOTUBE REINFORCED POLYSULFONE LOOSE NANOFILTRATION HOLLOW FIBER MEMBRANES FOR EFFICIENT DYE AND SALT SEPARATION

***Abstract**: In this chapter, a simple and novel loose nanofiltration (NF) membranes were prepared by the addition of tannic acid-functionalized halloysite nanotubes (THNTs) in polysulfone (PSF) membrane matrix via phase inversion method. The membrane permeation studies were carried out with a sequence of salts (NaCl and Na_2SO_4) and dyes (Reactive black 5 and Reactive orange 16). The resulted membranes exhibited increased hydrophilicity, porosity, water uptake, antifouling performance, along with higher dye rejection (>99 % for Reactive black 5 and >90 % of Reactive orange 16) and low salt rejection (2.5 % of NaCl and 7.5 % of Na_2SO_4) properties. The nanocomposite membrane also exhibited the highest pure water flux of 92 L/m^2h compared to the pristine membrane of 18 L/m^2h made it a worthy candidate for the wastewater purification.*

2.1 INTRODUCTION

The increased concentration of pollutants is inflowing water provisions through anthropogenic sources, affecting in the insufficient entry to clean water for the rising worldwide inhabitants (Shannon *et al*. 2008). The wastewater from the industries such as a dye, paper, paint and tanneries are needed to treat appropriately before discarding or recycling. The direct discharge of organic dyes into the water stream leads to severe environmental imbalance, as most of them are non-biodegradable, toxic and consume dissolved oxygen (Forgacs *et al*. 2004, Rafatullah *et al*. 2010, Wu *et al*. 2013). More complex structures, high molecular weight and synthetic origin of reactive dyes make them more stable, particularly even just 1.0 mg/L concentration in drinking water possibly will impart color (Salleh *et al*. 2011, Xing *et al*. 2015).

In the dye industry, water is employed primarily as steam for the heat treatment of the bath and then for transferring dyes into the fibers. The dyeing of about 1 kg of cotton needs around 152 L of water, ~ 0.8 kg of NaCl and somewhere around 60 g of dyestuff (Dupont). Therefore, the reclamation of dye from wastewater has excessive importance. Furthermore, inorganic salts such as NaCl (~ 6 wt%) and Na_2SO_4 (~ 5.7 wt%) were incorporated to improve the dye pickup ability of the cotton and during synthesis of dye, quite large amount of low molecular weight intermediates are produced (Yu *et al*. 2001). The occurrence of inorganic salts not only restraining the biodegradation of dyes but complicates the treatment processes as well (Luo *et al*. 2011, Xie *et al*. 2011). In the thought of sustainability, the recovery of dyes and salts from the wastewater needs a new technique that is cost-effective,

less time consuming and environmental friendly. Conventional methods, such as electrochemical (Lin *et al*. 1994, Vlyssides *et al*. 2000), oxidation (Tratnyek *et al*. 1994), coagulation by polymeric aluminum species (Shi *et al*. 2007) are having the similar disadvantages that the resources are not recycled adequately (Zheng *et al*. 2006).

The employment of loose nanofiltration (NF) membrane has been recognized as the complementary nominee for the wastewater management, as it has advantages like low cost, low operating pressure, environmentally friendly, less energy consumption, high dye rejection and high salt permeability (Liao *et al*. 2014, Ong *et al*. 2014, Zhu *et al*. 2016). Even though NF has the capacity to reject more than 99 % of dyes, it has a high rejection of inorganic salts (> 30 % NaCl), membrane fouling, concentration polarization and molecular weight cut-off (MWCO) of 100-1000 Da signifying the near pore size of 1 nm. Unavoidably, NF requires a high frequency of chemical cleaning, which would affect the lifespan of membranes. The above shortcomings make the NF as an insignificant candidate for the separation of dye/salt mixture (Koyuncu *et al*. 2003, Koyuncu *et al*. 2004, Mohammad *et al*. 2015, Wu *et al*. 2016). Therefore, it is of prime importance to study the loose NF membranes.

Lin and group members reported the separation of direct dye and salt in aqueous solution. The results exhibited that, 99.0 % of dye retention with 95 % of NaCl permeation (Lin *et al*. 2015). According to Yu *et al*., the poly (ionic liquid) functionalized SiO_2 loose NF membrane showed the increased permeation of salts with high rejection of dyes (Yu *et al*. 2015). Xing *et al*. prepared negatively charged PSS-SiO_2 incorporated PES membranes for the high rejection of dyes with less than 11 % of salt rejection (Xing *et al*. 2015). Yu *et al*. reported the positively charged hydrotalcite nanosheets modified by poly (ionic liquid). The loose NF membrane could reject 95 % of Reactive black 5 and around 90 % of reactive red 49 with non-zero salt rejection properties (Yu *et al*. 2016). Zhu *et al*. investigated the effect of adding chitosan-montmorillonite nanosheets to loose NF membranes and the modified membrane exhibited high rejection of reactive red 49 and Reactive black 5 along with high salts permeation (Scheme 2.1) (Zhu *et al*. 2015).

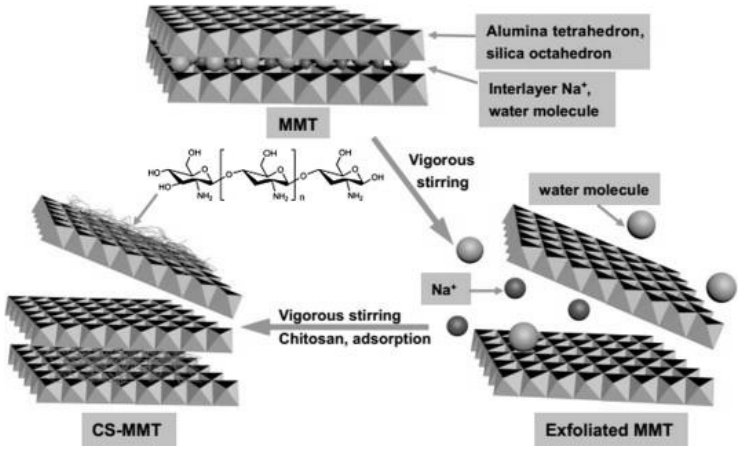

Scheme 2.1 Preparation of chitosan–montmorillonite (CS–MMT) nanosheets (Zhu *et al*. 2015)

Polysulfone (PSF) is one of the perfect polymeric material for the preparation of membranes, because of its high thermal stability, long-range of pH and chlorine tolerance along with outstanding chemical resistance (Nabe *et al*. 1997, Kim *et al*. 2002, McVerry *et al*. 2013). However, the pristine PSF membranes are suffering from severe fouling. The fouling of membrane can be ascribed mainly due to the lesser hydrophilicity of the membrane. Since the PSF membrane is less hydrophilic, it would foul very fast and the lifespan of the membrane would be reduced to a great extent. Consequently, the maintenance cost of the membrane would be enhanced. Of late, the significant extent of efforts has been taken to improve the innovative composite polymeric membranes for obtaining better surface hydrophilicity and antifouling performances (Ismail *et al*. 2013, Yang *et al*. 2014, Pereira *et al*. 2015, Moideen K *et al*. 2016). Sharma *et al*. prepared PSF ultrafiltration membranes using racemic and enantiomeric tartaric acid as an additive. It is reported that the as-prepared membrane exhibited the enhanced removal crystal violet dye (Sharma *et al*. 2016). Chai *et al*. demonstrated the preparation of PSF-Fe_3O_4/GO mixed matrix membranes for humic acid rejection (Chai *et al*. 2017). In 1966, Mahon prepared the first hollow fiber (HF) membranes (Mahon 1966). Related to flat sheet membranes, the HF membrane is the superior of membrane since it has the following advantages: (i) the increased surface area per unit volume of the membrane module, which renders enhanced efficiency; (ii) easy cleaning, handling and preparation; (iii) consistent results; (iv) it does not need any mechanical support (Chung *et al*. 2000, Wang *et al*. 2004). In recent days, HF membranes are also used in gas separation, reverse osmosis (RO), ultrafiltration (UF), dialysis and pervaporation.

Over the past decades, Halloysite nanotubes (HNTs) has received greater attention from the researchers due to its efficacy in the different fields. Figure 2.1 denotes the increased attention paid towards the HNTs for the past few years. These data are attained based on the Scopus database. Moreover, HNTs are cheaper, non-toxic and extensively found in soils worldwide. On the other hand, the foremost morphology of HNTs is elongated tubule with a diameter of 50-100 nm and length of 100-2000 nm (Yu *et al*. 2016). Figure 2.2 represents the structure of HNTs. Moreover, the lumen surface of HNTs is covered with alumina and the outer surface is covered with silica predominantly, as a result, it is having the net negative charge on the outer surface (Cavallaro *et al*. 2013, Owoseni *et al*. 2014). The presence of plenty of hydroxyl groups on the surface of HNTs makes the nanomaterial more hydrophilic and easier for further modifications. Nevertheless, to reject the anionic dyes based on the electrostatic repulsion, the HNTs must be functionalized with selected worthy materials.

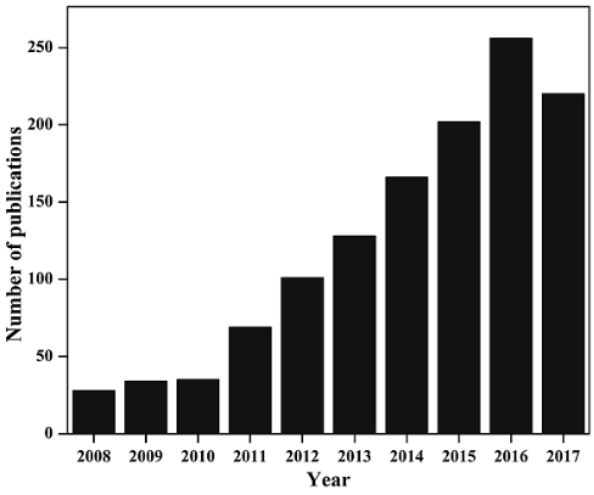

Figure 2.1 The number of publications based on the keyword "Halloysite nanotube" (Scopus; as on 06th Jan 2020)

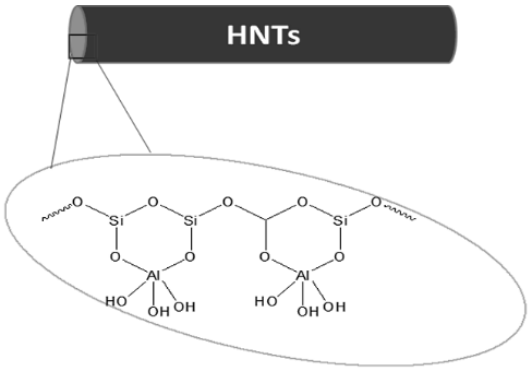

Figure 2.2 Structure of halloysite nanotubes (HNTs)

Messersmith *et al*. reported facile and one-step modification using polydopamine (pDA) as an effective modifier (Lee *et al*. 2007). According to Hebbar *et al*. the pDA coated HNTs enhanced the flux, porosity, antifouling and antibiofouling properties of the as-prepared membranes (Hebbar *et al*. 2016). Although pDA is unsophisticated to use on any substrate and offers many potential applications, the cost of dopamine and typical dark color of pDA coating would impairment some hands-on applications (Sileika *et al*. 2013, Pan *et al*. 2015,). Tadas *et al*. described the usage of polyphenols as an active alternative to pDA for the surface coatings (Sileika *et al*. 2013). Inspired by the phenomenon of staining of teacups by the tea water, the plant-based polyphenol such as tannic acid (TA) was identified as the universal coating material. These types of biomolecules consist of dense gallol functional groups and thus exhibit strong solid-liquid interfacial properties (Wei *et al*. 2015). TA is the low-cost, environmental friendly polyphenol. The commercial slight yellowish amorphous TA powder is straight away extracted from the plants. In tanneries, TA is used for the tanning of leathers. TA holds numerous advantages similar to pDA and deposits under similar conditions. Moreover, it is hundredfold cheaper and delivers colorless multifunctional coatings. The presence of plenty of hydroxyl groups in TA make the coating more hydrophilic and enhance the surface charge. In addition, it has excellent resistant towards the fouling by bacterial and mammalian cells (Tang *et al*. 2015).

The effect of adding TA coated graphene was studied by Liu and group members. The results indicated that the functionalized graphene showed excellent adsorption capacity towards Rhodamine B from the aqueous solution (Liu *et al*. 2015). According to Xu *et al*. the maleimido-containing TA coated stainless steel surface exhibited outstanding antifouling character (Xu *et al*. 2016). Zhang *et al*. stated the co-deposition of TA and diethylenetriamine (DETA) on the commercially available polypropylene and poly (vinylidene fluoride). The modified membranes displayed high water flux, hydrophilicity and more surface wettability (Scheme 2.2) (Zhang *et al*. 2016). Yan *et al*. examined the performance of the NF membrane via interfacial polymerization of TA and trimesoyl chloride. The thin film composite membrane exhibited enhanced permeation and antifouling performances along with excellent chemical stability (Zhang *et al*. 2013). Lin *et al*. demonstrated the use of TA coating on iron ions via coordination. The results showed that, the increased ratios of dye and salt rejection with the antioxidant ability (Fan *et al*. 2015). Xi *et al*. reported that the as-formed interlayer using TA and diethylenetriamine in

the thin-film composite membrane, enhanced the flux and rejection capacity as the interlayer assisted in the formation of defect-free polyamide layer (Zhang *et al*. 2016).

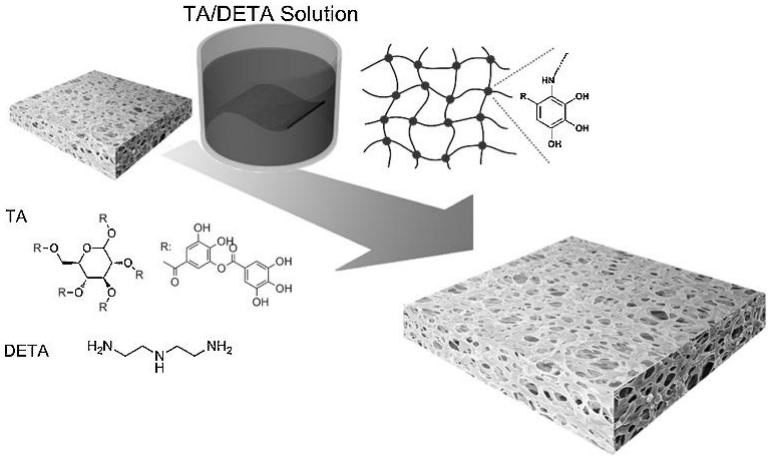

Scheme 2.2 Schematic representation of co-deposition of tannic acid (TA) and diethylenetriamine (DETA) on the membrane surface (Zhang *et al*. 2016)

In the contemporary study, facile, low-cost, green and one-step modification of HNTs with tannic acid via self-polymerization has been reported. The modified HNTs were used as an additive to fabricate the PSF loose NF membrane via a dry/wet phase inversion method. The effect of the addition of novel additive was thoroughly examined in terms of surface hydrophilicity, porosity, anti-fouling and water uptake. The purpose of using TA not only for the organic modification of HNTs but also to enhance the surface charge of the nanomaterial, which would enhance the surface charge of the hollow fiber membrane. The prepared novel PSF loose NF membrane also studied for the rejection capability towards the reactive dyes with high inorganic salt permeation ability. Besides, the loose NF membranes eliminate the formation of the toxic intermediates during the course of the dye degradation and improve the dye and salt recovery as well. This is the first such report of tannic acid-functionalized HNTs (THNTs) for the preparation of loose NF membranes.

2.2 EXPERIMENTAL

2.2.1 Materials and methods

Polysulfone (PSF, Udel P-3500), polyvinylpyrrolidone (PVP-K30), Tris(hydroxymethyl) aminomethane (Tris base), halloysite nanotubes (HNTs), Reactive black 5 and Reactive orange 16 were purchased from Sigma-Aldrich (India). Tannic acid (TA) was purchased from Loba chemicals. 1-Methyl-2-pyrrolidinone (NMP), NaCl and

Na_2SO_4 were obtained from Merck, India. Bovine serum albumin (BSA) was procured from Himedia.

The functional groups present in the HNTs and THNTs were analyzed using FT-IR (Bruker alpha spectrometer). Every single spectrum was recorded at a resolution of 2 cm^{-1} by 24 scans using KBr pellets in the range of 4000-500 cm^{-1}. The TGA measurements were performed in a nitrogen atmosphere with a flow of 100 mL min^{-1} by employing HITACHI EXSTAR 6300. In this experiment, 5 mg of the sample was heated at 10 ^oC min^{-1} from room temperature to 800 ^oC. In the TEM analysis, the nanoparticles were dispersed in ethanol by means of sonication for 1 h. Then, the dispersed particles were moved into a carbon-coated copper grid (200 meshes). After evaporation of the solvent, the samples were examined using JEOL JEM 123 under 200 kV acceleration voltage.

The elemental composition of nanoparticles before and after the modification was carried out using EDX analysis (X-act Oxford instruments). The zeta potential of both pristine and modified nanoparticles was analyzed by using the HORIBA SZ-100 nanoparticle analyzer. About 5 mg of the sample was dispersed in distilled water (pH ~ 6.4) and transferred into the cell. The pristine and THNTs embedded loose NF membrane surface charge was characterized by zeta potential, which was analyzed in the electrokinetic analyzer (Surpass Anton Paar) by streaming current method. The hollow fiber membranes were cut into the area of 2 cm x 1 cm and placed on the adjustable gap cell. Successively, 0.001 M KCl was used as the background electrolyte and pH was adjusted with 0.5 M HCl or 0.5 M NaOH.

The morphology of the as-prepared membranes was studied using SEM. The prerequisite amount of prepared hollow fiber membranes were dipped in methanol for 5 min. Further, the membranes were fractured in liquid nitrogen. The fractured membranes were sputtered with platinum to avoid charging. The cross-sectional images of the hollow fiber membranes were observed by using the TM3000 HITACHI tabletop microscope. The water contact angle of the hollow fiber membrane surface was measured by contact angle goniometer (15EC OCA, Dataphysics) at room temperature with 60 % of relative humidity. To make the contact angle more authentic, for every sample the contact angle was analyzed at five separate locations and the average was calculated.

2.2.2 Preparation of functionalized halloysite nanotubes (THNTs)

The halloysite nanotubes (HNTs) were functionalized via a step self-polymerization of tannic acid (TA) (Sileika *et al*. 2013). In short, 0.5 g of HNTs was dispersed in 50 mL of Tris base (0.61 g of the base and 1.76 g of NaCl) by means of sonication (40 kHz, 60 W Spectralab ultrasonic cleaning bath) for 30 min and the pH was adjusted to 7.8 with 0.1 M HCl. Subsequently, 0.05 g of tannic acid was added and stirred at room temperature for 24 h. The resultant reaction mass was centrifuged (3500 rpm for 30 min) to obtain THNTs and washed with water (3 x 20 mL). The schematic representation of the preparation of THNTs is presented in Scheme 2.3.

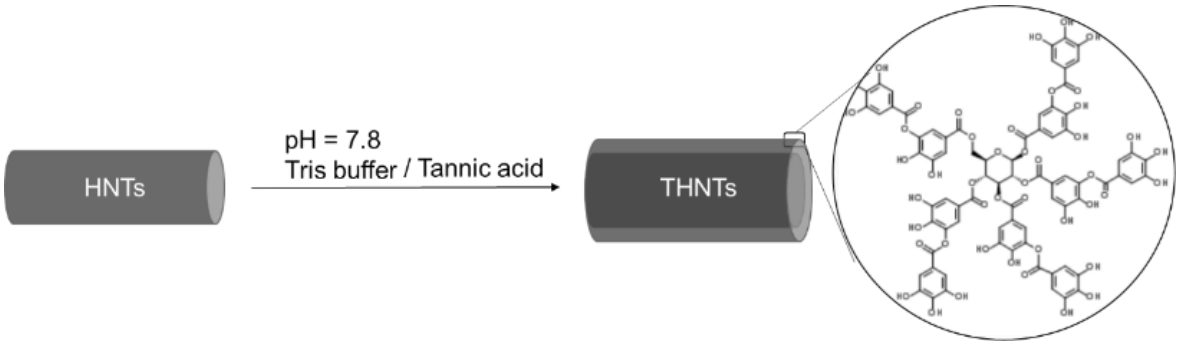

Scheme 2.3 The schematic representation of THNTs preparation

2.2.3 Preparation of functionalized halloysite nanotubes (THNTs) nanocomposite loose nanofiltration membranes

The PSF and PVP were dried in a vacuum oven at 50 ^{o}C for 12 h to remove the absorbed moisture. The detailed spinning parameters and dope solution composition are presented in Table 2.1 and 2.2 correspondingly. All the hollow fiber membranes were prepared via the dry/wet phase inversion method. For the preparation of HM-2, 0.36 g of THNTs was dispersed in 77.7 mL of NMP and sonicated (40 kHz, 60W Spectralab) for 30 min. Subsequently, 18 g of PSF and 2 g of PVP were added and heated to 50 ^{o}C for 12 h to get the homogeneous dope solution. All the dope solutions were degassed before spinning. The dry/wet spinning technique was used to spin the hollow fiber membranes by keeping the dope and bore extrusion rate constant. The as-prepared fibers were submerged in distilled water for 24 h with changing of water occasionally to eliminate the residual solvents. Then, the membranes were retained in 20 wt% glycerol aqueous solution for 24 h to get rid of pore collapse. The post-treated membranes were dried at room temperature for further usage.

Table 2.1 Hollow fiber membrane spinning parameters

Parameter	Spun fiber values
Dope extrusion rate (mL min^{-1})	4
Bore fluid	Distilled water
Bore flow rate (mL min^{-1})	2
Air gap (cm)	1
Spinneret dimensions (mm)	1.1/0.55 (OD/ID)
Humidity (%)	60

Table 2.2 Dope solution composition

Membrane code	PSF (g)	PVP (g)	NMP (mL)	THNTs (g)
HM-0	18	2	77.7	0
HM-1	18	2	77.7	0.18
HM-2	18	2	77.7	0.36
HM-3	18	2	77.7	0.54

2.2.4 Water uptake and porosity

The water uptake study was done as per the literature procedure (Pereira *et al*. 2016). In brief, the as-prepared membranes were cut into 2 cm of length and immersed in distilled water for 24 h. The membranes were taken out and swabbed with blotting paper. The wet weight of the membranes was logged and dried at 50 ^{o}C till constant weight. The dry weight of the membranes was recorded. The percentage of water uptake was calculated by equation (2.1). The percentage of porosity (ε) was assessed by the gravimetric method (Kumar *et al*. 2013) which is denoted by the equation (2.2).

$$\% \text{ Water intake} = \left(\frac{W_w - W_d}{W_w}\right) \times 100 \quad (2.1)$$

$$\varepsilon\,(\%) = \frac{W_w - W_d}{A \times l \times p} \times 100 \quad (2.2)$$

Where 'W_w' and 'W_d' are the wet and dry weight of the membrane samples. $'l'$ is the thickness of the membrane, 'A' is the area of the membrane (m^2) and 'p' is the density of pure water (0.998 g cm^{-3}).

2.2.5 Membrane filtration study

To determine the pure water permeability (PWP), salt and dye separation results, 5 number of fibers with a length of 10 cm (total area 8.635 cm^2) were potted in a stainless-steel adaptor using epoxy resin. The potted adaptors were dried at room temperature for 24 h. The experiments were run using a lab-made cross-flow filtration setup. Initially, the membranes were compacted for 30 min at 3 bar pressure. Subsequently, the PWP was studied at 2 bar pressure for 60 min and calculated by equation (2.3). The salt (1000 ppm) and dye (10 ppm) separations were completed at 1 bar pressure as defined in equation (2.4). The salt concentration was measured using a conductivity meter (Systronics 306 conductivity meter). The solute concentration of dye and BSA rejection were analyzed with a UV-Vis spectrophotometer (HORIBA UV-1800). All the experiments were carried out at room temperature.

$$J_w = \frac{Q}{A \times \Delta P \times \Delta t} \quad (2.3)$$

$$\%\ R = \left(1 - \frac{C_p}{C_f}\right) \times 100 \quad (2.4)$$

Where 'J_w' is the permeate permeability and expressed in L /m^2 h bar, 'Q' is the amount of water collected (L) through a 'Δt' (h) time, 'A' is the effective area of the hollow fiber membrane (m^2), 'C_p' and 'C_f' are permeate and feed solute concentrations correspondingly.

2.2.6 Molecular weight cut-off (MWCO) study

The MWCO study was carried out using polyethylene glycol (PEG) of different molecular weight ranging from 2000 to 10000 Da. The separation performance depends mostly on the MWCO and mean pore size of the membrane via a sieving mechanism. The filtration study was performed using 500 ppm of PEG at 2 bar pressure as reported elsewhere (Qin *et al*. 2016). The rejection of PEG was calculated according to the equation

(2.4). In general, the ultrafiltration membrane would have the MWCO of 1000-100000 Da (Ng *et al*. 2013). The MWCO of the membrane can be defined as the molecular weight of solute which has above 90 % rejection. The concentration of PEG in the feed and permeate was analyzed in terms of total organic carbon (TOC) with TOC-L SHIMADZU TOC analyzer.

2.2.7 Membrane antifouling performance study

To analyze the antifouling performance of the as-made hollow fiber membranes, BSA (0.8 g L^{-1}) was used as a model foulant. Initially, the PWP was performed for 40 min and depicted as $J_{w.}$ Later the BSA filtration was performed for another 40 min and represented as J_p. Subsequently, the membranes were washed with deionized water thoroughly. The cleaned membrane water permeability was measured as J_{w1} for another 40 min. To estimate the antifouling property of each membrane, the flux recovery ratio (FRR) was calculated as shown in equation (2.5).

$$\text{FRR (\%)} = \left(\frac{J_{w1}}{J_w}\right) \times 100 \tag{2.5}$$

2.3 RESULTS AND DISCUSSION

2.3.1 Characterization of functionalized halloysite nanotubes (THNTs)

The morphology of HNTs and modified THNTs were investigated by TEM. Figure 2.3 denotes the TEM images of pristine HNTs and THNTs. Figure 2.3a shows that HNTs have a tubular structure with both ends are open with a thickness of 10-15 nm. The diameter of HNTs ranges from 50-100 nm and lengths of 100-2000 nm. TEM image was used to calculate the inner and outer diameter of the nanotube before and after modification, in order to interpret the morphology changes of the pristine HNTs and THNTs. The results showed that the outer diameter was enlarged to nearly 10 nm and inner diameter was reduced to approximately 5 nm. It designates the formation of the TA layer on the inner and outer surface of the HNTs. Cho *et al*. reported the modification of HNTs using polydopamine (pDA) and similar reports were observed (Chao *et al*. 2013).

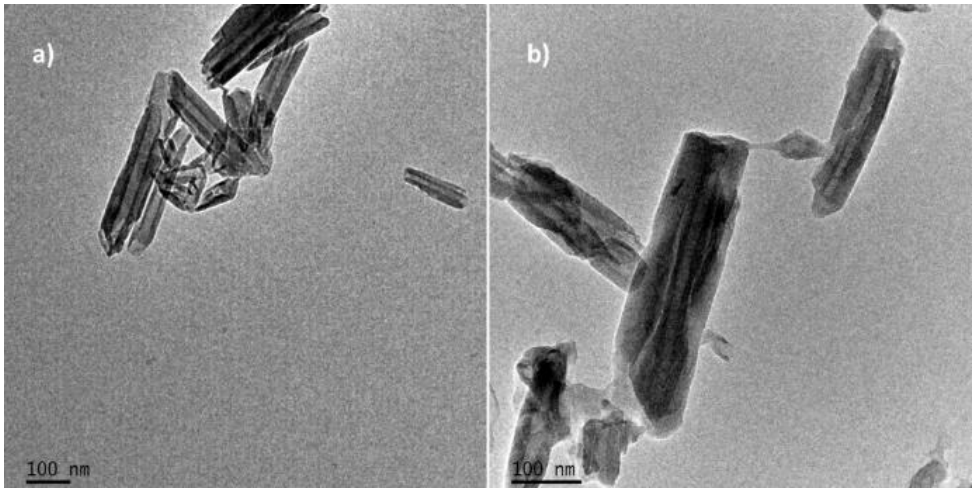

Figure 2.3 TEM micrographs of a) HNTs and b) THNTs

The organic modification of HNTs using TA was confirmed by FT-IR and Figure 2.4, which represents the FT-IR spectra of HNTs and THNTs. The peak at 3694 cm^{-1}, 3622 cm^{-1} are designated to Al_2-OH stretching vibrations and the peak at 1625 cm^{-1} is ascribed to the bending vibration of an adsorbed water molecule. The peak at 1038 cm^{-1} represents the in-plane Si-O stretching vibration. The peak at 913 cm^{-1} is attributed to the bending vibration of Al-OH. The new bands at 1711 cm^{-1} and 3451 cm^{-1} are ascribed to the carbonyl stretching frequency of the ester group and –OH groups present in TA. The presence of these new peaks confirmed the modification of HNTs by TA.

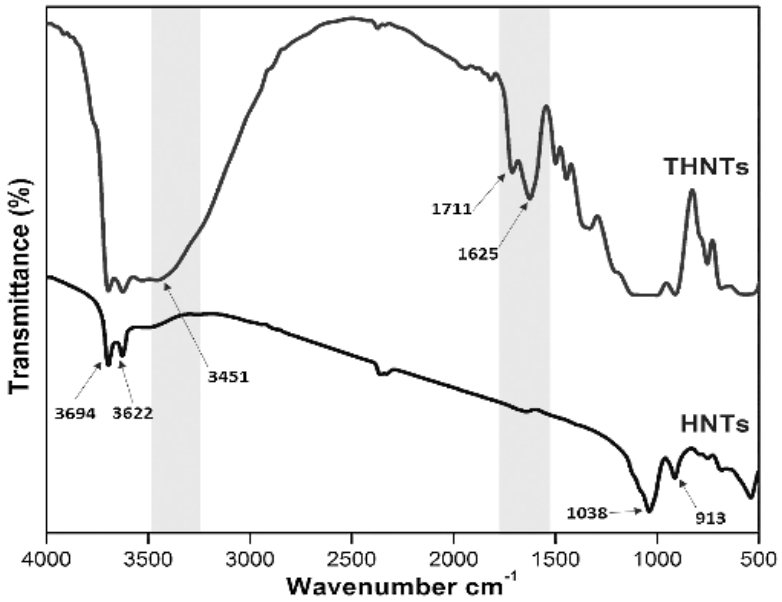

Figure 2.4 FT-IR spectra of HNTs and THNTs

The thermal stability of HNTs and THNTs was determined using TGA. The experimental results further confirmed the modification. Figure 2.5 represents the TGA curves of HNTs and THNTs. In HNTs, the weight loss between 50 and 150 ^{o}C was ascribed to the loss of adsorbed water (as HNTs are hydrophilic in nature). Another weight loss in the range of 450-550 ^{o}C was attributed to the dehydroxylation of the Al-OH group (Zhang *et al*. 2012). For THNTs, weight loss below 110 ^{o}C due to adsorbed water (presence of adsorbed water is consistent with FT-IR spectra) and the new weight loss between 240 and 365 ^{o}C was attributable to the loss of coated tannic acid. In summary, the TGA results confirmed the successful modification of HNTs with TA.

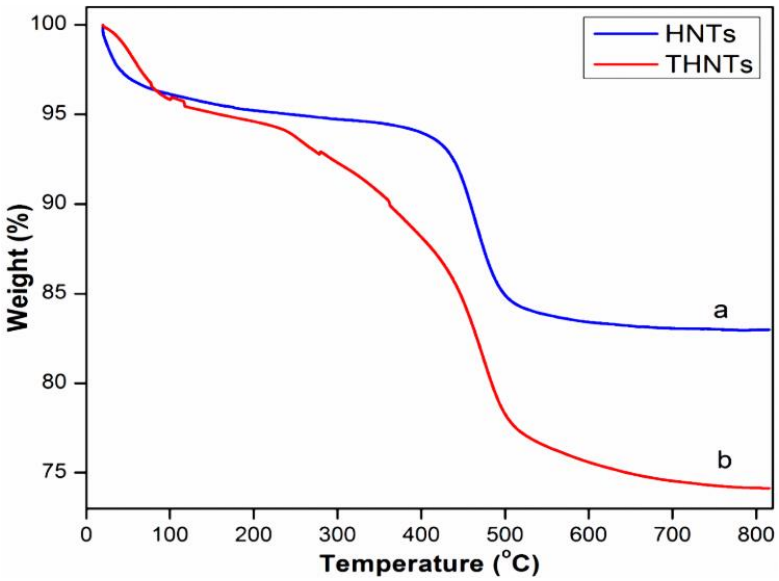

Figure 2.5 TGA curves of a) HNTs and b) THNTs

The zeta potential analysis is one of the useful techniques to determine the surface charge of the nanomaterial. In addition, the increased zeta potential would improve the colloidal stability (Günister *et al*. 2006, Qin *et al*. 2016). The presence of the Si-OH group on the outer side of the HNTs provide the negative charge and it was calculated as -26 mV (pH~ 6.4) (Levis *et al*. 2002, Joo *et al*. 2013). The zeta potential was further enhanced to -91 mV (pH~6.4) after modification of the HNTs, which was due to the presence of plenty of –OH groups present in TA. Figure 2.6 represents the zeta potential value of HNTs and THNTs. Therefore, the analysis result ascertains the presence of TA on the surface of the HNTs.

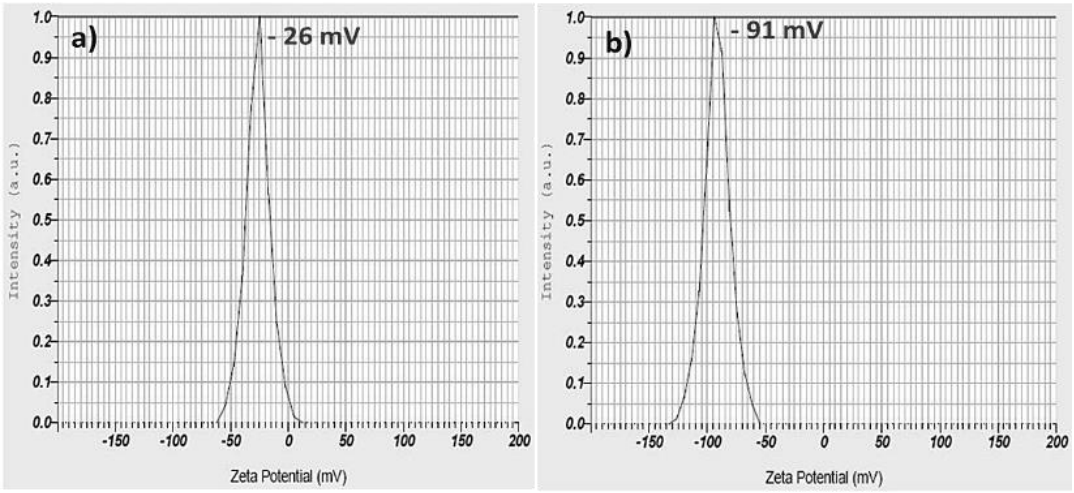

Figure 2.6 Zeta potential curves of a) HNTs and b) THNTs

2.3.2 Morphology of the hollow fiber membranes

In general, the permeation and rejection properties of the membranes can also be determined from the cross-sectional images of the membranes significantly (Hebbar *et al*. 2014). The cross-sectional SEM images of the as-prepared pristine and nanocomposite loose NF membrane with different amounts of THNTs are presented in Figure 2.7. As shown, all the membranes have produced an asymmetric structure with finger-like voids in both inner and outer surfaces and the sponge-like structure in the middle upon phase inversion. Despite the fact that, increasing the concentration of hydrophilic additive THNTs, the number of macro-voids increases in the inner and outer layers. This fact is well-suited while comparing cross-sectional images of the pristine HM-0 and nanocomposite membranes (HM-1, HM-2 and HM-3). In the HM-2 and HM-3, the vertical voids are more noticeable than the horizontal voids. The vertically connected voids let the water to permeate more with less internal resistance, high permeability compared to other membranes. This accounting for the membrane HM-2 to exhibit enhanced permeability. However, HM-3 exhibited reduced permeability owing to the agglomeration of nanoparticles. Further, HF membrane inner diameter (ID) and outer diameter (OD) was measured using SEM and presented in Table 2.3.

In addition, the presence of THNTs on the membrane was confirmed using EDX analysis. The presence of Silica (Si), Alumina (Al) and Oxygen (O) in the EDX spectrum (Figure 2.8b) confirmed the successful incorporation of THNTs into the membrane.

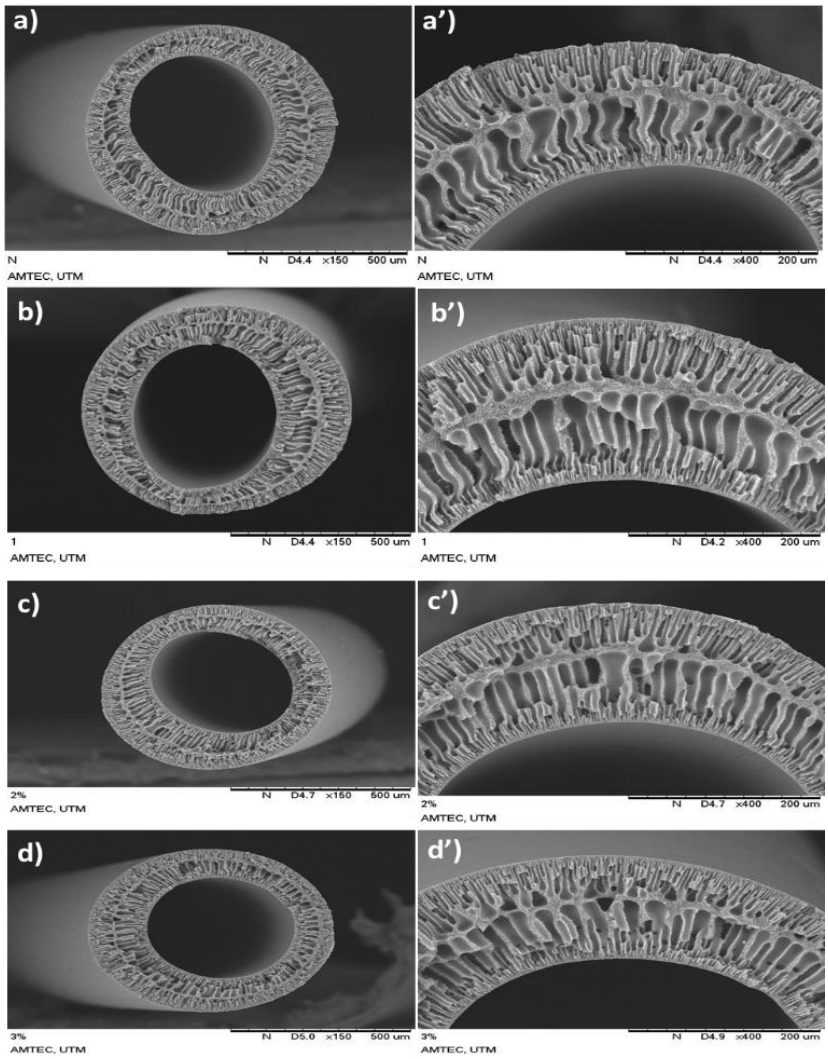

Figure 2.7 SEM cross-sectional images of HM-0 (a and a'), HM-1 (b and b'), HM-2 (c and c') and HM-3 (d and d')

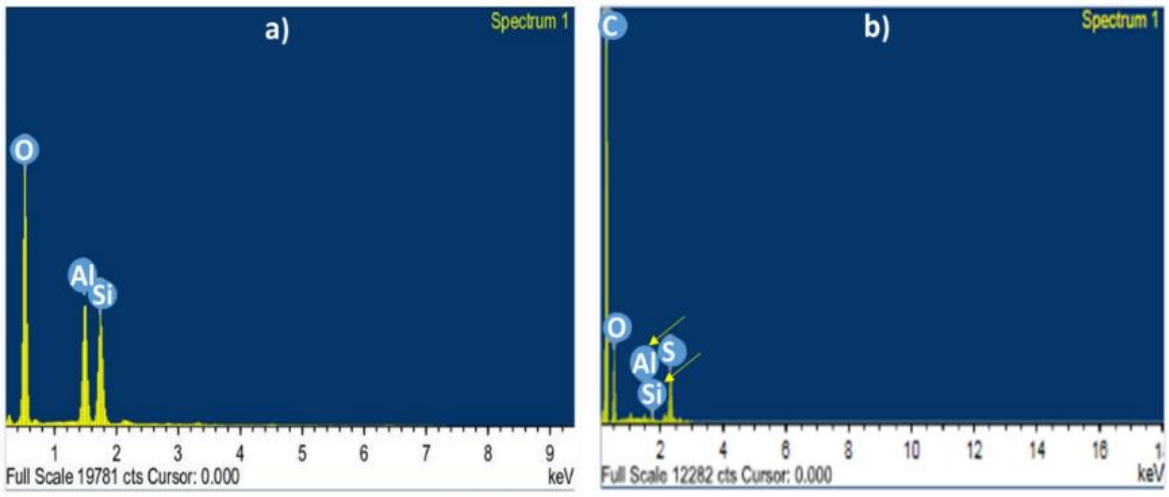

Figure 2.8 EDX analysis of a) HNTs and b) HM-2 membrane

2.3.3 Membrane hydrophilicity

The surface hydrophilicity of the as-made membranes was measured by static water contact angle analysis. The contact angle values of the membranes are represented in Figure 2.9A. The formation of a rigid and dense hydration layer depends on the hydrophilicity of the membrane surface, which inhibits the absorption of the hydrophobic foulants and enhances the permeation ability. As a general rule, lower the contact angle, the more will be surface hydrophilicity and energy which ease the water to wet the surface of the membrane (Liu *et al*. 2012). Comparative to the pristine membrane, the membrane HM-1 has exhibited the contact angle of 70^{o} which is 9^{o} less than the HM-0. Further increasing the concentration of THNTs, the contact angle was reduced to 66^{o} for HM-2 when THNTs content was 2 wt% and still reduced to 63^{o} for HM-3. The change in the hydrophilicity of the membrane surface was attributed to the addition of THNTs. During phase inversion, the nanomaterials migrated towards the surface of the membrane, which reduced the water contact angle. The surface hydrophilicity of the PEI membrane blended with MHNTs was reported by Hebbar *et al*. (Hebbar *et al*. 2016) and the results are comparable to the present experimental results.

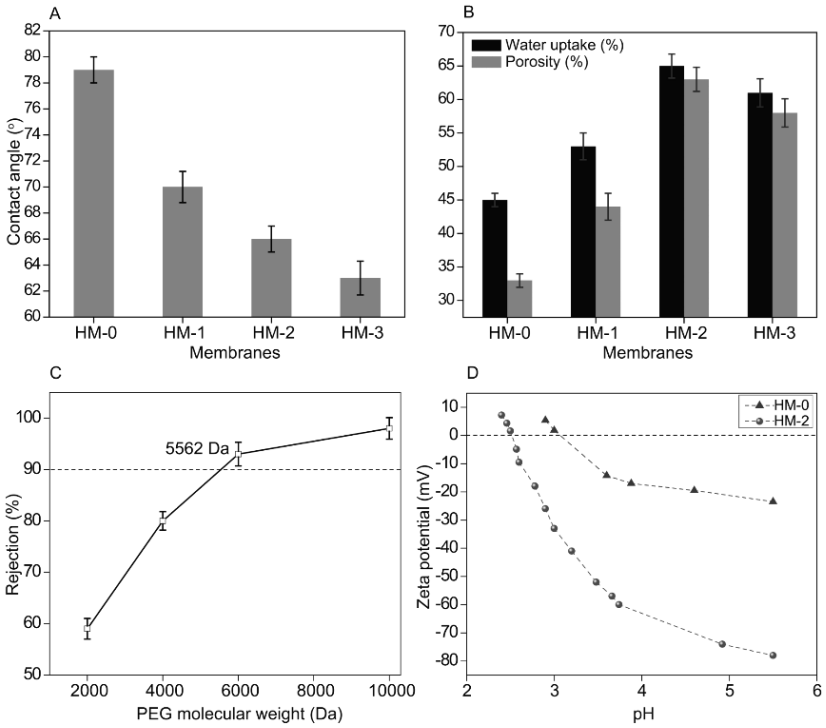

Figure 2.9 A**)** Water contact angle, B) Porosity and water uptake of hollow fiber membranes, C) molecular weight cut-off (MWCO) study of the HM-2 membrane and D) Zeta potential of HM-0 and HM-2 membranes as a function of pH

2.3.4 Porosity and water uptake of the membranes

The porosity and water uptake of the as-made membranes are signified in Figure 2.9B. The porosity of the prepared nanocomposite membranes exhibited increased porosity than the pristine membrane. The membrane HM-2 displayed porosity of 63 % compared to the HM-0 membrane of 33 %. The membrane porosity increases while increasing the amount of THNTs and then decreases. Specifically, for the HM-3 membrane, the porosity was reduced to 58 % compared to HM-2. The reduced porosity can be attributed to the partial agglomeration of the nanomaterial on the surface of the membrane. Additionally, the increased concentration of THNTs would have increased the viscosity of the dope solution. As a result, the non-solvent inflow rate would have reduced with an increase of the solvent outflow rate. Which possibly will cause the reduced porosity (Pereira *et al*. 2016, Salimi *et al*. 2016).

The water uptake capacity of the membranes depends on the porosity of the asymmetric membrane (Mi *et al*. 2003). As shown in Figure 2.9B, the percentage of water uptake capacity was increased while increasing the porosity of the membrane. On the other hand, the membrane HM-3 exhibited reduced water uptake of 61 % as the porosity decreases owing to the agglomeration of the THNTs.

2.3.5 Pure water permeability and molecular weight cut-off (MWCO) study of the membranes

The pure water permeability (PWP) primarily depends on the hydrophilicity and porosity of the membrane. Table 2.3 illustrates the PWP of the nanocomposite membranes. Proportional to the pristine membrane (HM-0), the PWP of the nanocomposite membrane increased with the addition of THNTs, which was reliable with the results of contact angle and porosity. Unambiguously, the pristine membrane exhibited PWP of 9 L/m^2 h bar,

Table 2.3 Properties of fabricated hollow fiber membranes

Membrane code	PWP (L/m^2 h bar)	FRR (%)	BSA rejection (%)
HM-0	09 $\pm$0.481	27	98.1
HM-1	35 $\pm$0.453	63	97.0
HM-2	46 $\pm$0.429	74	97.2
HM-3	41 $\pm$0.431	68	97.7

nevertheless, the membrane HM-2 exhibited the increased PWP of 46 L/m^2 h bar respectively. However, the PWP of HM-3 was reduced to 41 L/m^2 h bar because of the reduced porosity. In summary, the PWP had been increased noticeably by adding THNTs into the polymer matrix and this undeniably corresponding to the increased hydrophilicity and porosity of the membrane.

The pore size of the membrane can be easily understood from the MWCO analysis. As presented in Figure 2.9C, the rejection of PEG increases as the molecular weight of the PEG increases. The MWCO of the HM-2 membrane is about 5562 Da, which suggests that the as-prepared membrane is loose nanofiltration membrane (Liu *et al*. 2017).

2.3.6 The surface charge of the membranes

The surface charge measurement is one of the prime factors to determine the loose NF membrane capability to separate the charged solutes. Herein the surface charge was measured in terms of the zeta potential of loose NF membrane and it is presented in Figure 2.9D. The pristine membrane (HM-0) is negatively charged. Moreover, the membrane HM-2 surface charge was increased after incorporating the THNTs compared to the pristine membrane. A conceivable justification is that THNTs is negatively charged, which enhances the negative charge of the nanocomposite membrane. As a whole, the zeta potential measurements substantiate that the as-prepared loose NF membranes are negatively charged.

2.3.7 Dye and salt separation

The performance of the loose NF membrane was evaluated using anionic dyes such as Reactive black 5 (RB 5) and Reactive orange 16 (RO 16). Table 2.4 presents some of the literature towards the capability of HNTs and modified HNTs for the dye removal application. Figure 2.10A denotes the effect of the rejection of dyes and salts along with solute permeability. Moreover, based on PWP, porosity and water uptake, the membrane HM-2 was chosen as a best-performed membrane and HM-2 was utilized for separation of dyes and salts. The HM-2 had been exhibited the rejection of > 99 % of RB 5 and > 90 % of RO 16 owing to the presence of THNTs. It was obvious that the as-made loose NF membrane exhibited characteristically high rejection of dye molecules, analogous to the NF membrane. The higher rejection of RB 5 contrast to RO 16 could be attributed to the higher molecular weight of RB 5. It has been reported in literate that, the development of

thin filter cake layer on the surface of the membrane by the electrostatic interaction of negatively charged dyes with the positively charged membrane surface (Zhu *et al*. 2015), which may affect the water permeability of the membrane in the course of the prolonged usage. In the present study, the formation of such a layer was avoided to some extent by making the membrane surface negatively charged. Furthermore, the HM-2 exhibited the permeation permeability of 43.5 L/ m^2 h for RB 5 and 44 L/ m^2 h for RO 16 at 1 bar. In summary, the rejection of negatively charged dye molecules based on the electrostatic repulsion, which is the possible justification. As presented in Figure 2.10A, the rejection of salts followed the order Na_2SO_4 > NaCl. Especially the HM-2 membrane exhibited the rejection of 7.5 % of Na_2SO_4 and 2.5 % of NaCl respectively. Here, the electrostatic effect and sieving effect played a vital role in the rejection. The rejection ratio varies as the size of NaCl is smaller than Na_2SO_4 (Schaep *et al*. 1998). Moreover, the rejection of Na_2SO_4 could be due to both electrostatic effect and sieving effect, whereas in the case of NaCl sieving effect conquers the dominant role (Han *et al*. 2013). Thus, the as-prepared loose NF membrane could enhance the separation efficacy and has potential application in the wastewater treatment. The digital images of the RB 5 and RO 16 feed and permeate are depicted in Figure 2.10B.

To examine the membrane stability, a short-term of the filtration test was executed. The dye solution permeability for the period of 12 h is presented in Figure 2.10C. There was a slight drop in the dye solution permeability. This trend could be ascribed to the formation of the dye cake layer over time. Similar results were reported by Jiuyang *et al*. (Lin *et al*. 2015).

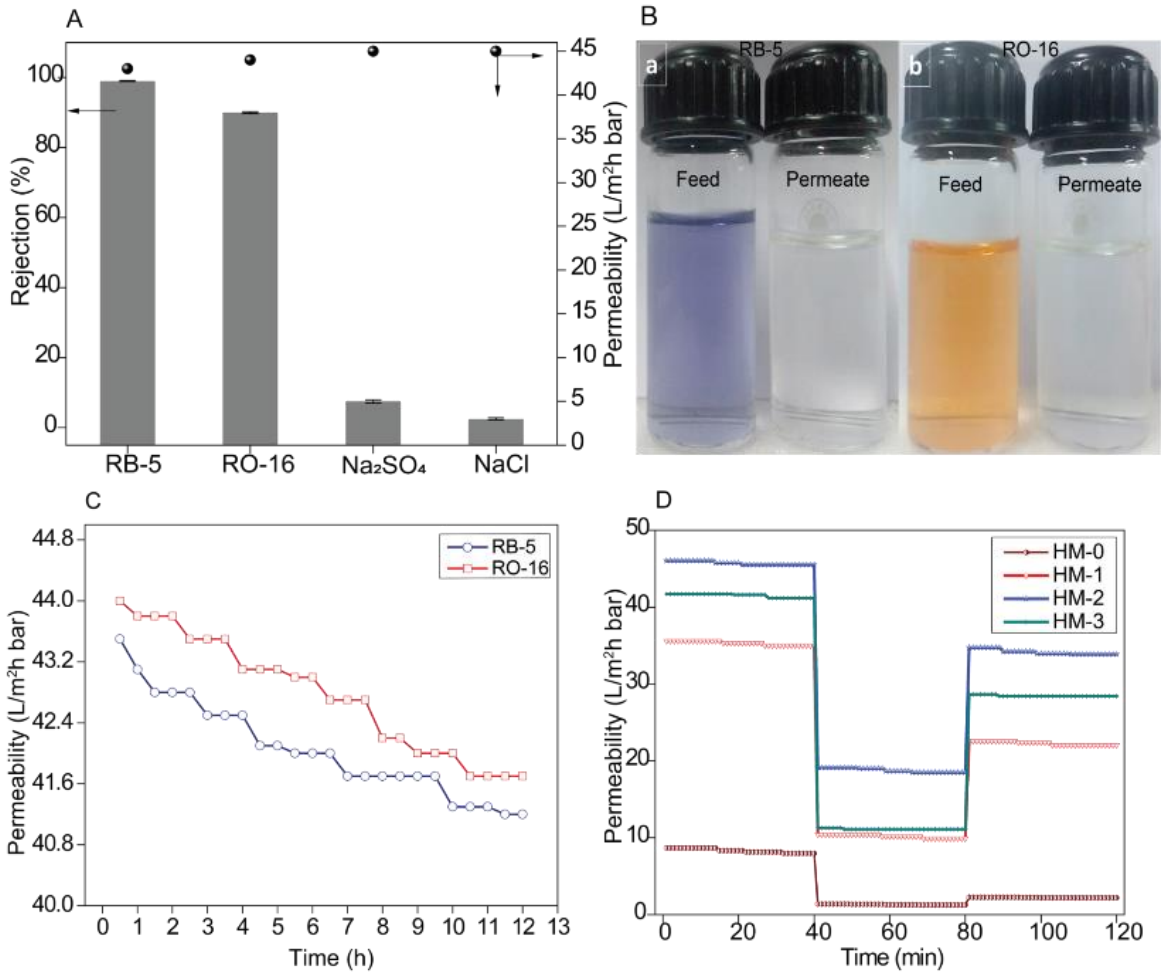

Figure 2.10 A), B), C) HM-2 membrane solution permeability and rejection of dyes and salts, RB-5 and RB-16 feed and permeate digital images and D) anti-fouling studies of all the membranes.

Table 2.4 The dye removal ability of halloysite nanotubes (HNTs) incorporated membrane

Dyes	Nanoparticle	Feed (ppm)	Removal (%)	Mechanism	Ref.
Methyl violet	HNTs	100	>99	Adsorption	(Liu *et al*. 2011)
Methyl violet	HNTs-Fe_3O_4	150	>99	Adsorption	(Duan *et al*. 2012)
Rhodamine 6G / Chrome azurol S	HNTs	1000	> 99/ >99	Adsorption	(Zhao *et al*. 2013)
Reactive black 5/ Reactive red 49	HNTs-poly(NASS)	500	90/91	Donnan effect	(Zhu *et al*. 2014)
Reactive black 5/ Reactive red 49	HNTs-SO_3H	1000	95/90	Donnan effect	(Wang *et al*. 2015)
Reactive black 5/ Reactive Red 102	m-aminophenol modified HNTs	10	94/97	Adsorption	(Hebbar *et al*. 2017)
Reactive black 5/ Reactive orange 16	**THNTs**	**10**	**99/90**	**Donnan effect**	**Present study**

2.3.8 Antifouling study of membranes

The antifouling property of the membrane determines the prolonged usage and filtration performance. Especially in the case of wastewater treatment, the membrane used to foul in

a while attributed to the adsorption and aggregation of foulants on the membrane surface. Therefore, the low fouling tendency is one of the prerequisites for the nanocomposite membranes. In the meantime, BSA molecules are larger in size, they could not be penetrated through the pores and causes fouling on the membrane surface. In the present study, the antifouling performance of both pristine and nanocomposite membrane was analyzed by measuring the flux recovery ratio (FRR) after the membrane was stained via BSA solution.

Figure 2.10D represents the water permeability of before and after BSA solution filtration. As it is evident from the experimental results, the water permeability had been decreased during the BSA filtration, which was due to the fouling and concentration polarization (Matthiasson *et al*. 1980, Hoek *et al*. 2003). However, HM-3 membrane BSA solution permeability was similar to HM-1, because, in the case of HM-3 membrane at a higher concentration of nanoparticles there was a considerable amount of nanoparticle agglomeration on the membrane surface. Consequently, there was a considerable decline in the permeability. Still, in the case of the HM-2 membrane, the agglomeration was less and the surface charge was also high. As a result, it could avoid the adsorption of BSA molecules on the surface. Hence, there was an increase in the BSA solution permeability when compared to other membranes. After washing with deionized water, the membrane HM-2 exhibited the FRR of as high as 74 % compared to the pristine membrane (HM-0) of 27 % and the values are tabulated in Table 2.3.

The enhanced FRR of the nanocomposite membrane could be attributed to the addition of THNTs, which has improved the surface hydrophilicity. It is understood that the more hydrophilic membrane surface could form the hydration layer through electrostatic attraction and hydrogen bonding. The as-formed hydration layer avoids the adsorption of foulants by acting as a barrier flanked by the membrane surface and foulants (Holmlin *et al*. 2001, Chen *et al*. 2010, McCloskey *et al*. 2012, Zinadini *et al*. 2014). Moreover, BSA is negatively charged protein, bring about to the electrostatic repulsion between the membrane surface and BSA molecules led to reduced adsorption of BSA. Further, all the prepared membranes exhibited above 97 % of BSA molecules rejection as tabulated in Table 2.3. In summary, the membrane antifouling property had been improved to a greater extent by incorporating hydrophilic THNTs.

2.4 CONCLUSIONS

Halloysite nanotubes were successfully modified with tannic acid in a facile one-step self-polymerization method. The tannic acid modified HNTs incorporated loose nanofiltration membranes were prepared by phase inversion method. The functionalized halloysite nanotubes were characterized and confirmed the successful modification. The effect of The functionalized halloysite nanotubes (THNTs) on the membrane hydrophilicity, morphology, water uptake, porosity, pure water permeability and antifouling performance were well studied. The as-prepared loose NF membranes exhibited enhanced efficacy towards dye removal with the high permeation of salts. Precisely, the nanocomposite membrane HM-2 loaded with 2 wt % functionalized halloysite nanotubes (THNTs) exhibited as high as pure water permeability of 46 L/m^2 h bar. In addition, the nanocomposite membrane exhibited the rejection of > 99 % of Reactive black 5 and > 97.5 % of Reactive orange 16 with the dye solution permeability of 43.5 L/m^2 h and 44 L/ m^2 h bar respectively. In conclusion, the as-prepared membrane has the potential to act as a good candidate for the separation of dyes in textile wastewater. It is anticipated that this surface functionalization strategy can be applied to other nanoparticles, bestowing them with distinctive properties.

CHAPTER 3

NOVEL, ONE-STEP SYNTHESIS OF ZWITTERIONIC POLYMER NANOPARTICLES VIA DISTILLATION-PRECIPITATION POLYMERIZATION AND ITS APPLICATION FOR DYE REMOVAL MEMBRANE

Abstract: *In this chapter, zwitterionic polymer nanoparticles were synthesized in one-step reaction via distillation-precipitation polymerization (DPP), and were characterized. [2-(methacryloyloxy)ethyl]dimethyl-(3-sulfopropyl)ammonium hydroxide (SBMA) as monomer, and N, N'-methylene bis(acrylamide) (MBAAm) as cross-linker are used for the synthesis of nanoparticles. The newly synthesized nanoparticles were further employed for the surface modification of polysulfone (PSF) hollow fiber membranes for dye removal. The modified hollow fiber membrane exhibited the improved permeability (56 L/m^{2}h bar) and dye removal (>98 % of Reactive black 5 and >80.7 % of Reactive orange 16) with the high permeation of salts. Therefore, the as-prepared membrane can have potential applications in textile and industrial wastewater treatment.*

3.1 INTRODUCTION

In recent years, the discharge of colored micropollutants into the water stream has elevated widespread concerns as dyes are toxic, non-biodegradable and carcinogenic (Shannon *et al*. 2008, Wang *et al*. 2013, Chethana *et al*. 2016). Anionic dyes are recognized as contaminants in wastewater, which are broadly employed in industries like paper, textiles and plastics (Liu *et al*. 2012). The dyes can be categorized into three types, viz. azo, anthraquinone and triphenylmethane. Reactive black 5 and Reactive orange 16 are falling below the category of azo dyes. These acid dyes are used for coloring the cellulose-based fabrics, such as cotton. Since reactive dyes are accompanying moderate rates of fixation, dyeing with reactive dyes always associated with serious environmental problems (Jiraratananon *et al*. 2000).

The complex structure of the acid dyes makes it insensitive to biodegradation and chemical oxidation. Consequently, it produces secondary pollutants during oxidation (Baughman *et al*. 1994, Weber *et al*. 1995). With the intention of solving this environmental pollution, it is critical to eliminate dyes from the effluent before discharging. A number of methods such as flocculation, adsorption, photodegradation and chemical oxidation are available for the treatment of wastewater (Ciardelli *et al*. 2001, Pala *et al*. 2002, Lee *et al*. 2006, Al-Degs *et al*. 2008, Wang *et al*. 2015). However, these methods are not cost-effective, less energy-efficient, produces solid wastes and so on (Yu *et al*. 2010). Therefore, a new method for treating this wastewater is very much required. Membrane separation techniques have been proved to be the potential alternative (Chen *et al*. 1997, Cassano *et*

al. 2001, Joshi *et al*. 2001, Marcucci *et al*. 2002, Fersi *et al*. 2005,) to remove dye from the wastewater. In addition, it has many advantages like energy-efficient, low-cost, non-toxic, easy to scale up, comprising no chemical reaction, high efficiency and produces less solid waste (Baker 2000). In general, rejection of these low molecular weight dye molecules is carried out using nanofiltration (NF) and reverse osmosis (RO) membranes (Tang *et al*. 2002, Bes-Piá *et al*. 2005, Suksaroj *et al*. 2005, Shen *et al*. 2016). Nevertheless, these separation processes are suffering from some downsides such as low permeability and high cost (Van der Bruggen *et al*. 2001, Van der Bruggen *et al*. 2005, Al-Amoudi *et al*. 2007, Mondal *et al*. 2012). Ultrafiltration (UF) is one of the emerging pretreatment technology for the RO and NF (Rosberg 1997). Specifically, hollow fiber UF membranes are dominating over the flat sheet due to their increased surface area per unit of module volume (Ong *et al*. 2014, Hebbar *et al*. 2017). In addition, UF membranes are talented to remove suspended solids, bacteria and high molecular weight solute from water (Mulder 2012).

Polysulfone (PSF) is one of the versatile polymeric material for the preparation of hollow fiber (HF) membranes. It has very high thermal, mechanical and chemical resistance along with outstanding film-forming ability (Ho *et al*. 1992, Ulbricht *et al*. 1996). The other polymeric materials such polyetherimide (PEI) undergoes hydrolysis under basic condition (Jang *et al*. 1994), chitosan (CS) which is insoluble in organic solvents (Nishimura *et al*. 1991) and polyphenylsulfone (PPSU) is brittle in nature (Brostow *et al*. 2008). Therefore, PSF is superior to other polymeric materials. Nonetheless, the PSF membrane is vulnerable to severe fouling of very short duration. The fouling is caused by the less hydrophilic nature of the PSF material. Consequently, the foulant forms a cake-like layer, which reduces the permeation rate of the water as well as increase the hydrophobicity and operational cost (Quintanilla 2010, Sun *et al*. 2013).

The effect of adding PEI modified silver nanoparticles into PSF UF membranes was reported by Mauter and co-workers. The results indicated that surface-modified PSF membranes exhibited increased antifouling and antimicrobial activity (Scheme 3.1) (Mauter *et al*. 2011). Fan *et al*. explored the antifouling and hydrophilicity of the PANI/PSF nanocomposite membranes. The nanocomposite membrane demonstrated enhanced hydrophilicity and antifouling nature, as a result, the nanocomposite membrane exhibited high permeability without losing its rejection performance (Fan *et al*. 2008). Joseph *et al*. reviewed that the incorporation of zwitterionic thin or thick film on the surface reduced the

protein adsorption (Schlenoff 2014). Tao *et al*. improved the blood compatibility of the PSF membrane by the chemical modification of PSF with a zwitterionic polymer brush. The results also indicated that the introduction of the zwitterionic functional group increased surface hydrophilicity (Xiang *et al*. 2014). Haijun *et al*. investigated the effect of grafting of the zwitterionic molecule on the PSF UF membrane. The results showed that surface hydrophilicity and antifouling nature enhances while increasing the grafting time (Yu *et al*. 2009). In current years, it has been reported that the incorporation of zwitterionic nanoparticles exhibited improved hydrophilicity, permeability and antifouling performances (Xuan *et al*. 2009, Jiang *et al*. 2010, Shao *et al*. 2015, Zhu *et al*. 2016).

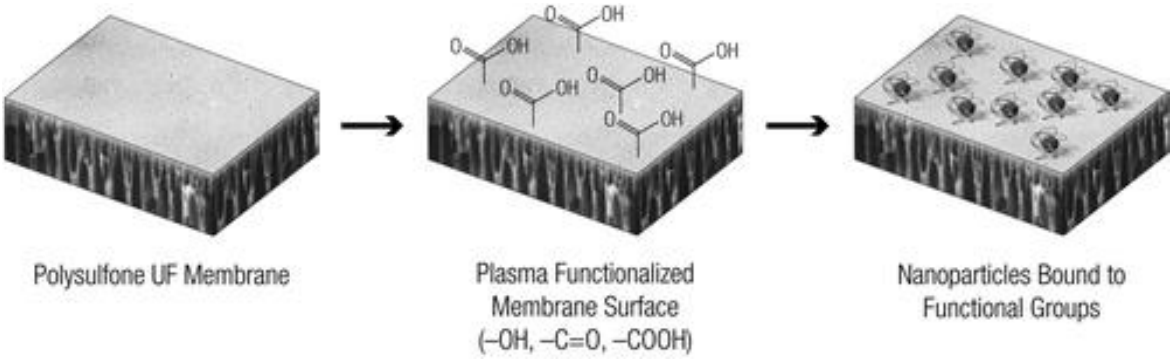

Scheme 3.1 Preparation of biocidal nanomaterials incorporated polysulfone membrane (Mauter *et al*. 2011)

The zwitterionic material has ample ionic groups that provide strong electrostatic interaction with water molecules, therefore it provides stronger and denser hydration layer over the membrane surface (Zhao *et al*. 2016). In addition, the polymer matrix is well miscible with hydrophobic chains of the zwitterionic polymers. Ye *et al*. employed a zwitterionic polymer brush on the TFC membrane to bestow anti-biofouling activity (Scheme 3.2) (Ye *et al*. 2015). Liu *et al*. investigated the effect of adding zwitterionic-CNT for the preparation of the ion-selective membrane. The added nanomaterial enhanced the mono/multivalent ion selectivity when compared to the pristine CNT nanocomposite membrane (Liu *et al*. 2015).

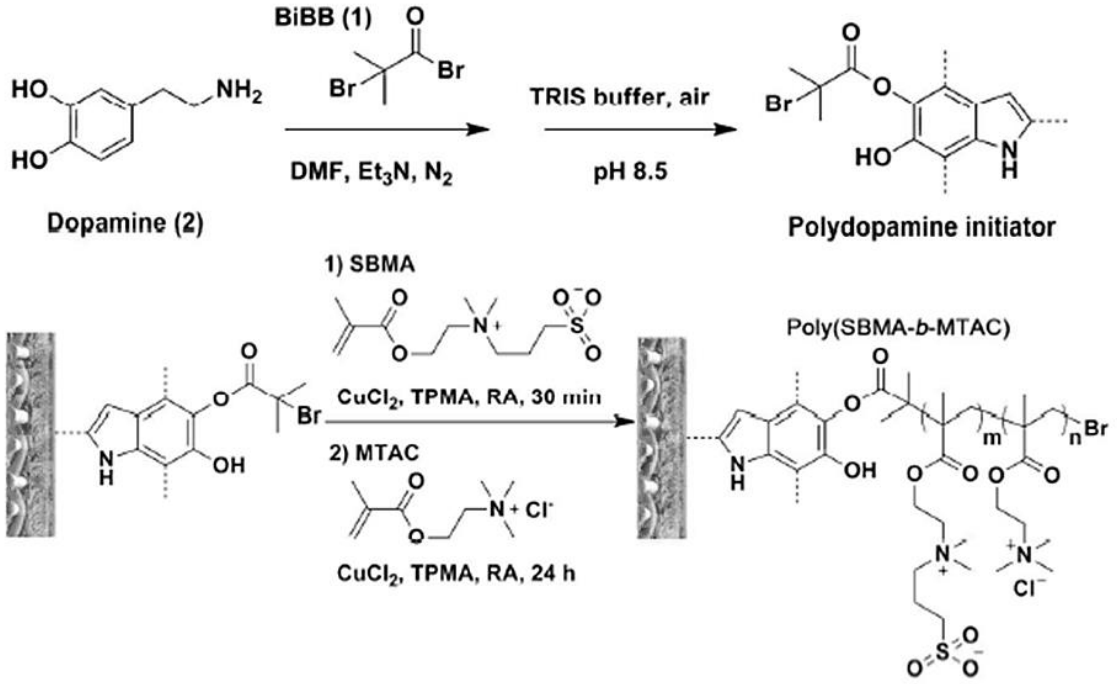

Scheme 3.2 Zwitterionic functionalization of thin film composite membrane (Ye *et al*. 2015)

Among the polymerization processes, distillation-precipitation polymerization (DPP) is the facile process and recently developed by Bai *et al*. (Bai *et al*. 2004). It is a unique method to prepare nanoparticles with uniform size and shape without adding any surfactant or stabilizer (Romack *et al*. 1995, Sosnowski *et al*. 1996). Additionally, this process can be scaled up since the refluxing solvent can bestow an effective mixing and oxygen-free environment (Yang *et al*. 2009). In comparison with the classical polymerization processes such as atom-transfer radical-polymerization (ATRP), group transfer polymerization (GTP), catalytic chain transfer polymerization and radical polymerization, DPP holds superior advantages like lesser reaction time (typically 2-3 h), cheap starting materials, no metal catalyst and ligand are required, no sophisticated apparatus required, reaction at atmospheric condition, atom economy and easy isolation method. The mechanism of DPP follows the order of radical initiation of monomer or cross-linker and subsequent chain propagation by chain addition, which results in precipitation of polymeric nanomaterial. The increased colloidal stability of the prepared nanoparticles could be attributed to the surface charge, which is affecting through electrostatic repulsion. Thus, the aggregation of the nanoparticles was circumvented. According to Feng *et al*. the nanoparticle size increases with the increase of monomer and initiator concentration (Bai *et al*. 2004). The

increased concentration of cross-linking agent such as MBAAm increases the hydrophilicity of the material (Liu *et al*. 2016). Among the solvents, ACN was chosen as the reaction solvent, however, protic solvents such as ethanol or methanol forms aggregate through hydrogen bond formation (Liu *et al*. 2007).

In the present study, poly(MBAAm-co-SBMA) zwitterionic polymer nanoparticles were synthesized by SBMA as monomer and MBAAm as a cross-linking agent via distillation-precipitation polymerization (DPP). The as-synthesized nanoparticles were characterized by FT-IR, TEM, SEM, BET, TGA, XRD and zeta potential analysis. The PSF HF membranes were prepared with the different amounts of nanoparticles by dry/wet phase inversion method. SEM, contact angle, porosity, water uptake, zeta potential, pure water permeability and antifouling study characterized the as-made PSF HF membranes. Furthermore, the nanocomposite membrane explored for the dyes such as Reactive black 5 (RB 5) and Reactive orange 16 (RO 16) rejections.

3.2 EXPERIMENTAL

3.2.1 Materials and methods

Polysulfone (PSF, P-1700) was purchased in the form of pellets from Solvay Specialty Polymers (China). The solvents N-methyl pyrrolidone (NMP) and acetonitrile (ACN) were obtained from Merck. Polyvinylpyrrolidone (PVP K-30), bovine serum albumin (BSA), [2-(methacryloyloxy)ethyl]dimethyl-(3-sulfopropyl)ammonium hydroxide (SBMA), N,N′-methylene bis(acrylamide) (MBAAm), Reactive black 5 (RB 5), Reactive orange 16 (RO 16) and azobisisobutyronitrile (AIBN) were procured from Sigma-Aldrich.

Morphology of the synthesized poly(MBAAm-co-SBMA) nanoparticles was visualized using transmission electron microscopy (TEM) (JEOL JEZM-2200FS) with an accelerating voltage of 200 kV and Field Emission scanning electron microscopy (FESEM) (HITACHI SU5000). The elemental mapping was carried out using Energy-dispersive X-ray spectroscopy (EDX) (X-act Oxford Instruments). The functional group identification was done by FT-IR (Bruker Alpha) spectrophotometer. Each sample was made into a KBr pellet and analyzed at the resolution of 2 cm^{-1} with 24 scans in the range of 4000-500 cm^{-1}. The thermal stability was measured by using thermogravimetric analysis (TGA) (HITA CHI EXSTAR 6300) in the temperature range of 30-800 ^{o}C at a heating rate of 10 $^{o}C\ min^{-1}$ under N_2 atmosphere.

The Bruner-Emmet-Teller (BET) surface area, pore volume and mean pore diameter were measured using Smart instruments (Smart Sorb 92/93). The zeta potential and hydrodynamic diameter of the nanoparticles were measured by dispersing 5 mg of sample in distilled water (pH ~6.5) using the HORIBA SZ-100 nanoparticle analyzer. The polymorphism of the poly(MBAAm-co-SBMA) nanoparticles was analyzed by benchtop powder X-ray diffractometer (XRD) (Rigaku, mini Flex 600) with Cu Kα as an X-ray source. The as-prepared membrane samples were dried at 50 ^{o}C for 12 h before the analysis. The cross-sectional images of the membranes were visualized by SEM (HITACHI TM3000). The samples were sputtered with platinum to bestow conductivity. The surface hydrophilicity of the membranes was measured using a water contact angle analyzer (OCA, Dataphysics instrument) at room temperature. The zeta potential of the membrane surface was analyzed by the electrokinetic analyzer (Surpass Anton Paar) with 0.001 M KCl as the background electrolyte. The presence of nanoparticles in the membrane matrix was confirmed by X-ray photoelectron spectroscopy (XPS, THERMO FISHER Scientific K-ALPHA) analysis. Al Kα radiation (1486.6 eV) was used as an X-ray source and the take-off angle was 20^{o}.

3.2.2 Synthesis of poly(MBAAm-co-SBMA) nanoparticles

In a typical DPP process, SBMA (0.2 g, 0.71 mmol), MBAAm (1.0 g, 6.4 mmol), AIBN (0.0225 g, 0.13 mmol), ACN (100 mL) were taken in a 250 mL single neck round bottom flask (RBF), purged with N_2 for 30 min to remove the dissolved oxygen. The RBF containing reaction mass (RM) was connected to the Dean-Stark receiver. The RM was heated to 75 ^{o}C for 10 min. The temperature of the oil bath was slowly increased to 100 ^{o}C to keep the reaction proceeding under reflux. About 35 mL of ACN was distilled out from the RM through Dean-Stark receiver over 1 h. Then the RM was cooled to room temperature and stirred for 1 h. The nanoparticles were filtered and washed with (2×20 mL) ACN to remove the unreacted monomer and oligomer. The nanoparticles were dried under vacuum (-25 Hg) at 50 ^{o}C for 12 h to yield 1.12 g of white powder. The synthetic route of nanoparticles is represented in scheme 3.3.

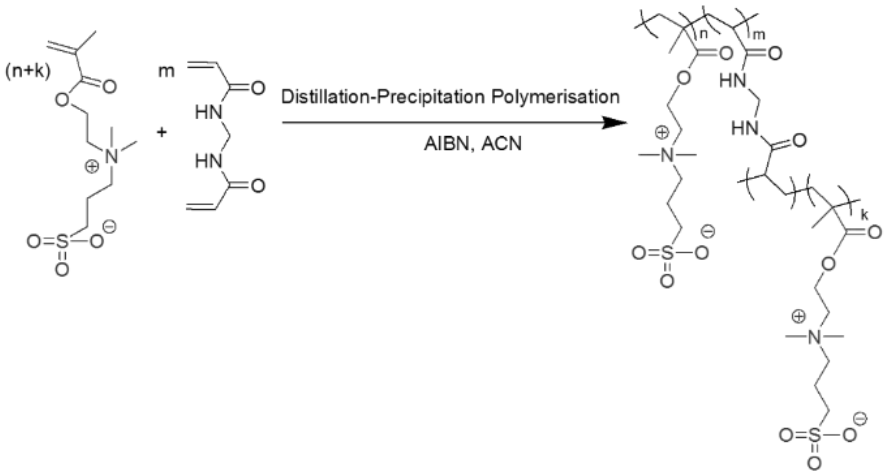

Scheme 3.3 Synthetic route to poly(MBAAm-co-SBMA)

3.2.3 Hollow fiber (HF) membrane preparation

The PSF/poly(MBAAm-co-SBMA) HF membranes prepared by the dry/wet phase inversion method (Hebbar *et al*. 2017). The dope solution compositions are depicted in Table 3.1 and spinning parameters are tabulated in Table 3.2. For the preparation of ZM-3, 0.1 g of poly(MBAAm-co-SBMA) nanoparticles were dispersed in 79 g of NMP by sonicating (40 kHz, 60 W Spectralab) for 30 min. Added 20 g of PSF and 1 g of PVP as a pore-forming agent to the dope solution and stirred at 60 ^{o}C for 12 h. The dope solution was degassed for 30 min using sonication. The HF membranes were spun by keeping the bore and dope extrusion rate constant. The extruded HF membrane underwent phase inversion in the coagulation bath. The as-made HF membranes were immersed in distilled water for 24 h by changing the water periodically. The membranes were retained in 20 wt% glycerol in water for a further 24 h to avoid the pore shrinkage. The post-treated membranes were dried at room temperature for future usage. The illustration scheme of HF membrane preparation has been given in scheme 3.4.

Table 3.1 The dope solution composition

Membrane	PSF (g)	PVP (g)	NMP (g)	poly(MBAAm-co-SBMA) (g)
ZM-0	20	1	79	0
ZM-1	20	1	79	0.02
ZM-2	20	1	79	0.05
ZM-3	20	1	79	0.10
ZM-4	20	1	79	0.20

Table 3.2 Spinning parameters of PSF/poly(MBAAm-co-SBMA) HF membranes

Parameters	Conditions
Spinneret (mm)	1.1/0.55 (OD/ID)
Dope extrusion rate (mL/min)	3.0
Bore flow rate (mL/min)	2.5
Bore fluid	Distilled water
Air gap (cm)	1.0
Humidity (%)	60
Coagulation bath	Tap water
Coagulation bath temperature (^{o}C)	27.0
Collection drum speed (RPM)	7.0

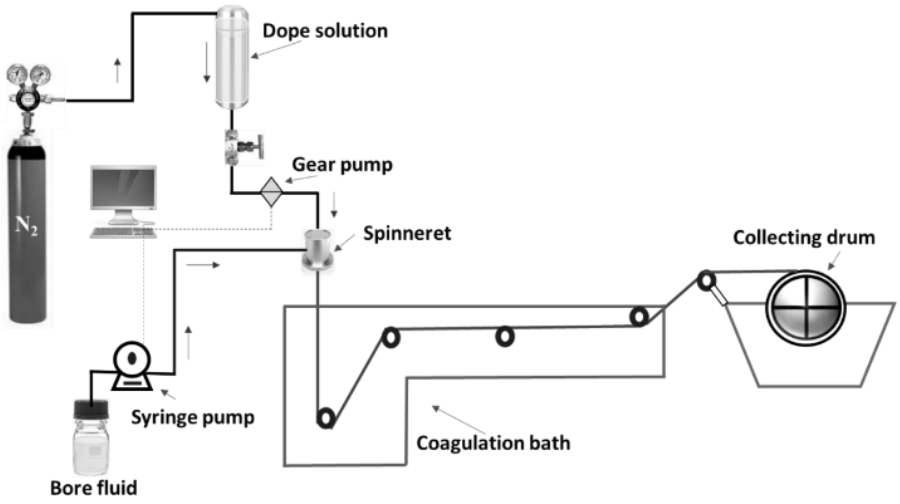

Scheme 3.4 An illustration scheme of hollow fiber membrane preparation

3.2.4 Porosity and water uptake studies

The porosity and water uptake studies were carried out to understand the surface properties of the membranes. Porosity and water uptake studies were carried out as mentioned in chapter 2, section 2.2.4.

3.2.5 Molecular weight cut-off (MWCO) study

The MWCO of the ZM-3 membrane was determined by filtering a series polyethylene glycol (PEG) with an average molecular weight of 2000, 4000, 6000 and 10,000 Da (Tang *et al*. 2016). The analysis was performed as mentioned in chapter 2, section 2.2.6.

3.2.6 Permeation and antifouling study

In the permeation study, a 10 cm length of HF membrane sample was cut and potted using epoxy adhesive. All the experiments were carried out in the lab-made cross flow apparatus. At first, the membranes were compacted for 30 min at 2 bar pressure. The pure water permeability (PWP) 'J_w' was measured at 1 bar for 60 min. An aqueous solution of RB 5 and RO 16 was prepared at the concentration of 100 ppm. The solute concentration was measured using a UV-Vis spectrophotometer (HACH DR 5000) at the λ_{max} of 592 nm and 494 nm for RB 5 and RO 16. The PWP, dye rejection and antifouling studies were executed as mentioned in chapter 2, section. 2.2.5 and 2.2.7.

3.3 RESULTS AND DISCUSSION

3.3.1 Characterization of poly(MBAAm-co-SBMA) nanoparticles

FT-IR spectra in Figure 3.1A represents the functional groups present in the poly(MBAAm-co-SBMA) and MBAAm. The peaks at 1656 cm^{-1} and 1529 cm^{-1} designate the stretching vibration of amide C=O and bending vibration of NH-CO. The peaks at 1722 cm^{-1} and 1043 cm^{-1} indicate the ester (C=O) and sulfonate (S=O) stretching vibrations (Suart 2004, Ji *et al*. 2012). The peak at 1626 cm^{-1} attributed to the alkene C=C stretching vibration of MBAAm, which was not observed in the poly(MBAAm-co-SBMA) due to the polymerization reaction. This change is one of the reliable confirmation that the reaction had been completed. The peak at 3271 cm^{-1} indicates the stretching vibration of N-H in the amide group of poly(MBAAm-co-SBMA). The peak at 1229 cm^{-1} due to the C-N stretching vibration of the amide group. However, the peak at 954 cm^{-1} owing to the presence of C-N stretching vibration of the quaternary ammonium group (Shang *et al*. 2009, Ji *et al*. 2011, Ji *et al*. 2012). The above results indicated that the poly(MBAAm-co-SBMA) was comprised of the monomer SBMA and cross-linker MBAAm.

The morphology of the as-prepared poly(MBAAm-co-SBMA) nanoparticles was visualized using field emission scanning electron microscope (FESEM) and transmission electron microscopy (TEM). As depicted in Figure 3.1B, the nanoparticles exhibited comparatively uniform shape and size, with a diameter in the region of around less than 60 nm. Kaiguang *et al*. reported that in DPP the size of the nanoparticles does not depend on the amount of solvent removed, whereas the reaction temperature (Yang *et al*. 2009), AIBN and monomer concentration (Bai *et al*. 2004) directly affects the size of the nanoparticles.

Figure 3.1d presents the selected area electron diffraction (SAED) pattern of the nanoparticles. It is clear from the picture that, the as-prepared nanoparticles exhibit small spots creating up a ring. It indicates that the nanoparticles are polycrystalline in nature (Egerton 2005). In addition, the nanoparticles show slight agglomeration, which is clear from the TEM pictures. The possible justification for such agglomeration may be due to the electrostatic attraction between the counterions. Figure 3.2 depicts the schematic representation of nanoparticle synthesis and the possible mechanism of agglomeration. A similar kind of observation had been reported elsewhere (Chang *et al*. 2013, Wang *et al*. 2017). Further, the elemental mapping analysis was carried out to confirm the presence of all the elements. Figure 3.3a-d show the distribution of C, N, O and S elements in poly(MBAAm-co-SBMA) nanoparticles, among them S is the characteristic element of SBMA monomer.

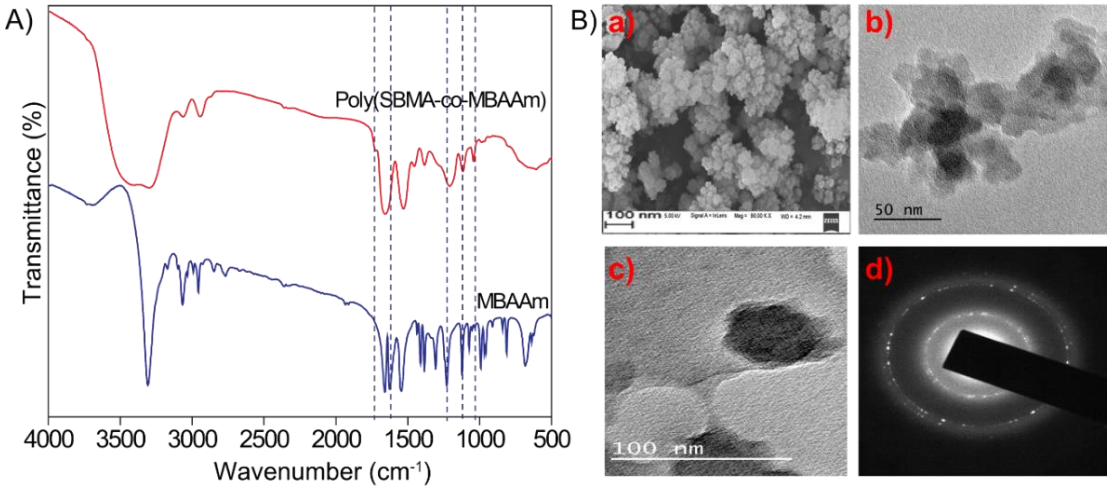

Figure 3.1 A) FT-IR spectra of poly(MBAAm-co-SBMA) and MBAAm and B) FESEM (a), TEM (b, c) images and d) selected area electron diffraction (SAED) pattern of poly(MBAAm-co-SBMA) nanoparticles

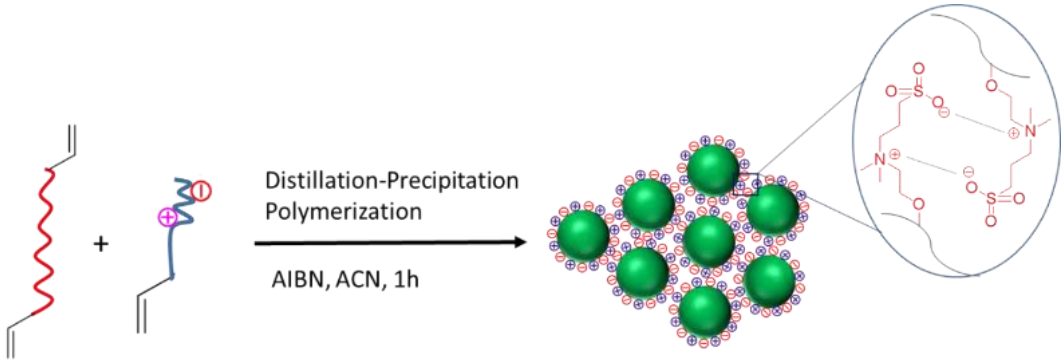

Figure 3.2 The schematic representation of nanoparticles synthesis

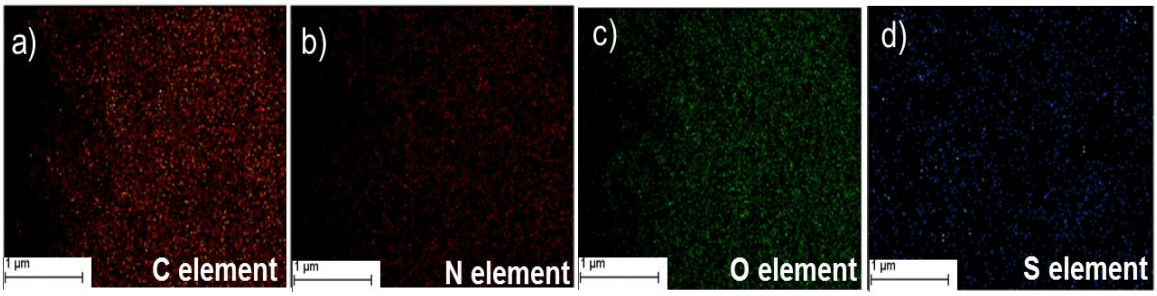

Figure 3.3 Elemental mapping of poly(MBAAm-co-SBMA) (a-d)

3.3.2 Surface properties and hydrodynamic diameter

The zeta potential of the synthesized poly(MBAAm-co-SBMA) nanoparticles was measured. As shown in Figure 3.4a, the nanoparticles exhibited the zeta (zeta) potential of -47.7 mV. The negative zeta-potential of the nanoparticles could be attributed to the presence of the sulfonate group. The pK_a value of the sulfonate group is 2 (Grainger *et al.* 2010) and the pK_b value of the quaternary ammonium group is 5 (Janson 2012). Consequently, the quaternary ammonium group signifies a weaker base than the sulfonate group as acid. Therefore, the overall surface charges of the as-synthesized nanoparticles exhibit a negative charge in aqueous solution. According to Dorian *et al*., the dispersibility of the nanomaterial could be enhanced by coating with the carboxylic acid group, which provides negative zeta-potential to the material. As a result, the nanoparticle maintains the suspension over the extensive range of pH deprived of any agglomeration (Hanaor *et al*. 2012). Similarly, the synthesized nanoparticles exhibit the negative zeta-potential and develop an electrical double layer, which avoids the nanoparticles from aggregating and preserves the stable dispersion in a variety of solvents through electrostatic repulsion.

Furthermore, the nanoparticles exhibited the BET surface area of 89.2 m^2/g and a mean pore diameter of 37 nm with the pore volume of 0.12 cc/g. In addition, the hydrodynamic diameter of the nanoparticle was 331 nm, which is presented in Figure 3.4b. The increase in the size was due to the slight aggregation of nanoparticles in water. Russell *et al*. reported that the sulfonate group has a strong tendency to form hydrogen bonding (Russell *et al*. 1997). Therefore, the aggregate formation was attributed to the formation of hydrogen bonding between the sulfonate group and water.

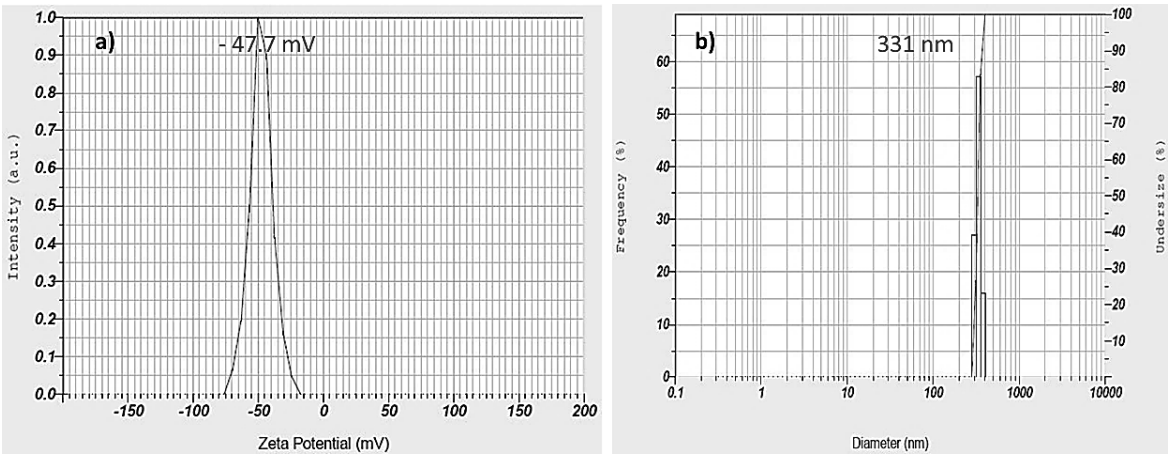

Figure 3.4 a) Zeta potential and b) hydrodynamic diameter of nanoparticles

3.3.3 Thermal stability study

The thermal stability of the nanoparticles was analyzed using TGA. The TGA analysis showed that the synthesized nanoparticle is thermally stable, as the onset of degradation is above 250 ^{o}C. Moreover, the curve contains three-stage degradation. The first weight loss between 25 and 105 ^{o}C due to the adsorbed water. The second weight loss from ~ 255 to 333 ^{o}C attributed to the degradation of a quaternary ammonium group. The third stage degradation in the region of ~ 340 to 450 ^{o}C ascribed to the removal of more stable oxygen functionalities. Figure 3.5A shows the TGA curves of the nanoparticles, along with its differential thermogravimetry (DTG) curve.

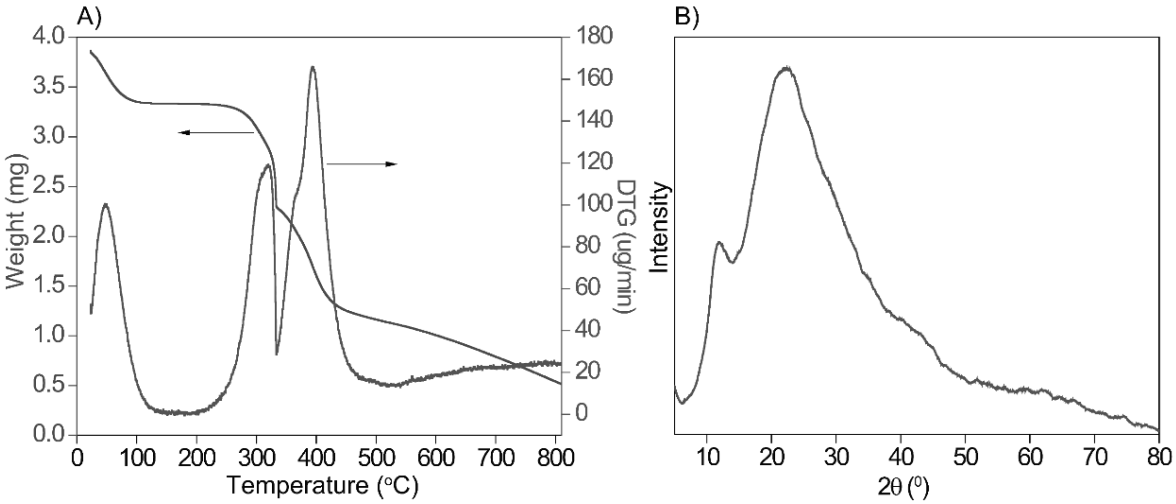

Figure 3.5 A) TGA, DTG curves and B) PXRD pattern of poly(MBAAm-co-SBMA) nanoparticles

3.3.4 XRD analysis

Figure 3.5B depicts the XRD pattern of the poly(MBAAm-co-SBMA) nanoparticles. Two intense broad bands centered at 2θ of ~11.88^{o} and ~22.68^{o} demonstrates that these nanoparticles are polycrystalline in nature. This result is well-aligned with the SAED pattern of the nanoparticles.

3.4 Characterization of membranes

3.4.1 Surface hydrophilicity

The hydrophilicity of the as-prepared membranes was evaluated by measuring the contact angle and water uptake capacity. In general, it is believed that lower the contact angle higher will be the hydrophilicity (Hurwitz *et al*. 2010, Moideen K *et al*. 2016). Since the pristine membrane (ZM-0) is less hydrophilic in nature, it exhibited a higher contact angle of 80.0^{o}. However, for the nanocomposite membranes such as ZM-1, ZM-2, ZM-3 and ZM-4, the contact angle was observed 76.1^{o}, 71.4^{o}, 67.0^{o} and 65.2^{o} respectively (Table 3.3). The decrease in contact angle was attributed to the incorporation of hydrophilic poly(MBAAm-co-SBMA) nanoparticles. The hydrophilic functional group such as sulfonate and amide group present in the nanoparticles was changed the interfacial free energy of the membrane. In addition, the sulfonic acid group has a greater water uptake capacity, which increases the surface hydrophilicity of the membrane.

Table 3.3 Membrane properties

Membrane	Contact angle (^{o})	Water uptake (%)	Porosity (%)
ZM-0	80.0	29.5	41.6
ZM-1	76.1	48.2	53.1
ZM-2	71.4	53.1	61.4
ZM-3	67.0	61.7	66.5
ZM-4	65.2	56.4	62.2

3.4.2 Membrane Morphology

The change in the morphology of the membranes upon the addition of nanoparticles was characterized using SEM. As shown in Figure 3.6, the nanocomposite hollow fiber membranes exhibit asymmetric structure with top skin layer, sub-layer and fingerlike macrovoids. The sub-layer is sandwiched between the top and bottom fingerlike layer. As stated by McKelvey *et al*. the growth of macrovoids depends on the change in diffusion rate between non-solvent and solvent during phase inversion (McKelvey *et al*. 1996). Since the pore-forming agent such as PVP was added to all the membranes invariably, the change in fingerlike projection between the prepared membranes was not observed distinctly upon the addition of nanoparticles. In addition, the air gap 1 cm was maintained throughout the spinning process to increase the permeability. Subsequently, the phase inversion occurred on both the outer and inner sides of the membranes at a nearly concurrent rate and led to the formation of two layers of the finger-like structure. The reported results are consistent with the literature (Subramaniam *et al*. 2017). The normal digital photographic image of the HF membrane is depicted in Figure 3.6F. Besides, the MWCO of the ZM-3 membrane is 9242 Da (Figure 3.7), which suggests that the as-prepared membrane is the UF membrane (Liu *et al*. 2017).

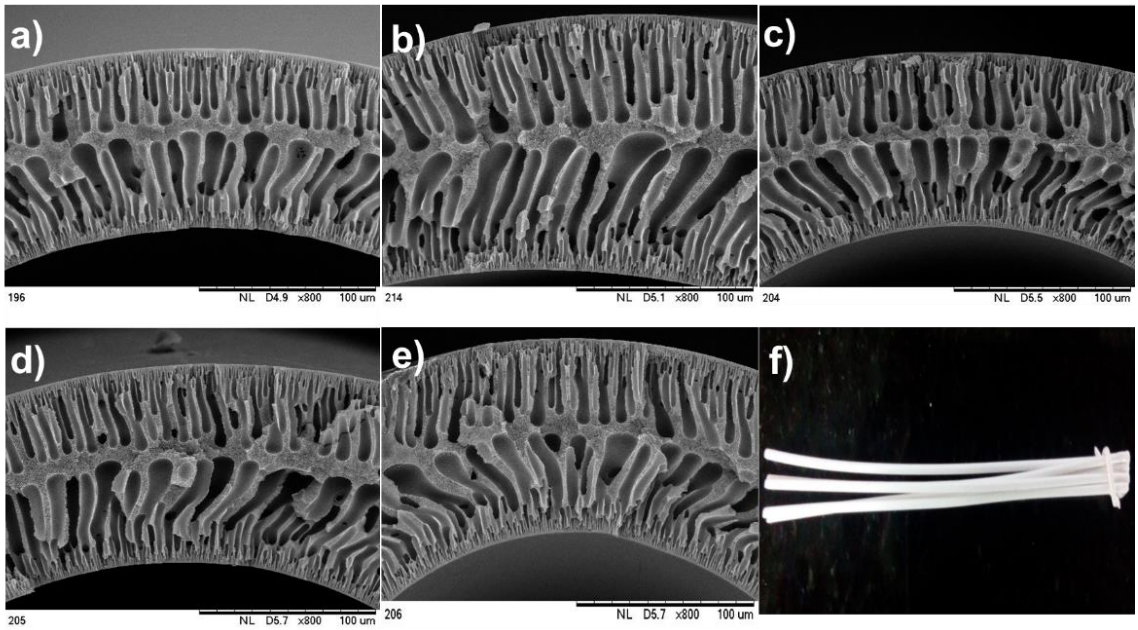

Figure 3.6 Cross-sectional SEM images of a) ZM-0, b) ZM-1, c) ZM-2, d) ZM-3 and e) ZM-4 membranes magnified at 800X and f) digital photographic image of ZM-3 membrane

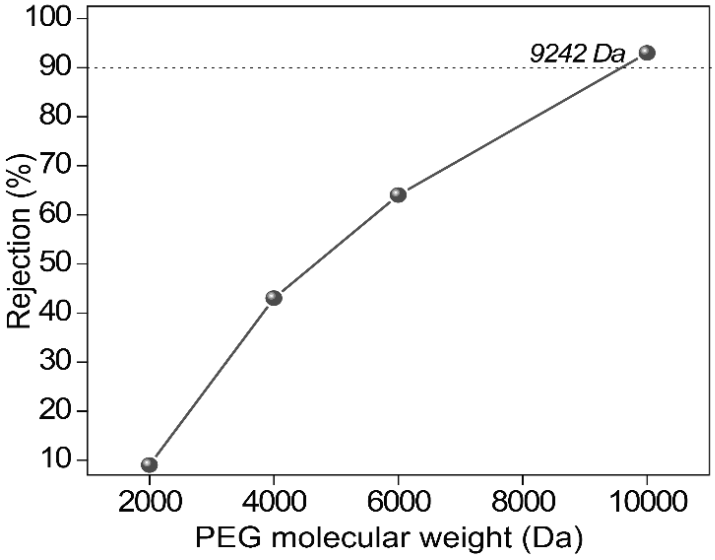

Figure 3.7 Molecular weight cut-off (MWCO) curve of ZM-3 membrane

3.4.3 XPS analysis

The ZM-3 membrane surface was analyzed by XPS and depicted in Figure 3.8. As shown in Figure 3.8A, the peaks at 168.38 eV, 285.18 eV, 400.18 eV and 532.18 eV were attributed to S 2p, C 1s, N 1s and O 1s elements. Additionally, the deconvoluted peaks of C 1s and N 1s are presented in Figures 3.8B and C. In Figure 3.8B, the peaks at 285.21 eV, 286.14 eV, 286.36 eV, 287.11eV and 288.15 eV were corresponding to C-C, C-N^+/C-SO_3^-, C-O/C-N, C=O and O-C=O. For N 1s, N-C=O, N-C and $^+NR_4$ were observed at 400.28 eV, 398.18 eV and 402.68 eV. The elemental composition (atomic %) of the nanocomposite HF membrane was observed as 77.35 %, 15.81 %, 2.76 % and 4.08 % for C, O, S and N elements respectively. Thereby, the existence of the nanoparticles in the membrane matrix was confirmed.

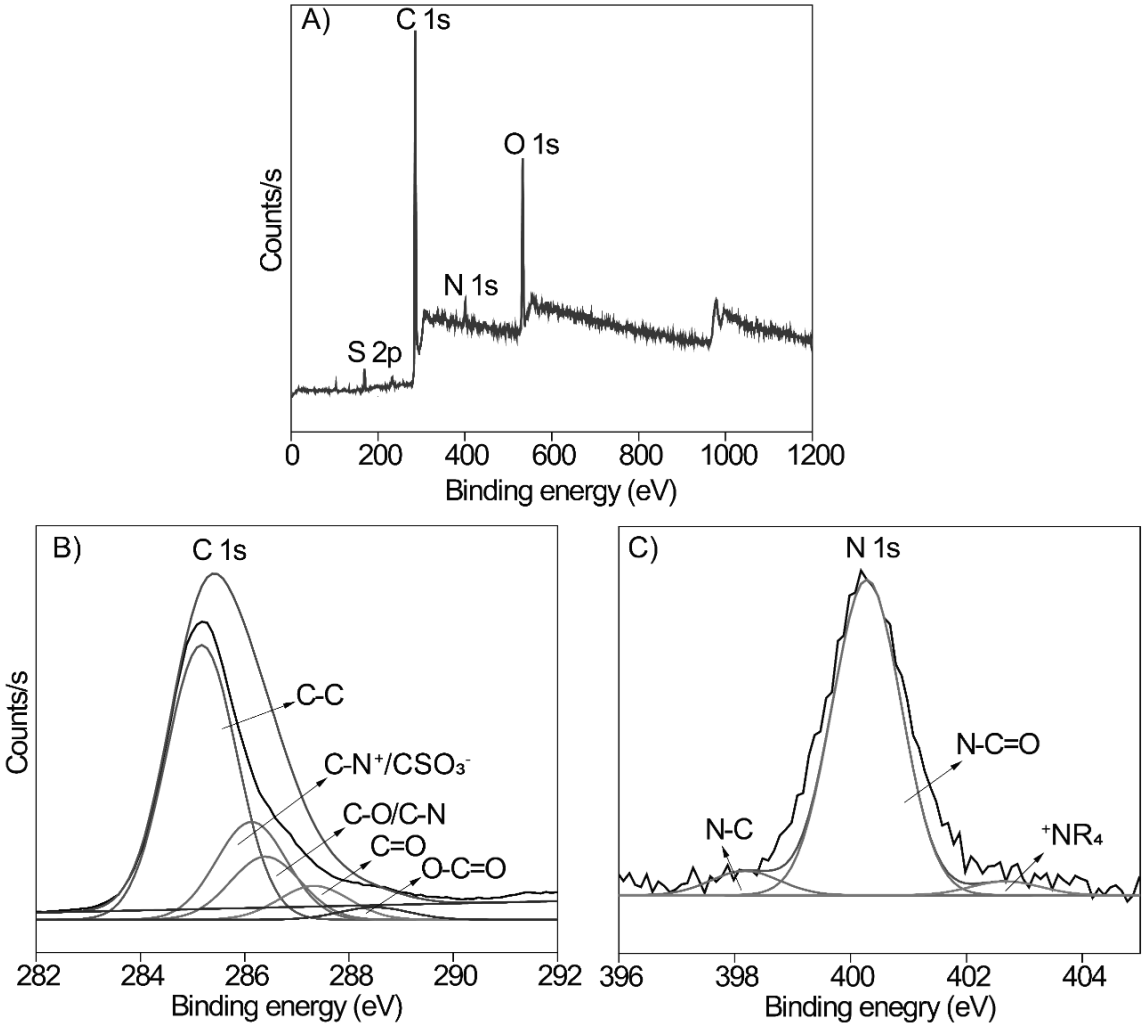

Figure 3.8 Long-range A) ZM-3 and high resolution XPS spectra of B) C 1s and C) N 1s

3.4.4 Surface charge of the membranes

As shown in Figure 3.9A, the membranes ZM-0 and ZM-3 exhibited the negative charge over the entire pH range of 4-10 and the absolute zeta potential value was decreased to acidic pH values. The isoelectric point (IEP) of the PSF neat (ZM-0) membrane was observed at pH 3.0, which is similar to the literature (Kim *et al*. 2002). However, the IEP of the ZM-3 membrane was detected at pH 3.4. The change in the IEP could be attributed to the incorporation of nanoparticles. In addition, the incorporated zwitterionic nanoparticles are negatively charged at pH 6.5. However, the zeta potential of ZM-3 was less at pH 7 when compared to the ZM-0 membrane. The reduced zeta potential could be attributed to the intervention of cation adsorption from background electrolyte (KCl) on the surface, which decreases the negative charge density of the sulfonate group. As a result, the zeta potential of the nanoparticle becomes less negative, which directly reduces the net

charge of the membrane surface. Overall, the as-prepared membrane could exhibit a negative charge over the large range of pH.

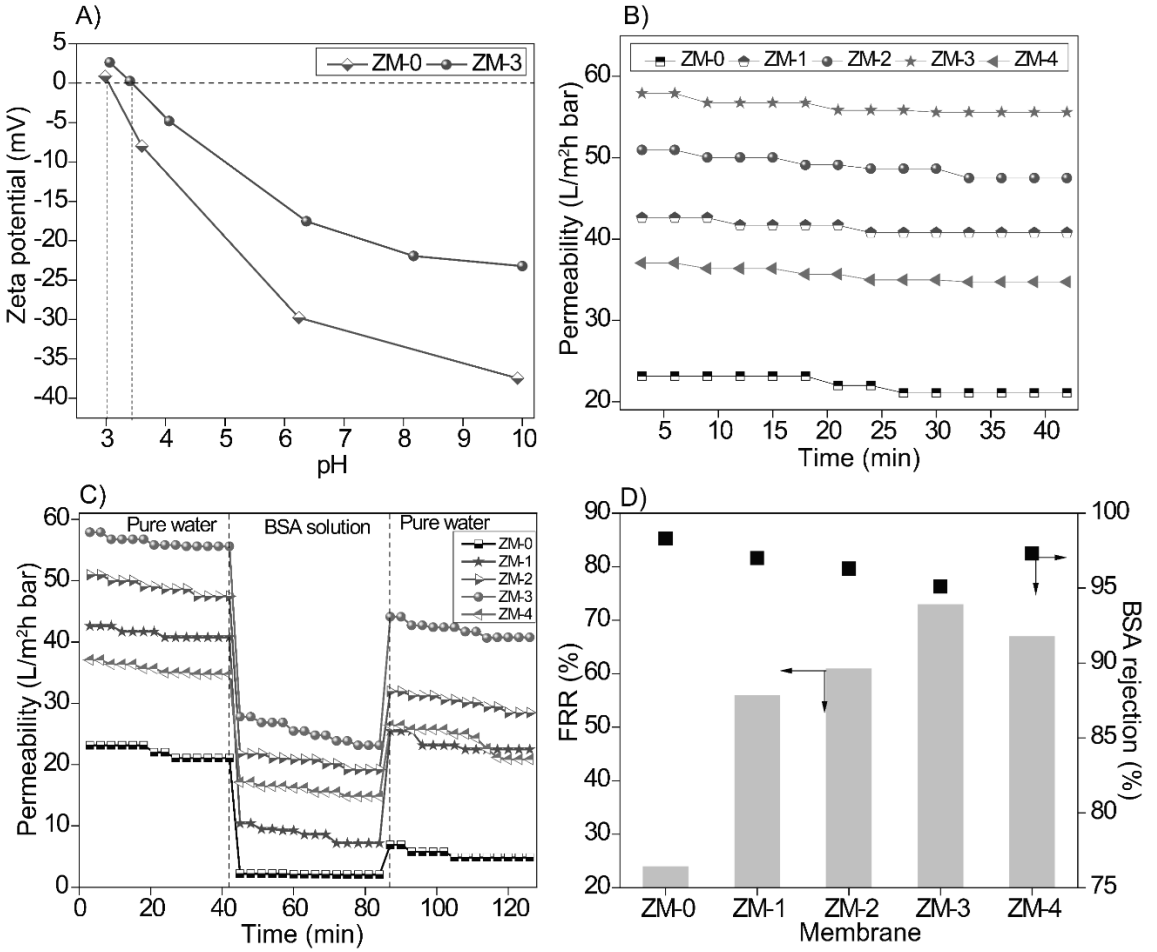

Figure 3.9 A) Zeta potential of ZM-0 and ZM-3 membranes, B) permeability, C) time depended permeability in different conditions of ZM-0, ZM-1, ZM-2, ZM-3 and ZM-4 membranes and D) flux recovery ratio (FRR) and BSA rejection of membranes

3.4.5 Permeability and antifouling performances

The permeation of water through the membrane is determined primarily by the surface hydrophilicity and pore size (Zhang *et al*. 2016). In order to evaluate the effect of the different poly(MBAAm-co-SBMA) nanoparticles content on the filtration performance of the as-made membranes, the pure water permeability (PWP) of all the UF membranes was measured; the results are presented in Figure 3.9B. As shown, the PWP of the membranes increases with the enhancement of the concentration of nanoparticles. The pristine (ZM-0) membrane exhibited the lowest PWP of 22 L/ m^2 h bar. The membrane ZM-3 embedded with 0.5 wt% of nanoparticles exhibited the PWP of 56 L/ m^2 h bar. A plausible explanation

is that the added nanoparticles could be increased the surface hydrophilicity of the membranes. The increased hydrophilicity would enhance the rate of demixing during phase inversion. Further, the non-solvent inflow and solvent outflow would be more. Consequently, the porosity showed an increasing trend. As shown in Table 3.3, the porosity and water uptake increased as the concentration of nanoparticles increases. The membrane ZM-3 showed the highest porosity of 66.5 % and water uptake of 61.7 % compared to the pristine membrane ZM-0 of 41.6 and 29.5 %. However, for the membrane ZM-4 with 1 wt% of nanoparticles, the porosity and water uptake reduced to 62.2 and 56.4 %. A similar trend had been observed in PWP of the ZM-4 membrane. The PWP was reduced to 35L/ m^2 h bar. The convincible reason for the reduction in porosity, water uptake and PWP is that the embedded nanoparticles may lead to partial agglomeration, consequently blocking the pores of the membranes and increase the resistance towards the water permeation (Hebbar *et al*. 2016, Zhu *et al*. 2016).

Figure 3.9C represents the time-dependent water permeability of the membranes at different conditions. The initial decline in the permeability of the water was due to the mechanical deformation of the membrane matrix (Reinsch *et al*. 2000). In addition, Figure 3.9C indicates the increase in water permeability as the concentration of nanoparticle increases. However, during the BSA filtration, there was a sudden decline in the water permeability. The sudden decline was attributed to the adsorption of BSA molecules on the membrane surface, which blocks the polymeric membrane pores. The antifouling capacity of the as-made membranes was measured in terms of flux recovery ratio (FRR) and it is depicted in Figure 3.9D. The membrane ZM-3 exhibited the FRR of 73 % compared to the pristine membrane ZM-0 of 24 %. The increased FRR of the ZM-3 was due to the increased hydrophilicity.

It has been accepted widely that membrane surface decorated with zwitterionic substances can bestow outstanding antifouling ability (He *et al*. 2008, Mi *et al*. 2012, Rohani *et al*. 2012, Hadidi *et al*. 2014). Further, it forms the hydration layer over the membrane surface, which avoids the adsorption of foulants on the membrane surface. Moreover, the prepared nanocomposite membranes are exhibiting negative charges at the neutral pH. As a result, the BSA molecules are poorly adsorbed via electrostatic repulsion as the BSA molecules are negatively charged at pH 7.4. However, membrane ZM-4 exhibited a reduced FRR of 67 %. The reduced FRR was owing to the agglomeration of

the nanoparticles, which encourages the adsorption of the foulant. In summary, the membrane with 0.5 % of nanoparticle loading is the optimal concentration for the preparation of the membrane.

3.4.6 Dye removal study

The filtration ability of the ZM-3 membrane for the different dye solutions as a function of pH is depicted in Figure 3.10. In the pH range of 3-10, the membrane performance varies with the solution pH. As shown in Figure 3.10, in acidic pH the permeability of the dye decreases and rejection increases. In general, the sodium salt of dye molecules is highly soluble in water. However, while decreasing the pH to the highly acidic side, the sulfonate groups present in the dye molecules are getting protonated and become a sulfonic acid group. As a result, the solubility and polarity of the dye molecules are decreased. Thus, the dye molecules are precipitated and aggregated largely at pH 3.

In summary, the increased rejection owing to the aggregation of dye molecules and declined permeability due to the precipitation of dye, which is in good agreement with the reported literature (Liu *et al*. 2017). At pH 10, the permeability of the dye was reduced to a smaller extent. The reduced permeability could be due to the swelling of the membrane at the basic pH. The swelling could increase the thickness of the membrane (Wang *et al*. 2016). Consequently, the permeability of the dye molecules was reduced to a smaller extent. Further, the rejection of RB 5 was high as compared to RO 16 at pH 7. The reason for the enhanced rejection was due to the size exclusion mechanism i.e., the higher molecular weight of the former compared to later. In conclusion, the optimum pH for the removal of both the dye molecules is 7. The digital photographs of the feed and permeate of RB 5 and RO 16 are depicted in Figure 3.11. The comparison of the dye removal capacity of polymeric membranes from recent literature and the present study is illustrated in Table 3.4. Generally, the effluent from the textile and dyeing industry usually consist of dyes and salts (Zhu *et al*. 2016). In that respect, salts such as NaCl and Na_2SO_4 rejection studies were carried out. The ZM-3 membrane exhibited the rejection in following order Na_2SO_4 (11 %) > NaCl (7 %), signifying that the nanocomposite membrane was negatively charged, which is consistent with the zeta potential result.

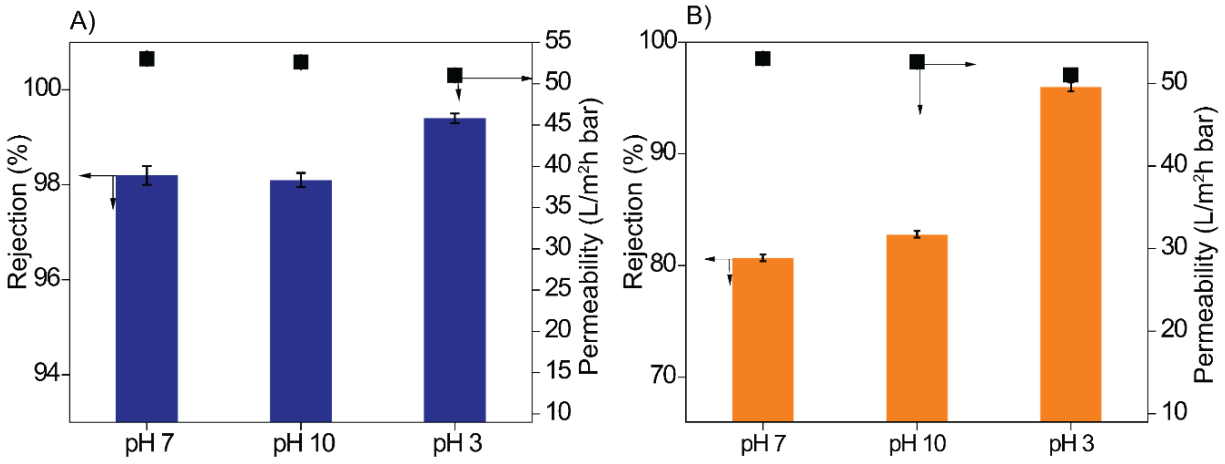

Figure 3.10 ZM-3 membrane permeability and rejection of A) RB 5 and B) RO 16 dye solution at different pH

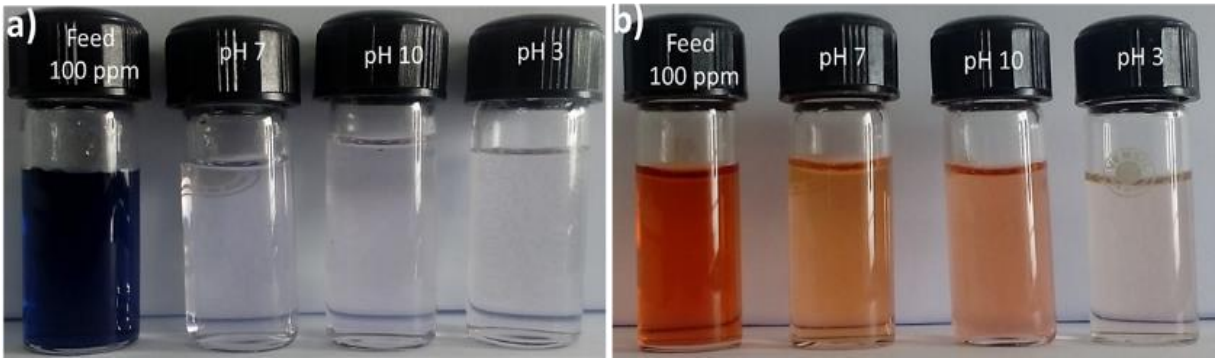

Figure 3.11 Digital photographs of a) RB 5, b) RO 16 feed and permeate at different pH

Table 3.4 Comparison of dye removal ability of polymeric membranes from recent literature and the present study

Membrane	Type of membrane	Dye	PWP (L/m^2 h bar)[a]	DSP (L/m^2h bar)[b]	Dye rejection (%)	Ref.
Sepro NF 2A	Loose NF	Direct red 80	10.5	9.6	99.98	(Lin *et al.* 2015)
Sepro NF 6	Loose NF	Direct red 80	13.7	13.2	99.95	(Lin *et al.* 2015)
PES / GO-PSBMA	Loose NF	Reactive black 5	11.98	9.4	99.2	(Zhu *et al.* 2016)
UH004 (Hydrophilic PES)	Tight UF	Direct red 80	27	26	99.9	(Lin *et al.* 2016)
PAEK-COOH	Tight UF	Congo red	29.5	25	99.0	(Liu *et al.* 2017)
PSF-poly(MBAAm-co-SBMA)	**UF**	**Reactive black 5/ Reactive orange 16**	**56**	**51/51.8**	**98/80.7**	**Present study**

a-pure water permeability; b-dye solution permeability.

3.5 CONCLUSIONS

The zwitterionic polymer nanoparticles were synthesized via distillation-precipitation polymerization. The as-synthesized nanoparticles exhibited high surface area (89.2 m^2/g), thermal and colloidal stability. The synthesized nanoparticles were successfully incorporated into the polysulfone membrane matrix and the membranes were prepared by dry/wet phase inversion method. The ZM-3 nanocomposite membrane showed high pure

water permeability of 56 L/ m^2 h bar and rejection of Reactive black 5 (>98 %) and Reactive orange 16 (>80.7 %) with the dye permeability of 51 L/ m^2 h bar and 51.8 L/ m^2 h bar at a dye concentration of 100 ppm, which has the molecular weight cut-off of 9242 Da. These results clearly reveal that the as-prepared membrane can be an attractive candidate for the treatment of industrial and textile wastewater treatment.

CHAPTER 4

TUNING THE SURFACE PROPERTIES OF Fe_3O_4 BY ZWITTERIONIC SULFOBETAINE: APPLICATION TO ANTIFOULING AND DYE REMOVAL MEMBRANE

Abstract: *In this chapter, zwitterionic nanoparticles were synthesized via covalent grafting and free radical polymerization, and were characterized. The as-synthesized nanoparticles were employed as a nanofiller to prepare superior antifouling polysulfone (PSF) hybrid hollow fiber (HF) membranes. The FM-2 membrane exhibited the maximum pure water permeability (PWP) of 61.1 L/m^{2}h bar with humic acid (HA) removal efficiency of 98 %. The fouling resistance was evaluated using humic acid as a foulant and the results suggested that the FM-2 membrane exhibited less amount of humic acid adsorption with a flux recovery ratio of 88.4 %. Furthermore, the FM-2 membrane demonstrated the Reactive black-5 (RB-5) and Reactive orange-16 (RO-16) removal of above 99 % and 84 % without much reduction in the dye solution permeability (DSP).*

4.1 INTRODUCTION

Currently, access to clean water is one of the important challenges in our life (Werber *et al*. 2016). The unexpected boom in industrialization, population growth and climate change have desperately affected the availability of clean water for both humans and which will become a prime concern in both developing and industrialized nations (Shannon *et al*. 2008, Ibrahim *et al*. 2018).

The natural organic matter (NOM) present in surface/groundwater determines the productivity of ultrafiltration (UF) membranes, as the fouling due to NOM is a serious concern. Humic acid (HA) is one of the most important constituents in NOM, which is produced during the degradation of plants and dead animals. When HA polluted water is in contact with a disinfectant such as chlorine, it produces disinfection by-products (DBPs). For instance, trihalomethanes (THMs) and other halogenated organic compounds. These DBPs are carcinogenic and assist the microbial regrowth in water (Peters *et al*. 1980). In addition, HA has the capability to absorb some of the cationic dye molecules and also coordinate with pesticides, herbicides and heavy metal ions in contaminated water (Shenvi *et al*. 2015). At the same time, the wastewater containing dye is also another toxic waste. In industries like paper, textile, pulp and paints, several types of reactive dyes were used to color cotton fabrics. These reactive dyes are not easy for chemical oxidation and biodegradation. Thus, it leaves a secondary pollutant during oxidation (Weber *et al*. 1995, Purkait *et al*. 2004). Therefore, the removal of HA and reactive dyes from the polluted

water has become a challenging task in water purification, especially in membrane science and technology.

To remove HA and reactive dyes from aqueous solution, the following methods have been reported in the literature. Nanofiltration (NF), reverse osmosis (RO), coagulation, adsorption, photocatalytic degradation and ozonation. However, NF and RO membranes have low water flux and suffering from severe fouling (Hong *et al*. 1997). Other methods were less efficient, time-consuming and produce solid wastes. Consequently, these methods are not viable to scale up. Hence it is mandatory to improve a UF membrane with great permeability and low fouling, which is more indispensable for the elimination of HA. Further, fouling is one of the severe concerns in the development of superior UF membranes, which come up from the interaction of HA on the membrane surface (Kaiya *et al*. 1996). According to Laîné *et al*. greater fouling was witnessed with larger pore size membranes and reduced fouling was reported for the hydrophilic membranes when compared to hydrophobic membranes (Laine *et al*. 1989). Song *et al*. stated that the charged membrane exhibited enhanced HA rejection over the uncharged membrane with reduced flux decline. The electrostatic repulsion between the HA and membrane surface increased the HA rejection. It is also mentioned that, governing the surface hydrophilicity will also help in the reduction of HA fouling (Song *et al*. 2011). Further, it is reported that less HA adsorption was observed on improved surface hydrophilicity and smoother surface membranes (Hwang *et al*. 2011). Therefore, developing a hybrid membrane with enhanced hydrophilicity, surface charge and reduced pore size will provide an effective solution to this problem.

It is well understood that the blending of zwitterionic materials with less hydrophilic polymeric materials will be a straightforward and cost-effective technique to mitigate the fouling (Schlenoff 2014, Galvin *et al*. 2014, Leng *et al*. 2018, Tang *et al*. 2018). Zwitterionic polymers are the substitute for broadly used poly(ethylene glycol) (PEG) polymers to prevent the nonspecific adsorption of protein molecules, as the PEG groups undergo enzymatic cleavage and oxidative cleavage in complex condition (Krishnan *et al*. 2008, Venault *et al*. 2016). Zwitterionic materials provide the ultra-hydrophilicity to the membrane surface and mitigate the adsorption of foulants by forming the hydration layer on the membrane surface (Jiang *et al*. 2010, Liu 2016). The zwitterionic materials for

instance phosphocholine, carboxybetaine and sulfobetaine were largely investigated for the antifouling performances. Among the zwitterionic materials, sulfobetaine methacrylate (SBMA) is commercially available and readily undergo polymerization (Scheme 4.1) (Lowe *et al*. 2002, Mi *et al*. 2014, Keating IV *et al*. 2016, Wang *et al*. 2016, Zhu *et al*. 2016, Bengani-Lutz *et al*. 2017). It binds with water molecules more strongly via electrostatic attraction than PEG chins. Also, it does not change the water hydrogen bonding structure (Kitano *et al*. 2002).

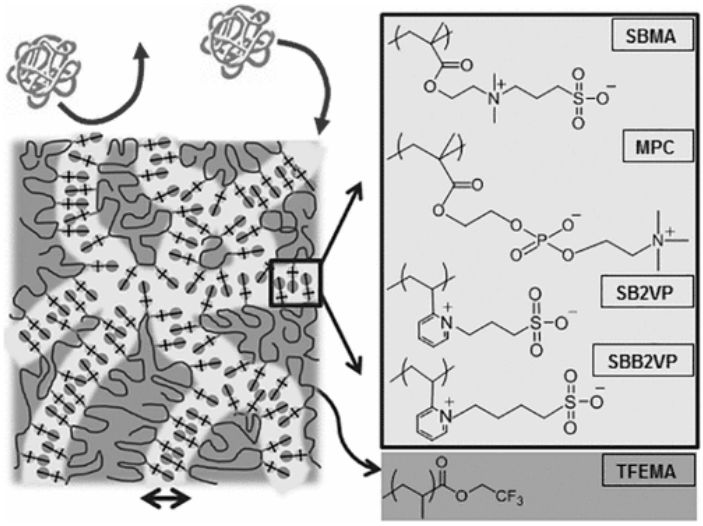

Scheme 4.1 Preparation of zwitterionic copolymer as a selective layer to mitigate fouling (Bengani-Lutz *et al*. 2017)

Recently, Fe_3O_4 has attracted great interest in the area of membrane science and technology, for the reason that Fe_3O_4 is non-toxic, low cost, good adsorbent, ease of chemical modification, antimicrobial and biocompatible (Jian *et al*. 2006, Sun *et al*. 2007, Daraei *et al*. 2012, Stanicki *et al*. 2014, Mukherjee *et al*. 2015). The zwitterionic modification of magnetic nanoparticles with carboxybetaine was demonstrated by Zhang *et al* (Zhang *et al*. 2010). The modification involved with many synthetic steps, which complicates the modification process. Similarly, Xiao *et al*. described the zwitterionic modification of magnetic nanoparticles, where the expensive and hygroscopic peptide coupling reagents were employed (Xiao *et al*. 2012). These observations have prompted us to modify the Fe_3O_4 with a simple reaction pathway and reagents. Mondini *et al*. reported the preparation of zwitterionic dopamine sulfonate coated iron oxide nanoparticles to explore the in vitro behavior (Scheme 4.2). Nevertheless, the costlier reagent dopamine hydrochloride and long reaction time (72 h) have made this modification expensive

(Mondini *et al*. 2020). Furthermore, the incorporation of zwitterionic Fe_3O_4 nanoparticles into the less hydrophilic PSF HF membrane matrix is unexamined. In our previous report, poly(SBMA-co-MBAAm) zwitterionic nanoparticles were synthesized by distillation-precipitation polymerization (Ibrahim *et al*. 2017). The formation of larger aggregates was observed due to a higher degree of crosslinking. Thus, it was planned to avoid the usage of the crosslinking agent.

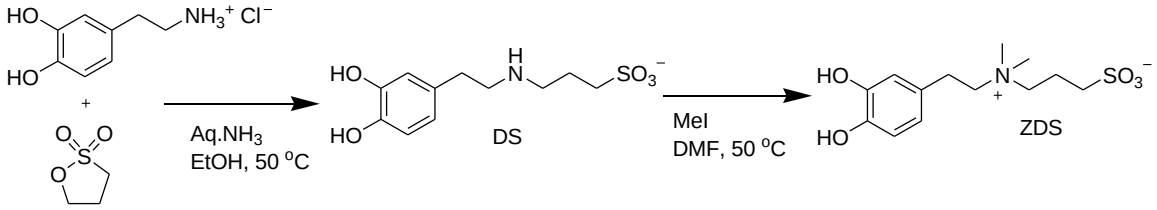

Scheme 4.2 Synthesis of zwitterionic dopamine sulfonate (ZDS) via dopamine sulfonate (DS) (Mondini *et al*. 2020)

Herein, the novel, zwitterionic functionalization of Fe_3O_4 in two steps is reported. In the first step, 3-(trimethoxysilyl)propyl methacrylate (MPS) was covalently grafted on the Fe_3O_4 surface to introduce the vinyl group. In the next step, zwitterionic sulfobetaine methacrylate (SBMA) was introduced via free radical polymerization. The as-synthesized nanoparticles were deployed to increase the surface charge, hydrophilicity, water uptake, porosity and antifouling properties of the polysulfone HF membrane. XPS was deployed to analyze the zwitterionic functionalization and the existence of nanoparticles on the membrane surface. The hybrid HF membranes were prepared by dry/wet phase inversion method. The as-prepared HF membrane performance was studied for HA rejection with different concentrations (10-50 ppm) and dye removal. The leaching of nanoparticles from the hybrid membrane matrix was analyzed. Further, the ability of a hybrid membrane in mitigating HA fouling was also demonstrated. This is a first-ever report to use zwitterionic PSBMA@Fe_3O_4 nanoparticles for fabricating antifouling polysulfone hollow fiber tight ultrafiltration membrane for HA and dye removal.

4.2 EXPERIMENTAL

4.2.1 Materials and methods

Polysulfone (PSF, Udel®, P-1700) obtained from Solvay chemicals. Sodium salt of humic acid, 3-(trimethoxysilyl)propyl methacrylate (MPS, 98 %), [2-(methacryloyloxy)ethyl]dimethyl-(3-sulfopropyl)ammonium hydroxide (SBMA, 95 %),

Reactive black -5 (RB-5, Dye content ≥50 %), reactive orange-16 (RO-16, Dye content ≥70 %), iron (II, III) oxide nanopowder (< 50 nm by TEM, Fe_3O_4), polyvinylpyrrolidone (PVP) K-30 (Mw 40,000 and ammonium persulfate (APS) were procured from Sigma-Aldrich. 1-Methyl-2-pyrrolidinone (NMP, 99.8 %), aqueous ammonia solution (25 %) were acquired from Loba Chemie.

The functional groups present in the nanoparticles were examined by BRUKER Alpha FT-IR. Morphology of PSBMA@Fe_3O_4 nanoparticles was observed by FESEM (ZEISS). PXRD (Rigaku Cu Kα as X-ray source) was used to identify the crystalline phase of the nanoparticles. The 2θ angles were investigated from 20° to 70° at a scan rate of 10° min^{-1}. The percentage weight loss of the nanoparticles was calculated using TGA (HITACHI EXSTAR 6300). Typically, the analysis was performed at a heating rate of 10 ^oC min^{-1} from RT to 900 ^oC under the nitrogen gas flow of 100 mL/min. Zeta potential analysis (HORIBA SZ 100) was carried out by dispersing ~ 4 mg of nanoparticles in DI water (pH 6.3). The presence of all the elements in the nanoparticle was characterized by EDX analysis (X-Max OXFORD instruments). XPS (THERMO FISHER Scientific K-Alpha) was utilized to analyze the surface elemental composition and confirmed the existence of PSBMA@Fe_3O_4 nanoparticles in the HF membrane matrix. The morphology of the HF membrane was characterized using HITACHI TM 3000 tabletop SEM.

The surface charge of the membranes was examined by the SurPASS electrokinetic analyzer using an adjustable gap cell and 0.001 M KCl as the background electrolyte. The pH was tuned using 0.2 M HCl or 0.2 M NaOH. The surface hydrophilicity of the HF membranes was evaluated using Data Physics OCA 25 contact angle analyzer. The thermal stability of the pristine and nanocomposite membrane was investigated by TGA. The effect of nanofiller on the membrane surface roughness was characterized using AFM. The permeation analysis was performed by the lab-scale cross-flow filtration system. For the PWP study, all the membranes first compacted for 30 min at 2 bar with DI water. Later, the pressure was reduced to 1 bar and PWP ($J_{w,}$ L /m^2 h bar) was calculated as mentioned in chapter 2, section 2.2.5.

The water uptake and porosity of the HF membranes were determined as mentioned in chapter 2, section 2.2.4. The membrane pore size (r_m) was estimated by the Guerout-Elford-Ferry equation in equation (4.1).

$$r_m = \sqrt{\frac{(2.9-1.75\varepsilon)8\eta l Q}{\varepsilon \times A \times \Delta P}} \quad (4.1)$$

Where 'η' is the viscosity (8.9×10^{-4} Pa s) of water, 'l' is the thickness of the membrane (m), 'Q' is the volume of permeated water per unit time (m^3/s), $'\varepsilon'$ is porosity, 'ΔP' is applied pressure (Pa) and 'A' is area of the membrane (m^2).

4.2.2 Synthesis of PSBMA@Fe_3O_4

In the first step, the vinyl group was attached to the Fe_3O_4 nanoparticles as reported elsewhere (Zhang *et al*. 2015). In brief, 2 g of Fe_3O_4 nanoparticles were dispersed in a mixture of deionized (DI) water/ethanol (100 mL/400 mL) for 30 min using an ultrasonic cleaner (USC-100, Anmanm industries). Added 5 mL of MPS and 15 mL of Aq. ammonia to the reaction mass (RM). The RM was aged at 60 ^oC for 24 h. Then, MPS@Fe_3O_4 nanoparticles were isolated by magnetic separation and washed with ethanol (3×25 mL) thoroughly. The isolated material was dried at 55 ^oC for 15 h to yield 1.9 g of MPS@Fe_3O_4 nanoparticles.

In the second step, PSBMA@Fe_3O_4 nanoparticles were synthesized via free radical polymerization. In short, 1.5 g of MPS@Fe_3O_4 nanoparticles were dispersed in 500 mL of DI water for 30 min. Added 9.0 g of SBMA and 0.36 g of APS to RM. The RM was purged with N_2 for 20 min followed by heating for 24 h at 60 ^oC under N_2 blanketing. The as-synthesized nanoparticles were isolated by magnetic separation and washed with DI water (3×15 mL) and ethanol (2×15 mL), then dried at 55 ^oC for 15 h to yield 1.45 g of PSBMA@Fe_3O_4 nanoparticles (scheme 4.3).

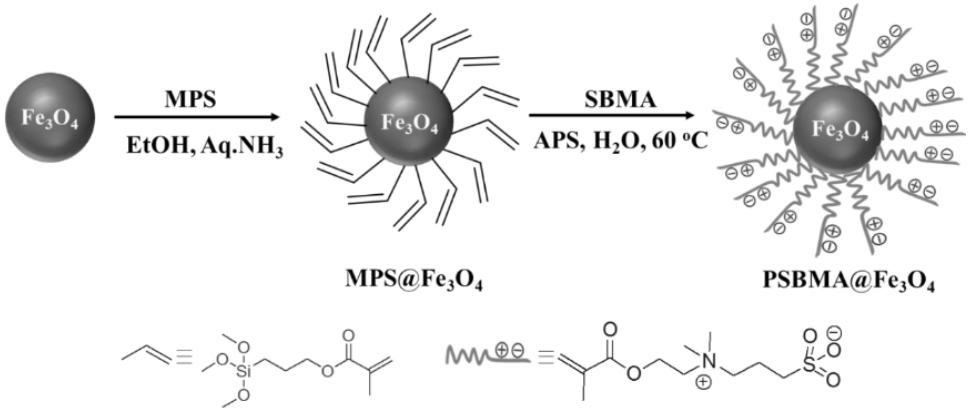

Scheme 4.3 The schematic route for the synthesis of PSBMA@Fe_3O_4 zwitterionic nanoparticles

4.2.3 PSBMA@Fe_3O_4 / PSF hollow fiber membranes preparation

In the typical preparation of the dope solution, PSBMA@Fe_3O_4 nanoparticles were first dispersed in NMP using a probe sonicator (QSONICA, 50 % amplitude with on time of 1 second and off time of 10 seconds) for 15 min at RT. Then, pre-dried PVP and PSF pellets were added to the solvent mixture. The solution was agitated using a mechanical stirrer at 50 ^oC for 14 h to obtain a homogeneous solution. The as-prepared dope solution was degassed for 30 min at room temperature. The dope solution composition is depicted in Table 4.1. HF membranes were produced by the dry/wet phase inversion method. The homogeneous dope solution and bore fluid were extruded through an annular spinneret to get the HF membranes. The HF membrane spinning parameters depicted in Table 4.2. The as-prepared HF membranes were submerged in DI water for 24 h to exclude the residual solvent with a change of water periodically. To circumvent the pore collapse, finally, the membranes immersed in 10 wt% glycerol solution for an additional 26 h before air-drying. The representative scheme of HF membrane fabrication is reported in our previous publication (Ibrahim *et al*. 2017).

Table 4.1 The dope solution composition

Membrane code	PSF (g)	NMP (g)	PVP (g)	PSBMA@Fe_3O_4 (g)	PSBMA@Fe_3O_4 (wt%)*
FM-0	20	79	1.0	0	0
FM-1	20	79	1.0	0.1	0.5
FM-2	20	79	1.0	0.2	1.0
FM-3	20	79	1.0	0.3	1.5

* W.r.t. PSF weight.

Table 4.2 Hollow fiber membrane spinning parameters

Spinning parameters	value
Dope extrusion rate	3.0 (mL/min)
Bore extrusion rate	2.5 (mL/min)
Spinneret dimension	1.1/0.55 (OD/ID)
Air gap	1.0 (cm)
Bore fluid	DI water
Bore fluid temperature	25.0 (^{o}C)
Collecting drum speed	7.0 (RPM)
Coagulation bath	Tap water
Humidity	60.0 (%)
Coagulation bath temperature	25.0 (^{o}C)

4.2.4 Antifouling and humic acid (HA) removal experiments

The antifouling study by adsorption was performed as follows. Typically, 10 ppm of HA solution was made by dissolving the calculated quantity of sodium salt of humic acid in DI water. The prepared HA solution was utilized to assess the antifouling capability of the nanocomposite membrane. In the HA adsorption study, the HF membrane area of 1.727 cm^2 was cut and both of the ends were sealed with epoxy resin. Then it was submerged in 10 mL of 10 ppm HA solution at pH 7. The solution containing the sample was kept in an orbital shaker (100 rpm) for 24 h at room temperature to attain the equilibrium of adsorption. The concentration of HA before and after adsorption at 254 nm was measured using a PerkinElmer LAMBDA 950 UV-Vis spectrophotometer. The quantity of HA adsorbed per unit area of the membrane, 'Q' (μg/cm^2) was determined using equation (4.2).

$$Q = \frac{(C_0 - C_e) \times V}{A} \tag{4.2}$$

Where, 'C_0' and 'C_e' are the initial and equilibrium concentration (μg/L) of HA, 'V' is the volume of the adsorbate solution (L) and 'A' is the area of the HF membrane (cm^2).

Further, the antifouling ability of the HF membranes was evaluated by filtration. Before starting the experiment, all the membranes compacted for 40 min at 2 bar. Then PWP (J_w) was measured for 60 min by filtering DI water at 1 bar. After PWP, DI water in the feed

tank was replaced with 10 ppm of HA solution and filtered for 60 min and HA solution permeability was measured as $J_{HA.}$ Subsequently, the membranes were cleaned carefully with 0.05 M aq. NaOH solution for 30 min. The PWP ('J_{w1}') of the cleaned membrane was measured for another 60 min. To estimate the antifouling property of the HF membranes, flux recovery ratio (FRR) was calculated using the equation (4.3).

$$\text{FRR (\%)} = \left(\frac{J_{w1}}{J_w}\right) \times 100 \tag{4.3}$$

Furthermore, the HF membrane fouling was studied carefully by estimating the irreversible fouling (R_{ir}), reversible fouling (R_r) and total fouling (R_t) using the below-mentioned equations (4.4, 4.5 and 4.6).

$$R_{ir}\ (\%) = \left(\frac{J_w - J_{w1}}{J_w}\right) \times 100 \tag{4.4}$$

$$R_r\ (\%) = \left(\frac{J_{w1} - J_{HA}}{J_w}\right) \times 100 \tag{4.5}$$

$$R_t\ (\%) = \left(\frac{J_w - J_{HA}}{J_w}\right) \times 100 \tag{4.6}$$

HA removal of the HF membranes was evaluated using different HA concentrations (10, 20, 40 and 50 ppm) at pH 7. Briefly, a known concentration of HA solution was filtered through the HF membranes at pH 7. The initial and final concentration of HA was assessed by a UV-Vis spectrophotometer (HACH DR 5000) at 254 nm. Furthermore, 100 ppm of RB-5 and RO-16 dye solutions were prepared separately and a dye removal study was performed at 1 bar pressure. The dye concentration in the feed and permeate was analyzed by a UV-Vis spectrophotometer at 592 nm for RB-5 and 494 nm for RO-16. The percentage of removal was determined by equation (4.7).

$$\text{Removal (\%)} = \left(1 - \frac{C_p}{C_f}\right) \times 100 \tag{4.7}$$

Where 'C_p' and 'C_f' are the permeate and feed solute concentrations.

4.2.5 Iron leaching study

In order to identify the leaching of iron from the membrane matrix, DI water was filtered for 24 h at pH 7 and 1 bar. 10 mL of sample was collected after 24 h of filtration.

A standard solution with a varying concentration of 0.2 mg/L to 5 mg/L was made by dissolving iron in 2 % aqueous nitric acid solution. The absorbance values were calculated using a SHIMADZU AA-6800 atomic absorption spectrophotometer (AAS). A calibration curve was plotted by taking the absorbance in the y-axis and concentration on the x-axis. Through which the concentration of iron in permeate was measured.

4.3 RESULTS AND DISCUSSION

4.3.1 Characterization of prepared nanoparticles

The surface charge of the as-synthesized nanoparticles was calculated by zeta potential analysis and presented in Figure 4.1a, b and c. The change in the zeta potential value in each stage confirms the functionalization of Fe_3O_4. Figure 4.1a depicts the zeta potential of Fe_3O_4, which was – 47 mV (pH 6.3). After covalently bonded with MPS (Figure 4.1b), the zeta potential value was increased to – 60 mV (pH 6.3). The increase in the surface charge was owing to the presence of a hydroxyl group, which was formed by the hydrolysis of the methoxy group. However, Figure 4.1c shows the zeta potential of – 36 mV (pH 6.3). The decrease of negative charge was accounted for the presence of PSBMA on the nanoparticle surface. SBMA has both anionic and cationic functional groups, which provide a neutral charge to it. Consequently, it reduces the negative charge of the Fe_3O_4. The acquired results are in agreement with the literature (Susanto *et al*. 2007). As stated by Hanaor *et al*., the nanoparticles with high zeta potential value will form a stable dispersion, as the agglomeration and settling were inhibited by the electrostatic repulsion (Hanaor *et al*. 2012). However, Fe_3O_4 nanoparticles were started settling down after 15 min owing to Oswald ripening (Babu *et al*. 2009). More interestingly, PSBMA@Fe_3O_4 nanoparticles were stable up to a longer time and the increased stability was ascribed to the presence of the polymer chain, which acts as the steric stabilizer. Therefore, the as-synthesized PSBMA@Fe_3O_4 nanoparticles will form a stable dispersion.

The formation of the vinyl group and grafting of SBMA on Fe_3O_4 was confirmed by FT-IR analysis. As illustrated in Figure 4.1d, e and f, the bands at 580 cm^{-1} and 1631 cm^{-1} are due to the Fe-O stretching and adsorbed water O-H bending vibration. In Figure 4.1e, the new peaks at 1700 cm^{-1} and 1155 cm^{-1} are ascribed to the ester group C=O stretching and Si-O-Si group. These two new peaks substantiated the presence of MPS on the surface of Fe_3O_4. However, the reduced stretching frequency of the ester (C=O) group was

attributed to the presence of conjugation in the MPS (Suart 2004, Silverstein *et al*. 2014,). In Figure 4.1f, the new characteristic peak at 1721 cm^{-1} is designated to C=O stretching, peaks at 1183 cm^{-1} and 1044 cm^{-1} are linked with sulfonate group stretching vibration (Silverstein *et al*. 2014, Zhu *et al*. 2017). Additionally, in the case of PSBMA@Fe_3O_4, the ester group C=O stretching vibration was observed at the little higher frequency. The characteristic shift was ascribed to the absence of conjugation. Therefore, this shift further confirmed the polymerization of MPS and SBMA monomers.

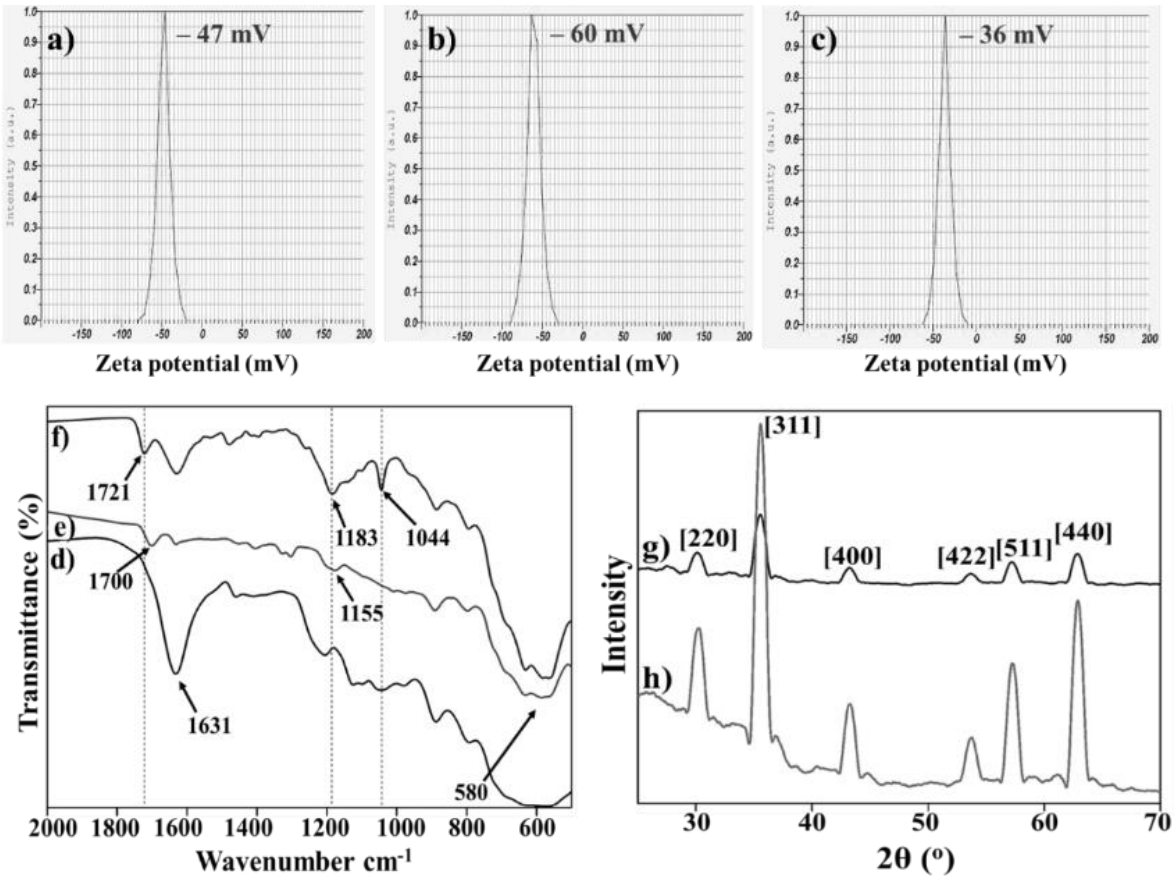

Figure 4.1 Zeta potential of a) Fe_3O_4, b) MPS@Fe_3O_4 and c) PSBMA@ Fe_3O_4 at pH 6.3, FT-IR spectra of d) Fe_3O_4, e) MPS@Fe_3O_4 and f) PSBMA@ Fe_3O_4 and PXRD of g) Fe_3O_4 and h) PSBMA@Fe_3O_4

The PXRD diffraction pattern of the Fe_3O_4 and PSBMA@Fe_3O_4 nanoparticles is illustrated in Figure 4.1g and h. The characteristic diffraction peaks for Fe_3O_4 were detected at 30.1º, 35.8º, 43.1º, 53.6º, 57.6º, 63.0º resultant to the Miller indices [220], [311], [400], [422], [511] and [440] correspondingly (Figure 4.1g). As presented in Figure 4.1h, the modified nanoparticles were also exhibited the same diffraction pattern as Fe_3O_4 and well-

matched with JCPDS file number 75-1609. In summary, there was no noticeable change was observed in the crystal structure of the nanoparticles after functionalization.

The thermal stability of the nanoparticles at various stages was examined using TG analysis and shown in Figure 4.2a. In Fe_3O_4 (Figure 4.2a), the weight loss between 50 and 150 ^oC was caused by adsorbed water molecules. The major weight loss between 200 and 270 ^oC was ascribed to the decomposition of surface hydroxyl groups and the weight loss at 900 ^oC was 5.7 wt%. After vinylation, the weight loss at 900 ^oC was 9.0 wt%. From this, the grafting ratio of the vinyl group was calculated as 3.3 wt%. In the final step, the weight loss at 900 ^oC was 11.2 wt% and the grafting ratio of PSBMA was calculated as 2.2 wt%. Therefore, the change in weight loss confirms the modification of the nanoparticles.

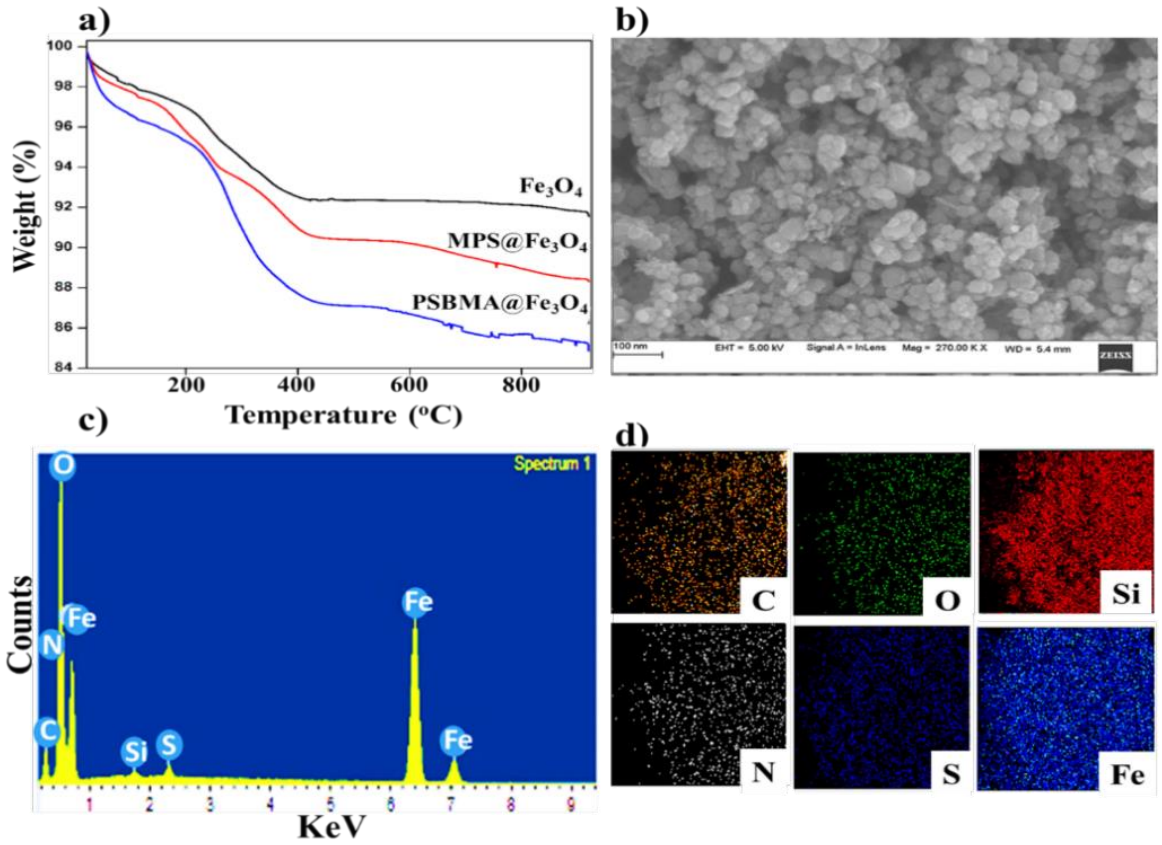

Figure 4.2 a) TGA curves of Fe_3O_4, MPS@Fe_3O_4, PSBMA@Fe_3O_4 and b) FESEM image (scale bar 100 nm), c) EDX spectrum and d) elemental mapping of PSBMA@Fe_3O_4 nanoparticles

The morphology and elements present in the zwitterionic nanoparticles were examined by FESEM and EDX analyses. As described in Figure 4.2b, the nanoparticles exhibited uniform size and shape. The presence of elements such as sulfur (S), nitrogen (N), silicon

(Si) and carbon (C) confirmed the functionalization of Fe_3O_4 nanoparticles (Figure 4.2c). Further, the uniform distribution of all the elements in the nanoparticles was explored by EDX elemental mapping (Figure 4.2d).

4.3.2 Characterization of membranes

The TGA curve of membranes is represented in Figure 4.3. As shown, the nanocomposite membrane (FM-2) exhibited improved thermal stability than the pristine (FM-0) membrane. The two membranes exhibited a small amount of weight loss between 50 and 150 ^oC due to adsorbed water. For FM-0 membrane, one-step weight loss was observed between 470 and 626 ^oC, due to the decomposition of the polymer main chain. The weight loss at 900 ^oC for FM-0 was 71.2 wt%, which was decreased to 62.8% for the FM-2 membrane. Further, the onset decomposition temperature of FM-0 was 470.5 ^oC, however, the FM-2 membrane exhibited a higher onset decomposition temperature of 480.2 ^oC. Overall, the FM-2 membrane demonstrated decreased decomposition ratio, which was due to the incorporation of the zwitterionic PSBMA@Fe_3O_4 nanoparticles.

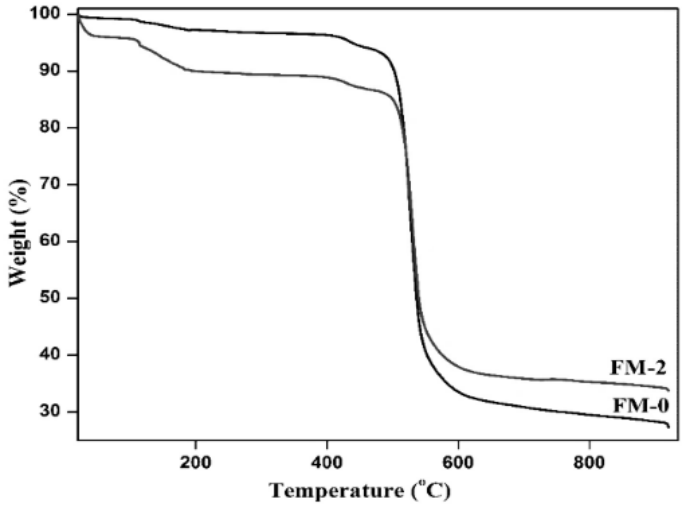

Figure 4.3 TGA curves of a) FM-0 and b) FM-2 membranes

The cross-sectional images of HF membranes spun with various concentration of zwitterionic PSBMA@Fe_3O_4 are depicted in Figure 4.4. All the as-prepared membranes exhibited asymmetric morphology with the finger-like structure in the inner and outer side and sponge-like structure in the middle. It is curious to observe that, the added nanoparticles increased the number of macrovoids and reduced the skin layer thickness of HF membranes. Furthermore, the improved hydrophilicity caused an increased rate of

demixing between the solvent and non-solvent. Consequently, the more porous membrane was formed.

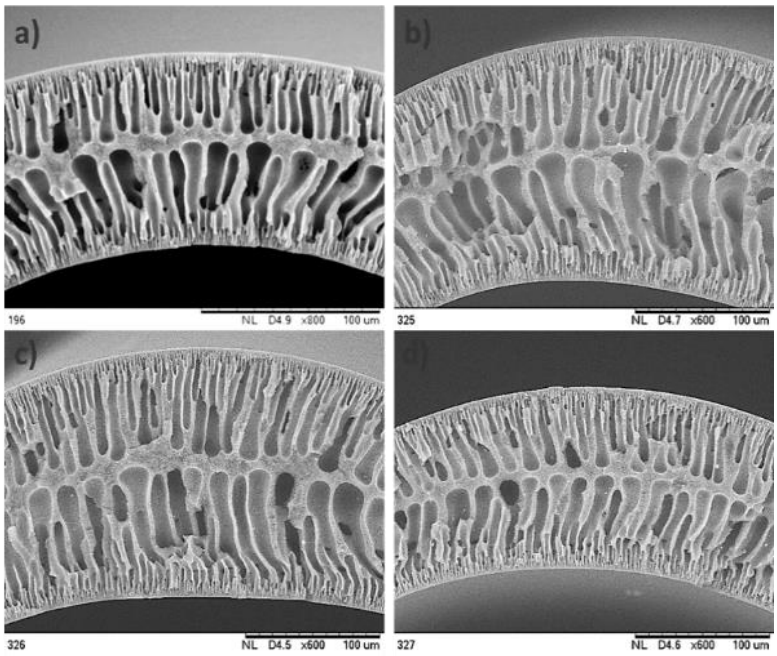

Figure 4.4 SEM cross-sectional images of a) FM-0, b) FM-1, c) FM-2 and d) FM-3

The FM-2 membrane high resolution XPS spectra are presented in Figure 4.5. Figure 4.5a represents that, the presence of two peaks at 710.16 and 727.05 eV were due to Fe $2p_{3/2}$ and Fe $2p_{1/2}$. As depicted in Figure 4.5b, the high resolution C 1s spectrum can be deconvoluted into six peaks at 283.24 (C-Si), 284.82 (C=C/C-C), 286.27 (CN^{+}/C-SO_3^{-}), 286.96 (C-N/C-O), 287.53 (C=O) and 289.54 eV (O-C=O) (Lin *et al*. 2017). The O 1s peak was deconvoluted into four peaks at 530.61 (Fe-O), 531.55 (C=O/O-C=O), 531.9 (SO_3^{-}) and 532.72 eV (Si-O/C-O) (Figure 4.5c) (Zhao *et al*. 2010, Sunkara *et al*. 2013). The obtained XPS data confirmed the zwitterionic functionalization of Fe_3O_4 and the presence of nanoparticles on the FM-2 membrane surface. In addition, the FM-2 HF membrane surface elemental composition (atomic %) was calculated as 87.81 %, 0.94 %, 7.42 %, 0.60 %, 1.46 % and 1.74 % of C 1s, N 1s, O 1s, Si 2p, Fe 2p and S 2p elements respectively.

The analysis of the zeta potential of the membrane surface is useful in understanding the relationship between the membrane surface and the solution in contact with it. The membrane surface charge determines the fouling and rejection properties of the membrane. The zeta potential of the outer surface of the membranes FM-0 and FM-2 HF membrane at different pH is represented in Figure 4.5d. As shown, the isoelectric point (IEP) of the FM-

0 membrane was identified at pH 3.07. In FM-0, the positive charge below the IEP was ascribed to the adsorption of cations by the electronegative sulfone group. However, negative zeta potential value was observed above the IEP, which was owing to the adsorption of anions (OH^-/Cl^-) on the membrane surface from the electrolyte (Kumar *et al*. 2013). The IEP of the FM-2 membrane was observed at pH 2.84. As discussed above, the as-synthesized nanoparticles were negatively charged at pH 6.3. Consequently, the FM-2 membrane surface negative charge was enhanced when compared to the FM-0 membrane, which was due to the presence of negatively charged PSBMA@Fe_3O_4 nanoparticles.

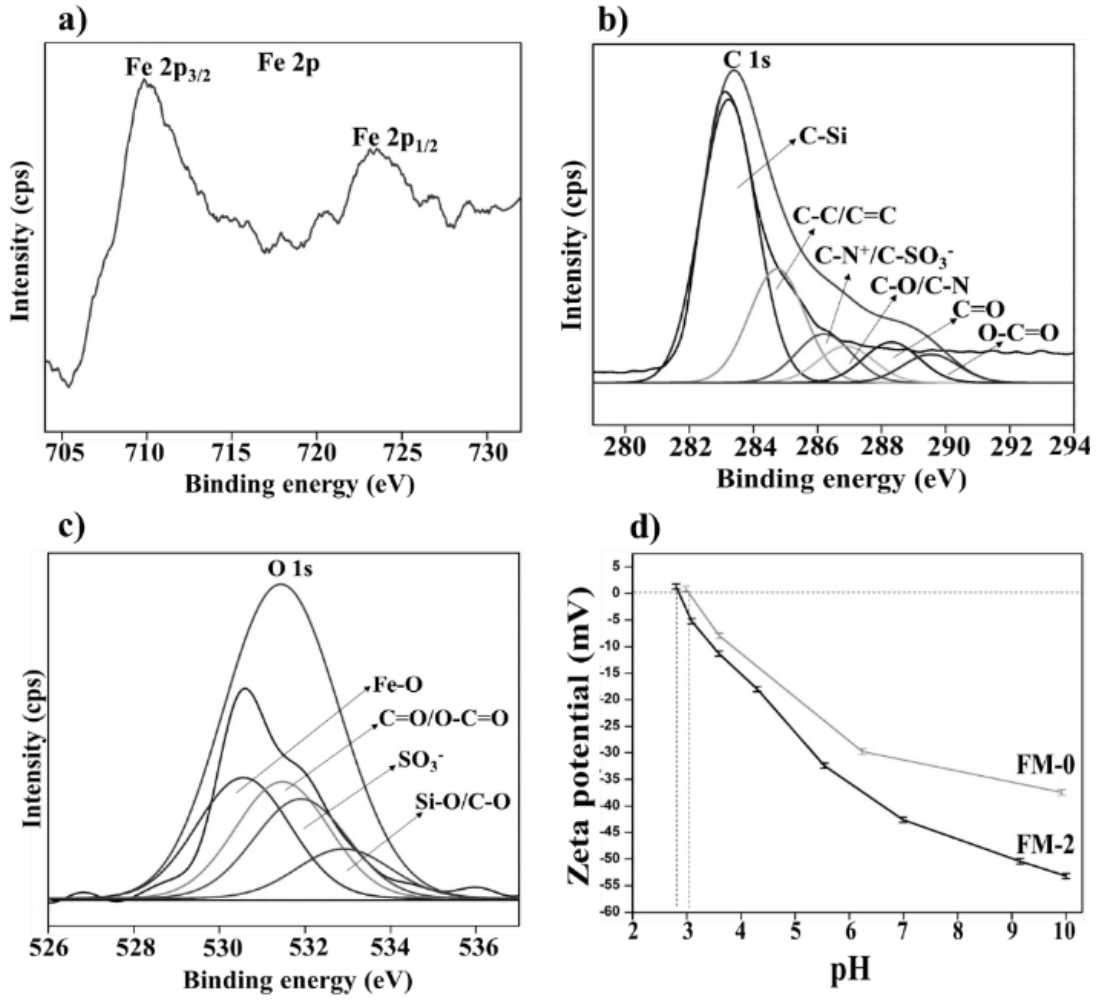

Figure 4.5 XPS high resolution spectra of FM-2 membrane a) Fe 2p, b) C 1s, c) O 1s and d) zeta potential of FM-0 and FM-2 membranes as a function of pH

The effect of PSBMA@Fe_3O_4 zwitterionic nanoparticles on the contact angle, water uptake, pore size and porosity of the fabricated membrane are presented in Table 4.3. The porosity was improved with the addition of PSBMA@Fe_3O_4 nanoparticles. In the FM-1

membrane, porosity was enhanced by 14 % compared to the pristine FM-0 membrane. The highest porosity of 61.5% was observed for the FM-2 membrane with 1.0 wt% of zwitterionic nanoparticles. The same trend was observed for pore size and water uptake of the hybrid membrane. Since the added nanoparticles are hydrophilic in nature, it increases the diffusion rate between non-solvent and solvent exchange and leads to the formation of porous membranes. However, the porosity was decreased with a higher concentration (1.5 wt%) of nanoparticles. Consequently, pore size and water uptake of the membrane were also reduced. The higher concentration of nanoparticles will be partially agglomerated (Hebbar *et al*. 2016) and increase the viscosity of the dope solution, thus slow down the demixing process during phase inversion (Jiang *et al*. 2014). Therefore, it reduces the membrane porosity, pore size and water uptake. Similarly, the contact angle of the hybrid membrane was reduced with the addition of PSBMA@Fe_3O_4 nanoparticles. The lowest contact angle of 67.2^o was obtained for the FM-3 membrane, which is 12.6^o less than the pristine FM-0 membrane. The decreased contact angle of the hybrid membrane was ascribed to the formation of a tight hydration layer and enhanced porosity (Zhao *et al*. 2015).

Table 4.3 Properties of hollow fiber membranes

Membrane	PWP (L/m^2 h bar)	Contact angle (^{o})	Porosity (%)	Water uptake (%)	Pore size (nm)	HA adsorption ($\mu g/cm^2$)	Surface roughness (nm)		
							R_a	R_q	R_{max}
FM-0	22.6 ±1.6	79.8 ±1.3	43.2 ±0.3	32.4 ±0.9	10.1 ±0.1	43.5 ±0.5	3.88	4.94	41.6
FM-1	53.4 ±0.8	73.5 ±0.9	57.4 ±0.9	47.9 ±0.2	10.9 ±0.3	29.1 ±0.8	3.76	4.68	31.9
FM-2	61.1 ±1.1	69.3 ±0.3	61.5 ±0.2	58.1 ±0.4	11.6 ±0.2	17.3 ±0.2	2.94	3.66	30.8
FM-3	45.9 ±0.6	67.2 ±0.7	58.1 ±0.6	55.3 ±1.0	10.4 ±0.1	17.9 ±0.3	3.15	3.94	47.7

4.3.2.1 Permeability of membranes

The PWP of all the prepared membranes is illustrated in Table 4.3. The improved PWP of the FM-2 membrane over pristine (FM-0) membrane was ascribed to the increased surface hydrophilicity, porosity and water uptake. The PWP was enhanced with an increased concentration of PSBMA@Fe_3O_4 up to 1 wt%. In general, the water molecules first adsorb on the membrane surface and then permeate across the membrane. The zwitterionic nanoparticles contain both sulfonate and quaternary ammonium groups, which has a strong affinity for water molecules via electrostatic attraction, As a result, it forms a strong hydration layer on the membrane surface. This layer has increased the interaction between the membrane surface and water molecules. Subsequently, the water molecules adsorbed more easily on the membrane surface and become permeate. Thus, the resistance to the water permeability was reduced significantly. However, with a higher concentration (1.5 wt%) of nanoparticles, the PWP was reduced. The reason for the reduction in PWP was because of the partial agglomeration of zwitterionic nanoparticles, which has blocked the membrane pores. Consequently, there was a noticeable reduction in the passage of the water molecules.

4.3.2.2 Antifouling studies of membranes

The antifouling capability of the as-prepared hybrid membranes was studied by both adsorption and filtration. The HA static adsorption of the membrane at pH 7 was carried out and values are tabulated in Table 4.3. As shown, the adsorption of hybrid membranes was less related to the pristine membrane. The adsorption was decreased with an increase in the concentration of nanoparticles. The reason for the reduction in the HA adsorption was owing to the increased negative charge (Ibrahim *et al*. 2017) and hydrophilicity (Chiag *et al*. 2011, Jain *et al*. 2017). As the HA is negatively-charged molecules, (Hebbar *et al*. 2015) when it comes in contact with the negatively charged membrane surface, HA molecules excluded through electrostatic repulsion. Also, the improved hydrophilicity, which offered from the zwitterionic nanoparticles forms a strong hydration layer on the membrane surface. The as-formed hydration layer hardens the contact between the HA and the membrane surface.

The time-dependent pure water and HA solution permeability of all the membrane is depicted in Figure 4.6. The total fouling (R_t), reversible fouling (R_r) and irreversible fouling

(R_{ir}) are estimated and shown in Figure 4.7a. As shown, the hybrid membranes exhibited decreased R_t compared to the pristine (FM-0) membrane. The R_t value was decreased from 60.3 % to 50.1 % for the FM-2 membrane, which was as a result of the improved surface charge and hydrophilicity of the FM-2 membrane. Thus, the FM-2 membrane prevented the adsorption of HA on the membrane surface or pore walls (Hwang *et al*. 2011). Conversely, for the FM-3 membrane, the R_t value was slightly higher than the FM-2 membrane. Because, with 1.5 wt % of nanoparticles, the hybrid membrane surface roughness was higher than the FM-2 membrane (Table 4.3), which overwhelmed the effect of surface charge and hydrophilicity. The rough surface of the membrane has a higher surface area and active sites, which increased the adsorption of HA molecules (Rechendorff *et al*. 2006, Yang *et al*. 2011). As expected, the same trend was observed in the case of R_r and R_{ir}. The FM-2 membrane exhibited the higher R_r and lower R_{ir} tendency with respect to the pristine FM-0 membrane. The AFM 3D images of all the membranes are presented in Figure 4.7b.

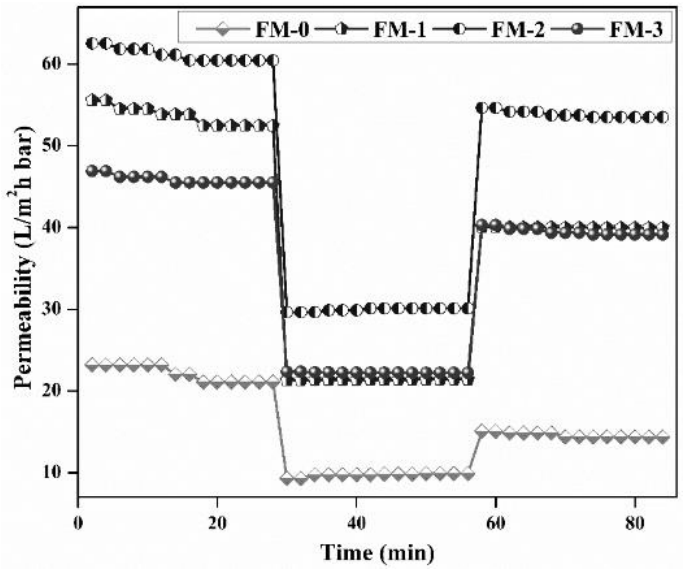

Figure 4.6 Time-dependent pure water and HA solution permeability of membranes

The recycling property of the hybrid membranes was estimated by calculating the flux recovery ratio (FRR). As presented in Figure 4.7a, the FRR value was increased from 66.2 % for FM-0 to 88.4 % for the FM-2 membrane. The increase in FRR value was owing to the reduced surface roughness, improved surface hydrophilicity and the surface charge. The formation of a negatively charged hydrophilic skin layer avoids the adsorption of HA molecules. Therefore, the hybrid membrane could recover easily with simple aqueous

caustic washing. Still, there was a small decline in the FRR of the FM-3 membrane, which can be ascribed to the enhanced surface roughness (Table 4.3). It is well documented that, fouling will be more on the highly rougher surface (Rana *et al*. 2010). Therefore, the hybrid FM-2 hollow fiber membrane exhibited improved permeability and antifouling.

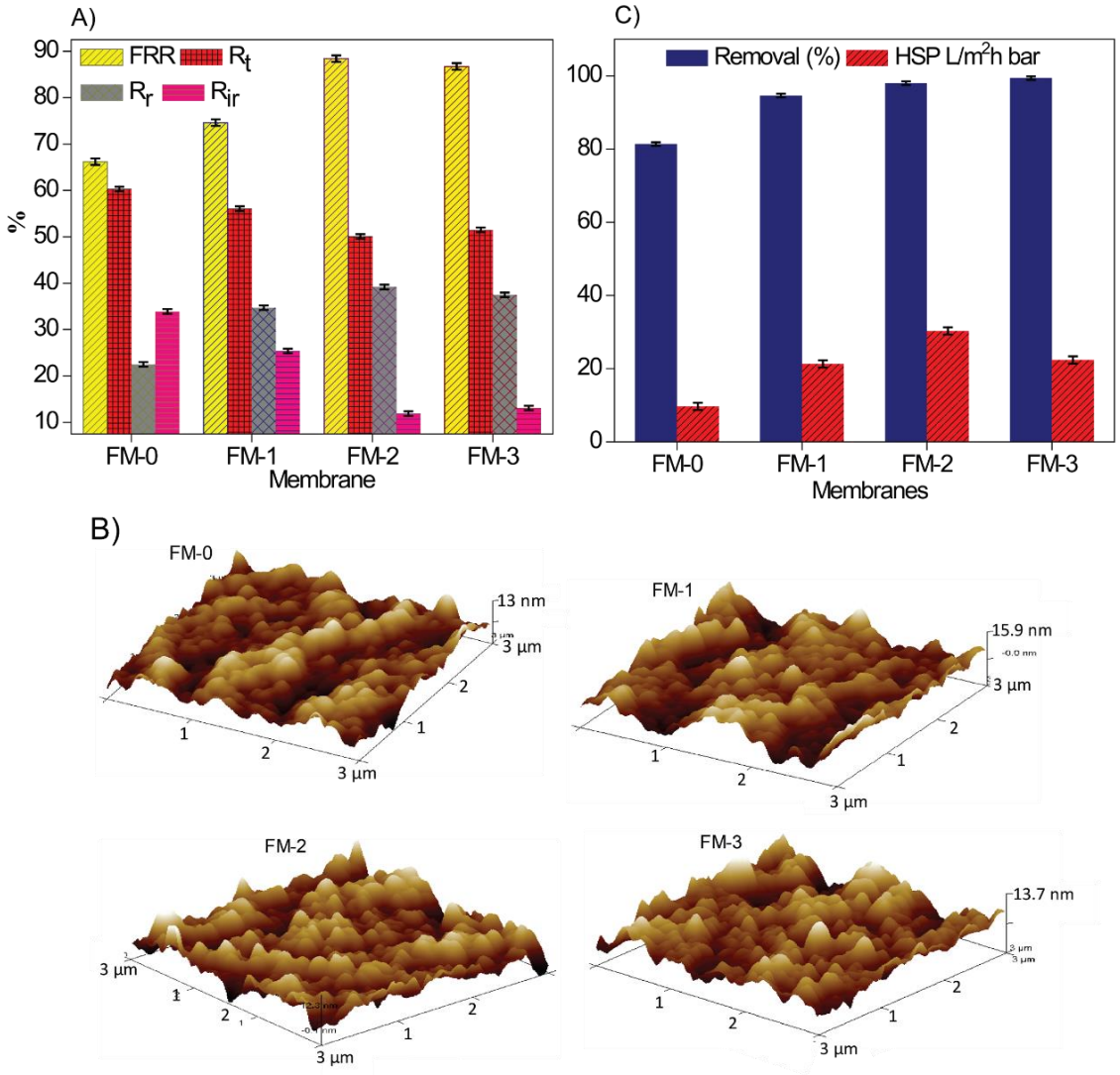

Figure 4.7 A) Percentage of flux recovery ratio (FRR), total fouling (R_t), reversible fouling (R_r), irreversible fouling (R_{ir}), B) AFM 3D images of membranes and C) HA removal and HA solution permeability (HSP) of membranes at pH 7 and 1 bar

4.3.2.3 Humic acid removal

The HA removal and HA solution permeability (HSP) of the membrane is demonstrated in Figure 4.7c. All the hybrid membranes exhibited enhanced HA removal than the pristine membrane. The HA removal was improved from 81.4 % of FM-0 to 99 % of the FM-2 membrane with HSP of 9.7 L/m^{2}h bar and 30.3 L/m^{2}h bar. Generally, HA removal efficacy

of the hybrid membrane is decided by membrane surface hydrophilicity, pore size and surface charge. In this work, the pore size of the hybrid membranes is larger than the size of HA molecules (typically less than 1 nm). Thus, the predominant mechanism for the removal of HA was based on the electrostatic repulsion and hydration layer formation. As reported in the literature, the presence of –COOH and –OH group make the HA negatively charged molecules at pH 7 (Hwang *et al*. 2011). The as-prepared HF membrane also exhibited negative charge at pH 7, which was confirmed in the zeta potential analysis. Consequently, there was a strong electrostatic repulsion between the membrane surface and HA molecules. Further, the as-formed hydration layer reduced the adhesion force between the membrane surface and HA. Therefore, HA molecules were prevented from the permeation across the membrane due to increased electrostatic repulsion and hydration layer. At the same time, the FM-3 membrane showed the HA removal of 99.4 %, which is slightly higher than the FM-2 membrane. The slight increment in the HA removal was ascribed to the reduced porosity, pore size and increased nanoparticle concentration, which would further increase the surface charge density.

The HA removal in different concentrations at pH 7 and 1 bar also studied using the FM-2 membrane. The FM-2 membrane was selected as it exhibited higher permeability compared to other hybrid membranes. As represented in Figure 4.8a, the HA removal percentage was reduced with an increase in the concentration of HA. The FM-2 membrane demonstrated the HA removal of 88.3 % at the HA concentration of 50 ppm. The reason for the reduction in the HA removal with increasing concentration of HA was owing to the inadequate availability of active sites. While increasing the concentration of the HA molecules, there was a severe competition between the negatively charged HA molecules and negatively charged active sites of the membrane. Thereby, some of the HA molecules could permeate across the hybrid membrane and the same trend was observed in the literature (Kumar *et al*. 2016, Hebbar *et al*. 2017). In summary, the FM-2 hollow fiber membrane performed well at the HA concentration of 10 ppm. The digital photographic images of feed (50 ppm) and permeate after UF using the FM-2 membrane is displayed in Figure 4.8b.

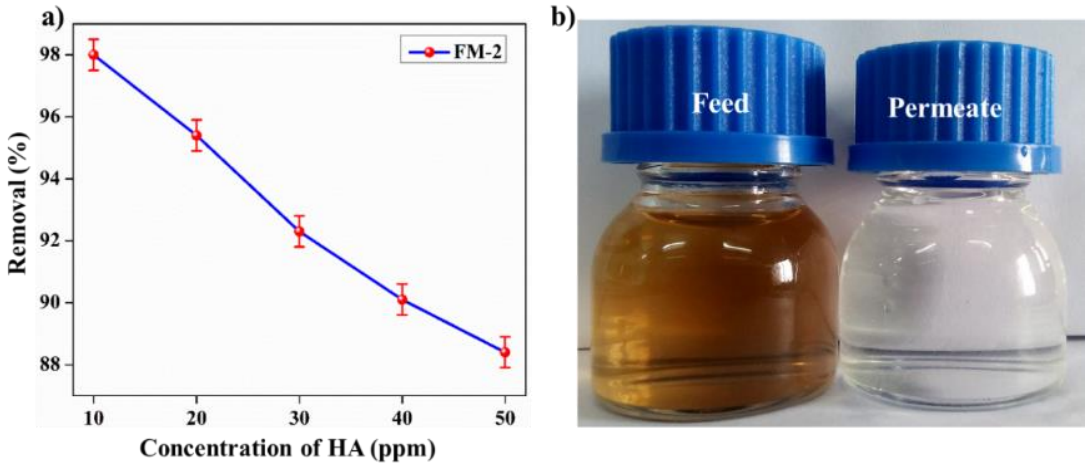

Figure 4.8 a) FM-2 membrane HA rejection in different concentration and b) digital photographic images of feed (50 ppm) and permeate after UF using FM-2 membrane at pH 7 and 1 bar

Further, the stability of the FM-2 membrane with a surface area of 8.635 cm^2 was studied using 20 ppm of HA as feed for 10 h at pH 7 and 1 bar. As indicated in Figure 4.9, the HA concentration was decreased after 5 h and then attained a steady state. The HA concentration in permeate was less than the permissible limit of 2 ppm throughout the analysis. There was a slight decrement in the permeability as well, which was caused by the growth of a thin cake layer on the membrane surface. In summary, the negatively charged membrane surface facilitated the electrostatic repulsion against the negatively charged HA molecules. Henceforth, the FM-2 membrane lifetime was able to extend beyond 10 h. The observed results are in agreement with the literature (Panda *et al*. 2015).

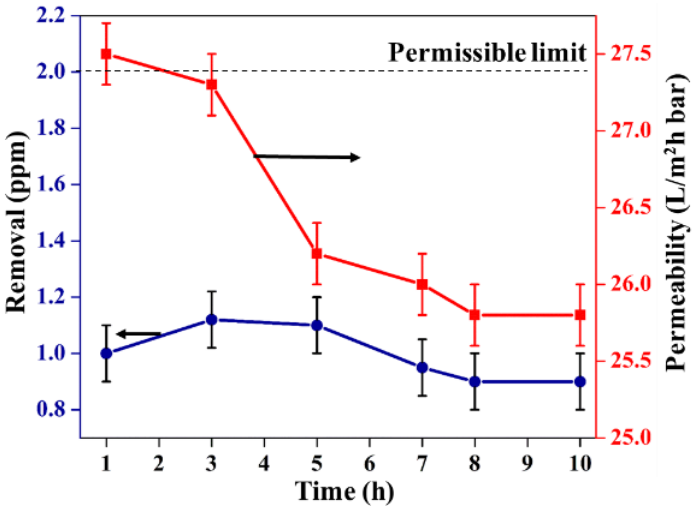

Figure 4.9 Longtime study of the FM-2 membrane using 20 ppm of HA as feed at pH 7 and 1 bar

4.3.2.4 Dye removal study of hollow fiber membranes

Based on the PWP and FRR, the FM-2 HF membrane was chosen for the dye removal study. The dye removal and DSP of the FM-2 membrane at different pH are represented in Figure 4.10. As depicted in Figure 4.10a, the RB-5 rejection was above 99 % at all the pH studied. However, at pH 10 and 3, the DSP was slightly reduced. The reduced DSP at pH 10 was attributed to the swelling of the HF membrane, which increased the thickness of the membrane (Wang *et al*. 2016). At pH 3, the reduced DSP was due to the precipitation of dye molecules. In general, the sodium salt of dye molecules is highly water-soluble. At acidic pH, the sulfonate group was protonated to become a sulfonic acid group and solubility of a dye molecule was reduced. Furthermore, the precipitated dye molecules blocked the membrane pores and led to the reduced permeability.

In the case of RO-16 (Figure 4.10b), the HF membrane exhibited the rejection of above 84 %. At pH 7 and 10, the rejection was 84.7 % and 86.8 %. Nevertheless, at pH 3, the rejection was increased to 96.2 %. The increased rejection of RO-16 at pH 3 was again ascribed to the decreased solubility of RO-16 at pH 3. Similarly, the DSP has followed the same trend as observed in RB-5 rejection. The enhanced removal ability of the FM-2 HF membrane towards the negatively charged reactive dyes was also attributed to the surface charge of the membrane. The incorporated nanoparticles bestowed the negative charge to the HF membrane. Thus, the adsorption of dye molecules on the membrane surface was circumvented through electrostatic repulsion, which improved the dye removal with less reduction in the DSP. Furthermore, the higher rejection of RB-5 compared to RO-16 was due to the size exclusion mechanism. Therefore, the larger molecular weight RB-5 exhibited a higher rejection percentage than the lower molecular weight RO-16. The observed results are good accord with the reported literature (Ibrahim *et al*. 2017, Liu *et al*. 2017).

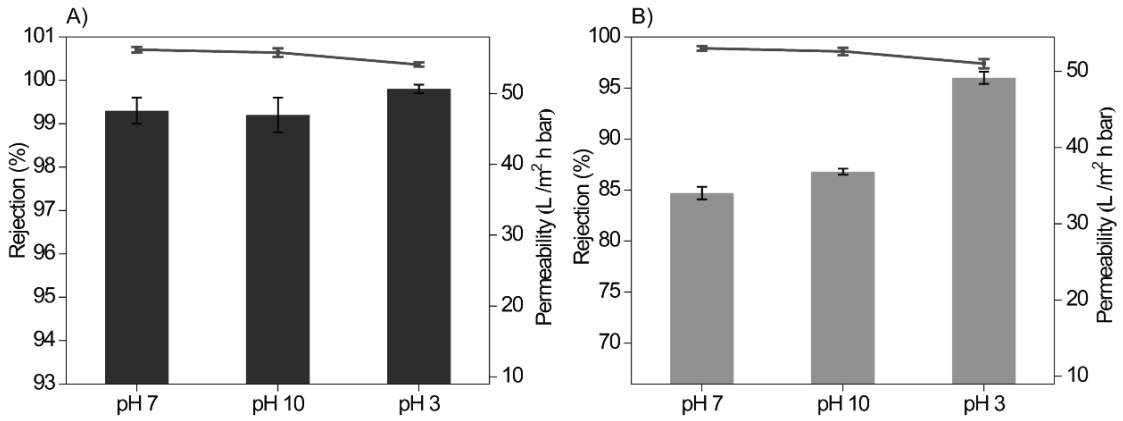

Figure 4. 10 FM-2 membrane rejection and permeability of A) Reactive black -5 and B) Reactive orange-16 at different pH

Table 4.4 Comparison of dye removal ability of nanocomposite membrane with literature

Membrane	Dye	PWP[a]	DSP[b]	Dye rejection (%)	Type of membrane	Ref.
Sepro NF 2 A	Direct red 80	10.5	9.6	99.98	Loose NF	(Lin *et al.* 2015)
UH004 (Hydrophilic PES)	Direct red 80	27	26	99.9	Tight UF	(Lin *et al.* 2016)
PSF/poly(MBAAm-co-SBMA)	Reactive black 5/ Reactive orange 16	56	51/51.8	98/80.7	Tight UF	(Ibrahim *et al.* 2017)
GR82PP	Direct red 80/ Reactive orange 16	37.4	~31/~33	~99.9/~94	Tight UF	(Jiang *et al.* 2018)
PSF/ PSBMA@Fe_3O_4	**Reactive black 5/ Reactive orange 16**	**61.1**	**56.2/53**	**99.3/ 84.7**	**Tight UF**	**Present study**

[a]PWP: Pure water permeability (L/m^2h bar); [b]DSP: Dye solution permeability (L/m^2h bar)

4.3.2.5 Iron leaching study

According to the World Health Organization (WHO), the permissible limit of iron in drinking water is 0.3 to 3.0 mg/L (Mukherjee *et al*. 2017). However, the concentration of iron in permeate measured by AAS was below the detection of 0.11 mg/L after 24 h of filtration, which confirmed that there was no any leaching of iron nanoparticles from the membrane matrix. Thus, these hybrid hollow fiber membranes are suitable for long-term usage.

4.4 CONCLUSIONS

Poly(sulfobetaine)@Fe_3O_4 (PSBMA@Fe_3O_4) zwitterionic nanoparticles were synthesized, characterized and used as an additive to fabricate polysulfone hollow fiber ultrafiltration membranes. The influence of zwitterionic poly(sulfobetaine)@Fe_3O_4 nanoparticles on membrane surface charge, hydrophilicity, water uptake, porosity, pore size, morphology and humic acid removal was examined and improved with respect to the concentration of the poly(sulfobetaine)@Fe_3O_4 nanoparticles. The hybrid membranes were less susceptible to adsorption of humic acid and the possible mechanism was predicted as hydration layer formation and electrostatic repulsion, which was offered by the zwitterionic nanoparticles. The FM-2 membrane exhibited improved antifouling property with a flux recovery ratio of 88.4 % and irreversible fouling of 11.9 %. The highest humic acid removal was demonstrated by the FM-3 membrane. However, owing to the partial agglomeration of nanoparticles, the permeability of the FM-3 membrane was reduced when compared to the FM-2 membrane. In addition, the FM-2 membrane demonstrated the high removal of reactive dyes with a concentration of 100 ppm. In conclusion, the hybrid FM-2 hollow fiber membrane can be used for the effective removal of humic acid with a concentration of 10 ppm at pH 7 and Reactive black 5 and Reactive orange 16 with a concentration of 100 ppm at pH 7.

CHAPTER 5

ONE-STEP SYNTHESIS OF NOVEL ZWITTERIONIC GRAPHENE OXIDE NANOHYBRID: APPLICATION TO POLYSULFONE ULTRAFILTRATION HOLLOW FIBER MEMBRANE

Abstract: *In this chapter, zwitterionic graphene oxide (GO) nanohybrid was synthesized using monomers [2-(methacryloyloxy)ethyl]dimethyl-(3-sulfopropyl)ammonium hydroxide (SBMA) and N,N'-methylenebis(acrylamide) (MBAAm) (GO@poly(SBMA-co-MBAAm) and incorporated into polysulfone (PSF) hollow fiber membrane for the effectual rejection of dye from the wastewater. The dye removal ability of the nanocomposite membranes was studied using Reactive black 5 (RB-5) and Reactive orange 16 (RO-16) as model dyes and antifouling performance was evaluated using Bovine Serum Albumin (BSA) as a model protein. The as-prepared tight ultrafiltration hollow fiber membrane exhibited high rejection of Reactive black 5 (99 %) and Reactive orange 16 (74 %) at a dye concentration of 10 ppm and pure water flux (PWF) of 49.6 L/m^{2}h.*

5.1 INTRODUCTION

In recent times, wastewater generated from the textile industries is becoming detrimental environmentally demanding effluent. It is mainly composed of a large amount of organic dyes and inorganic salts, properly 5.6 wt % of Na_2SO_4 and 6 wt % of NaCl (Zhu *et al*. 2016, Ibrahim *et al*. 2017). Among the organic dyes used, reactive dyes have gained significant attention owing to the low tendency of fixing on the fibers. Accordingly, a considerable amount of inorganic salts should be used to enhance the binding capability, which led to the existence of a large number of dyes and salts in the wastewater stream (Burkinshaw *et al*. 2011).

The discharge of untreated wastewater effluents into the environment, not only affect human beings but also restrict the permeation of light which will affect the aquatic flora and fauna to a greater extent (Wang *et al*. 2008, Geng *et al*. 2012). Further, the discharged dye molecules are highly vulnerable to hydrolysis or oxidation to degrade into different toxic substances. Reactive dyes are capable of causing skin diseases like contact dermatitis and respiratory diseases like asthma (Thorén *et al*. 1986). In the matter of sustainability, dyes and inorganic salts should be separated from the wastewater and recycled rather than dye removal or water purification by reverse osmosis (RO). Additionally, the recycled dye can be used in the dyeing process and salts can work well as draw solution in forward osmosis (FO) (Lin *et al*. 2015, Lin *et al*. 2015, Zhu *et al*. 2015).

Membrane separation is one of the efficient and popular techniques for the purification of wastewater (Hebbar *et al*. 2018, Ibrahim *et al*. 2018, Ibrahim *et al*. 2019). In the 1980s,

the nanofiltration (NF) membrane was introduced and has become an attractive technology, due to the improved selectivity, high permeation, low operating pressure and less maintenance cost (Mariën *et al*. 2016, Du *et al*. 2017). NF membrane has a pore size of ~0.5-2.0 nm and molecular weight cut-off (MWCO) between 200 and 1000 Da, which renders the opportunity to stand superior in wastewater purification (Sun *et al*. 2012). The mechanism of NF membrane separation is based on size exclusion and electrostatic repulsion (Donnan effect). However, NF membrane performances are severely affected by concentration polarization and membrane fouling (Tang *et al*. 2011). Essentially, in textile wastewater treatment, the flux decline is triggered by the cake layer formation and pore blockage (Koyuncu *et al*. 2004, Lin *et al*. 2015). According to Koyuncu, membrane fouling can be reduced by increasing the cross-flow velocity (Koyuncu 2002).

In addition, the hydrophobic interaction and electrostatic attraction will also contribute to the reduced flux via the accumulation of dye molecules in the membrane pore structure (Koyuncu *et al*. 2003). Consequently, it increases the frequency of chemical cleaning, which reduces membrane life. Besides, the high concentration of inorganic salts reduces the permeate flux due to the increase in osmotic pressure (Xu *et al*. 1999). Therefore, advanced NF membranes having dye removal capacity with low salt rejection and high flux are highly anticipated in the field of textile wastewater treatment.

The use of tight ultrafiltration (T-UF) can be recognized as an operative approach for the bifurcation of dye/salt mixture (Lin *et al*. 2016, Liu *et al*. 2017). Lin and co-workers demonstrated the fractionation of dye/Na_2SO_4 using the UH004 T-UF membrane (MWCO 4700 Da) from textile wastewater. The results revealed that the membrane could reject > 98.9 % of both reactive blue 2 and direct dyes along with the high permeation of Na_2SO_4 (Lin *et al*. 2016). Liu *et al*. applied a positively charged T-UF membrane with MWCO of 12700 Da for separation of dye, which allowed 99.9 % rejection of Congo red with dye solution permeation of 84 L/m^2 h bar (Liu *et al*. 2017). Hydrophilic polyaryletherketone (PAEK)-COOH T-UF membrane was reported by the Liu group (Scheme 5.1). The prepared membrane exhibited a rejection of 99.8 % Congo red (100 ppm) with the complete permeation of NaCl and < 10 % rejection to Na_2SO_4 (Liu *et al*. 2017). Hence, the T-UF membrane having both high permeability of water and inorganic salts with high rejection of dye molecules is highly desirable since the textile effluents increase day by day.

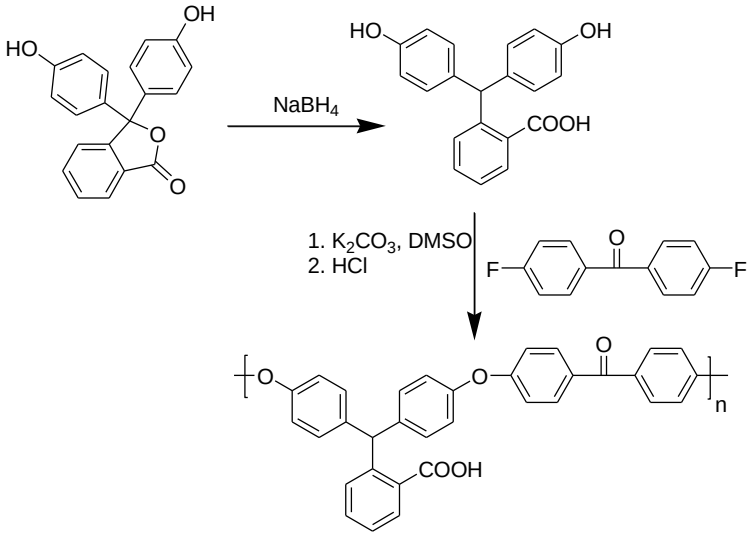

Scheme 5.1 Synthesis of carboxylated cardo poly(arylene ether ketone)s (PAEK-COOH) (Liu *et al*. 2017)

The carbon-based nanomaterials have been demonstrated many interesting properties such as adsorption of organic dyes and heavy metals, desalination and antimicrobial activity (Machida *et al*. 2006, Ai *et al*. 2011, Liu *et al*. 2011, Kumar *et al*. 2019). Graphene oxide (GO) consists of reactive functional groups such as -OH, epoxy and -COOH has designated as an effective substitute for constructing the nanocomposite membranes owing to its characteristic 2D structure, high chemical stability, strong hydrophilicity and high surface area (Liu *et al*. 2012). GO has been incorporated into the membrane matrix for constructing nanocomposite membranes with enhanced flux and antifouling properties (Goh *et al*. 2015, Tang *et al*. 2015). Nevertheless, graphene derivatives are susceptible to form aggregation in dope solution, as a result, it forms a random dispersion.

Furthermore, the compatibility between the membrane matrix and GO is poor, which may enhance the defects in the matrix. Consequently, there will be a compromise in the selectivity and mechanical strength of the nanocomposite membrane (Wang *et al*. 2015, Zhu *et al*. 2016). For that reason, surface modification of GO for the betterment of improved performance and compatibility is mandatory. Zwitterionic materials bearing both anionic and cationic groups have been developed as favorable antifouling and superhydrophilic materials. It establishes a strong hydration layer on the membrane surface, which is essential for reducing the adsorption of foulants capability and enhancement of flux (Shao *et al*. 2015).

The nanocomposite membrane will have improved compatibility, as the hydrophobic chains in the zwitterionic polymers are miscible with the polymer matrix. Zhu *et al*. described the preparation of zwitterionic GO via reverse atom transfer radical polymerization (RATRP), which is overall in three steps (Scheme 5.2) (Zhu *et al*. 2016). Zhao *et al*. prepared zwitterionic GO via free radical polymerization at 60 ^{o}C under a nitrogen atmosphere. The prolonged reaction time (40 h) and inert atmosphere still increase the operational cost (Zhao *et al*. 2016). He *et al*. stated the functionalization of GO in two steps. In the first step, GO was vinylated by 3-(methacryloxy) propyltrimethoxysilane (MPS) followed by reaction with some of the monomers via surface-initiated precipitation polymerization (He *et al*. 2015).

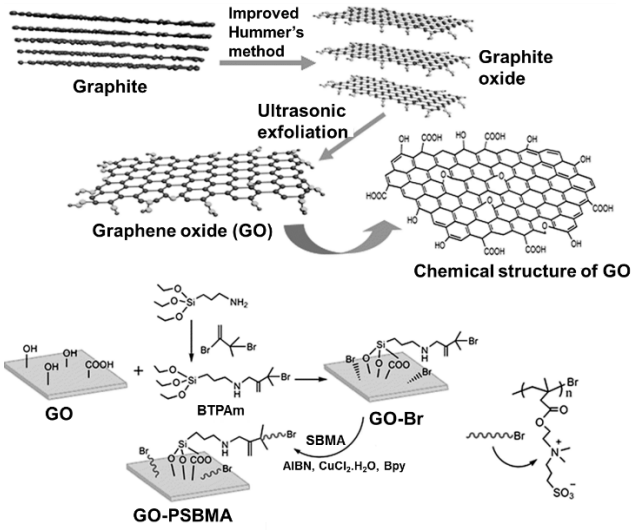

Scheme 5.2 Synthesis of zwitterionic GO via reverse atom transfer radical polymerization (RATRP) (Zhu *et al*. 2016)

Distillation precipitation polymerization (DPP) is one of the developing methods for the preparation of uniform-sized micro and nanoparticles. It was first reported by Bai *et al*. for the preparation of poly(divinylbenzene) microspheres (Bai *et al*. 2004). It is described that the size of particles can be altered by changing the concentration of the monomer and radical initiator. In addition, the increased degree of cross-linking also influences the size of the particles. DPP is i) Time-saving (<2 h) and facile method compared to the conventional polymerization process. ii) No stabilizer and pH adjustment are required. iii) As reaction proceeds at refluxing temperature, no need for the inert atmosphere. iv) Prepared particles show excellent colloidal stability in various solvents without adding any

stabilizing agents. In the typical process, acetonitrile (ACN) was chosen as a reaction solvent, since the monomers and initiator are highly soluble and synthesized nanoparticles are insoluble.

The preparation of functionalized Fe_3O_4 nanoparticles via DPP was reported by Zhang *et al*. The as-prepared hydrophilic nanoparticles demonstrated the improved binding capacity towards glycoproteins (Scheme 5.3) (Zhang *et al*. 2015). Guangwei *et al*. modified the MWCNTs with functional groups such as –COOH, $–SO_3H$ and PO_3H_2 by DPP. It was stated that the modified MWCNTs improved proton conductivity (He *et al*. 2014).

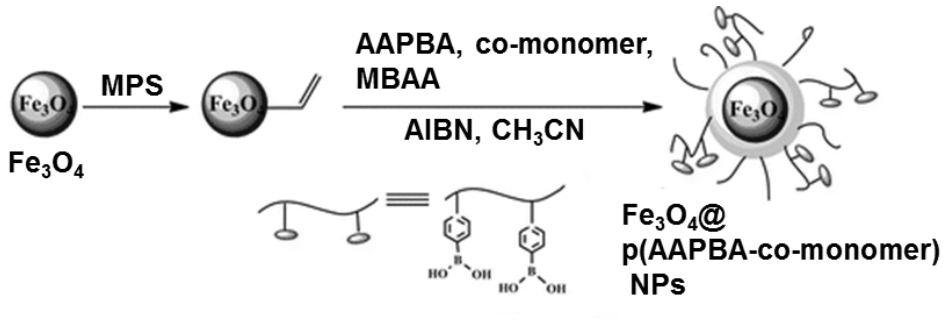

Scheme 5.3 Synthesis of functionalized Fe_3O_4 magnetic nanoparticles via DPP (Zhang *et al*. 2015)

Jianfeng *et al*. reported the first paper on the surface functionalization of multiwalled carbon nanotube (MWCNTs) with poly(acrylic acid) and poly(acrylamide) via in situ radical polymerizations (Shen *et al*. 2008). Later, the GO surface was functionalized with poly(acrylic acid) and poly(acrylamide) via covalent bonding, which was reported by Shen *et al*. (Shen *et al*. 2009). In 2011, Kan *et al*. demonstrated the functionalization of GO with different polymer chains via free radical polymerization (Scheme 5.4) (Kan *et al*. 2011). It was stated that after functionalization, the aggregation of GO was reduced to a greater extent. In this typical reaction, polymer chains are directly attached to the C=C bond of GO and the rest of the active functional groups were intact.

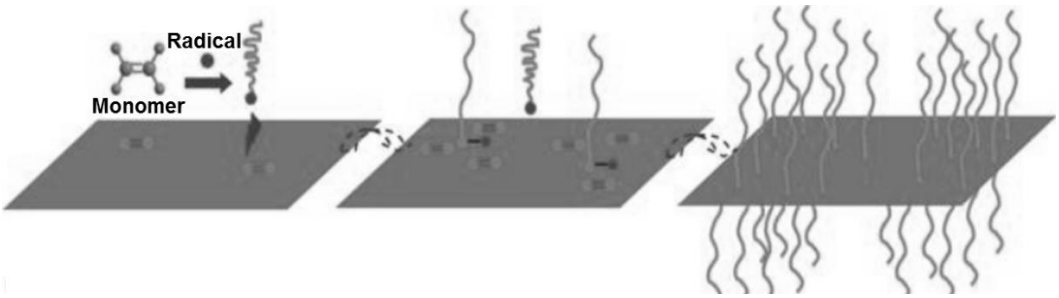

Scheme 5.4 Functionalization of GO via free radical polymerization (Kan *et al*. 2011)

Further, by combining the advantages of this method and DPP would provide a simple and cost-effective methodology for the functionalization of GO. In this typical polymerization process, the vinyl monomers are initiated by radical polymerization and the formed radicals are added to C=C bonds of GO via propagation. Consequently, there is a formation of many radicals on the GO surface, which undergoes further chain propagation and termination. Conversely, so far no experimental evidence has been reported to support the above-said mechanism (Kan *et al*. 2010). Additionally, the functional groups such as –COOH and –OH of GO are intact. Thus, there was no compromise in the hydrophilicity of GO after functionalization.

Inspired by the above reports, GO@poly(SBMA-co-MBAAm) nanohybrid was synthesized via DPP using GO as the backbone, MBAAm as a cross-linking agent and SBMA as a zwitterionic monomer. This material was used as an additive to prepare ultrafiltration (UF) hollow fiber (HF) membranes, using polysulfone (PSF) as the membrane material. The presence of all the elements and membrane morphology were studied using XPS and SEM analyses. The effect of incorporated nanocomposite on UF HF membranes was examined based on surface hydrophilicity, water uptake, MWCO and pure water permeability. The as-prepared membrane's filtration performance was demonstrated for dye and salt separation using negatively charged reactive dyes as model pollutants in detail. Additionally, the dye rejection at different concentrations of dye and salt, different pH, various pressure and antifouling performances have also been studied. To the best of our understanding, this is the first such paper which describes the synthesis of novel GO@poly(SBMA-co-MBAAm) nanohybrid and used as an additive in PSF UF HF membrane.

5.2 EXPERIMENTAL

5.2.1 Materials and methods

Azobisisobutyronitrile (AIBN), graphite powder, acetonitrile (ACN), N-methyl-2-pyrrolidone (NMP), polyvinylpyrrolidone (PVP) and MBAAm were obtained from Loba chemicals. Polysulfone pellets (PSF, Udel® P-1700) was purchased from Solvay chemicals. SBMA, RB-5, RO-16 and bovine serum albumin (BSA) were procured from Sigma Aldrich. Sodium sulfate (Na_2SO_4), sulfuric acid (H_2SO_4), sodium chloride (NaCl),

hydrogen peroxide (H_2O_2), potassium permanganate ($KMnO_4$), phosphoric acid (H_3PO_4) acquired from Merck.

The morphology of GO@poly(SBMA-co-MBAAm) was examined by transmission electron microscopy (TEM - JEOL JEM-2100). The presence of all the elements in the nanohybrid was confirmed and elemental mapping was performed using energy dispersive X-ray (EDX, X-Max Oxford instruments) analysis. FT-IR spectra with a scanning range of 4000-600 cm^{-1} were measured using a BRUKER ALPHA ECO FT-IR spectrometer as KBr pellets. The thermal stability of the as-synthesized nanohybrid was determined by thermogravimetric analysis (TGA, HITACHI EXSTAR TG/DTA 6300). The nanocomposite was heated from room temperature to 800 ^oC at a heating rate of 10 $^oC\ min^{-1}$ under nitrogen gas. The polymorphism of GO and nanohybrid was recorded using powder X-ray diffractometer (PXRD, Rigaku Miniflex) in the range of 5 to 40^o using Cu Kα as an X-ray source. The surface charge of the nanohybrid was characterized using the HORIBA nanoparticle analyzer. SEM (HITACHI TM3000) was used to observe the cross-section images of the membranes. Surface hydrophilicity was analyzed by the static water contact angle, which was performed in contact angle goniometer (Data Physics instruments, OCA20). The membrane elemental composition and presence of nanohybrid were studied by X-ray photoelectron spectroscopy (XPS, THERMO FISHER Scientific K-ALPHA) analysis. Al Kα radiation (1486.6 eV) was employed as an X-ray source and the take-off angle was 90^o.

5.2.2 Preparation of graphene oxide

Graphene oxide (GO) was prepared as stated in the literature (Marcano *et al*. 2010). In brief, 2 g of graphite was added to the mixture of 240 mL of Conc.H_2SO_4 and 27 mL of H_3PO_4 at 10 ^oC. 12 g of $KMnO_4$ was added lot-wise undercooling. The reaction mass was cooled to RT and heated to 50 ^oC for 12 h. Furthermore, the reaction mass was cooled to RT and slowly poured into 130 mL of ice-cooled water containing 2 mL of 30 % H_2O_2. The supernatant was decanted and the remaining solid was again washed with 130 mL of Conc. HCl (30 %). The GO nanosheets were washed with water until the neutral pH and finally with 1×130 mL of ethanol and isolated by centrifugation.

5.2.3 Synthesis of zwitterionic graphene oxide nanohybrid (GO@poly(SBMA-co-MBAAm))

The GO@poly(SBMA-co-MBAAm) nanohybrid was synthesized via a one-step DPP technique. Typically, 0.1 g of GO was dispersed in 100 mL of acetonitrile in a dried round bottom flask by using an ultrasonic cleaning bath (Anmanm industries USC-100). Added 0.2 g (0.71 mmol) of SBMA, 0.8 g (5.18 mmol) of MBAAm and 0.02 g (0.12 mmol) of AIBN and stirred for 15 min at room temperature. The reaction mass was purged with nitrogen gas for 20 min to eliminate the dissolved oxygen. Later the reaction was performed by attaching Dean-Stark receiver and heated in an oil bath to 75 ^{o}C for another 15 min. The oil bath temperature was gradually rose to 110 ^{o}C to continue the polymerization reaction at reflux. When 40 mL of acetonitrile has removed over 40 min through Dean-Stark receiver, the reaction mixture was allowed to room temperature and agitated for an additional 1 h. The nanoparticles were isolated and washed with acetonitrile to remove the oligomer and unreacted monomer. The material was dried at 55 ^{o}C for 15 h (Yield = 0.9 g). The synthetic route of GO@poly(SBMA-co-MBAAm) nanohybrid is represented in Scheme 5.5.

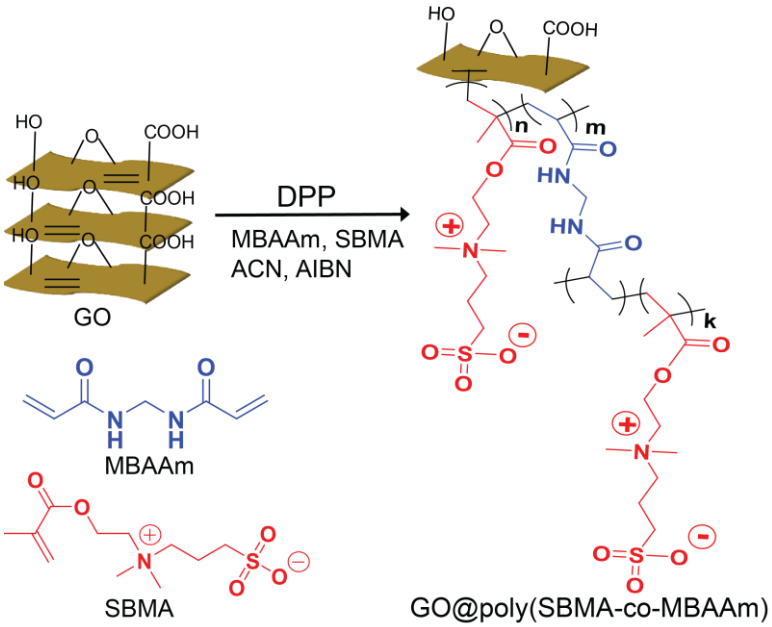

Scheme 5. 5 GO@poly(SBMA-co-MBAAm) nanohybrid synthesis

5.2.4 Preparation of ultrafiltration hollow fiber membranes

PSF ultrafiltration (UF) hollow fiber (HF) membranes were prepared by the dry/wet phase inversion method. The PSF and PVP were dried at 60 ^{o}C for 24 h prior to dope solution preparation to eliminate the adsorbed water molecules. Details of the spinning parameter and dope solution composition are depicted in Table 5.1 and 5.2. In the preparation of TM-2, 0.05 g of GO@poly(SBMA-co-MBAAm) nanohybrid dispersed in 79 g of NMP using a probe sonicator (QSONICA, 50 % amplitude with on time of 1 second and off time of 10 seconds) for 10 min. Added 1 g of PVP and stirred for 10 min at room temperature. 20 g of PSF was added to the dope solution lot wise and stirred at 60 ^{o}C for 24 h to obtain the homogeneous solution. The dope solution was degassed for 6 h to remove any residual air bubbles. The as-prepared dope solution was used to spin the UF HF membrane. The schematic representation of the HF membrane spinning system is represented in our previous report (Ibrahim *et al*. 2017). The as-made HF membranes were dipped in deionized water for 24 h to complete the phase inversion followed by 20 wt% glycerol solution for another 24 h to circumvent any pore collapse. The membranes were air-dried for future usage. The membranes prepared with different GO@poly(SBMA-co-MBAAm) concentration of 0, 0.1, 0.25 and 0.5 wt% from now denoted to as TM-0, TM-1, TM-2 and TM-3.

Table 5.1 Spinning parameters of hollow fiber membrane

Parameters	Conditions
Coagulation bath	Tap water
Spinneret (mm)	1.1/0.55 (OD/ID)
Coagulation bath temperature (^{o}C)	27
Bore flow rate (mL/min)	2.5
Dope extrusion rate (mL/min)	3
Bore fluid	Distilled water
Air gap (cm)	1
Collecting drum speed (RPM)	7
Humidity (%)	60

Table 5.2 The hollow fiber membrane dope solution composition

Membrane	PSF (g)	PVP (g)	NMP (g)	GO@poly(SBMA-co-MBAAm) (g)	GO@poly(SBMA-co-MBAAm) (wt%)*
TM-0	20	1	79	0	0
TM-1	20	1	79	0.02	0.1
TM-2	20	1	79	0.05	0.25
TM-3	20	1	79	0.1	0.5

* With respect to PSF

5.2.5 Characterization of membranes

The water uptake, porosity and PWP of the HF membranes were determined as mentioned in chapter 2, section 2.2.4 and 2.2.5.

The rejection experiments were conducted using a different concentration of RB-5 and RO-16. The concentration of salts was measured from conductivity (JENWAY 4520 conductivity meter) analysis and concentration of dye molecules was measured using UV-Vis spectrophotometer (DR6000 HACH). The percentage rejection, '*R*' was determined using this equation (5.1).

$$\text{R}\,(\%) = \frac{C_f - C_p}{C_f} \times 100 \tag{5.1}$$

Where 'C_p' and 'C_f' are the solute concentration in permeate and feed respectively.

The molecular weight cut-off (MWCO) of the membrane was characterized by filtering sequence of polyethylene glycol (PEG) with a molecular weight of 2000, 4000, 6000 and 10000 Da at the concentration of 100 ppm at 1 bar. The PEG concentration in both feed and permeate was evaluated using a total organic carbon analyzer (TOC, SHIMADZU). The PEG rejection, '*R*' was determined using equation 5.1. MWCO is the molecular weight of solute upon which at least 90% of rejection can be attained. Furthermore, the Stokes radius of PEG solute was determined [equation (5.2)] from its average molecular weight. Where 'r_p' is in nm and molecular weight (MW) in Da.

$$r_p = 16.73 \times 10^{-12} \times MW^{0.557} \tag{5.2}$$

The antifouling performance of the UF HF membrane was evaluated using 800 ppm BSA solution as feed at room temperature and 1 bar pressure. FRR, R_{ir}, R_r and R_t were calculated as explained in chapter 4, section 4.2.4.

5.3 RESULTS AND DISCUSSION

5.3.1 Characterization of GO@poly(SBMA-co-MBAAm) nanohybrid

GO and GO@poly(SBMA-co-MBAAm) were examined by FT-IR and are presented in Figure 5.1A and B. In GO, the peak at 3365 cm^{-1} due to O-H stretching vibration and the C=O peak was observed at 1735 cm^{-1}. The peaks at 1624, 1219 and 1056 cm^{-1} were owing to C=C, C-O and C-O-C vibrations respectively (Lin *et al*. 2011). For GO@poly(SBMA-co-MBAAm), peaks at 3065 and 2947 were ascribed to C-H stretching vibrations. The ester group present in SBMA was observed at 1722 cm^{-1} (Zhao *et al*. 2016). The amide group C=O stretching and N-H bending vibrations were detected at 1657 and 1530 cm^{-1}. More importantly, peaks at 1043 and 1117 cm^{-1} were assigned to the symmetric and asymmetric stretching vibrations of the sulfonate (SO_3^-) group. The peak at 1209 cm^{-1} was bestowed by C-N stretching vibration (Suart 2004). In that way, the modification of GO was confirmed by FT-IR. The formation of intermolecular hydrogen bonding improves the compatibility between PSF and nanohybrid and homogeneous distribution of nanohybrid across the membrane matrix.

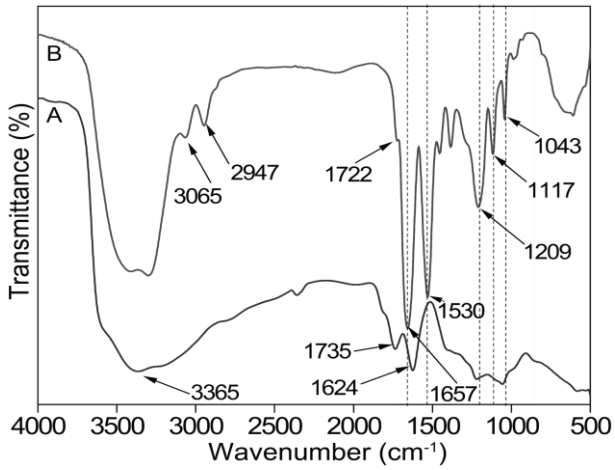

Figure 5.1 FT-IR spectra of A) GO and B) GO@poly(SBMA-co-MBAAm)

The morphology of zwitterionic GO was observed in TEM and shown in Figure 5.2. In Figure 5.2A, GO exhibits a distinct crystal clear and distorted laminar structure. However, in Figure 5.2B, GO is uniformly covered by nanosize poly(SBMA-co-MBAAm) nanoparticles, which are homogeneously spread on the surface of GO. The surface of the GO was comparatively smooth and no wrinkles were observed. Conversely, the modified GO shown some of the wrinkles and folding under the same condition. In addition, many

irregular dark dots are present on the modified GO surface, which makes the modified GO darker and rougher than unmodified GO. The magnified image of functionalized GO is shown in Figure 5.2C, which further confirmed that some of the poly(SBMA-co-MBAAm) nanoparticles are intercalated between the GO layers (Urbanova *et al*. 2018). In summary, the morphological changes in TEM images confirmed the functionalization of GO.

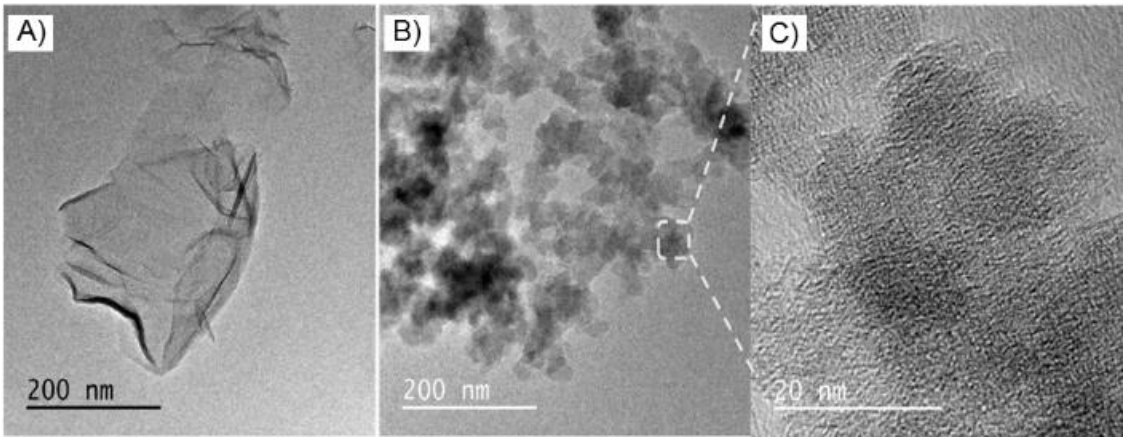

Figure 5.2 TEM images of A) GO, B) and C) GO@poly(SBMA-co-MBAAm) in different magnifications

Figure 5.3A represents the powder X-ray diffraction (PXRD) pattern of both GO and GO@poly(SBMA-co-MBAAm). GO has peak at $2\theta = 9.8^{o}$, resultant to the [001] diffraction peak with an interlayer spacing of 9.0Å (Marcano *et al*. 2010, Huang *et al*. 2013, Wang *et al*. 2016). However, in the case of GO@poly(SBMA-co-MBAAm), the [001] reflection of GO at $2\theta = 9.8^{o}$ was not detected as the regular stack of GO was demolished by the intercalation of nanosize poly(SBMA-co-MBAAm) and the increased disorder, which provides additional confirmation of intercalation of the poly(SBMA-co-MBAAm) at GO. The obtained result is well aligned with the literature (Xu *et al*. 2008, Chen *et al*. 2010, Han *et al*. 2014, Huang *et al*. 2015, Zhao *et al*. 2016). Furthermore, the increased interlayer spacing and disorder of the GO@poly(SBMA-co-MBAAm) nanohybrid would have more amount of active sites than the GO.

TGA was used to understand the thermal properties of GO and GO@poly(SBMA-co-MBAAm) and presented in Figure 5.3B. In GO, the weight loss below 100 ^{o}C owing to adsorbed water. The major weight loss around 200 ^{o}C was due to CO, CO_2 and steam release (Stankovich *et al*. 2007, Yu *et al*. 2013) and slower weight loss between 450 and 900 ^{o}C was ascribed to the decomposition of more stable oxygen-containing functionalities

(Shen *et al*. 2009). In addition, the total weight loss of GO was ca. 65.1 %. However, in the case of GO@poly(SBMA-co-MBAAm) the total weight loss was ca. 80.8 %. The difference in weight loss validates the successful functionalization of GO. Therefore, the loading density of MBAAm and SBMA on GO was ca. 157 mg/g. The increased thermal stability of the modified GO was due to the formation of hydrogen bonding.

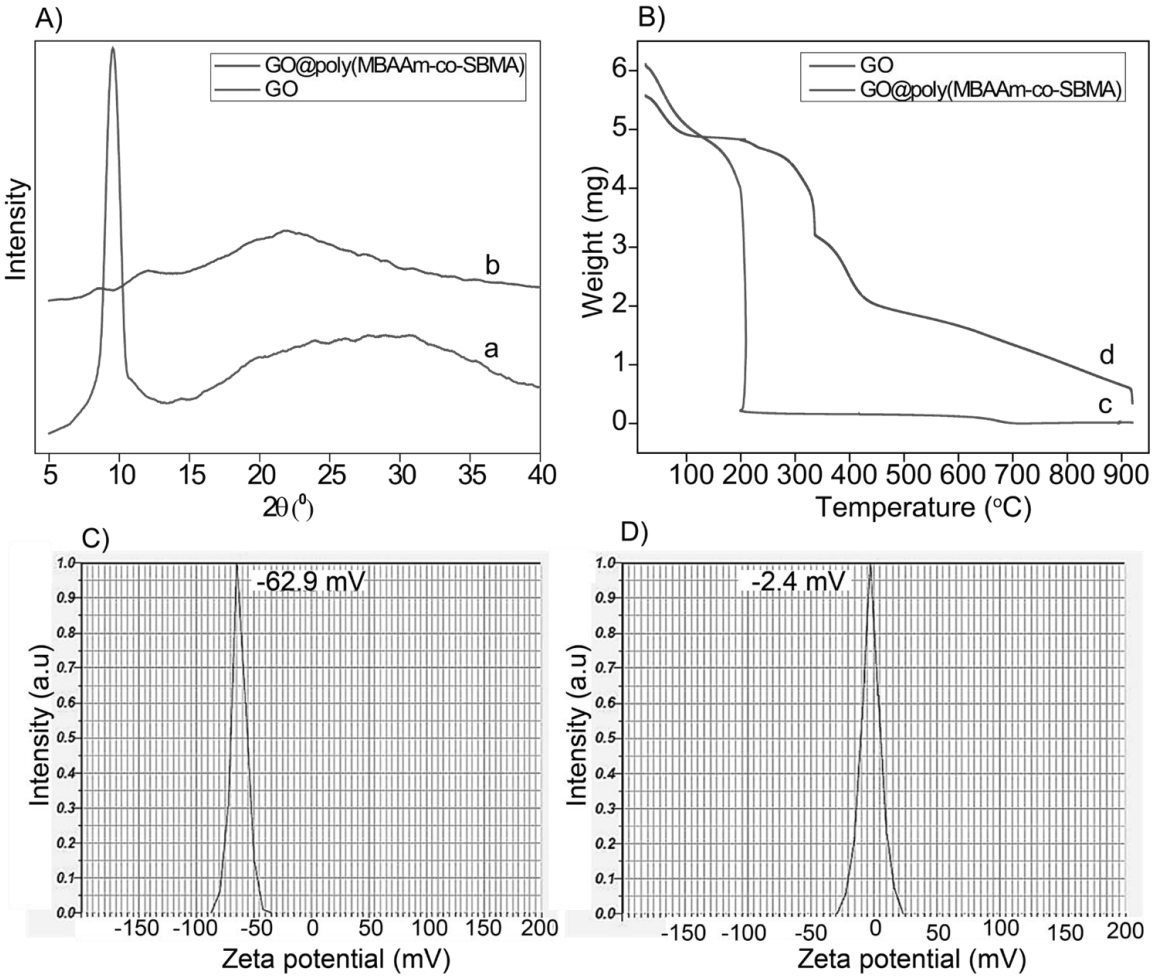

Figure 5.3 A) PXRD of (a) GO, (b) GO@poly(SBMA-co-MBAAm), B) TGA curve of (c) GO, (d) GO@poly(SBMA-co-MBAAm), C) and D) zeta potential of GO and GO@poly(SBMA-co-MBAAm)

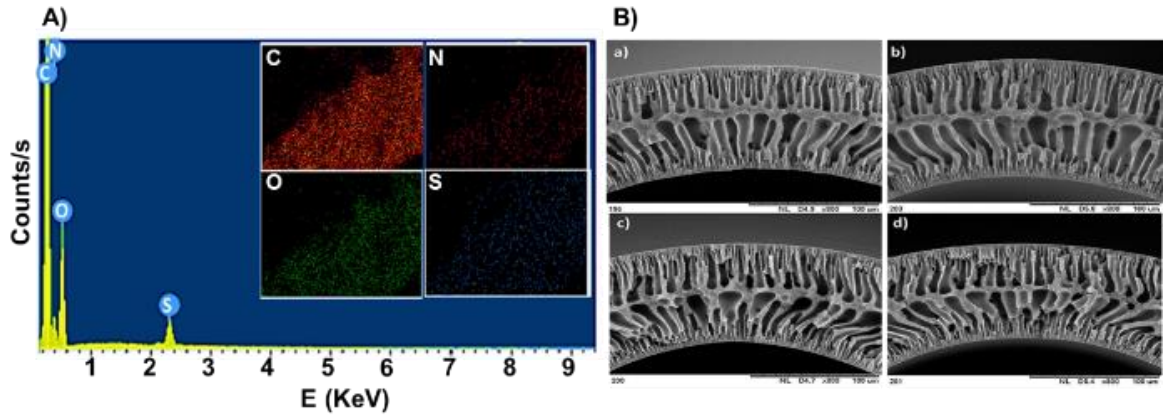

Figure 5.4 A) EDX and elemental mapping (inset) analyses of GO@poly(SBMA-co-MBAAm) and B) Cross-section SEM images of (a) TM-0, (b) TM-1, (c) TM-2 and (d) TM-3 membranes

The surface charge of the nanohybrid was analyzed and depicted in Figure 5.3C and D. As far as the GO is concerned, it forms very stable aqueous colloids (Kotov *et al*. 1996, Cassagneau *et al*. 2000). The prepared GO (Figure 5.3C) exhibited a negative charge (-62.9 mV at pH 6.3) in the aqueous medium is related to the results by Li *et al*. (Li *et al*. 2008). The negative charge of GO again confirmed the presence of carboxylic acid and hydroxyl groups. Nevertheless, after functionalization (Figure 5.3D) the nanomaterial exhibited zeta potential value of - 2.4 mV (pH 6.3). The reduction in zeta potential could be attributed to the existence of evenly distributed zwitterionic poly(sulfobetaine) (PSBMA). This trend was comparable to the results reported by the Ulbricht group (Susanto *et al*. 2007). Further, the presence of all elements in the nanohybrid was confirmed in EDX and elemental mapping confirmed the distribution of all the elements (Figure 5.4A).

5.3.2 Morphology of hollow fiber membranes

The cross-section images of the pristine PSF HF membrane and nanocomposite HF membranes with various concentrations of GO@poly(SBMA-co-MBAAm) are presented in Figure 5.4B. It was found that the as-prepared HF membranes demonstrated typical asymmetric structure with sponge-like intermediate layer sandwiched between the top and bottom finger-like macro-voids. Since the coagulant (water) was intruded from both the top and bottom of the membrane, finger-like macro-voids were extended up to the sponge-like dense layer. However, there were no significant morphological changes were observed between the pristine and nanocomposite membranes in SEM, as PVP was added invariably.

5.3.3 XPS analysis of membranes

Figure 5.5A depicts the wide range XPS spectra of both TM-0 and TM-2 membrane. For the TM-2 membrane, the peak at 284.98 eV corresponds to the C 1s element. O 1s element peak detected at 532.48 eV. The peak at 167.98 eV can be ascribed to the S 2p element. The new peak at 400.48 eV was due to the existence of the N 1s element, which was not observed in the pristine membrane (TM-0). Further, the C 1s and N 1s elemental peaks were deconvoluted and depicted in Figure 5.5B and C. In Figure 5.5B, C 1s was deconvoluted into five different peaks with binding energies of 284.9, 286.1, 286.3, 287.6 and 291.58 eV, which are assigned to C-C/C=C, CN^{+}/CSO_3^{-}, C-O/C-N, C=O and O-C=O respectively. In Figure 5.5C, N 1s was deconvoluted into three peaks namely N-C=O and N-C and R_4N^{+} with the binding energies of 400.48, 398.18 and 402.28 eV. The atomic % of all the elements present in the membrane are as follows. For TM-0 membrane, C - 83.10 %, O - 12.21 % and S - 4.69 % and for TM-2 membrane, C - 81.85 %, O - 13.88 %, S - 2.84 % and N - 1.44 %. Therefore, XPS analysis confirms the occurrence of nanohybrid in the membrane matrix.

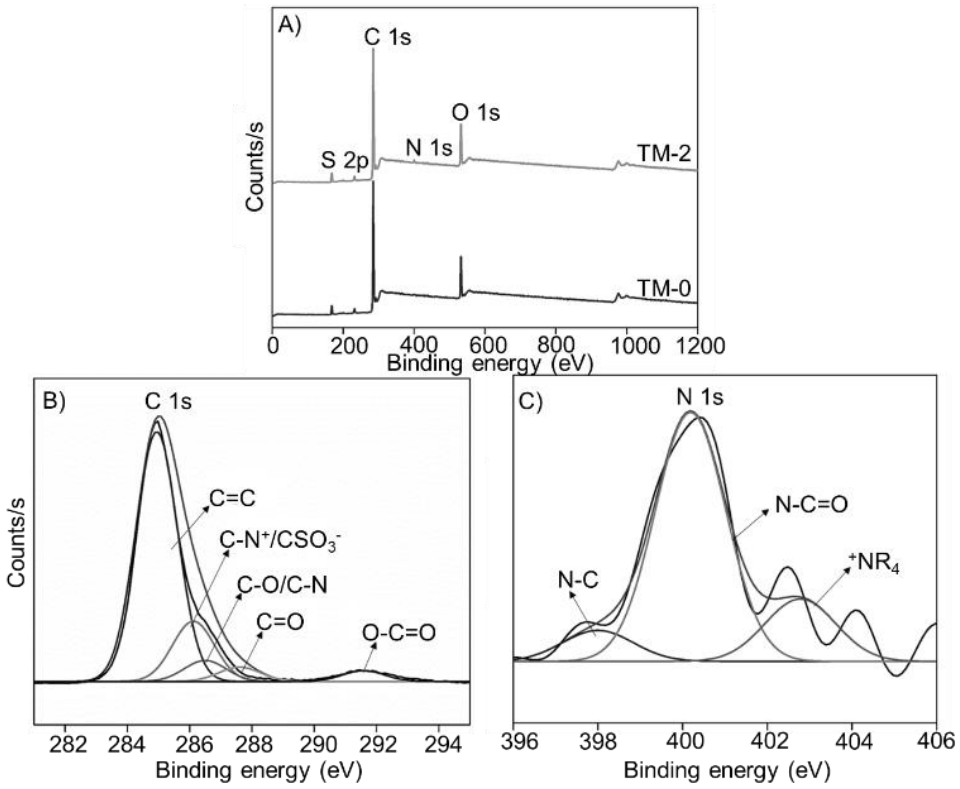

Figure 5.5 A) XPS wide-scan TM-0 and TM-2 membrane spectra, B) high resolution C 1s and C) N 1s spectra of TM-2 membrane

5.3.4 Surface properties of hollow fiber membranes

The hydrophilicity of the membrane was measured by contact angle analysis. In general, the hydrophilic membrane surface is less prone to fouling (McCloskey *et al*. 2012, Li *et al*. 2014), which is necessary for reducing the maintenance cost and to increase the membrane lifecycle. Figure 5.6A depicts the contact angle of membranes. The contact angle of the pristine membrane (TM-0) was 80 $\pm$1.2^{o}, however, in the case of the TM-2 membrane, the contact angle was 68 $\pm$1.5^{o}. The reduction in contact angle could be ascribed to the addition of hydrophilic GO@poly(SBMA-co-MBAAm). The presence of both anionic and cationic functional groups in SBMA, render more affinity to bind with "free water" molecules, which results in reduced contact angle. Further, during the phase inversion, the added nanomaterials tend to transfer towards the top layer to reduce the interfacial energy. In contrast, while increasing the nanomaterial concentration from 0.25 to 0.5 wt%, the contact angle was increased to 70 $\pm$1^{o} due to the presence of hydrophobic alkyl functional groups in functionalized GO. To understand the surface hydrophilicity further, water uptake capacity of the pristine and nanocomposite membrane was carried out and presented in Table 5.3. The nanocomposite membrane TM-2 exhibited the highest water uptake capacity of 60.3 $\pm$1.8 % compared to the TM-0 membrane of 39.6 $\pm$1.4 %. Conversely, for the TM-3 membrane, it was reduced to 57.1 $\pm$1.5 % as hydrophilicity was reduced. The obtained result is in good agreement with the contact angle result.

As shown in Table 5.3, with an increase in the concentration of nanohybrid, porosity was also increased related to the pristine membrane. As shown, the TM-2 membrane exhibited an increased porosity of 61.1 $\pm$0.34 %. Conversely, the TM-3 membrane shown the reduced porosity of 57.8 $\pm$0.52 %. The reduced porosity was attributed to the agglomeration of nanohybrid at a higher concentration.

Table 5.3 Properties of UF HF membranes

Membrane	PWP (L/m^2 h bar)	Water uptake (%)	Porosity (%)	Fouling (%)			
				FRR	R_t	R_r	R_{ir}
TM-0	22.5 ±0.67	39.6 ±1.4	42.4 ±0.42	41.2 ±0.5	81.8 ±0.23	21.2 ±0.11	38.8 ±0.34
TM-1	40.3 ±0.41	51.5 ±2.1	49.7 ±0.71	53.4 ±0.45	76.3 ±0.31	34.7 ±0.32	24.1 ±0.41
TM-2	49.6 ±0.54	60.3 ±1.8	61.1 ±0.34	73.9 +0.36	71.1 ±0.33	39.1 +0.3	17.4 ±0.38
TM-3	42.1 ±0.73	57.1 +1.5	57.8 ±0.52	70.5 ±0.71	72.7 ±0.28	36.8 ±0.43	20.7 ±0.51

The MWCO of the as-prepared UF (UF) HF membrane was determined from the rejection of PEG with different molecular weights. As can be seen from Figure 5.6B, while increasing the molecular weight of the PEG, the rejection percentage also increases correspondingly. MWCO of TM-2 membrane was 10665 Da and Stokes radius of PEG solute was 2.93 nm respectively, which confirmed that the as-prepared membrane is ultrafiltration membrane.

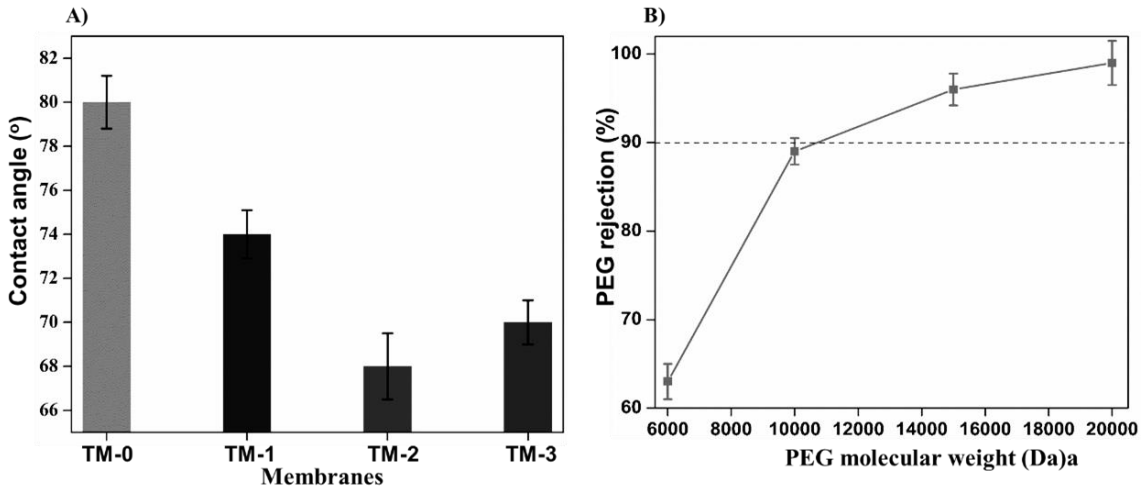

Figure 5.6 A) The contact angle of hollow fiber membranes and molecular weight cut-off (MWCO) curve of TM-2 membrane

5.3.5 Pure water permeability study

The pure water permeability (PWP) of as-prepared membranes is represented in Table 5.4. In general, PWP is mainly associated with the hydrophilicity and slack structure of nanocomposite membranes. It was observed that PWP was enhanced due to the incorporation of GO@poly(SBMA-co-MBAAm) nanohybrid, which was coherent with the obtained results of contact angle and water uptake. To a more precise, pristine membrane (TM-0) revealed the PWP of 22.5 L/m^2 h bar. However, in the case of the TM-2 membrane, PWP was improved to 49.6 L/m^2 h bar. This enhancement was attributed to the incorporation of nanohybrid, which provided improved hydrophilicity, porosity and slack structure of the nanocomposite membrane.

The zwitterionic materials have a functional group such as sulfonate and a quaternary ammonium group, which has a strong attraction towards the water molecules via electrostatic attraction. Therefore, the attraction between the water molecules and the membrane surface will be more. Further, the incorporated nanohybrid in the polymer matrix can diminish the interaction of polymer chains to some extent. Therefore, it decreases the resistance to the transport of water molecules across the membrane and led to increased permeability. Nevertheless, for the TM-3 membrane the PWP, hydrophilicity and porosity were decreased. The reason for this reduction is as follows. With a further increase of nanohybrid, tend to agglomerate and obstruct the pathway of permeation. As a result, PWP and porosity were reduced. The decreased hydrophilicity was due to the enhancement of hydrophobic alkyl groups in the MBAAm and SBMA. In summary, the as-prepared UF HF membrane noticeably exhibited an increased PWP compared to the pristine membrane.

5.3.6 Dye separation performance of the membrane

5.3.6.1 Effect of dye concentration

To evaluate the dye removal capacity of the as-prepared membrane, the rejection experiment was carried out with various concentrations of RB-5 and RO-16. Among all the prepared membranes, TM-2 was preferred for the dye removal studies. Figure 5.7 presents the percentage of dye rejection with dye solution permeability. As it is clear from Figure 5.7, the membrane demonstrated the highest rejection of 99 % for RB-5 and 74 % of RO-16 at 10 ppm of dye concentration. However, for both dyes, the dye rejection and dye

solution permeability were decreased with the increase of dye concentration, which is in accordance with the results reported by Liu *et al*. (Liu *et al*. 2017).

The four charged RB-5 demonstrated the highest rejection than the two charged RO-16. In general, the higher the charge of the dye molecules, the greater would be the degree of hydration. Consequently, the size of the dye molecule increases. As shown in Figure 5.8, the greater hydration degree and higher molecular weight of RB-5 could be attributed to the higher rejection compared to low molecular weight and less hydrated RO-16. Further, the reason for decreased rejection was due to the increased concentration of impurities such as Cl^-, SO_4^{2-} and HCO_3^- in the feed solution. The presence of such ionic species would increase the electrostatic shielding effect, thereby decreasing the rejection of dyes (Lin *et al*. 2015). A similar report had been published for the decreased rejection of direct red 23 (Lin *et al*. 2016). Meanwhile, the permeated dye molecules cause fouling, which results in decreased dye solution permeability slightly.

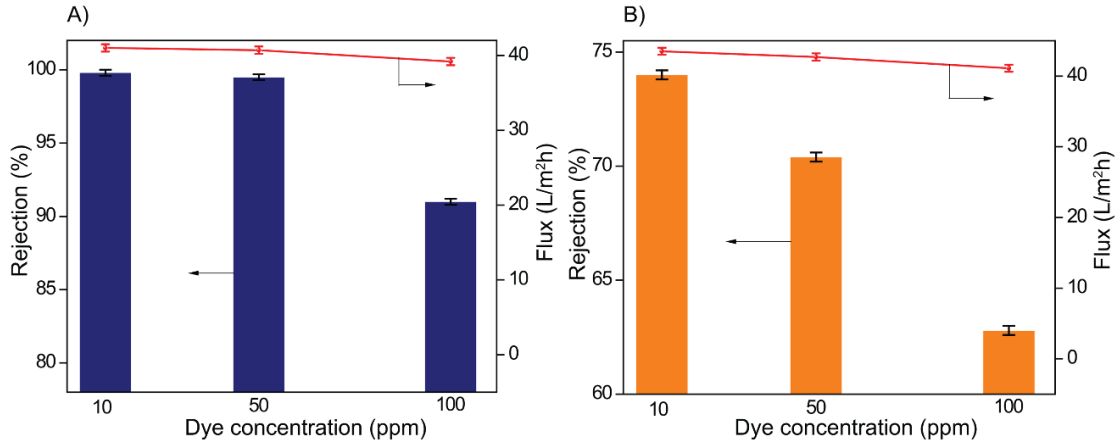

Figure 5.7 TM-2 membrane performance as a function of dye concentration for A) RB-5 and B) RO-16 (1 bar and pH 7)

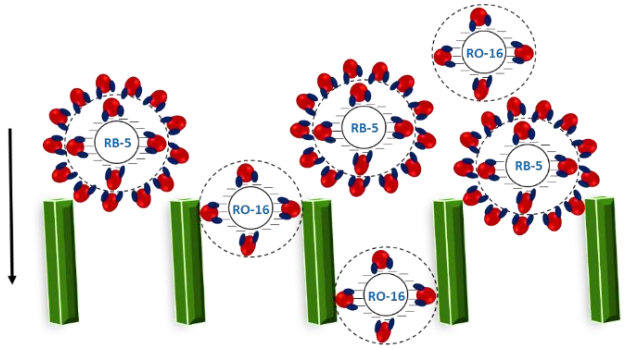

Figure 5.8 Schematic representation of hydration of dye molecules

5.3.6.2 Effect of pressure

The performance of the TM-2 membrane with respect to applied pressure is depicted in Figure 5.9A and B. Dye solution permeability increases with the increase of pressure for both the dyes, however, dye rejection was decreased. The decreased rejection could be attributed to the enhancement of concentration polarization effect, which improves the permeation of dye molecules. The observed results are in parallel with the results reported by Petrinić *et al*. (2007) and Lin *et al*. (2016).

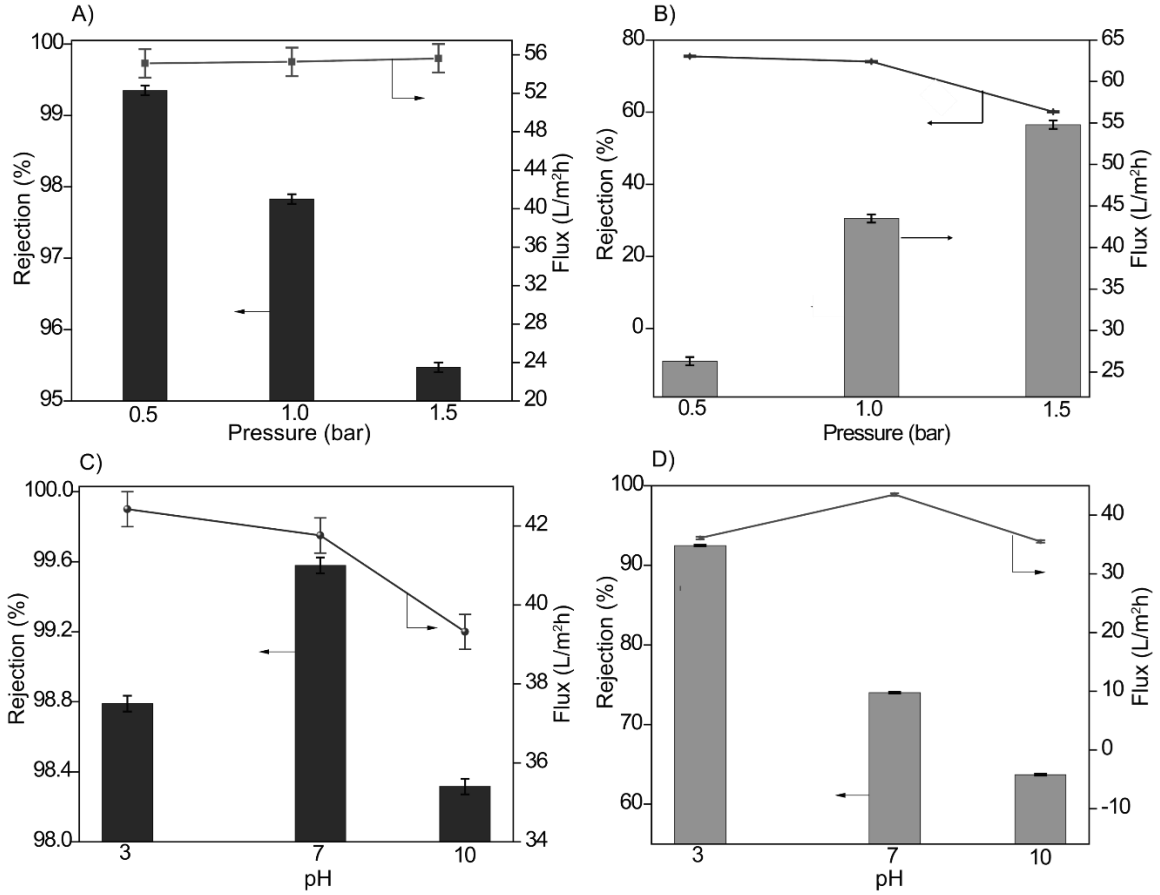

Figure 5.9 TM-2 membrane performance as a function of pressure for A) RB-5 and B) RO-16 (10 ppm and pH 7) and as a function of pH C) RB-5 and D) RO-16 (10 ppm and 1 bar)

5.3.6.3 Effect of feed solution pH

The separation efficiency of membranes can be effectually altered by the solution pH since the electrochemical properties of the membrane surface and the dye molecules are directly affected. Figure 5.9C and D describe the effect of solution pH on dye rejection and dye solution permeability. The optimum state of greater rejection and permeability was observed at pH 7. However, at pH 10 both rejection and permeability were declined. In the

case of basic condition, the membrane surface is highly ionized and undergoes severe swelling. The swelling could effectively make the membrane surface (skin layer) thicker (Wang *et al*. 2016), therefore, membrane permeability decreases. Furthermore, the decreased rejection can be ascribed to the inferior electrostatic repulsion between the membrane surface and dyes. At high basic conditions, the electrostatic interaction is screened by the presence of OH^- ions. It was noted that at pH 3, dye rejection was increased and permeability was declined. In acidic conditions, dye molecules get protonated to a greater extent, which in turn solubility of dye molecules are reduced and get precipitated in the feed tank. As a result, rejection increases owing to precipitation, while permeability decreases because of membrane fouling from dye precipitation on the membrane surface. The feed and permeate digital photographic images of RB-5 and RO-16 is depicted in Figure 5.10.

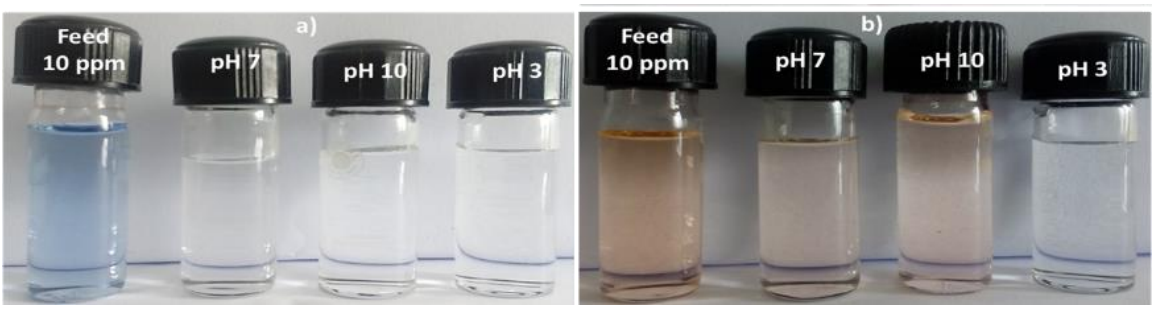

Figure 5.10 Digital photographic images of (a) RB-5 and (b) RO-16

5.3.6.4 Salt and salt/dye mixture filtration

As textile wastewater is a mixture of dye and inorganic salts, it is important to study the rejection profile of salt and salt/dye mixture. Further, the added salt has a direct impact on membrane performances (Van der Bruggen *et al*. 2001, Akbari *et al*. 2007, Zheng *et al*. 2013). Subsequently, a membrane with high rejection of dye molecules with high salt permeation is highly needed to process the textile wastewater. TM-2 membrane exhibited complete permeability to NaCl and <5 % rejection of Na_2SO_4. The filtration performance of the TM-2 membrane for RB-5 and RO-16 at different concentrations of Na_2SO_4 is illustrated in Figure 5.11. As reported by Nilsson *et al*. salt/dye solution permeability was decreased with the increase of salt concentration. The reduced permeability was attributed to the change in the osmotic pressure, which reduces the net driving pressure. In spite of the TM-2 membrane exhibits lower rejection for Na_2SO_4, water transports faster than salt

("Dilute effect") due to steric exclusion (Fang *et al*. 2014). However, the rejection was increased as the dye molecules form aggregates under the influence of added salt. Some of the recent literature reported and commercially available membranes are summarized in Table 5.4.

Table 5.4 Summary of reported literature and commercially available membranes for dye rejection.

Membrane	Dye	PWP* (L/m^2 h bar)	DSP** (L/m^2h bar)	Rejection (%)	Ref.
Commercial Sepro NF 6	Direct red 80	13.7	13.2	99.9	(Lin *et al*. 2015)
GO-PSBMA/PES loose NF	Reactive red 49/Reactive black 5	11.9	8.8	97.2/99.2	(Zhu *et al*. 2016)
UH004 (hydrophilic PES)	Direct red 80, direct red 23 and congo red	27.5	27.0	98.9	(Lin *et al*. 2016)
PAEK-COOH T-UF	Congo red	29.5	25.0	99.8	(Liu *et al*. 2017)
GO@poly(SBMA-co-MBAAm)/PSF UF	**Reactive black 5 / Reactive orange 16**	**49.0**	**41.0/43.5**	**99.0/74.1**	**Present study**

*- Pure water permeability, **- Dye solution permeability.

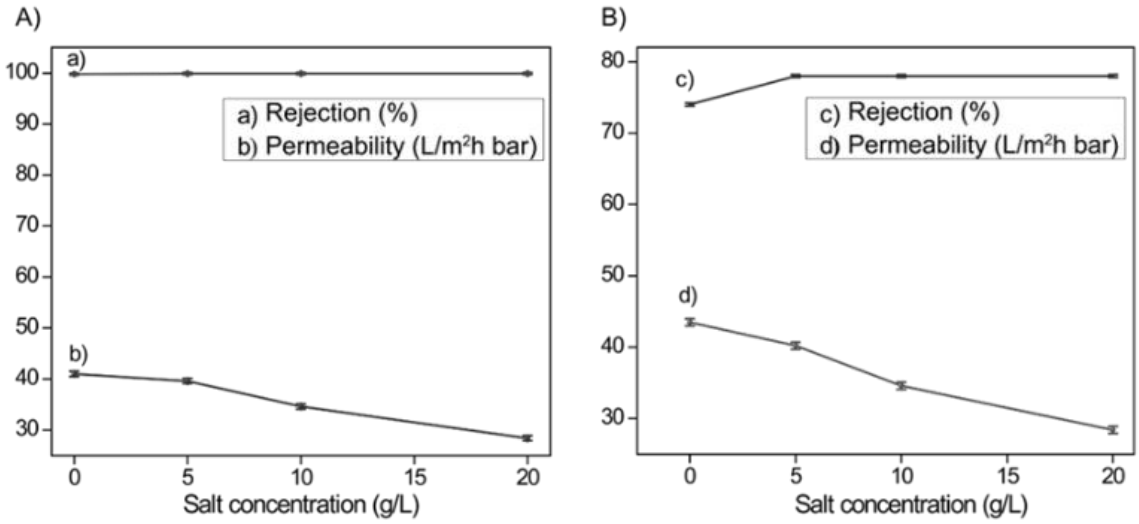

Figure 5.11 TM-2 membrane performance of salt/dye mixture for A) RB-5 and B) RO-16 (10 ppm of dye, 1 bar and salt is Na_2SO_4)

Furthermore, a short-term stability study was performed and depicted in Figure 5.12. During the 24 h of filtration, there was a slight decrease in the dye solution permeability and a small increment in the rejection was observed. The change in the rejection and permeability was ascribed to the formation of the dye cake layer and cake-enhanced concentration polarization.

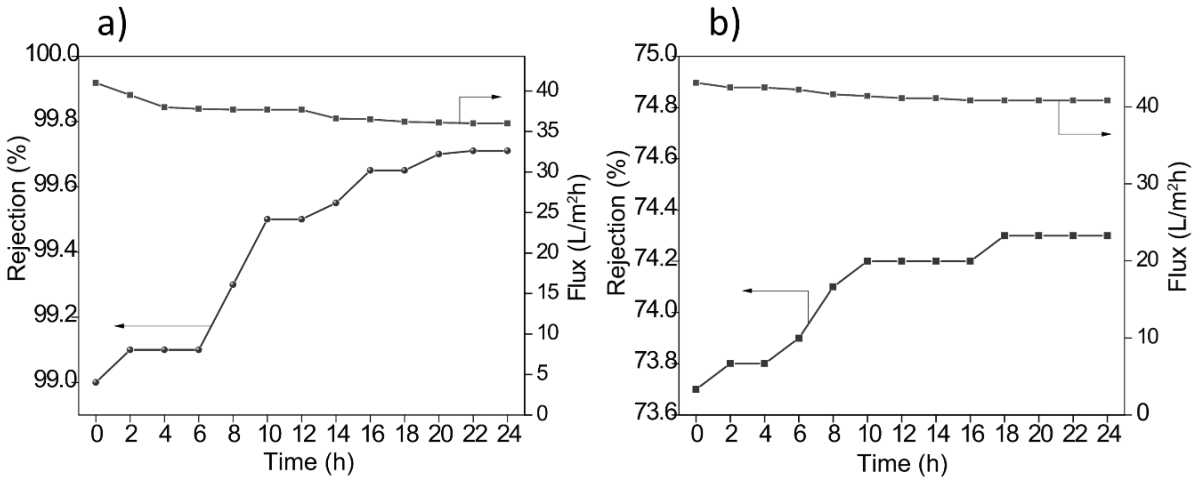

Figure 5.12 Short-term stability study of TM-2 membrane at 1 bar and 10 ppm, (a) RB-5 and (b) RO-16

5.3.7 Antifouling study

The membrane filtration performance greatly depends on the antifouling property. Typically, membranes used in wastewater treatment are more vulnerable to membrane

fouling, which was ascribed to the adsorption and aggregation of foulants on the hydrophobic membrane surface. Consequently, membrane permeability is reduced. As the foulants are contacting the membrane surface via hydrogen bonding, electrostatic interaction and weak van der Walls force (Zhao *et al*. 2013), simple hydraulic cleanings will not help to recover the maximum membrane flux until the membrane has antifouling property. Hence, high flux, low fouling tendency and high rejection capability are the prerequisites of the nanocomposite membrane. In the present study, BSA was used as a model protein. Generally, as the size of BSA molecules is larger than the membrane pore size, it adsorbs on the membrane surface rather than penetrate the pore. Thus, it causes severe fouling on the membrane surface.

Figure 5.13 signifies the water permeability before and after BSA filtration. The water permeability was reduced to a greater extent after BSA filtration, which was attributed to the blockage of membrane pores by adsorption of BSA molecules on the membrane surface and concentration polarization. However, after washing, the nanocomposite membrane could recover the maximum water permeability while compared to the pristine (TM-0) membrane.

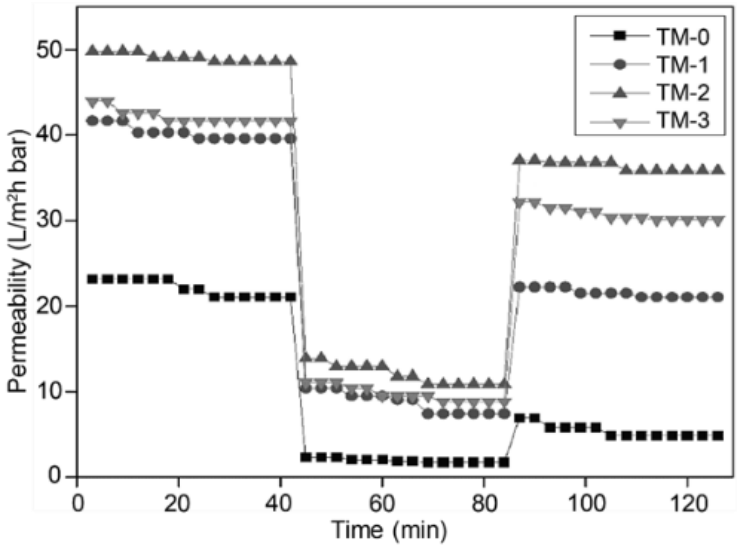

Figure 5.13 Water and BSA solution permeability of pristine and nanocomposite membranes

The calculation of the flux recovery ratio (FRR) would be useful to determine the antifouling performance of the membranes. In addition, total organic fouling (R_t),

reversible fouling (R_r) and irreversible fouling (R_{ir}) were also calculated for better understanding and values are tabulated in Table 5.3. The TM-2 membrane showed the FRR of 73.9 % compared to the TM-0 membrane of 41.2 %. The enhanced FRR of the nanocomposite membrane was owing to the improved hydrophilicity and surface charge by the addition of GO@poly(SBMA-co-MBAAm) nanohybrid.

The better hydrophilicity of the nanocomposite membrane assists to form a hydration layer on the membrane surface, which hinders the adsorption of protein molecules (Zinadini *et al*. 2014). Thus, the loosely adsorbed foulants were easily removed with a simple hydraulic water wash. Moreover, since the as-prepared nanocomposite membrane is negatively charged at pH 7.4, it also would help to inhibit the adsorption of negatively charged BSA molecules through electrostatic repulsion. The R_t of the pristine membrane was 81.8 %, which shows the inferior antifouling nature of TM-0. The nanocomposite membrane TM-2 demonstrated the R_{ir} of 17.4 %, which confirmed the loose adhesion of foulants on the membrane surface. In the case of TM-0, R_{ir} was 38.8 % as the foulants had a strong attraction towards the membrane surface. Still, TM-3 membrane performance was less compared to TM-2. The reason for the reduced performance of TM-3 could be attributed to the agglomeration of nanohybrid at the higher concentration. In summary, the antifouling property of the TM-2 membrane was significantly enriched.

5.4 CONCLUSIONS

The prepared graphene oxide surface was functionalized with zwitterionic sulfobetaine via distillation precipitation polymerization. The as-synthesized nanohybrid was incorporated into the polysulfone membrane matrix and ultrafiltration hollow fiber membranes were prepared by dry/wet phase inversion method. The modification of graphene oxide was confirmed by spectroscopic and microscopic techniques. The existence of nanohybrid in the membrane matrix was investigated by XPS analysis. The impact of nanohybrid on the hydrophilicity, water uptake, porosity, molecular weight cut-off, morphology, permeability and antifouling capacity of nanocomposite membranes were explored. The nanocomposite membrane (TM-2) exhibited high pure water permeability (49.6 L/m^2 h bar) and reactive dyes such as Reactive black 5 (99.0 %) and Reactive orange 16 (74.1 %) rejection with high salt permeability, which was owing to the presence of nanohybrid. TM-2 membrane with 0.25 wt% loading of nanohybrid exhibited the

irreversible fouling of 17.4 %, signifying enhanced antifouling ability; the as-prepared novel ultrafiltration hollow fiber membrane demonstrates a potential application for salt/dye mixture separation in textile wastewater.

CHAPTER 6

PERFORMANCE INTENSIFICATION OF POLYSULFONE ULTRAFILTRATION MEMBRANE BY BLENDING WITH COPOLYMER ENCOMPASSING NOVEL DERIVATIVE OF POLY(STYRENE-CO-MALEIC ANHYDRIDE) FOR HEAVY METAL REMOVAL FROM WASTEWATER

Abstract: *In this chapter, the hydrophilic polymer was synthesized by the aminolysis of poly(styrene-co-maleic anhydride) cumene terminated (PSMAC) using p-aminohippuric acid. The effect of the blend ratio of polysulfone (PSF) and poly[styrene-alt-(N-4-benzoylglycine-maleamic acid)] cumene terminated (PAH) on morphology and permeation were studied. The blend membrane was also screened for heavy metal ion removal. The M-3 membrane was screened for heavy metal ion removal and achieved the removal of 91.5 % of Pb^{2+} and 72.3 % of Cd^{2+} ions, respectively. The adsorption parameters indicated that the Langmuir isotherm model fits well for both Pb^{2+} and Cd^{2+} ions adsorption on the M-3 membrane. The adsorption capacity attained from the Langmuir isotherm model was 19.35 and 9.88 mg/g for Pb^{2+} and Cd^{2+} ions correspondingly.*

6.1 INTRODUCTION

The intensifying obligation for clean, freshwater and declining obtainability from natural resources, water needs to be conserved effectually to come across future requirements (Service 2006). This deteriorating condition fascinated the attention of global researchers towards non-conventional sources, such as ocean water, treated water and groundwater. Membrane separation processes such as ultrafiltration (UF), nanofiltration (NF), reverse osmosis (RO) and forward osmosis (FO) have been established briskly in the past decade into the leading technology for the effective water treatment (Petersen 1993). The UF membrane separation process is currently considered as the improved water purification method since it is cost-effective, efficient and reduced potential for fouling. In addition, it serves as a pretreatment filter for RO and NF membranes during desalination of seawater (Rosberg 1997).

The scarcity of water across the globe has directed to reuse wastewater. Industries such as paper, battery, electronics, tanneries, metal plating and pesticides are discharging heavy metals directly or indirectly into the environment in large quantities. In addition, the practice of untreated wastewater for irrigation would increase the accumulation of heavy metal concentration in soil (Li *et al*. 2016). As stated by the Environmental Protection Agency, lead (Pb^{2+}) and cadmium (Cd^{2+}) are highly toxic materials (Demirbas 2008). Furthermore, lead can damage the kidney, central nervous system, liver, reproductive system and strongly bound to serum protein in the blood, which can change the functional properties of serum protein (Ayranci *et al*. 2004). Cadmium has been classified as a

probable human carcinogen and chronic exposure leads to kidney dysfunction (Fu *et al*. 2011). Thus, spreading out the efforts to regulate the wastewater treatment as an important way to avoid the entry of heavy metals into soil and food chain.

Researchers have proposed quite a lot of methods for the removal of heavy metals from water such as using a water-soluble polymer as a complexing agent (Geckeler *et al*. 1996), adsorption (Duman *et al*. 2010), precipitation (Gharabaghi *et al*. 2012), ion-exchange (Alam *et al*. 2014), thermal and chlorination treatment (Liu *et al*. 2015), NF (Zhang *et al*. 2015), polymer nanocomposite (Chavan *et al*. 2015) and the rest. Polymer enhanced ultrafiltration (PEUF) is also one of the most popular methods, in which the heavy metal-containing solution is treated with a complexing agent such as polyethylenimine to form the larger complexes, which is filtered through UF membranes (Hebbar *et al*. 2016). Nevertheless, most of the methods are expensive thus making it less economical. Moreover, it generates solid waste also time and energy-consuming. UF membrane containing metal coordinating polymer would be one of the most effective methods which can overcome the above drawbacks.

Polysulfone (PSF) is one of the commercially available pressures driven UF membrane polymeric material which is having the superior capacity to remove pathogens, macromolecular natural organic matter, viruses, bacteria and inorganic colloidal particles from water (Cheryan 1998). Furthermore, PSF is stable over a wide range of pH, thermally labile and chlorine resistant (Ibrahim *et al*. 2017). However, the membranes prepared by using PSF as the polymeric material is lesser hydrophilic (Ibrahim *et al*. 2017) in nature and hence it fouls at a very faster rate. Fouling is one of the core problems in membrane technology. Typically, the adsorption of foulants on the membrane due to the hydrophobic nature of the membrane, which results in irreversible fouling that significantly interrupts the membrane permeation performances throughout the filtration processes (Sawada *et al*. 2012). As a result, the membranes need to be cleaned by using chemicals or backwashes, which leads to an increase in operational cost and reduces lifetime (Kuzmenko *et al*. 2005). In addition, the PSF membrane does not have any metal coordinating site for forming the complex with heavy metal ions for adsorptive removal. Furthermore, the pore size of the PSF UF membrane is larger than the heavy metal ions. As a result, an additional complexing agent such as polyethylenimine (PEI) to be employed before filtration.

Therefore, the PSF polymer to be modified with metal coordinating groups such as $–NH_2$, -COOH, etc. The PSF membrane hydrophilicity can be enhanced by grafting with hydrophilic polymers (Helin *et al*. 2008), the addition of hydrophilic nanomaterial (Ong *et al*. 2016), or water-soluble additives (Moideen K *et al*. 2016) to the casting solution and plasma oxidative post-treatments (Kim *et al*. 2002). Nevertheless, these events enhance the hydrophilicity and deliver only short-term influence, which involves more tedious steps for preparation and scale-up.

The blending of PSF with a polymer with an ability to form coordination polymer (Joseph *et al*. 2003) and hydrophilic polymer (Meng *et al*. 2009) is one of the conventional methods for intensifying hydrophilicity, pore size and heavy metal removal. Styrene-maleic anhydride (SMA) was used as a hydrophilic additive to polyethersulfone membranes and stated that the SMA was hydrolyzed during membrane formation. Consequently, the prepared membranes unveiled better hydrophilicity and protein adsorption resistance (Zhu *et al*. 2007). Tang *et al*. prepared electrospun sodium salt of SMA cross-linked with diethylene glycol hydrogel nanofibers and indicated that the nanofiber is able to show better water swelling character (Tang *et al*. 2007). Thomas *et al*. indicated that hydrolyzed poly(styrene-co-maleic anhydride) (HPSMA) for adsorption of a Pb^{2+} ion from a solution of Pb^{2+} and Zn^{2+} ions and results revealed that it has the capacity to adsorb Pb^{2+} ion to better extend via complex formation than Zn^{2+} ion (Thomas *et al*. 2008). Zhu et al. synthesized graft copolymer of methoxyl poly(ethylene glycol) and SMA as an additive. The studies exhibited that, the increase of surface hydrophilicity and improved anti-fouling properties over the neat membrane (Zhu *et al*. 2008). Shenvi *et al*. reported HPSMA as an additive that enhanced the permeation properties (Scheme 6.1) (Shenvi *et al*. 2014).

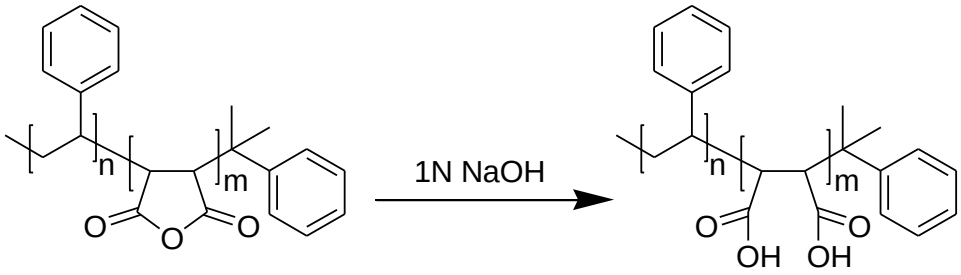

Scheme 6.1 Synthesis of hydrolyzed poly(styrene-co-maleic anhydride) (HPSMA) (Shenvi *et al*. 2014)

In the contemporary study, poly[styrene-alt-(N-4-benzoylglycine-maleamic acid)], cumene terminated (PAH) polymer was synthesized and blended with PSF in a different ratio. The PSF/PAH blend membranes were fabricated by phase inversion method. The result of the blending ratio on the morphology of the membrane and execution was premeditated in depth. The surface hydrophilicity was evaluated by dynamic contact angle analysis. The membrane cross-sectional morphology was characterized by SEM. The presence of PAH in the membrane matrix was confirmed by XPS analysis. The miscibility of the blend membrane was characterized by DSC analysis. The functioning of blended membranes was studied by means of pure water permeability (PWP), water uptake, porosity and surface charge. In addition, an attempt was made to explore the adsorptive heavy metal ion removal affinity of the as-prepared membranes.

6.2 EXPERIMENTAL SECTION

6.2.1 Materials and methods

Polysulfone (Udel P-3500) was acquired from Solvay chemicals. N-methyl pyrrolidone (NMP), dimethyl sulfoxide (DMSO) and thionyl chloride ($SOCl_2$) were purchased from Spectrochem, India. Poly(styrene-co-maleic anhydride), cumene terminated (PSMAC) (M_n ~16 kDa by GPC) was procured from Sigma-Aldrich, India. Cadmium nitrate tetrahydrate (assay 98 %) and lead (II) nitrate (assay 99.9 %) were obtained from Sigma- Aldrich Co., Bangalore, India. Glycine and *p*-aminobenzoic acid (PABA) were purchased from Loba Chemicals.

The ring-opening reaction of PSMAC with *p*-amino hippuric acid and the functional groups present in the isolated polymer was confirmed by recording its FT-IR spectra. The same was recorded using Bruker Alpha FT-IR spectrometer in the range of 4000 – 500 cm^{-1}. The dry polymer sample was mixed with KBr and pressed into a tablet. ^1H NMR spectrum was recorded on Bruker Avance-400 spectrometer (400 MHz) using DMSO-d_6 as a solvent and (TMS) as an internal standard with 32 number of scans. The unit of chemical shift is represented in δ (ppm). The cross-sectional SEM images were recorded employing a tabletop scanning electron microscope (TM3000, HITACHI, Japan). The membrane samples were dipped in methanol for 1 min followed by the cryogenic fracture in liquid nitrogen and sputtered with a thin layer of platinum using a sputtering apparatus

with the intention of spawning an electrically conductive surface. X-ray photoelectron spectroscopy (XPS, THERMOFISHER Scientific K-ALPHA) was employed to identify the presence of PAH on the membrane surface. Al Kα radiation (1486.6 eV) was used as an X-ray source and the take-off angle was 20^{o}.

6.2.2 Synthesis of *p*-aminohippuric acid

The synthesis of *p*-aminobenzoyl chloride was adopted from McMaster *et al*. (McMaster *et al*. 1928). In brief, thionyl chloride (40 mL, 0.54 mol) was added slowly into *p*-aminobenzoic acid (10 g, 0.07 mol) (1) in 100 mL round-bottomed flask (RBF) and heated to reflux for 4 h. After the completion of the reaction, the excess of thionyl chloride was distilled off completely to get pure *p*-aminobenzoyl chloride (2), which was transferred into addition funnel under the nitrogen atmosphere. In another RBF, charged sodium hydroxide (10.75 g, 0.26 mol) in 50 mL of demineralized water and cooled to 0-5 ^{o}C. Added glycine (4.35 g, 0.05 mol) to the RBF containing aqueous sodium hydroxide and stirred for 15 min. Then, *p*-aminobenzoyl chloride was added dropwise over 30 min at 0-5 ^{o}C. The progress of the reaction was monitored by TLC (absence of glycine was confirmed by ninhydrin test). Upon the completion of the reaction, the pH of the reaction mass was adjusted to 7.0 with 10 % of HCl and stirred for 1 h at 0-5 ^{o}C. The solid obtained was filtered, washed with demineralized water and dried. The attained yield was 58 %. The melting point of the compound was found to be 197-200 ^{o}C (decomposition) and it was corresponding to the literature [199-200 ^{o}C (decomposition)] (DeRuiter *et al*. 1989).

6.2.3 Synthesis of poly[styrene-alt-(N-4-benzoylglycine-maleamic acid)], cumene terminated (PAH)

The procedure was adopted from Chenglin *et al*. (Chenglin *et al*. 2012). The PSMAC (1 g) and *p*-aminohippuric acid (2 g) (3) were added to the RBF with a ratio of 1:2 and dissolved in dimethyl sulfoxide (10 mL). The reaction mass was heated in a water bath at 50 ^{o}C until the maleic anhydride group in the FT-IR spectrum (~1853 and 1778 cm^{-1}) completely disappeared (Figure 6.1). Upon the completion of the reaction, the reaction mass was allowed to cool to room temperature and added 20 mL of demineralized water dropwise to the reaction mass and stirred for 1 h at room temperature. The obtained solid was filtered and washed with demineralized water. The material was dried at 55 ^{o}C under

vacuum for 12 h. The schematic illustration of PAH synthesis is exemplified in Scheme 6.2.

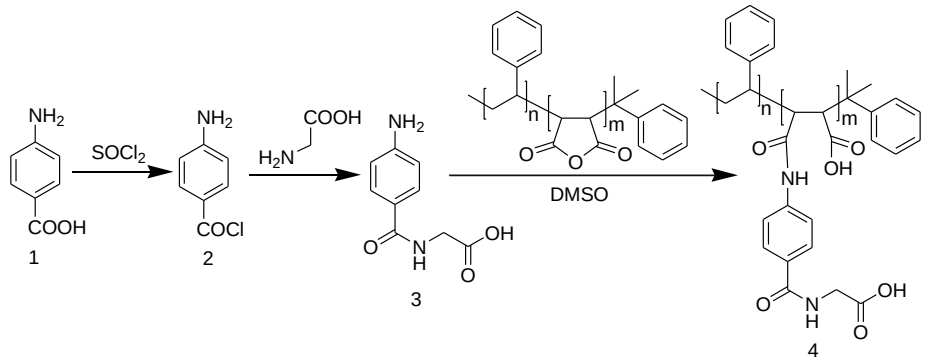

Scheme 6.2 The synthetic route for the poly[styrene-alt-(N-4-benzoylglycine-maleamic acid)], cumene terminated (PAH)

6.2.4 Preparation of polysulfone/poly[styrene-alt-(N-4-benzoylglycine-maleamic acid)], cumene terminated blend membranes

The PSF was dried at 50 ºC for 12 h to remove adsorbed water. For preparing the blend membrane, PSF and PAH (4) were dissolved in NMP at 60 ºC for 24 h to get the homogeneous solution. Subsequently, the polymer solution was sonicated (40 kHz, 60 W Spectralab ultrasonic cleaning bath) for 30 min at room temperature for removing the trapped air and then it was cast over glass plate using a glass rod. After casting, the solvent was endorsed to evaporate for 10 s and immersed in the coagulation bath containing demineralized water. The prepared membranes were retained in demineralized water for 24 h at room temperature with changing of water. Furthermore, it was washed several times with demineralized water followed by air-dried for further analysis. The details of the blending ratio of polymers are depicted in Table 6.1.

Table 6.1 Polysulfone (PSF)/poly[styrene-alt-(N-4-benzoylglycine-maleamic acid)], cumene terminated (PAH) blending ratio for preparing the membrane

Membrane code	PSF (g)	PAH (g)	NMP (g)	% composition (PSF : PAH)
M-0	2	0	8	100 : 0
M-1	1.9	0.1	8	95 : 5
M-2	1.8	0.2	8	90 : 10
M-3	1.7	0.3	8	85 : 15
M-4	1.6	0.4	8	80 : 20

6.2.5 Membrane permeation study

The hydrophilicity of the membrane is one of the key prerequisites for the membrane to uptake water (Ong *et al*. 2016). The water uptake study was done by the following reported procedure (Abbas *et al*. 2016). In short, membranes of 1 cm^2 area were cut and immersed in demineralized water for 24 h at room temperature. The wet membranes were taken out and the adsorbed water on the membrane surface was wiped out with blotting paper and weighed. The wet membranes were dried at 75 ^oC for 24 h and the dry weight of the membranes was recorded. The percentage of water uptake was calculated using the equation (7.1). The changes in hydrophilicity after blending was confirmed by measuring the contact angle of the membranes. The analysis was executed employing an OCA15 plus video-based optical contact angle measuring instrument (Data Physics instrument, Germany) by means of a sessile droplet method. The contact angle was measured thrice at different locations of the membrane and the average value was reported for minimizing the experimental error. The porosity of the prepared membranes was measured as explained in chapter 2, section 2.2.4. The permeation properties of the membrane were assessed by utilizing a lab-scale dead-end filtration unit. The permeation experiments were carried out on the round membrane disk with effective filtration of an area of 0.0025 m^2, where pure water was loaded in a feed tank. Every membrane was compacted for 30 min at 6 bar Transmembrane pressure (TMP) before initiating the experiment. Then the TMP was reduced to 5 bar and maintained at the same pressure for about 15 min to attain the stable flux. Subsequently, the pure water permeability (PWP, 'J_w') was measured at the same TMP for 80 min. The PWP was calculated using the equation (6.2).

$$\% \text{ Water uptake} = \left(\frac{W_w - W_d}{W_w}\right) \times 100 \tag{6.1}$$

$$J_w = \frac{Q}{\Delta t \times A \times \Delta P} \tag{6.2}$$

Where 'W_w' and 'W_d' are the weight of the wet and dry membranes, 'A' is the area of the membrane (m^2), 'ΔP' is the applied pressure, 'J_w' is expressed in (L m^{-2} h^{-1} bar^{-1}) and 'Q' is the amount of water collected through a Δt (h) time.

6.2.6 Surface charge of the membrane

The surface charge of the membranes was determined by measuring the zeta potential (SurPASS, Anton Paar, Austria) based on streaming current method. The membrane sample was cut and immobilized on the adjustable gap cell. The measurements were completed using 0.001 M KCl solution as background electrolyte and pH was adjusted using a 0.5 M HCl solution.

6.2.7 Molecular weight cut-off (MWCO) study

Polyethylene glycol (PEG) containing an average molecular weight of 6000, 10,000, 15,000 and 20,000 Da (100 ppm) was filtered through the membrane to determine the MWCO at 2 bar. The concentration of PEG in both feed and permeate was measured using a total organic carbon (TOC, SHIMADZU) analyzer. The percentage rejection of PEG was calculated using the equation (7.3). MWCO of the membrane is determined by minimum PEG rejection of 90 % and the Stokes radius of PEG (r_p) can be calculated (equation 6.4) on the basis of its average molecular weight (Liu *et al*. 2017).

$$\% \text{ R} = \left(1 - \frac{C_p}{C_f}\right) \times 100 \tag{6.3}$$

$$\text{r}_\text{p} = 16.73 \times 10^{-12} \times M^{0.557} \tag{6.4}$$

Where 'C_p' and 'C_f' are permeate and feed solute concentration and 'M' is the average molecular weight of PEG correspondingly.

6.2.8 Heavy metal ion removal study

The heavy metal ion removal experiments were carried out for various feed concentrations (prepared by dissolving a calculated amount of metal salt in water) of cadmium nitrate tetrahydrate and lead (II) nitrate aqueous solution as the feed separately and effect of pH and other ions (10 mg/L of each NaCl, $CaCl_2$, $MgCl_2$ and $FeCl_3$ aqueous solutions were used) were also studied. The feed and permeate were analyzed by using ICP-OES (Inductively coupled plasma optical emission spectroscopy, PerkinElmer) to identify the metal ion concentration and the percentage of metal ion removal ('% R') was calculated by equation (6.5). All the metal ion removal experiments were carried out using a self-constructed dead-end filtration system.

$$\% \text{ R} = \left(1 - \frac{C_p}{C_f}\right) \times 100 \quad (6.5)$$

Where 'C_p' and 'C_f' are permeate and feed metal ion concentration.

6.2.9 Adsorption study

The adsorptive ability of the M-3 membrane on Pb^{2+} and Cd^{2+} ions was evaluated as follows. 0.05 g of M-3 membrane sample was kept in interaction with 50 mL of each metal ion solution (concentrations varied from 20 – 100 mg/L) in a conical flask and placed in an orbital shaker (150 rpm) for 24 h with solution pH of 6 at room temperature. ICP-OES was used to analyze the initial (C_0) and equilibrium (C_e) concentrations in mg/L respectively. The percentage of removal (% R) by adsorption was calculated using the equation (7.6). In addition, the amount of metal ion adsorbed per unit gram of M-3 membrane (q_e) was calculated by equation (7.7).

$$\% \text{ R} = \left(1 - \frac{C_e}{C_0}\right) \times 100 \quad (6.6)$$

$$q_e = \frac{(C_0 - C_e)\, V}{m} \quad (6.7)$$

Where 'q_e' is equilibrium adsorption capacity (mg/g), 'V' is the total volume of metal ion solution (L) and 'm' is the weight (g) of the dry membrane, which was used for adsorption study.

6.3 RESULTS AND DISCUSSION

6.3.1. Characterization of polymer and membrane

The FT-IR spectra of PSMAC and PAH are represented in Figure 6.1. As shown in Figure 6.1b, the peak at 3336 cm^{-1} can be ascribed to the symmetric stretching of –OH group. The band at 1407 cm^{-1} is due to the C-O-H bending. The carboxylic acid C=O symmetric stretching vibration was observed at 1690 cm^{-1} due to the presence of hydrogen bonding. The peak at 1652 cm^{-1} was due to amide C=O symmetric stretching. The amide N-H bending was observed at 1598 cm^{-1}. The peak at 2920 cm^{-1} was depicted to the aliphatic C-H stretching. More importantly, stretching of anhydride peak was observed at 1853 cm^{-1} and 1778 cm^{-1} in PSMAC, which was not detected in the PAH sample spectrum.

In this manner, the ring-opening reaction of the PSMAC by the *p*-aminohippuric acid was confirmed by FT-IR.

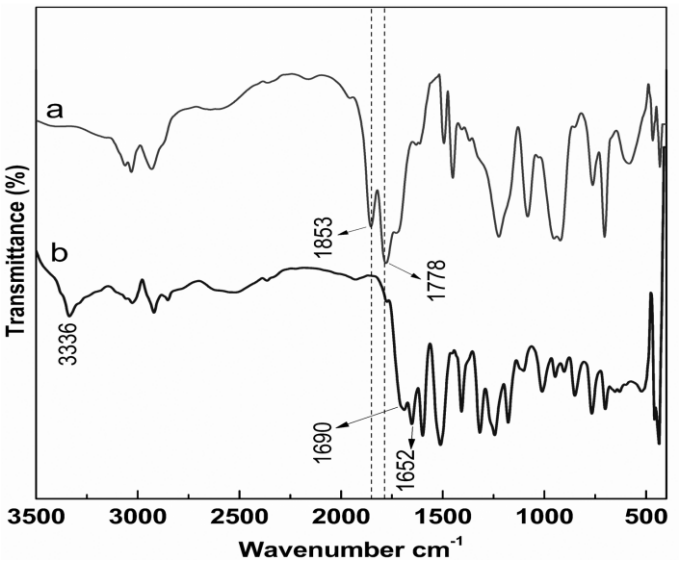

Figure 6.1 FT-IR spectra of a) PSMAC and b) PAH

^{1}H NMR spectrum of PAH is shown in Figure 6.2. It is very clear from the spectrum that, the multiplet at δ 6.6 to 7.9 resembles the aromatic protons. The amide N-H protons were detected at δ 10.0 and 10.4. The more deshielded active methylene group (-CH_2) protons were observed at δ 5.8 due to the presence of amide and carboxylic acid groups. The peak at δ 12.4 confirmed the presence of carboxylic acid group protons. Moreover, the aliphatic protons at δ 2.5 were merged with the DMSO-d_5 peak. These values are consistent with the proposed polymer structure.

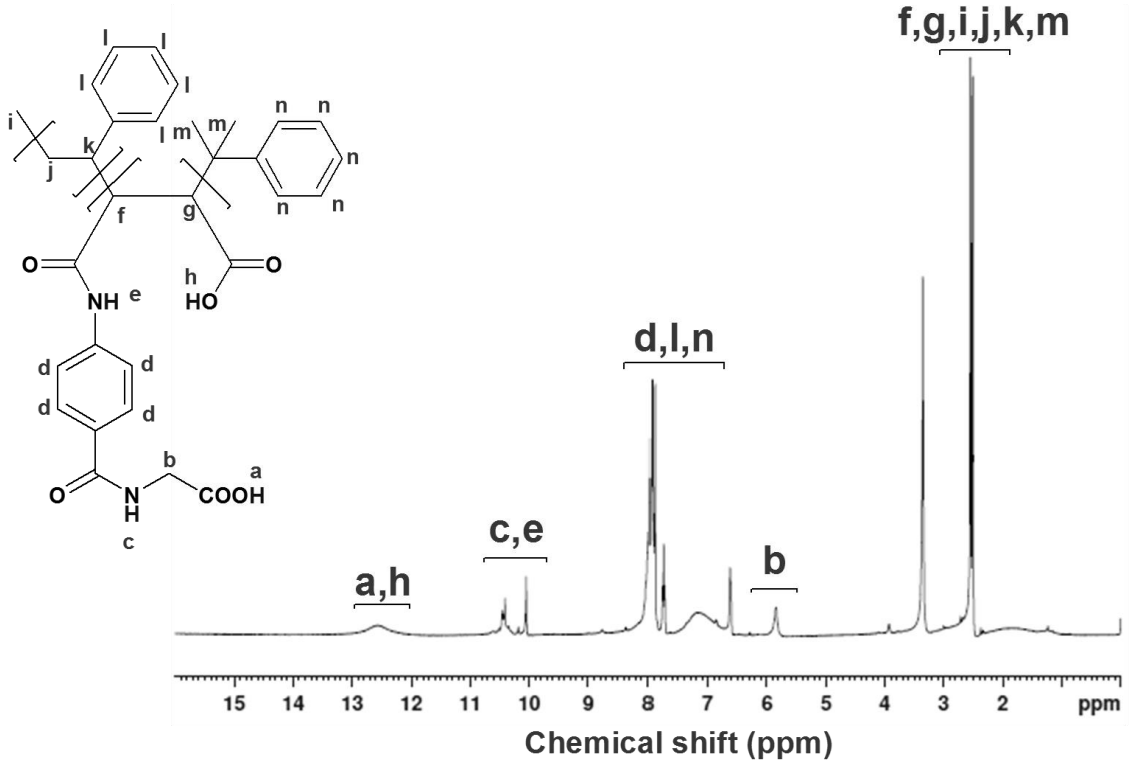

Figure 6.2 ^{1}H NMR spectrum of PAH

The thermal behavior of PSF/PAH blend membranes was studied from the DSC plots. It is observed that the blend membranes exhibited single T_g value and it can be ascribed to the presence of many weak Van der Waals interactions between the two polymers. In addition, the increased T_g value was attributed to the presence of hydrogen bonding (Kwei 1984) and the existence of hydrogen bonding was confirmed by the shift of -C=O and -OH absorption in FT-IR spectra as well. The possible interaction between PSF and PAH polymer by hydrogen bonding is schematically represented in Figure 6.3.

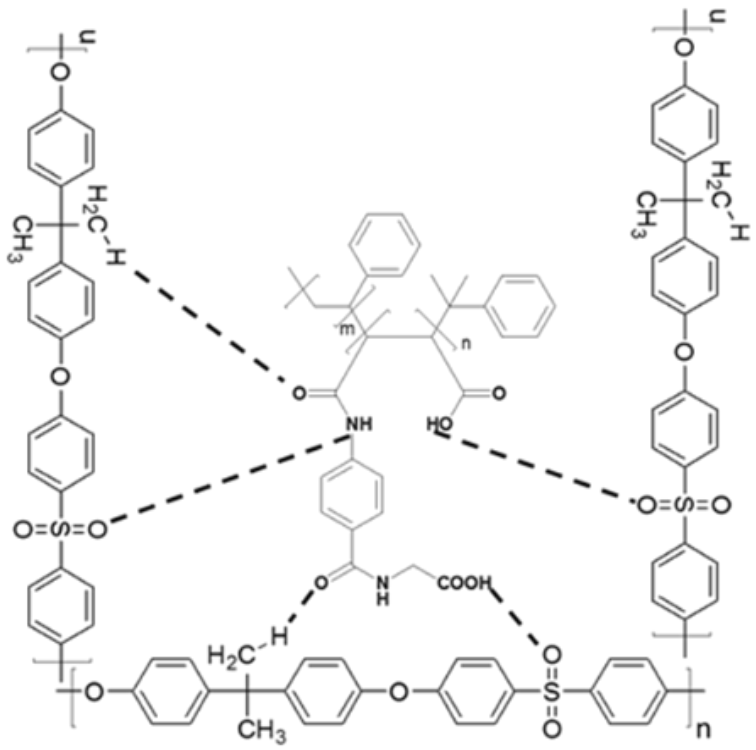

Figure 6.3 Possible interaction between PSF and PAH polymer via hydrogen bonding

XPS wide and narrow scan spectra of M-0 and M-3 membrane are presented in Figure 6.4. For M-0 membrane (Figure 6.4a), the presence of three major emission peaks at 284.98 eV, 532.08 eV and 167.88 eV were attributed to the presence of C 1s, O 1s and S 2p elements. Nevertheless, after blending with PAH polymer the new peak at 399.98 eV was observed and it was attributed to the presence of N 1s element. Furthermore, the C 1s and N 1s peaks were deconvoluted and presented in Figure 6.4b and c. The peak at 285.07 eV was due to C-C/C=C. The C=O peak was observed at 287.16 eV. The peak at 286.16 eV was attributed to the presence of C-O/C-N. The presence of the amide group (O-C=O) was detected at 290.84 eV. In the case of N 1s, two peaks were observed at 398.18 eV and 400.48 eV, which corresponding to N-C and N-C=O bonds in an amide. Thereby the presence of PAH on the membrane surface was confirmed by XPS analysis.

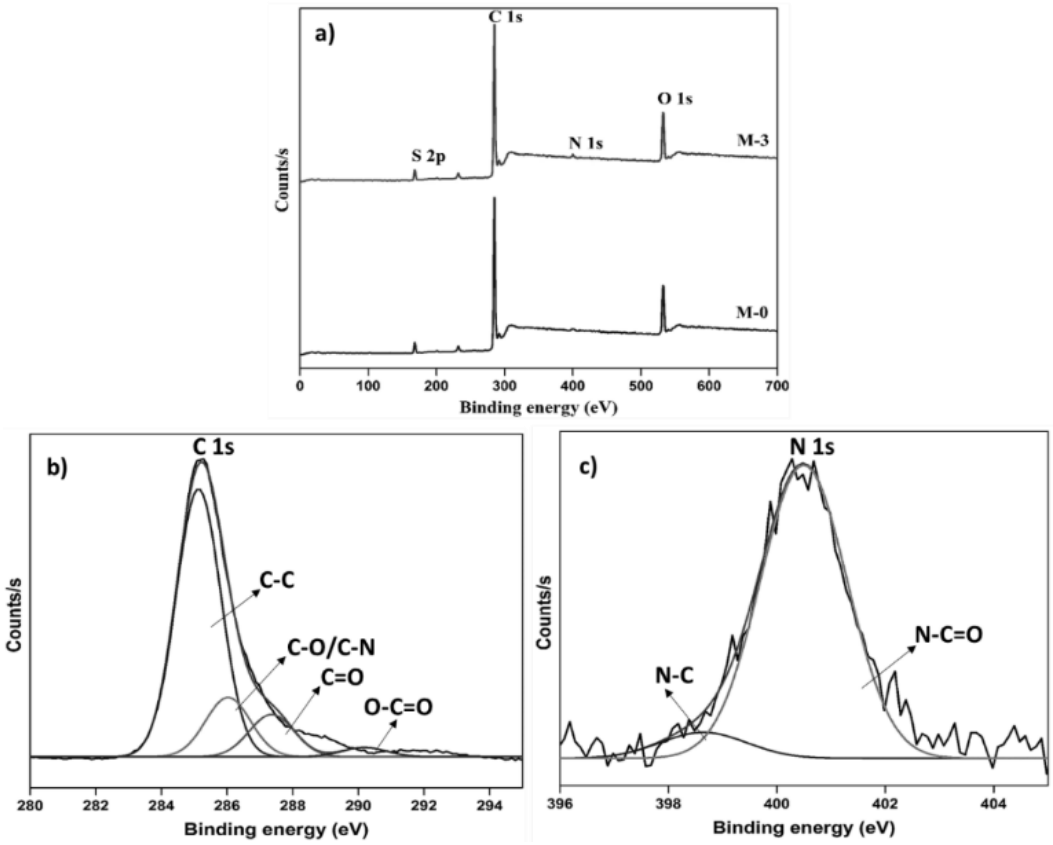

Figure 6.4 a) XPS wide scan spectra of M-0 and M-3 membranes, b) and c) M-3 membrane narrow scan spectra of C 1s and N 1s

6.3.2 Surface hydrophilicity of the membranes

The surface hydrophilicity is one of the key parameters in a membrane preparation. The surface hydrophilicity of the prepared membrane can be measured by the contact angle analysis. As per a general rule, if the contact angle is less, the membrane surface would be more hydrophilic and vice versa. The contact angle of the membrane surface can be reduced by incorporating hydrophilic substances. The membrane M-3 exhibited a less contact angle of 55^{o} compared to the pristine membrane (M-0) of 82^{o}. The contact angle is represented in Table 6.2. As the ratio of PAH increases, the water contact angle value was further decreased. However, over 20 % of PAH, the water contact angle was started increasing. The increase in water contact angle was attributed to the increase of hydrophobic alkyl group of PAH in the blend and it has dominated the effect of hydrophilic functional groups. The changes in the contact angle of the blend membranes could be comprehended in the following way. i.e., during the phase inversion process, to diminish the interfacial energy between the polymer blend solution and non-solvent bath, the hydrophilic PAH polymer

travels towards the surface of the membrane. As a result, the PAH polymer density will be more on the membrane surface and pore surface (Humplik *et al*. 2011). Additionally, as far as the asymmetric membrane is concerned, the skin layer controls the performance of the membrane rather than the sublayer.

Table 6.2 Membrane properties

Membrane code	Thickness (µm)	Contact angle (°)	Water uptake (%)	Porosity (%)	PWP* (L m^{-2} h^{-1} bar^{-1})
M-0	158 ±0.1	82 ±1.6	21.1 ±3.3	30.3 ±1.3	1.72 ±0.23
M-1	143 ±0.2	74 ±2.1	60.2 ±2.7	40.1 ±2.3	3.44 ±0.21
M-2	149 ±0.1	65 ±1.2	61.5 ±1.8	42.4 ±1.6	6.72 ±0.23
M-3	162 ±0.2	55 ±2.3	77.7 ±3.4	57.1 ±1.2	35.7 ±0.35
M-4	151 ±0.4	61 ±2.6	74.1 ±3.9	55.2 ±1.7	30.7 ±0.32

*PWP: Pure water permeability (L m^{-2} h^{-1} bar^{-1})

6.3.3 Water uptake, porosity and MWCO of membranes

In general, the water uptake capability of the membrane depends on the surface hydrophilicity. The M-3 membrane had shown the uppermost water uptake ability of 77.7 % compared to the pristine membrane (M-0), which was attributed to the presence of PAH polymer. However, the M-4 membrane had publicized the water uptake of 74.1 %. This abnormal tactic was ascribed to the decreased hydrophilicity of the M-4 membrane. The decreased hydrophilicity of the membrane reduces the hydration sphere which formed on the surface of the membrane. Furthermore, as the ratio of PAH increases, the hydrogen bonding between the blend membrane and water also increases (Manawi *et al*. 2016). Thereby, it can put up a number of a water molecule on the macrovoids present in the membrane. Whereas, in the case of M-4, the increased ratio of the alkyl group diminishes the hydrogen bonding. Since the alkyl group, the hydrophobic effect was less, there was a slight change in water uptake between M-3 and M-4 sequentially. The water uptake ability of blend membranes is tabulated in Table 6.2

The porosity of the blend membranes improved with an escalation in the ratio of PAH up to the M-3 membrane. It is evident from the literature that, the porosity can be improved by incorporating hydrophilic nanomaterials and pore-forming agents (Zhao *et al*. 2008). In

the current study, no nanomaterials and pore-forming agents were employed. The increased percentage of porosity can be enlightened with the following reasons. The first reason could be the formation of hydrogen bonding between water molecules and PAH. Secondly, the improved hydrophilicity enhanced the rate of demixing and led to the formation of more fingerlike projections. Consequently, the porosity was increased. The membrane M-4 had exhibited a decrease in porosity to a small extent. This phenomenon can be explained as follows. Due to the low miscibility and decreased hydrophilicity of PAH beyond 20 %, the interaction between PAH and water diminishes to a small extent. Therefore, the rate of demixing decreases and it led to the formation of the dense membrane, as captured in SEM images. Hence, the porosity was decreased (Ali *et al*. 2016, Dervin *et al*. 2016). The percentage of porosity is depicted in Table 6.2.

Figure 6.5 depicts the MWCO of the membrane. The MWCO of M-3 membrane was 15510 Da and the Stokes radius was 3.6 nm respectively. This result suggests that the prepared membrane is a UF membrane.

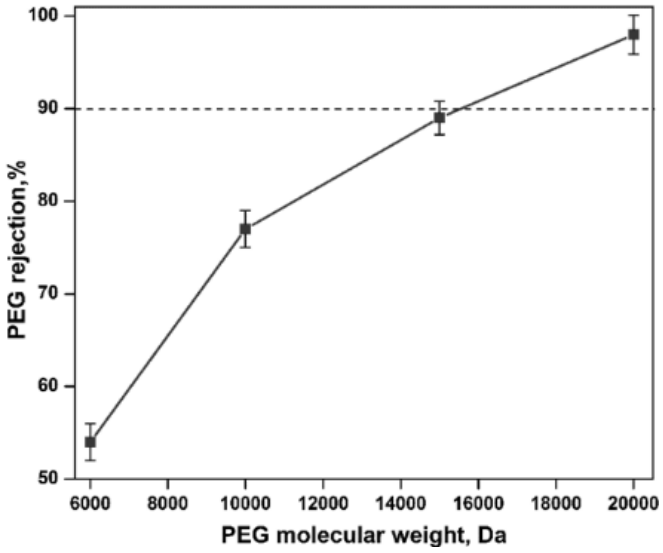

Figure 6.5 Molecular weight cut-off (MWCO) of M-3 membrane

6.3.4 Morphology of the membranes

In the direction of studying the membrane morphology, the cross-section of the membrane samples was witnessed in SEM, as displayed in Figure 6.6. The pristine PSF (M-0) membranes classically yielded in a dense skin layer at the surface reinforced by the fingerlike voids throughout phase inversion (Corry 2008). The membrane M-1 unveiled vertical microvoids, nevertheless, the horizontal macrovoids are less noticeable. Moreover,

the membranes M-2 and M-3 were exhibited vertical microvoids stretched up to the bottom layer of the membrane and no horizontal macrovoids were detected. In addition, M-4 had publicized vertical microvoids whereas the horizontal macrovoids are pronounced little more compared to the M-3 blend membrane. This is due to the diminished hydrophilicity of the membrane. Furthermore, it was understood that the water could flow through the vertical pore at ease as well as with less amount of in-house resistance. Whereas, in the case of water flow in the horizontal pore experiences more in-house resistance and led to less water flux.

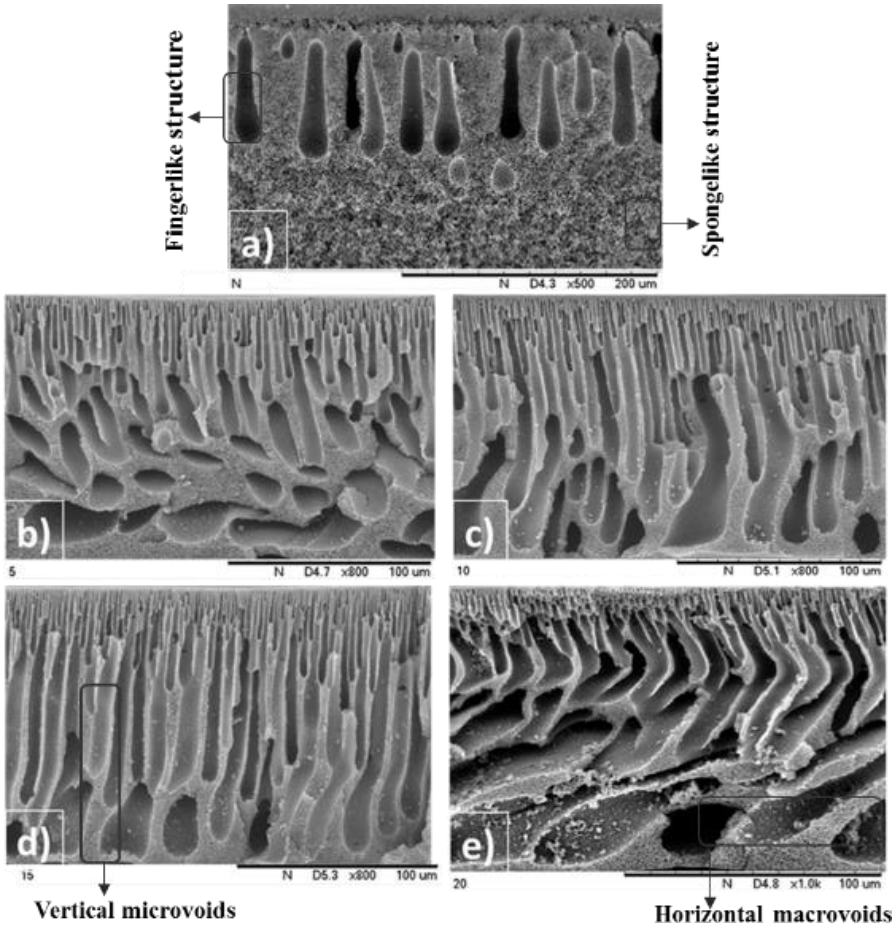

Figure 6.6 Cross-sectional SEM images of a) M-0, b) M-1, c) M-2, d) M-3 and e) M-4

6.3.5 Pure water permeability of membranes

The pure water permeability (PWP) of the prepared blend membranes was increased as the ratio of PAH increases, as illustrated in Table 6.2. The M-3 membrane exhibited the maximum PWP than the pristine (M-0) membrane. The improved flux could be attributed to the increased hydrophilicity and porosity of the blend membranes. As mentioned above,

the surface hydrophilicity and porosity decrease the resistance of permeation of water molecules through the membranes and unveiled better permeability. However, the M-4 membrane exhibited decreased PWP than the M-3 membrane owing to reduced hydrophilicity and porosity.

6.3.6 Surface charge of membranes

Surface charge is one of the key factors in determining the separation properties of the UF membranes. The M-3 membrane exhibited a higher negative charge than the pristine M-0 membrane, as depicted in Figure 6.7. The increased negative charge was attributed to the presence of the carboxylic acid groups in the membrane. Since the pH decreases to the acidic side, the carboxylate ions are protonated and as a result double layer thickness shrinks. The change in the zeta potential of the PSF membrane was ascribed to the incorporation of PAH polymer.

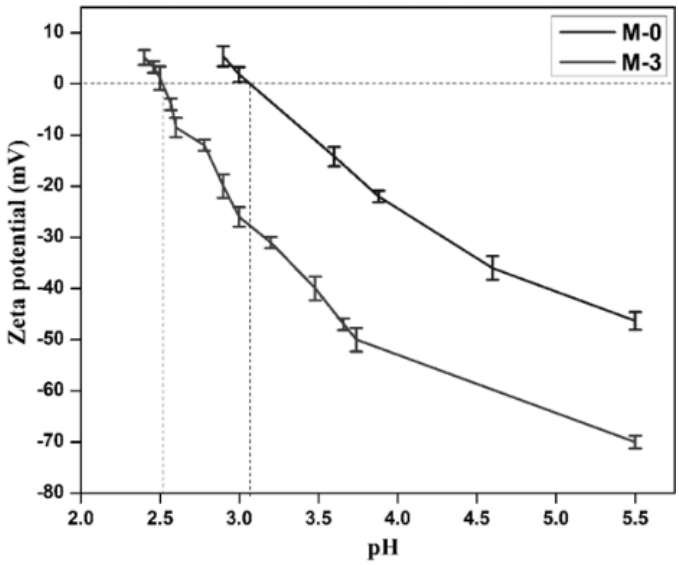

Figure 6.7 Zeta potential of membranes

6.3.7 Heavy metal ions removal study

Heavy metal ions are the most hazardous environmental pollutants and non-biodegradable in nature. In the current study, among all the prepared blend membranes, the well-performed membrane M-3 was favored for the heavy metal ion removal studies. The prepared novel polymer contains carboxyl groups, that acting as a coordinating site for the heavy metal ions (Hummer *et al*. 2001). Thereby metal ions were removed by adsorption on the surface of the membrane, as depicted in Figure 6.8.

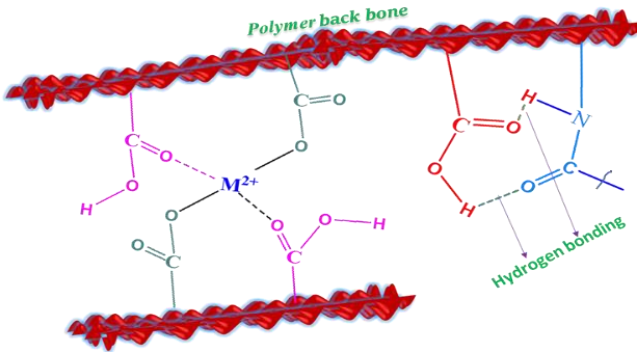

Figure 6.8 The proposed mechanism of complex formation with metal ions and hydrogen bonding

6.3.7.1 Effect of other ions

In the view of the real-time application, it is very important to carry out the metal ion removal experiment in the presence of other ions such as Na^{+}, Ca^{2+} Mg^{2+} and Fe^{3+} ions and presented in Figure 6.9. It was found that in the presence of Na^{+} ions the removal efficiency was reduced to a small extent. However, as the valency of other metal ion increases the removal percentage was decreased to a greater extent. The reason for this reduction was due to the reduced mobility of Pb^{2+} and Cd^{2+} ions towards the membrane surface. The other ions got involved in complex formation with PAH polymer, which makes less available active functional groups for Pb^{2+} and Cd^{2+} ions to bind. Furthermore, as explained by Miyoshi *et al*. (Miyoshi 1999) the formation of ion-pair between the other metal ions and membrane surface was also affected the membrane performances.

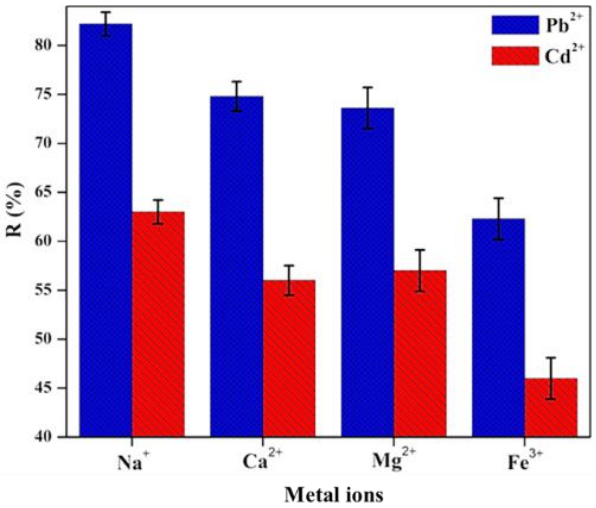

Figure 6.9 Removal of metal ions using M-3 membrane in the presence of other ions (2 bar, 10 mg/L and pH 6)

6.3.7.2 Time-dependent study

Figure 6.10 depicts the heavy metal ions removal as a function of time. It was observed that, removal and permeate solution flux started decreasing with time. Moreover, the percentage of removal of Pb^{2+} was higher than Cd^{2+}. The reason could be, the Pb^{2+} would have displayed a strong affinity to form the stable complex with polymer rather than Cd^{2+} i.e., the Pb^{2+}-polymer complex would be more stable than the Cd^{2+}-polymer complex. To evaluate this statement, the following literature helped in resolving the unknown fact. Junxia *et al*. reported Cd^{2+} and Pb^{2+} complexation using high molecular weight poly(acrylic acids). The results revealed that the Pb^{2+} was well bound to form stable complex than Cd^{2+}. Thus the metal binding capacity of poly(acrylic acids) for Pb^{2+} was higher than Cd^{2+}(Junxia *et al*. 2007, He *et al*. 2016). Similarly, glycogen-graft-poly (acrylic acid) copolymer exhibited the selective removal of Pb^{2+} over the other metal ions (Pal *et al*. 2015). The decreased removal of metal ions and reduced permeate solution flux can be attributed to the pore collapse and fouling on the membrane surface. Additionally, the adsorption of foulant on the membrane surface reduces the interaction of metal ions with the membrane surface by forming a cake layer. Consequently, the removal efficiency was decreased.

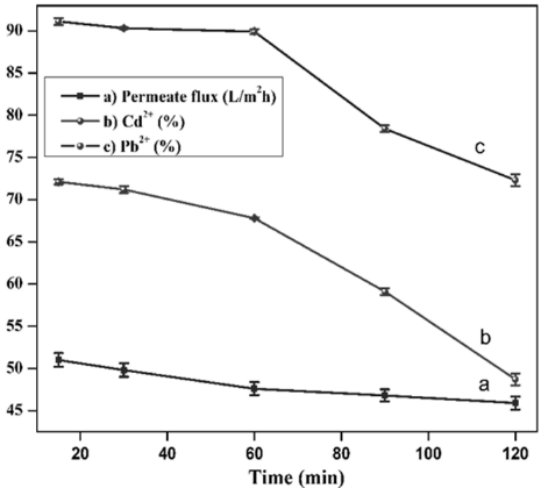

Figure 6.10 Heavy metal ion removal of M-3 membrane as a function of time with permeate flux (10 mg/L, 2 bar and pH 6)

6.3.7.3 Reusability test of membranes

In addition, the reusability of the M-3 membrane was characterized by simple acid treatment (0.2 M HNO_3) and had run for five cycles with 10 mg/L of feed solution (pH 6) at 2 bar pressure. The results indicated that the M-3 membrane manifested higher removal

of above 88 % of Pb^{2+} and 63 % of Cd^{2+} ions up to four cycles. However, in the case of the fifth cycle, the metal ion removal decreased to less than 76.1 % of Pb^{2+} and 60.3 % of Cd^{2+} ions (Figure 6.11). To further confirm the adsorption and desorption (after washing with acid) of heavy metal ions on the membrane surface, elemental mapping was carried out which is presented in Figure 6.12. It concludes that the novel membrane could be regenerated by simple acid treatment. Table 6.3 summarizes some of the recent literature reports towards the heavy metal ions removal by the UF membrane.

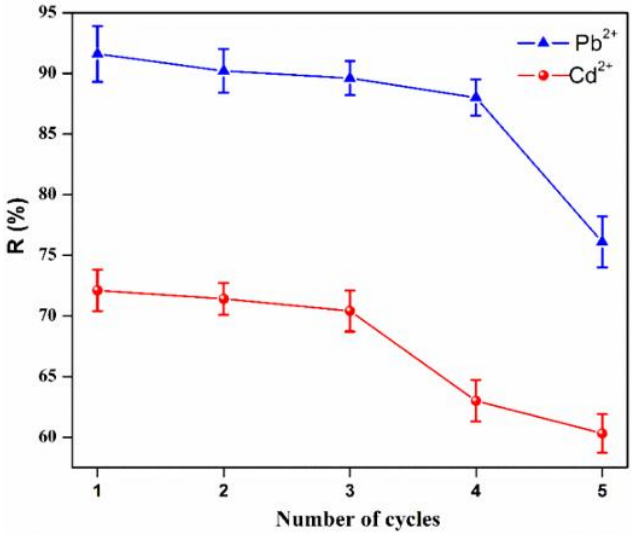

Figure 6.11 Reusability study of M-3 membrane

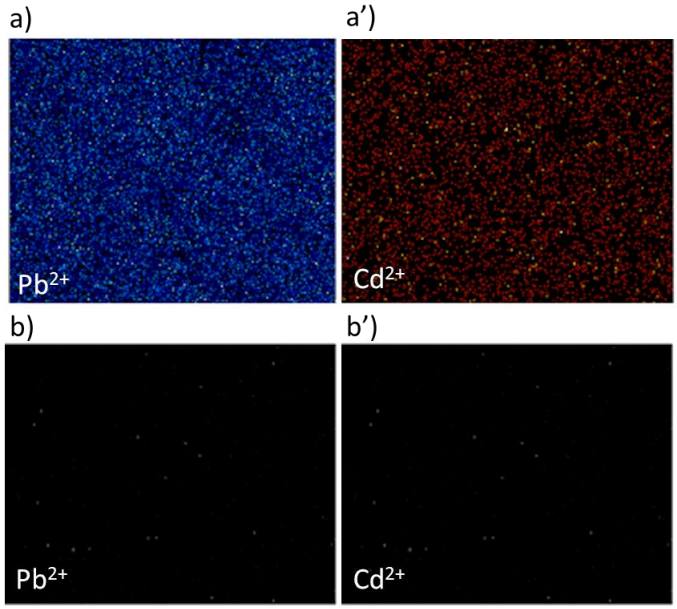

Figure 6.12 Elemental mapping of M-3membrane a) and a') after filtration and b) and b') after acid washing

Table 6.3 Summary of heavy metal ions removal by ultrafiltration membranes

Additive	Metal ions removed	Removal (%)	Adsorption capacity (mg/g)	Feed Conc. (ppm)	pH	Mechanism	Ref.
Poly 3-methyl 2-vinyl pyridinium nitrate	Cu^{2+} Pb^{2+}, Cd^{2+}	99.23, 89.61, 97.15	NA	1000	6	Molecular sieving	(Kalaiselvi *et al*. 2015)
Hydrous ferric oxide nanoparticles	Pb^{2+}	95%	13.2	0.1	7	Adsorption	(Abdullah *et al*. 2016)
Polydopamine coated halloysite	Pb^{2+}, Cd^{2+}	79, 73	NA	1000	6	Molecular sieving	(Hebbar *et al*. 2016)
Polydopamine nanoparticles	Pb^{2+}, Cd^{2+}, Cu^{2+}	NA	20.23, 17.01, 10.42	NA	5.4	Adsorption	(Fang *et al*. 2017)
Nickel iron oxide	Cu^{2+}, Cd^{2+}, Ni^{2+}, Zn^{2+}, Pb^{2+}, Cr^{6+}	98.6, 71.38, 62.51, 83.45, 98.14, 52.84	41.42, 23.87, 17.46, 35.25, 52.11, 17.45	50	4 - 10	Adsorption	(Mondal *et al*. 2017)
PAH polymer	**Pb^{2+}, Cd^{2+}**	**91.5, 72.3**	**19.35, 9.88**	**10**	**6**	**Adsorption**	**Present study**

6.3.7.4 Adsorption isotherm

The adsorption capacity (mg/g) of the M-3 membrane at different metal ion concentrations (mg/L) is presented in Figure 6.13. The heavy metal ion adsorption on the membrane surface was studied by fitting the adsorption data into Langmuir and Freundlich isotherm models. The linear form of the Langmuir model is depicted in equation (6.8). It bestows the homogeneous system with single layer adsorption.

$$\frac{C_e}{q_e} = \frac{1}{bq_{max}} + \frac{C_e}{q_{max}} \tag{6.8}$$

Where 'C_e' and 'q_e' are the concentration and amount of metal ion adsorbed at equilibrium (mg/g), 'q_{max}' is the maximum adsorption capacity (mg/g) and 'b' is the Langmuir constant (L/mg), which is related to the affinity of the binding site.

Equation (6.9) depicts the linear form of the Freundlich isotherm model and it designates the multilayer adsorption in a heterogeneous system.

$$ln\ q_e = ln\ K_F + \frac{1}{n}\ ln\ C_e \tag{6.9}$$

Where 'K_F' ($mg^{1-1/n}\ L^{1/n}\ g^{-1}$) and '$n$' are Freundlich constants.

The obtained isotherm parameters of both the isotherm models are tabulated in Table 6.4. It is clear from the Table that, the adsorption parameters follow Langmuir isotherm more satisfactorily rather than Freundlich isotherm with the regression coefficient R^2 value of 0.99 for Pb^{2+} and 0.98 for Cd^{2+} ions. It was observed from Figure 6.13 that, the order of metal ion adsorption is Pb (II) > Cd (II). The adsorption was assisted by the electrostatic interaction between PAH polymer and metal ions. The increased adsorption of Pb^{2+} ion was ascribed to the decreased hydration energy (1345 kJ/mol) and first hydrolysis constant (pK_1 7.71) of Pb^{2+} ion compared to the Cd^{2+} ion (1575 kJ/mol and $pK_1$10.08) (Barnum 1983, Marcus 1991, Mondal *et al*. 2017). In general, lower the first hydrolysis constant and hydration energy facilitates the formation of the metal hydroxide (MOH^+) (Qiu *et al*. 2009, Nguyen *et al*. 2015, Sounthararajah *et al*. 2015). Therefore, lead (II) forms more metal hydroxide and led to enhanced adsorption than cadmium (II).

Table 6.4 Langmuir and Freundlich isotherm parameters for Pb^{2+} and Cd^{2+} adsorption on M-3 membrane at pH 6

Metal ion	Langmuir model			Freundlich model		
	q_{max} (mg/g)	b (L/mg)	R^2	K_F ($mg^{1-1/n}$ $L^{1/n}$ g^{-1})	1/n	R^2
Pb^{2+}	19.35	0.1417	0.9978	6.81	0.2309	0.9124
Cd^{2+}	9.88	0.0589	0.9871	2.26	0.2955	0.947

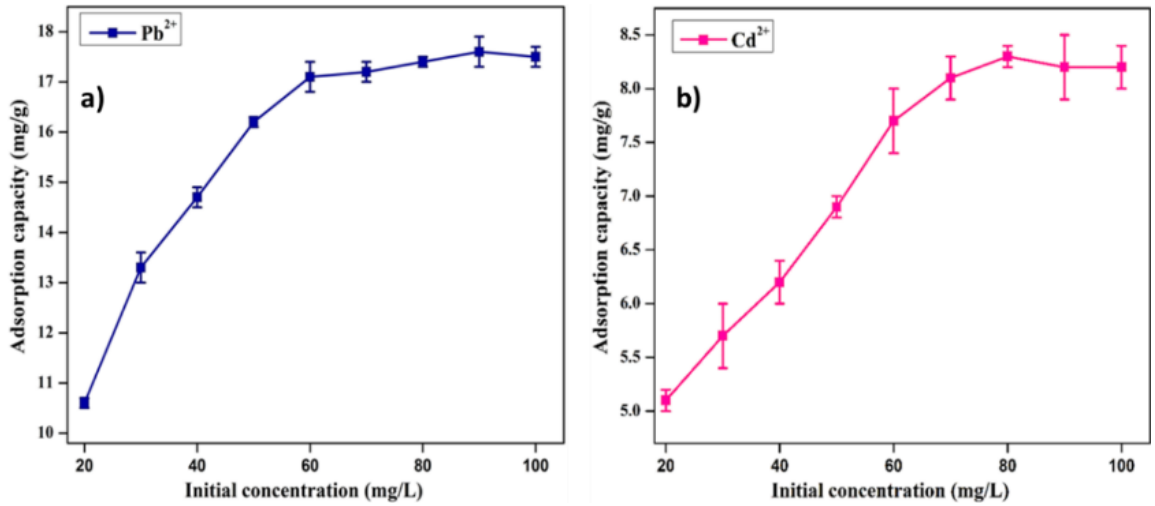

Figure 6.13 The adsorption capacity of the M-3 membrane at pH 6 a) Pb^{2+} and b) Cd^{2+}

6.4 CONCLUSIONS

The poly[styrene-alt-(N-4-benzoylglycine-maleamic acid)], cumene terminated polymer was synthesized and used as an additive to the polysulfone blend membrane. The polysulfone/poly[styrene-alt-(N-4-benzoylglycine-maleamic acid)], cumene terminated blend ultrafiltration membranes were prepared by phase inversion method with a different ratio of poly[styrene-alt-(N-4-benzoylglycine-maleamic acid)], cumene terminated copolymer. The optimum ratio of polysulfone/poly[styrene-alt-(N-4-benzoylglycine-maleamic acid)], cumene terminated was found to be 85:15 (M-3) with pure water permeability of 35.7 L /m^2 h bar. In addition, the M-3 membrane exhibited 91.5 % of Pb^{2+} and 72.3 % of Cd^{2+} ions removal with a feed concentration of 10 mg/L. The results also revealed that the further increase of polysulfone/poly[styrene-alt-(N-4-benzoylglycine-maleamic acid)], cumene terminated amount beyond 20 % diminished the hydrophilicity,

porosity and pure water permeability. The porosity of the blend membrane (M-3) was increased to 57.1 % compared to the pristine polysulfone membrane. As a whole, the novel polymer polysulfone/poly[styrene-alt-(N-4-benzoylglycine-maleamic acid)], cumene terminated would be the prospective nominee for improving the membrane performances.

CHAPTER 7

POLY(HOMOPIPERAZINE-AMIDE) THIN FILM COMPOSITES FOR NANOFILTRATION OF HEAVY METAL IONS

***Abstract**: In this chapter, poly(homopiperazine-amide) thin-film composite (HTFC) nanofiltration (NF) membranes fabricated using homopiperazine (HP) as a novel monomer. The effect of crosslinking degree and post-treatment time were studied. The HTFC membrane salt and heavy metal rejection and antifouling performance were also evaluated in this chapter. The HTFC NF membranes prepared with 2 wt% of homopiperazine and 0.15 wt % of 1,3,5-benzene tricarboxylic acid chloride (TMC) and post-treatment with ethylenediamine (EDA) in isopropyl alcohol (IPA) bestowed the improved performances, among which the HTFC-1 membrane demonstrated increased pure water permeability (PWP) of 7.0 L/m^{2}h bar with Na_2SO_4, $MgSO_4$ and NaCl rejection of 97.0 %, 97.4 % and 23.3 % respectively. The HTFC-1 membrane also exhibited higher rejection on Pb^{2+} and Cd^{2+} ions of 98.1 % and 96.3 % and flux recovery ratio (FRR) of 96.9 % without any chemical treatment.*

7.1 INTRODUCTION

The continuous deterioration and contamination of surface and groundwaters by heavy metal ions, existing in industrial wastewater, have increased the demand for development of advanced technologies for water purification (Karan *et al*. 2015, Werber *et al*. 2016, Ibrahim *et al*. 2017, Wang *et al*. 2018). Complete removal of such ions from water resources is of critical importance due to their hazardous impact on human health (Fu *et al*. 2011).

Heavy metals are typically named after the elements with a specific gravity greater than 5.0 and atomic weight between 63.5 and 200.6 (Srivastava *et al*. 2008). Among the heavy metals fitting in this range, Lead (Pb^{2+}) and cadmium (Cd^{2+}) ions are the most common ones found in industrial wastewater; these two elements have various applications in industries such as batteries, paint, fertilizer, pigments, electroplating, etc. The overexposure of humans and animals to these metal ions can cause severe health issues and ultimately death. As an example, Cd^{2+} has been classified as a probable human carcinogen by the U.S. Environmental Protection Agency (Fu *et al*. 2011, Zhang *et al*. 2014). Also, the ingestion of Pb^{2+} could damage the kidney, liver, nerve and reproductive system (Hebbar *et al*. 2016, Moideen *et al*. 2016, Nayak *et al*. 2019). Therefore, there is a high demand for the development of technologies to entirely remove heavy metal ions from water resources (<100 ppb).

The conventional methods for treating the water resources, contaminated with heavy metal ions, are coagulation-flocculation, ion-exchange and adsorption (Barakat 2011, Fu *et al*. 2011, Yang *et al*. 2019). However, the usage of a large quantity of chemicals, challenges in sludge management and difficulties in the separation of adsorbent after adsorption hamper the effective usage of the mentioned techniques (Barakat 2011, Fu *et al*. 2011). Furthermore, since the concentration of the heavy metals in wastewaters is very low (<10 ppm), the removal of the ions, using the conventional methods, is challenging.

Currently, membrane-based purification is the most promising and scalable approach for the removal of heavy metal ions from water resources. That is, the considerable improvements in the membrane technologies have made it more suitable for heavy metal removal compared to the conventional techniques. Currently, among all the membrane-based techniques, reverse osmosis (RO) and nanofiltration (NF) are considered as the state-of-the-art technology for water purification and desalination. Especially, NF plays a vital role in the wastewater purification and desalination as it acts as an intermediate between RO and ultrafiltration (UF). NF operates at a lower pressure than RO and exhibits solute rejection in the range of 100 to 1000 Da (Wang *et al*. 2018, Dai *et al*. 2019).

The applications of NF membranes have been extended from desalination to pesticide removal (Berg *et al*. 1997), heavy metal (Ye *et al*. 2019), dyes (Bai *et al*. 2019), and pharmaceuticals waste (Peeva *et al*. 2019) removal. The state-of-the-art NF membranes are thin-film composite (TFC) membranes and prepared via interfacial polymerization (IP), which consists of active polyamide (PA) layer on the UF or microfiltration (MF) membrane substrate (Scheme 7.1). The NF membrane performance is primarily depending on the quality of the PA layer, which curbs the permeability and solute rejection of the NF membrane. The performance of the PA layer formed during IP can be adjusted by properly choosing the type of monomer, monomer and initiator concentrations, miscibility of phases, reaction time and post-treatment (Kim *et al*. 2005).

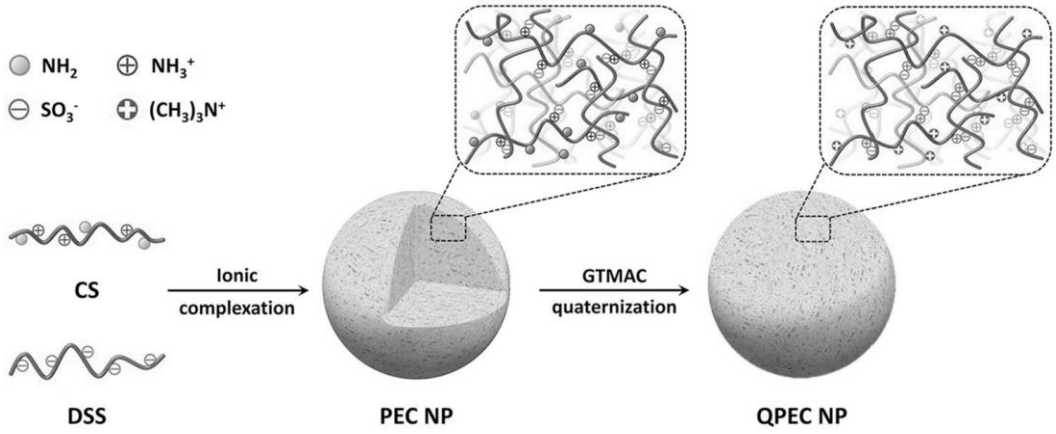

Scheme 7.1. Fabrication of quaternized polyelectrolyte complex incorporated nanofiltration membrane (Ye *et al*. 2019)

In this chapter, the synthesis of poly(homopiperazine-amide) TFC (HTFC) membranes by reacting homopiperazine (HP), as novel amine and 1,3,5-benzene tricarboxylic acid chloride (TMC), as a crosslinker, at the aqueous-organic interface is reported. The as-prepared HTFC membranes were further post-treated with ethylenediamine (EDA) in isopropyl alcohol (IPA) to fine-tune the HTFC membrane surface properties. The effect of post-treatment time on the membrane permeability, surface roughness, hydrophilicity and metal ion rejection was carefully examined. In addition, the antifouling property of the TFC membranes was carried out by using humic acid (HA) as a model foulant in dynamic crossflow filtration mode.

7.2 EXPERIMENTAL

7.2.1 Materials and methods

Polysulfone (PSF, M_n ~22,000), homopiperazine (HP, 98 %), sodium hydroxide (NaOH, $\geq$98 %, pellets), lead nitrate ($Pb(NO_3)_2$, 99.9 %), cadmium nitrate tetrahydrate ($Cd(NO_3)_2.4H_2O$, 98%), humic acid sodium salt (HA) and ethylenediamine (EDA, $\geq$99 %) were purchased from Sigma-Aldrich. 1,3,5-Benzenetricarboxylic acid chloride (TMC, 98 %) was purchased from Acros. Polyethylene glycol (PEG) of different molecular weight and N, N-dimethylformamide (DMF, anhydrous, 99.8 %) were procured from Loba Chemie. Isopropyl alcohol (IPA, $\geq$99.8 %) was obtained from Merck. Isopar-G was purchased from Univar, USA. Poly(ethylene terephthalate) nonwoven fabric (PET, K#01 3249) was purchased from Hollytex, USA. Sodium chloride (NaCl, $\geq$99.5 %), anhydrous sodium sulfate (Na_2SO_4, $\geq$99.0 %) and anhydrous magnesium sulfate ($MgSO_4$, $\geq$98.0 %)

were obtained from Fisher Scientific. Reverse osmosis (RO) water was used to prepare the salt solution and in the coagulation bath for phase inversion.

Attenuated total reflectance Fourier-transform infrared spectroscopy (ATR- FTIR) was performed using a Bruker Alpha spectrometer. Accordingly, a small area of the HTFC membrane was cut (1 cm × 1 cm) and placed on the diamond window of the ATR module. The data was collected with a resolution of 4 cm^{-1} and averaged over 24 scans.

The wettability of the membrane surfaces was evaluated by measuring the water contact angle (KRUSS DSA 100E) on each sample. To do so, a 5 μL water droplet was placed on the dried membrane and contact angle was measured after 10 s using the sessile drop method. The measurements were performed on three different locations of each sample. The reported values show the average of three measurements with one standard deviation.

The surface charge of NF membranes was measured using a streaming potential analyzer (SurPASS, Anton Paar). The membranes were attached to parallel planar surfaces (sample holders) of an adjustable gap cell (Anton Paar). Subsequently, the membranes (1 cm × 2 cm) were fixed on the sample holders. The gap between the samples was adjusted to be ca. 100 μm using two knobs. The electrolyte solution (1mM KCl) flowed at different pressures along the gap between the samples. The electrolyte flow generated a streaming potential from which the zeta potential of the membrane surface was calculated using the Helmholtz–Smoluchowski equation (Mohammadi Ghaleni *et al*. 2018). The measurements were done using electrolyte solutions having different pH values. The pH of the electrolyte was adjusted by the automatic addition of KOH or HCl during the measurements.

Scanning electron microscopy (SEM) images were collected using a FEI Helios NanoLab 660 instrument. The membranes were air-dried overnight, cut in size and adhered to the conductive carbon tape and sputter-coated with ~60 nm of gold using a Ted Pella sputtering machine (108 Auto), before taking the SEM images. For cross-section images, the membrane samples were dipped in liquid nitrogen and freeze-fractured before the drying stage.

The surface morphology of NF membranes was acquired using Bruker Dimension Icon atomic force microscopy (AFM) at ambient conditions. The analysis was executed in peak force tapping mode (SCANASYST-Air) using a silicon tip with a nominal tip radius of 2

nm and resonance frequency (f_o) of 70 kHz. The measurements were performed in 3 μm × 3 μm area of the sample and the average roughness was determined over the entire area.

The surface elemental composition and degree of crosslinking were identified using X-ray photoelectron spectroscopy (XPS) (K-alpha, ThermoFisher Scientific). XPS survey spectra were obtained over the spot size of ~400 μm, range of 0-1200 eV with 100 ms dwell time, 200 eV pass energy and averaged over four scans. High-resolution XPS core electron spectra were obtained with 50 eV pass energy, 50 W beam power, 100 ms dwell time and averaged over four scans.

7.2.2 Fabrication of poly(homopiperazine-amide) TFC (HTFC) membranes

The PSF beads were dried in vacuum (~ 25 inHg) at 60 ^{o}C for 12 hours to remove adsorbed water. The PSF supports were fabricated through the nonsolvent induced phase separation (NIPS) method. Briefly, 15 wt% PSF was dissolved in DMF and stirred for eight hours at 60 ^{o}C. The solution was deaerated by keeping the dope solution at room temperature for six hours without stirring. The nonwoven PET fabric was secured on the glass plate by taping it from the backside, and prewetted with DMF; the excess DMF was removed by Kimwipes (Kimberley-Clark). The dope solution was poured on the fabric and cast on the wet PET using a casting knife (Gardco) with an adjustable gap set at 50 mils. After the solution was cast, the substrates were immediately immersed in a coagulation bath containing water. After gelation (five minutes), the membranes were transferred to another water bath and soaked for 24 hours to remove the residual solvent. The as-prepared PSF support membrane exhibited a thickness of ~100 μm measured by a micrometer at different locations. The PSF substrate membranes were stored in deionized water at 4 ^{o}C until use.

The poly(homopiperazine-amide) thin-film composite (HTFC) nanofiltration (NF) membranes were prepared by performing interfacial polymerization (IP) on the prepared PSF support. All the TFC membranes were prepared at room temperature (20 ^{o}C) and relative humidity of 60%. In brief, PSF substrates were sandwiched between the glass plates and HDPE frames, creating wells 1 cm deep. Next, 30 mL of DI water containing 2 wt% HP and 0.35 wt% NaOH was poured on the substrate, and the substrate allowed to rest for two minutes. The excess of HP solution was drained by keeping the frame in the vertical position for one minute. The residual droplets of the HP solution were removed by gently

padding the support, using a Kimwipe. In the second step, 30 mL of Isopar-G solution containing 0.15 wt% of TMC, was poured into the well and left for one minute to allow the reaction to complete. Subsequently, the excess solution was drained by keeping the frame in a vertical position for one minute. The as-formed PA films were post-treated with 20 mL of IPA containing 1 wt% of EDA. The duration of the post-treatment step was chosen as a variable. Membranes post-treated for one, two and three minutes were labeled as HTFC-1, HTFC-2, and HTFC-3, respectively. Subsequently, the excess EDA solution was removed, and the membranes were cured in a convective oven for eight minutes at 60 ^{o}C (Scheme 7.2). The membranes that did not go through any postprocessing and one was washed for one minute with IPA were labeled as control and HTFC-IPA respectively. The as-prepared membranes were stored in deionized water at 4 ^{o}C until use. The synthetic scheme of the active layer of the NF membrane is presented in scheme 7.3. The details of reactant concentration and post-treatment are given in Table 7.1.

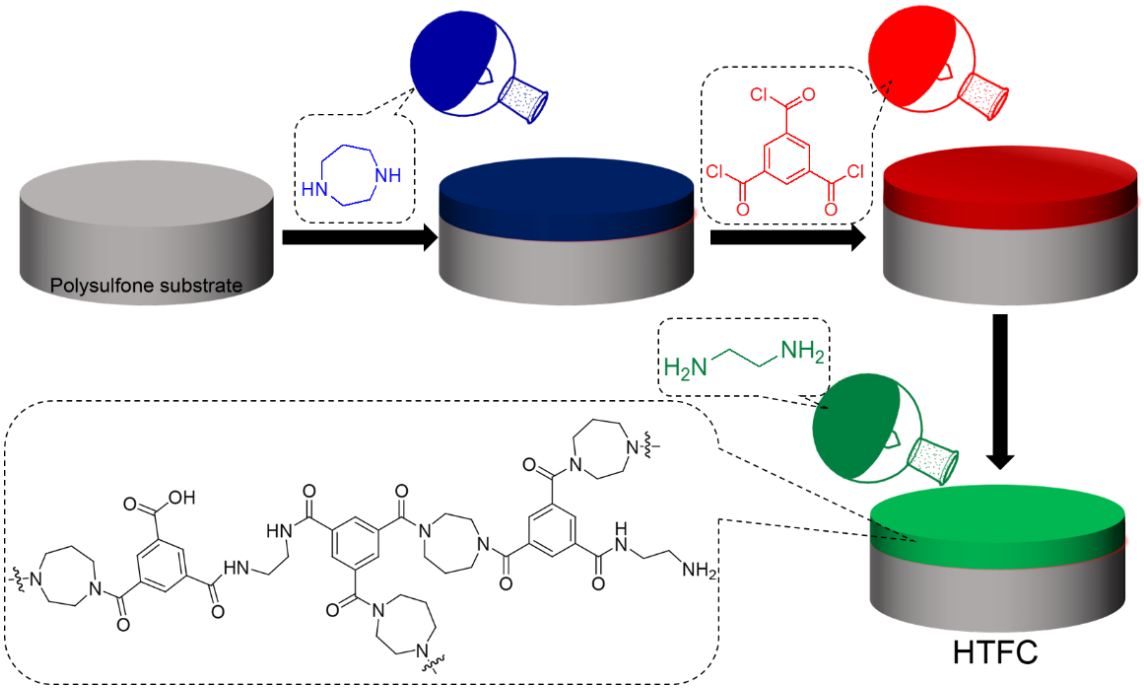

Scheme 7.2 Schematic representation of HTFC NF membrane preparation

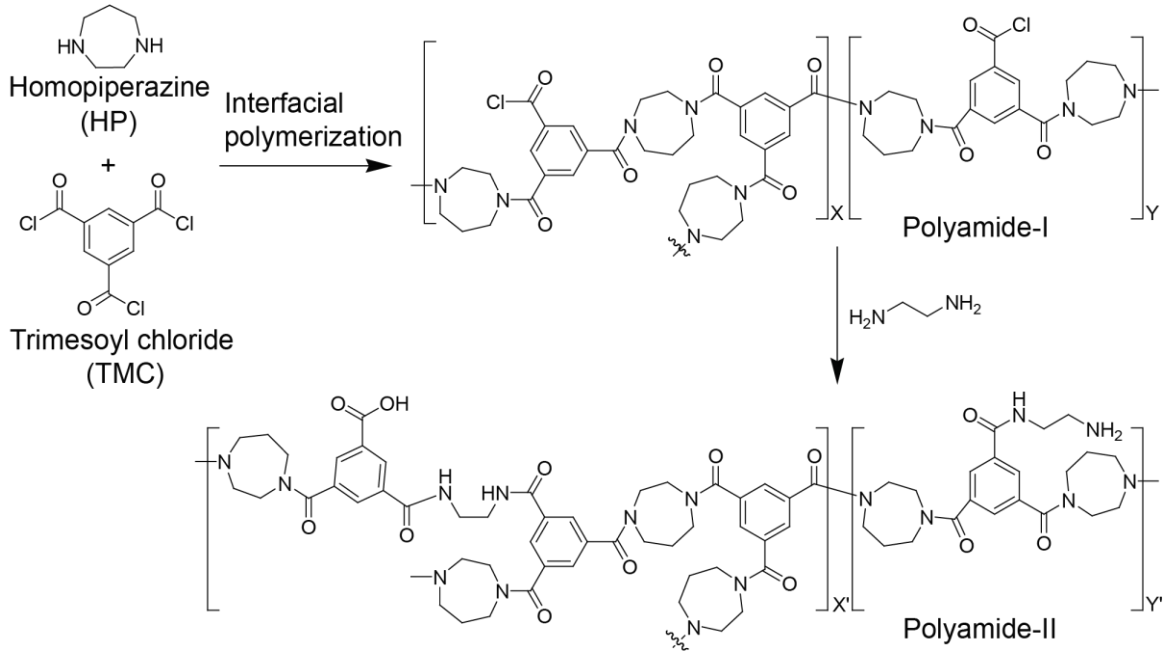

Scheme 7.3 Synthetic scheme of poly(homopiperazine-amide) thin-film composite (HTFC) membrane preparation. In the first step, homopiperazine (HP) and trimesoyl chloride (TMC) reacted via Schotten–Baumann reaction to give polyamide-I. In the second step, ethylenediamine (EDA) was post-treated with the as-formed polyamide-I layer to react with residual acyl chloride group and yield polyamide-II

Table 7.1 Poly(homopiperazine-amide) thin-film composite (HTFC) membrane parameters

Membrane	Homopiperazine (HP) (wt%)	Trimesoyl chloride (TMC) in Isopar-G (wt%)	NaOH (g)	Post-treatment
Control	2	0.15	0.1	No post-treatment
HTFC-IPA	2	0.15	0.1	No EDA. Only IPA
HTFC-1	2	0.15	0.1	1 wt% EDA in IPA for 1 min
HTFC-2	2	0.15	0.1	1 wt% EDA in IPA for 2 min
HTFC-3	2	0.15	0.1	1 wt% EDA in IPA for 3 min

EDA-Ethylenediamine, IPA- Isopropyl alcohol

7.2.3 Characterization of poly(homopiperazine-amide) TFC (HTFC) membranes

The filtration performance of NF membranes was analyzed using custom-made crossflow stainless-steel membrane cell with an active area of 19 cm^2 at 20 ^oC. All the experiments were replicated at least three times. Before the pure water permeability (PWP) and solute rejection, each membrane was compacted at 170 psi (11.7 bar) for 1 h using DI water to reach the steady-state regarding permeability. Subsequently, PWP, 'J_w' (L $m^{-2}h^{-1}$ bar^{-1}) was measured at 150 psi (10.3 bar) using the following equation:

$$J_w = \frac{Q}{A \times \Delta t \times \Delta p} \tag{7.1}$$

where 'Q' is the permeate volume in litter, 'Δt' is the time in hour, 'Δp' is the operating pressure in bar and 'A' is the effective membrane area in the module (m^2).

The salt rejection efficiency of the NF membrane was analyzed by filtering 2000 ppm of NaCl, Na_2SO_4 and $MgSO_4$ solution at 150 psi (10.3 bar) and 20 ^oC. The conductivity of both feed and permeate were analyzed using Oakton CON 2700 conductivity meter. The heavy metal removal efficiency of the as-prepared NF membrane was determined by filtering 10 ppm aqueous solution of $Pb(NO_3)_2$ and $Cd(NO_3)_2$ at 150 psi (10.3 bar), 20 ^oC and pH 5 separately. The metal ion concentration in both feed and permeate was determined using ThemoFisher inductively coupled plasma mass spectrometry (ICP-MS). The % rejection ('R') was calculated using equation (7.2).

$$\%\,R = \left(1 - \frac{C_p}{C_f}\right) \times 100 \tag{7.2}$$

where 'C_p' and 'C_f' are the permeate and feed conductivity in salt rejection and 'C_p' and 'C_f' are the permeate and feed solute concentration in heavy metal and PEG rejection.

The molecular weight cut-off (MWCO) of the membrane was determined by filtering 200 ppm PEG molecule with different molecular weight (200, 400, 600 and 1000 Da) at 150 psi (10.3 bar) and 20 ^oC. The concentration of PEG solute in both feed and permeate was analyzed by total organic carbon (TOC) SHIMADZU TOC-L analyzer. The rejection (R) was calculated using equation (7.2). The PEG rejection curve was plotted, where the PEG solute rejection at 90 %, defined as the MWCO of the membrane (Gao *et al*. 2019). The Stokes radius ($r_{p)}$ (nm) of the PEG was determined based on its average molecular weight MW as presented in equation (7.3).

$$r_p = (16.73\times10^{-12}) \times MW^{0.557} \quad (7.3)$$

The antifouling performance of all the HTFC membranes was evaluated using 200 ppm of HA. Briefly, 'J_w' was measured initially at 150 psi (10.3 bar) and 20 ^oC for 8 h. Later, the feed solution was replaced with 200 ppm HA solution and the filtration was continued for another 8 h at 150 psi (10.3 bar) and 20 ^oC and HA solution permeability (J_p) was measured. After fouling with the HA solution, all the membranes were washed with RO water for another 1 h under the crossflow condition at 10 psi and 20 ^oC to remove the loosely adhered HA molecules on the membrane surface. Again, the water permeability ('J_w') was measured for another 8 h at 150 psi (10.3 bar) and 20 ^oC. The flux recovery ratio (FRR) was calculated using the following equation

$$FRR\ (\%) = \frac{J_{w1}}{J_w} \times 100 \quad (7.4)$$

7.3 RESULTS AND DISCUSSION

7.3.1 Characterization of poly(homopiperazine-amide) TFC (HTFC) membranes

The functional groups present on the HTFC membrane was characterized using ATR-FTIR. The ATR-FTIR spectra of the PSF substrate and all the HTFC membranes are presented in Figure 7.1A. All the HTFC membranes exhibited peaks at 2967 cm^{-1}, 1293 cm^{-1}, 1242 $cm^{-1,}$ and 1150 cm^{-1}, which were attributed to the characteristic aromatic C-H stretch, S=O asymmetric stretch, C-O-C stretch and S=O symmetric stretch of PSF support, respectively. When compared to the PSF substrate ATR-FTIR spectrum, the new peak at ~1625 cm^{-1} in all the HTFC NF membranes was observed. The new peak was attributed to the C=O stretching vibration of the amide group, which confirms the presence of the PA layer formed via IP on the PSF substrate (Zhang *et al*. 2019). Furthermore, the broad peak located at ~3401 cm^{-1} and the peak at 1725 cm^{-1} were ascribed to the -OH and C=O stretch of the residual carboxylic acid groups, respectively.

Furthermore, the elemental composition, chemical bonding and degree of crosslinking were analyzed using XPS measurement. As shown in wide-scan XPS spectra (Figure 7.1B), the presence of all the elements confirms the PA layer structure. The surface elemental composition (atomic %), O/N ratio and degree of crosslinking of all the HTFC NF membranes are depicted in Table 7.2. As depicted, the O/N ratio of the control membrane was 1.0 and the value was increased up to the HTFC-1 membrane and then reduced to 0.96

for the HTFC-3 membrane. Theoretically, for a fully crosslinked PA layer, the O/N ratio varies between 1.0 and for the fully linear structure it varies between 2.0. Using the XPS results, the degree of crosslinking was calculated by using the following equation (Kwon *et al*. 2008).

$$\text{Degree of crosslinking (\%)} = \frac{X}{X+Y} \times 100 \tag{7.5}$$

Where X and Y are the crosslinked and linear part of the PA layer and can be calculated from the experimental O/N ratio acquired from XPS analysis by the following equation,

$$\frac{O}{N} = \frac{3X+4Y}{4X+2Y} \tag{7.6}$$

As calculated, the control membrane exhibited the degree of crosslinking of 47.0 %. However, after post-treating with IPA, the degree of crosslinking was reduced to 40.3 % (HTFC-IPA). This reduction in the degree of crosslinking was attributed to the removal of unreacted monomers and hydrolysis of the acid chloride group in the PA layer by water-miscible solvent IPA, which reduced further crosslinking during heat treatment. However, the degree of crosslinking of HTFC-1, HTFC-2 and HTFC-3 NF membranes were not calculated as the post-treatment was performed with EDA in IPA.

The added EDA has changed the PA layer structure, which led to the different repeating units compared to the control and HTFC-IPA membranes. Still, the O/N ratio of HTFC-1 and HTFC-2 membranes confer the clue that, the degree of crosslinking is less compared to the control membrane. At the same time, the HTFC-3 membrane demonstrated a higher degree of crosslinking compared to all the NF membranes. This trend was attributed to the increased time of post-treatment with EDA. In 3 minutes of post-treatment time, the added EDA reacted with unreacted acid chloride and further increased the crosslinking density. For the control membrane, C 1s was deconvoluted into two peaks. The peaks at 284.71 eV and 287.11 eV were ascribed to C-C and N-C=O bond. The N 1s peak was deconvoluted into two peaks and peaks at 399.42 eV and 399.89 eV were attributed to C-N and N-C=O bond.

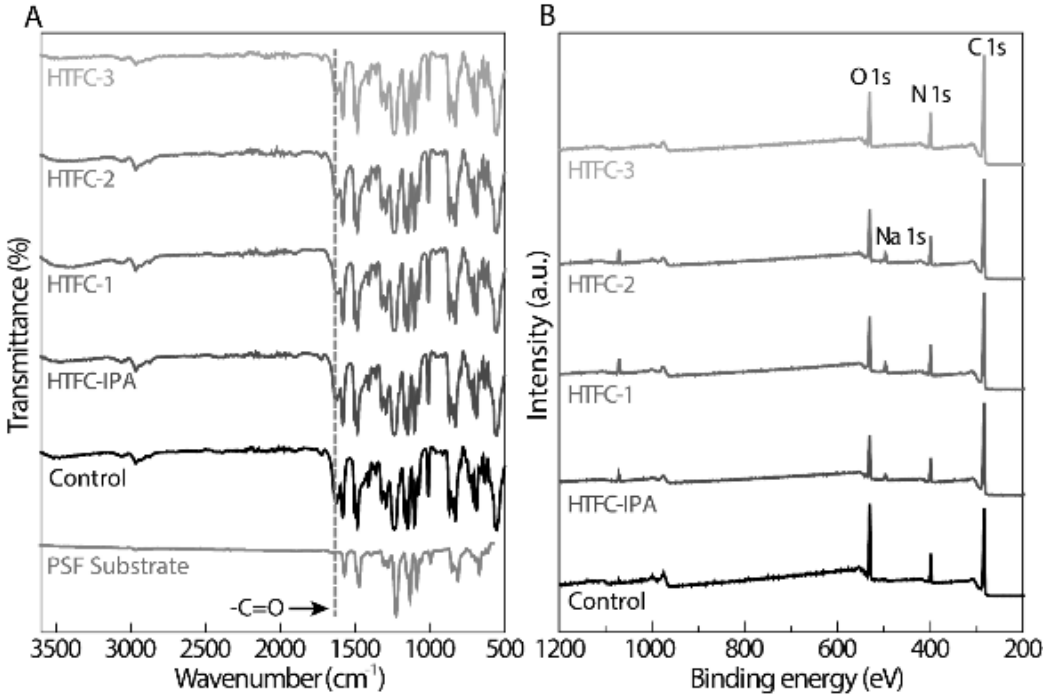

Figure 7.1 A) ATR-FTIR spectra and B) wide scan XPS spectra of HTFC membranes

Table 7.2 XPS elemental composition of poly(homopiperazine-amide) TFC (HTFC) membranes

Membrane	Atomic concentration (%)					O/N ratio	Degree of cross-linking (%)
	C 1s	O 1s	N 1s	Na 1s	Cl 2p		
Control	72.72	13.4	13.43	0.44	-	1.0	47.0
HTFC - IPA	73.71	13.73	11.08	1.16	0.31	1.24	40.3
HTFC -1	70.74	14.99	11.98	2.01	0.28	1.25	-
HTFC -2	72.21	13.52	12.07	1.84	0.35	1.12	-
HTFC -3	72.61	13.14	13.67	0.25	0.33	0.96	-

The surface morphology of the as-prepared HTFC NF membranes was observed by SEM and AFM and presented in Figure 7.2. As shown in Figure 7.2A, all the HTFC membranes exhibited nodules and globules structure with ‘nano cracks’ owing to the IP reaction of HP and TMC. When compared to the control membrane, the HTFC-IPA and

HTFC-1 membranes surface were less tightly packed with nodules and globules as these membranes were post-treated. As the HTFC-IPA membrane was post-treated only with IPA, it exhibited the least loose-packed surface morphology. At the same time, the HTFC-2 and HTFC-3 membranes surface were tightly packed as the control NF membrane. This phenomenon possibly results from the fact that the added NaOH catalyzed the amidation reaction between HP and TMC followed by post-treatment with EDA in IPA. As a result, the EDA molecule further undergoes an amidation reaction with unreacted TMC molecules, which resulted in increased crosslinking density and tightly packed surface morphology. The NF membranes exhibited a PA layer thickness of ~80 - 85 nm. The obtained SEM results are well aligned with XPS results (crosslinking density).

The AFM 2D images and average roughness (R_a) parameter of all the HTFC membranes with an area of 3 μm × 3 μm are presented in Figure 7.2B. The AFM 2D images of all the HTFC membranes confirm the nodule and globules structure. It is very interesting to note that, among all the membranes prepared control membrane exhibited a higher R_a value of 10.3 nm. Later, the R_a value was decreased to 6.58 nm for HTFC-IPA and then increased gradually to 9.43 nm (HTFC-1). Subsequently, the HTFC-2 and HTFC-3 membranes demonstrated the R_a values of 8.19 nm and 7.14 nm. The change in the R_a value for all the HFTC NF membranes can be explained based on the rate of amidation reaction and post-treatment. In the control membrane, the added NaOH increased the rate of amidation reaction between HP and TMC at the aqueous and organic interface, which left the minimum amount of TMC as unreacted. Thus, it forms a highly thicker and rougher PA layer (Xue *et al*. 2016). However, after post-treatment with IPA the R_a value was reduced (HTFC-IPA), which was attributed to the removal of a few low molecular weight PA layers and unreacted monomers. Meanwhile, after post-treatment with EDA in IPA for 1 min (HTFC-1), R_a value increased due to the further amidation reaction between EDA and unreacted acyl chloride. Correspondingly, the HTFC-2 and HTFC-3 membranes bestowed a decrease in R_a value respectively.

In summary, the NF membranes prepared with PIP as monomer demonstrated ridge and valley-like structure with R_a in the range of 30-45 nm (Lai *et al*. 2016, Lai *et al*. 2018). In the present study, the formation of nodules and globules structure with ‘nano cracks’ and reduced surface roughness of the HTFC NF membrane was attributed to the solubility and diffusivity of HP during IP reaction.

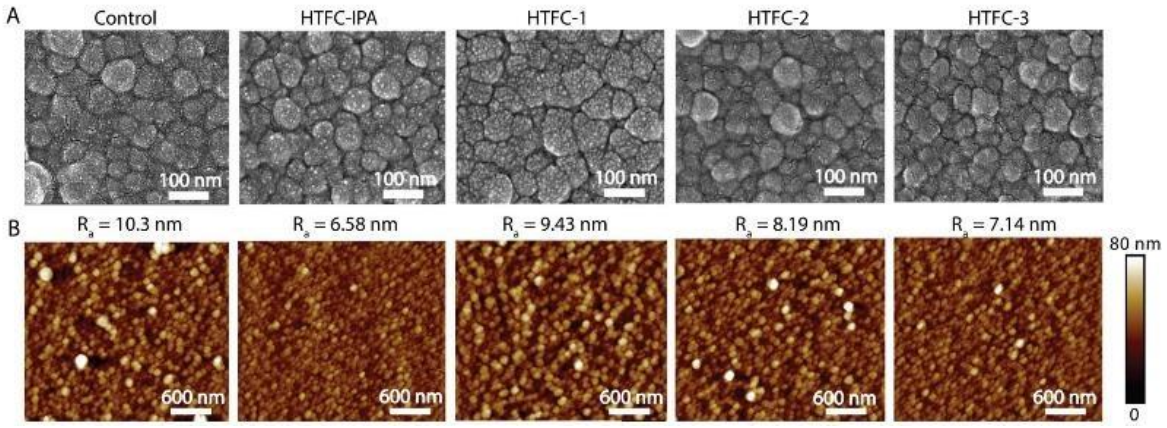

Figure 7.2 A) SEM and B) AFM 2D images of the HTFC NF membranes

The surface charge of all the HTFC NF membranes in the pH range of 5 to 9 is presented in Figure 7.3A. As shown, all the as-prepared HTFC membranes demonstrated positive charge below pH 6.2, which favors the rejection of divalent or multivalent ions via the Donnan effect (Van der Bruggen *et al*. 1999, Childress *et al*. 2000). The isoelectric point (IEP) for the control membrane was found to be at pH 6.47. Compared with the control samples, the IEP for the HTFC-1 membrane declines to pH 6.25. The reduced IEP (slightly increased negative charge) was attributed to the removal of unreacted monomers and oligomer during the post-treatment process. As the unreacted amine removed during the post-treatment, the unreacted acyl group (-COCl) in the PA layer hydrolyzed in the presence of water, forming a COOH group. As a result, the HTFC-1 membrane becomes more negative than the control membrane. By increasing the post-treatment time, it was expected that the unreacted carboxylic groups to be cross-linked by EDA, which results in an increased IEP.

Furthermore, the surface hydrophilicity of NF membranes can also be assessed by measuring the water contact angle (CA) (Lai *et al*. 2016). According to the Wenzel model, the increased surface roughness will reduce the contact angle (Wenzel 1949). As depicted in Figure 7.3B, the pristine control membrane exhibited the lowest water CA of 16.9^o due to higher R_a value when compared to all other HTFC membranes. After post-treatment with IPA, the HTFC-IPA membrane CA was increased to 18.7^o as there was a decrement in the R_a value. Subsequently, HTFC-1, HTFC-2 and HTFC-3 membranes were exhibited CA of 17.9^o, 18.3^o and 24.1^o. This increased trend of CA was attributed to the EDA crosslinking,

which increased the degree of crosslinking and reduced the availability of free carboxylic acid groups in the PA layer (Gorgojo *et al*. 2014).

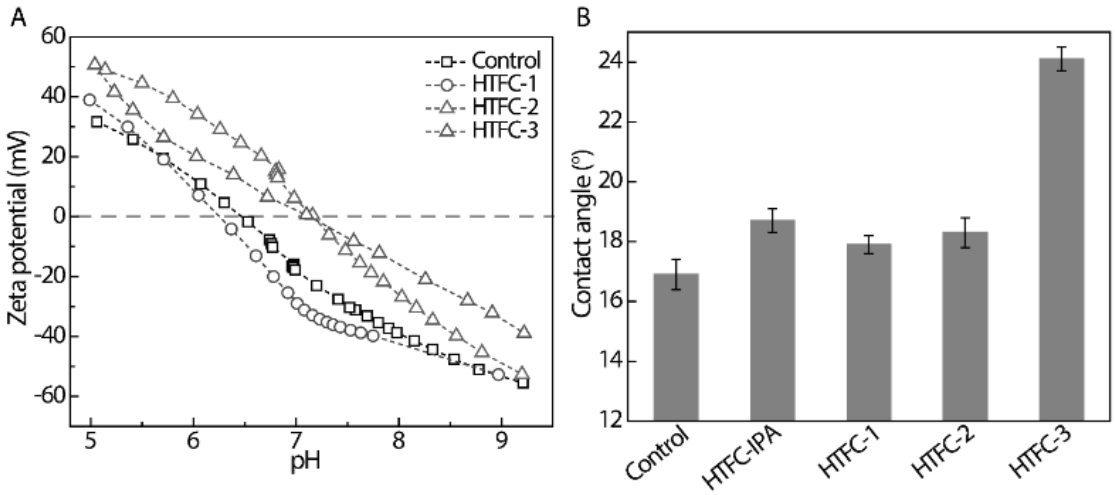

Figure 7.3 A) Zeta potential as a function of pH and B) contact angle of all the HTFC NF membranes

7.3.2. Poly(homopiperazine-amide) TFC (HTFC) membrane performance

Based on the crosslinking degree of the PA layer, it is possible to fine-tune the pore size and solute rejection of the HTFC membranes. In general, the higher crosslinking degree leads to smaller pore size and higher solute rejection. The different molecular weight PEG neutral solute rejection was evaluated by MWCO measurement and results are presented in Figure 7.4A. The results indicated that the MWCO of control, HTFC-IPA, HTFC-1, HTFC-2 and HTFC-3 membranes were 253 Da, 260 Da, 272 Da, 266 Da and 326 Da. Furthermore, the PEG solute Stokes radius (r_p) of all the HTFC NF membranes was also calculated as 0.36 nm, 0.37 nm, 0.38 nm, 0.37 nm and 0.42 nm respectively. The MWCO of all the NF membranes was almost in the same range except the HTFC-3 membrane. The slight decrement in the HTFC-3 membrane solute rejection was attributed to the increased time (3 min) of post-treatment. During post-treatment, not only amidation reaction between EDA and TMC happens but also the removal of a few low molecular weight PA layers happened. Consequently, there were some minor defects formed, which led to a slight reduction in solute removal.

The pure water permeability (PWP) of all the HTFC NF membranes is depicted in Figure 7.4B. The permeability of the NF membrane mainly depends on the porosity of the PA layer (Ji *et al*. 2000), surface hydrophilicity (Bano *et al*. 2015) and PA layer thickness

(Zhu *et al*. 2018). When compared to the pristine control membrane (PWP 3.6 L/m^2h bar), the HTFC-1 NF membrane exhibited the highest PWP of 7.0 L/m^2h bar. The increased permeability of the HTFC-1 membrane was attributed to the post-treatment with EDA in IPA and increased surface hydrophilicity.

The increased hydrophilicity of the HTFC-1 membrane improved water permeability by attracting water molecules towards the membrane matrix and reduced the mass transfer resistance across the membrane. As calculated by the crosslinking degree from XPS analysis (Table 7.2), the higher crosslinking degree (47 %) of the pristine control membrane attributed to reduced PWP. However, post-treatment with IPA reduced the crosslinking degree to 40.3 % by removing some of the low molecular weight PA layer and unreacted monomer. As a result, the reduction in thickness of the PA layer or unblocking of the permeation pathway would have happened (Gorgojo *et al*. 2014). Thereby the permeability was increased from 3.6 L/m^2h bar (control) to 6.0 L/m^2h bar (HTFC-IPA). Furthermore, the post-treatment with EDA in IPA for HTFC-1 NF membrane PWP further enhanced to 7.0 L/m^2h bar. Nevertheless, EDA in IPA post-treatment for HTFC-2 (2 min) and HTFC-3 (3 min) membranes exhibited a decreased trend of PWP, which was mainly due to the increased crosslinking density. The presence of EDA molecules in IPA reacted with unreacted acyl chloride and resulted in a higher crosslinking density. Thus, the HTFC-2 and HTFC-3 membranes demonstrated PWP of 6.4 L/m^2h bar and 5.5 L/m^2h bar. In summary, the improved PWP of the HTFC-1 membrane was ascribed to the increased surface hydrophilicity and reduced crosslinking degree.

The representative divalent and monovalent salts such as Na_2SO_4, $MgSO_4$ and NaCl rejection ability of the NF membranes were analyzed and depicted in Figure 7.4C. All the NF membranes demonstrated above 94 % rejection towards divalent salts of both Na_2SO_4 (control- 95.7 %, HTFC-IPA- 94.6 %, HTFC-1- 97.0 %, HTFC-2- 96.9 % and HTFC-3- 97.1 %) and $MgSO_4$ (control- 96.7 %, HTFC-IPA- 95.2 %, HTFC-1- 97.4 %, HTFC-2- 97.1 % and HTFC-3- 997.9 %). Subsequently, all the HTFC NF membranes exhibited below 30 % rejection of NaCl. The improved rejection of $MgSO_4$ was attributed to the Donnan effect. Because the control and HTFC-1 membranes were negatively charged and HTFC-2 and HTFC-3 membranes were positively charged at pH 7 (Figure 7.3A). Therefore, in the case of control and HTFC-1 membranes the SO_4^{2-} ions were

electrostatically repelled at the same time to maintain the electrical neutrality Mg^{2+} ions were also rejected.

Still, as HTFC-2 and HTFC-3 membranes were positively charged at pH 7, thus Mg^{2+} ions were rejected via electrostatic repulsion. In Na_2SO_4 rejection, as shown in Figure 7.3A, the control and HTFC-1 membranes were negatively charged at pH 7. However, HTFC-2 and HTFC-3 showed a slightly positive charge at pH 7. Thus, the control and HTFC-1 membranes were rejected the SO_4^{2-} ions via electrostatic repulsion (Donnan effect), as a result in order to maintain the electrical neutrality Mg^{2+} ions were also rejected. Yet, the HTFC-2 and HTFC-3 membranes were a little positively charged at pH 7.0 due to the reaction between EDA and acyl chloride during post-treatment. In addition, the HTFC-2 and HTFC-3 membranes exhibited r_p value of 0.37 nm and 0.42 nm. However, the hydrated ionic radius of SO_4^{2-}, Mg^{2+}, Cl^- and Na^+ ions are 0.4 nm, 0.43 nm, 0.33 nm and 0.36 nm (Brant *et al*. 2005, Marcus 1988). Thus, the Na_2SO_4 rejection mechanism for HTFC-2 and HTFC-3 membranes depends on the size exclusion. The obtained results are well aligned with the literature (Bera *et al*. 2018, Trivedi *et al*. 2018). In summary, all the membranes were highly selective towards the divalent salt (Na_2SO_4 and $MgSO_4$) rather than the monovalent salt (NaCl). The reason for the reduced rejection of the monovalent ions was due to reduced charge density and size of Cl^- and Na^+ ions.

From a practical application point of view, operational stability is one of the main requirements for the NF membrane. In that connection, based on the better permeability and salt rejection HTFC-1 membrane was chosen and characterized for long term tests (24 h) and results are presented in Figure 7.4D. As depicted, the HTFC-1 membrane demonstrated better stability, permeability and salt rejection over 24 h. The obtained results indicated that the as-prepared HTFC membranes are suitable for the desalination of brackish water.

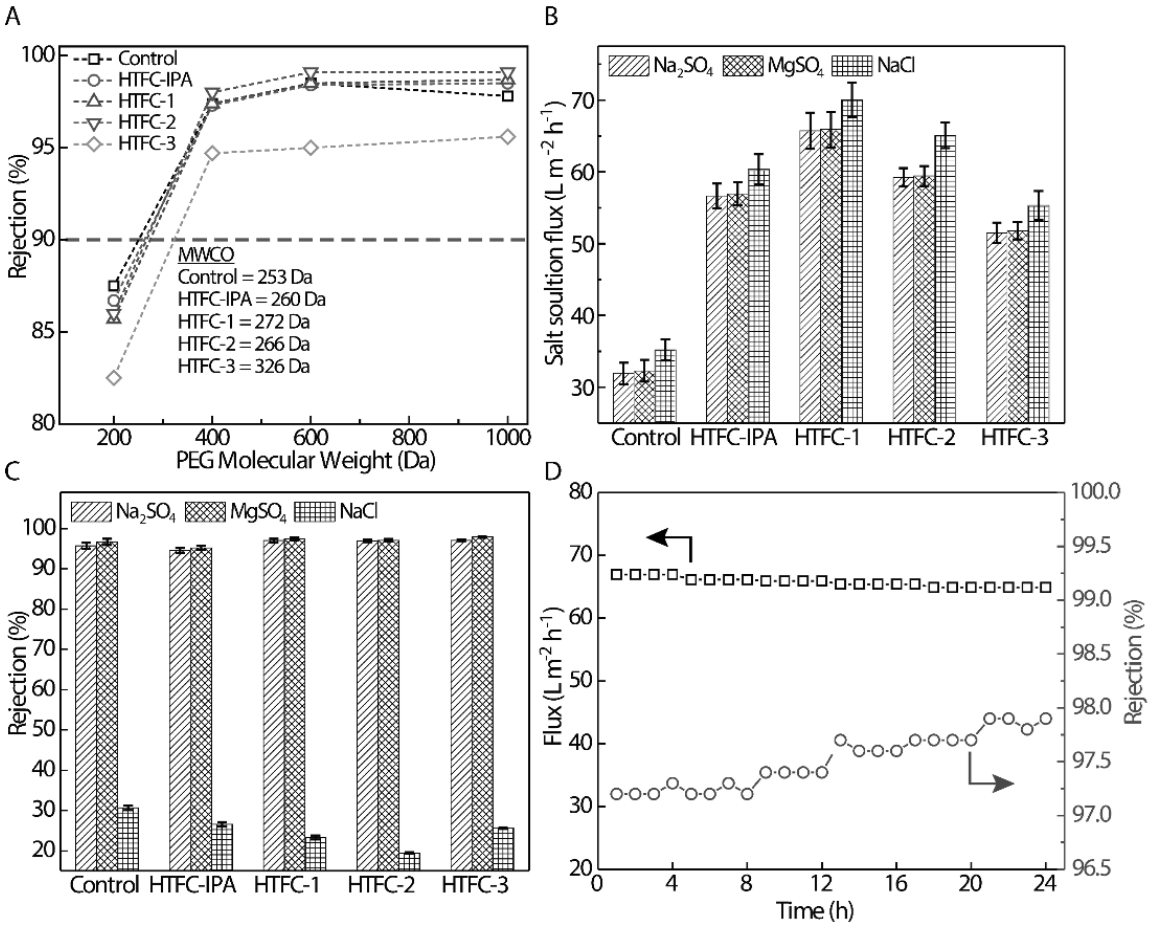

Figure 7.4 A) Molecular weight cut-off (MWCO), B) pure water permeability, C) salt rejection of HTFC membranes and D) long-time Na_2SO_4 rejection and permeability of HTFC-1 membranes at 150 psi and 20 ^oC

7.3.3 Heavy metal ions removal and antifouling study of poly(homopiperazine-amide) TFC (HTFC) membranes

In order to explore the versatility of the as-prepared HTFC NF membranes, the heavy metal ions rejection efficiency of all the HTFC NF membranes were tested and presented in Figure 7.5A. All the HTFC NF membranes exhibited >97 % Pb^{2+} and >94 % Cd^{2+} ions rejection at pH 5. As Pb^{2+} and Cd^{2+} ions form insoluble metal hydroxide at above pH 7 (Li *et al*. 2016, Ibrahim *et al*. 2018), in this study, the rejection experiment was performed at pH 5. While looking at the metal ion rejection results, the HTFC NF membranes demonstrated higher rejection towards Pb^{2+} than Cd^{2+} ions. This is unexpected, as the size of Pb^{2+} ions is smaller than Cd^{2+} ions. The reason for the higher rejection of Pb^{2+} over Cd^{2+} can be explained as follows. (i) Higher normalized volume charge density and (ii) lower ionic strength of $Pb(NO_3)_2$ solution than $Cd(NO_3)_2$ solution and (iii) increased hydrated

stability of Pb^{2+} at pH 5 than the Cd^{2+}. The increased hydrated stability of the Pb^{2+} bestowed better charge-charge repulsion between the Pb^{2+} ions and the positively charged membrane surface (Bouranene *et al*. 2008, Bera *et al*. 2018). Therefore, Pb^{2+} ions were rejected by > 97 % when compared to the Cd^{2+} ions (> 94 %). The heavy metal ion rejection ability of the as-prepared membrane is compared with literature and results were comparable with most of the membranes and superior to some of the NF membranes reported (Table 7.3).

Table 7.3 Comparison of heavy metal removal capacity of as-prepared NF membrane with literature

Membrane	PWP (L/m^2h bar)	Metal ion	Rejection (%)	Ref.
Dow membrane NF90	7.14	Pb^{2+} [$Pb(NO_3)_2$]	91-94	(Saikaew *et al*. 2010)
Dow membrane NF270	13.2	Pb^{2+} [$Pb(NO_3)_2$] Cd^{2+} [$Cd(NO_3)_2$]	~60 ~68	(Al-Rashdi *et al*. 2013)
Polybenzimidazole/ polyethersulfone dual-layer hollow fiber membrane	0.826	Pb^{2+} [$Pb(NO_3)_2$] Cd^{2+} [$Cd(NO_3)_2$]	93 95	(Zhu *et al*. 2014)
Matrimid/PEI/Nexar	2.4	Pb^{2+} [$Pb(NO_3)_2$] Cd^{2+} [$CdCl_2$]	99.8 98.2	(Thong *et al*. 2014)
PAN/SPEB blend	7.62	Pb^{2+} [$Pb(NO_3)_2$] Cd^{2+} [$CdCl_2$]	94.6 95.1	(Jia *et al*. 2019)
HTFC-1	**7.0**	**Pb^{2+} [$Pb(NO_3)_2$]** **Cd^{2+} [$Cd(NO_3)_2$]**	**98.1** **96.3**	**Present study**

The higher metal ions (Pb^{2+} and Cd^{2+}) rejection of all the as-prepared NF membranes were attributed mainly to the NF membrane surface charge. As all the prepared NF membranes were positively charged at pH 5, the metal ions (Pb^{2+} and Cd^{2+}) rejected via electrostatic repulsion (Donnan effect). The positive charge on the control and HTFC-IPA NF membrane at pH 5 was attributed to the higher crosslinking density, which led to the reduced unavailability of the free carboxylic acid group and for HTFC-1, HTFC-2 and HTFC-3 membranes, the presence of EDA increased the positive charge. However, the

membrane HTFC-5 membrane demonstrated slightly reduced metal ion rejection owing to the increased r_p value (0.42 nm) compared to other NF membranes prepared.

Furthermore, the fouling of the NF membrane is one of the bottlenecks during membrane filtration. The presence of NOM such as HA in the wastewater will affect the NF membrane flux by adsorbing on the membrane surface (Tang *et al*. 2007). In this study, the antifouling ability of all the prepared NF membranes was analyzed for 24 h and represented in Figure 7.5B. As shown, all the NF membranes exhibited a sudden drop in the water permeability when the feed solution was changed from water to HA solution. The sudden drop in water permeability was ascribed to the deposition of HA molecules on the membrane surface, which acted as a barrier for the water molecule to pass through the membrane. Then, the control and all HTFC NF membrane's antifouling efficiency was evaluated by measuring the flux recovery ratio (FRR). In general, the TFC NF membranes prepared with piperazine (PIP) as monomer exhibited FRR in the range of 60-70 % (Mansourpanah *et al*. 2013, Gol *et al*. 2014, Mansourpanah *et al*. 2015, Akbari *et al*. 2016). Therefore, further surface modification of PIP based NF membranes is needed (Guo *et al*. 2019). However, in this study, after simple water washing of all the NF membranes prepared using HP as monomer bestowed >94 % of FRR. When compared to all the NF membranes prepared in this study, the HTFC-1 membrane demonstrated higher FRR (96.9 %) and water permeability.

The improved antifouling performance of the as-prepared NF membranes can be explained based on the NF membrane surface physicochemical properties such as improved hydrophilicity and reduced surface roughness. All the HTFC membranes conferred the contact angle of less than 24.1^o, especially the HTFC-1 membrane exhibited contact angle of 17.9^o (Figure7.3B). As these HTFC NF membranes are more hydrophilic in nature, it forms strong hydration layer on the membrane surface easily (Ibrahim *et al*. 2017, Fu *et al*. 2019). The as-formed hydration avoided the adsorption of foulant molecules (HA) on the membrane surface. Furthermore, the as-formed minimum amount of foulant molecules on the hydrophilic membrane can easily be removed by simple water washing. In another way, as shown in Figure 7.2B, the reduced surface roughness of the HTFC NF membranes (especially HTFC-1 R_a = 9.43 nm) attributed to the reduced adsorption of foulant molecules (HA). Indeed, colloidal fouling in NF membranes can be directly related to the surface

roughness as these colloidal foulant molecules are clogged into the valleys of the rough membrane surfaces (Vrijenhoek *et al*. 2001). Therefore, the reduced surface roughness of the as-prepared HTFC NF membranes could demonstrate improved antifouling performance.

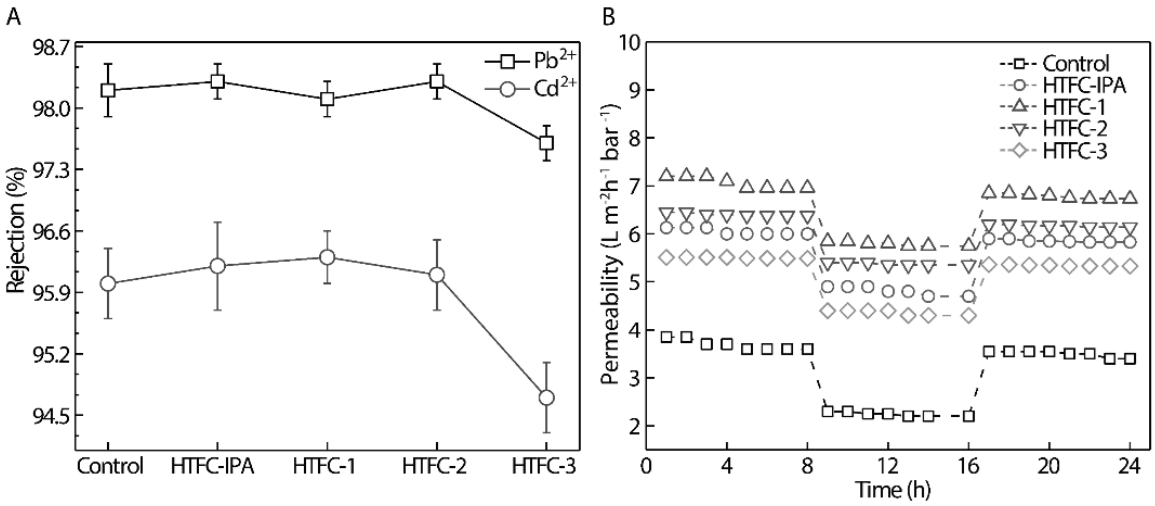

Figure 7.5 A) Pb^{2+} and Cd^{2+} rejection of HTFC-1 membrane at pH 5, 150 psi and 20 ^{o}C and B) antifouling performance of control, HTFC-IPA, HTFC-1, HTFC-2 and HTFC-3 membranes with 200 ppm of humic acid at 150 psi and 20 ^{o}C

7.4 CONCLUSIONS

In summary, a novel and easily scalable poly(homopiperazine-amide) thin-film composite nanofiltration membrane using homopiperazine as a monomer is fabricated. The influence of ethylenediamine in isopropyl alcohol post-treatment on the nanofiltration membrane performances were studied. The XPS analysis confirmed that the degree of cross-linking was reduced with post-treatment and then increased with an increase of post-treatment time. The as-prepared poly(homopiperazine-amide) thin-film composite nanofiltration membranes exhibited nodule and globules surface morphology. The zeta potential analysis revealed that the negatively charged membrane surface could be altered into positively charged by simple ethylenediamine post-treatment. The nanofiltration membrane prepared with 2 wt% of homopiperazine, 0.15 wt% of trimesoyl chloride and post-treatment with ethylenediamine in isopropyl alcohol for 1 min resulted HTFC-1 membrane, which was chosen as the best performing membrane in terms of pure water permeability (7.0 L/m^{2}h bar), Na_2SO_4 (97.0 %), $MgSO_4$ (97.4 %), NaCl (23.3 %), Pb^{2+} (98.1 %), Cd^{2+} (96.3 %) rejection and higher flux recovery ratio (96.9 %). Overall, the as-

prepared poly(homopiperazine-amide) thin-film composite nanofiltration membranes are having potential application towards the desalination and heavy metal ions removal.

CHAPTER 8

INTEGRATION OF ZWITTERIONIC POLYMER NANOPARTICLES IN INTERFACIAL POLYMERIZATION FOR ION SEPARATION

***Abstract**: In this chapter, the thin-film nanocomposite (TFN) membrane was developed by integrating zwitterionic polymeric nanoparticles into the active layer of the membranes. The effect of concentration of nanoparticles in the polyamide layer towards the permeability and solute rejection were evaluated. The TFN membrane antifouling and heavy metal rejection capabilities were also examined in this chapter. The fabricated TFN membranes exhibited pure water permeability (PWP) of 11.4 L/m^{2}h bar and salt rejection value of 97.6 % and 16.9 %, for sodium sulfate and sodium chloride, respectively. The fabricated membranes demonstrated metal ion removal efficiencies of 99.48 % and 95.67 % for Pb^{2+} and Cd^{2+} ions respectively.*

8.1 INTRODUCTION

The scarcity of potable water at the global scale begs for the development of methods and materials that allow for tapping into impaired water resources (Werber *et al*. 2016, Abraham *et al*. 2017, Ibrahim *et al*. 2017, Guo *et al*. 2019). Among the various waste streams, effluents of industrial wastewater plants are among the challenging streams for treatment. The high concentration of heavy metal ions is one of the major culprits. It is anticipated that the heavy metal contamination will become even a more pronounced, challenging issue, owing to the growth of industry and population (Wang *et al*. 2018). Heavy metal ions are toxic and nonbiodegradable and the need to develop separation technology that targets these contaminants is at high demand (Kumar *et al*. 2014, Bandara *et al*. 2019).

Membrane-based separation is among the most suitable candidates for treating impaired water resources. Compared with other separation technologies, such as mechanical vapor compression and multistage distillation, membrane-based separation often have a lower energy demand and carbon footprint; as a result, they are the more cost-efficient and eco-friendly solutions to water recovery and reuse (Ganesh *et al*. 2013, Hebbar *et al*. 2016, Werber *et al*. 2016, Zhang *et al*. 2016, Ibrahim *et al*. 2017). Currently, reverse osmosis (RO) and nanofiltration (NF) are the state-of-the-art technology for desalination and removal of heavy metal ions from wastewater streams (Ben-Sasson *et al*. 2016, Ibrahim *et al*. 2019, Jia *et al*. 2019, Yang *et al*. 2019). Nonetheless, the trade-off between the permeability and selectivity along with the fouling propensity of the RO membranes has limited the large scale deployment of this technology for heavy metal ion removal (Qi *et*

al. 2019). NF is an attractive process for removing heavy metal ions; however, to make this process an economically viable solution, challenges attributed to the fouling propensity and low permeability of the NF membranes should be addressed.

Thin-film nanocomposite (TFN) membranes are the promising choice of membranes for the NF application. TFN membranes are composed of a selective nanocomposite polyamide (PA) and a porous substrate layer (Lai *et al*. 2016). Recently, Hoek *et al*. reported on TFN membrane fabrication by incorporating zeolitic nanoparticles in the polyamide (PA) layer (Jeong *et al*. 2007). The as-prepared membrane exhibited an enhanced permeability without any change in the solute rejection. The improved performance of the TFN membrane was attributed to the flow of water molecules through the molecular sieve pores. In parallel, many efforts have been devoted to fabricating TFN by incorporating nanoparticles and fillers within the PA active layers (Lau *et al*. 2015). Different nanomaterials including zeolitic imidazolate framework, cellulose nanocrystals, modified TiO_2, carbon nanotubes and graphene and graphene oxides have been utilized to enhance the performance of TFN membranes (Zhao *et al*. 2014, Kim *et al*. 2015, Safarpour *et al*. 2015, Lai *et al*. 2016, Zhu *et al*. 2017, Bai *et al*. 2018, Maalige *et al*. 2018, Ibrahim *et al*. 2019), nonetheless, creating stable dispersions of these nanomaterials and the tight integration of these materials within the active layer of TFNs, is among the main challenges.

Herein, the integration of zwitterionic polymeric nanoparticles within the TFN active layer is reported. The polymeric nanoparticles are prepared via distillation-precipitation polymerization (DPP) (He *et al*. 2014). The as-prepared polymer nanoparticles contain residual vinyl groups, allowing for further chemical modification of the matrix. To impart zwitterionic properties to the nanoparticles, the "thiol-ene" reaction followed by covalent attachment of L-cysteine (L-Cys) was used. It has been well established that, the presence of zwitterionic moiety on the membrane surface impart improved hydrophilicity to the membrane via formation of hydration layer (Liu *et al*. 2017), which bestowed the improved antifouling property. The zwitterionic polymer nanoparticles P(MBAAm-co-SVBS)@L-Cys) were dispersed into organic solution, used as the precursor solution for PA synthesis. The fabricated membranes were characterized and their performance in removing heavy metal ions from a feed solution containing 10 ppm Pb^{2+}, Cd^{2+} were evaluated. The results indicate that the TFN membranes, fabricated using polymeric nanoparticles as an additive,

have lower fouling propensity and higher removal efficiency, exceeding 99 %, for the heavy metal ions. These attributes, along with the high permeate water permeability (11.4 L/m^2h bar) of the fabricated membranes, make these TFN membranes a suitable candidate for removing heavy metal ions from contaminated water resources.

8.2 EXPERIMENTAL

8.2.1 Materials and methods

Polysulfone (PSF, Udel® P-3500) was obtained from Solvay chemicals. N-methyl pyrrolidone (NMP, 99.8 %), acetonitrile (99.9 %), L-cysteine (L-Cys, 97 %), polyethylene glycol (PEG) 200, 400, 600 and 1000, polyvinylpyrrolidone (PVP) K-30, azobisisobutyronitrile (AIBN, 98 %) and N,N′-methylenebis(acrylamide) (MBAAm, 99 %) were purchased from Loba chemicals. Sodium 4-vinylbenzenesulfonate (SVBS, ≥90 %), lead nitrate ($Pb(NO_3)_2$, ≥99.0 %), cadmium nitrate tetrahydrate ($Cd(NO_3)_2 .4H_2O$, 98 %) and sodium dodecyl sulfate (SDS, ≥99.0 %) were procured from Sigma-Aldrich. Trimesoyl chloride (TMC, 99 %) and cyclohexane were obtained from Acros Organics and Merck, respectively.

The functional groups in the nanoparticles and membrane were identified by Fourier transform infrared (FT-IR) spectroscopy, using a Bruker Alpha Fourier-transform infrared spectrometer. The morphology of the as-synthesized nanoparticles was studied using a transmission electron microscope (TEM) JEOL JEM-2100. The particle solution was drop cast on a TEM copper grid and the sample was dried and transferred to the microscope. To evaluate the structural property of the sample, X-ray diffraction was performed by loading powder samples in a sample holder of a Rigaku SmartLab diffractometer (Cu Kα). The diffractogram was collected between 0-90 degrees in 2θ mode. The thermal stability of the nanoparticles was determined using HITACHI STA7000 thermogravimetric analysis (TGA).

The elemental mapping of the nanoparticles was evaluated by performing energy-dispersive X-ray (EDX) spectroscopy using a scanning electron microscope (SEM) equipped with an Oxford EDX detector. Briefly, the samples were spread on a conductive carbon tape (PELCO Tabs) and then mounted on an SEM stub. The data were collected using 10 KeV for the electron beam at the working distance of 10 mm. The cross-sectional

images of the membranes were collected using HITACHI TM3030 SEM. The samples were freeze fractured by submerging in liquid nitrogen. The surface roughness of all the membranes was measured using a BRUKER icon atomic force microscope (AFM). AFM cantilever with a tip radius of 2 nm and resonant frequency (f_0) of 70 kHz was used for all measurements; all measurements were performed in tapping mode.

The nanoparticles' elemental composition and surface chemistry were evaluated using AXIS ULTRA X-ray photoelectron spectroscopy (XPS, Al K-Alpha). Each XPS spectrum is the average of five scans; survey spectra were recorded with a pass energy of 200 eV and 100 ms dwell time. The surface charge of the membrane was analyzed using the SurPASS electrokinetic analyzer from Anton Parr. The water contact angle was measured using KRUSS Advance contact angle goniometer. The specific surface area and pore volume distribution were estimated by a nitrogen adsorption-desorption method, using Quantachrome® ASiQwin™. The pore size distribution was estimated using the Barrett-Joyner-Halenda (BJH) method (Lowell *et al*. 2012).

The pure water permeability (PWP) (L/m^2 h bar) was assessed using a lab-made crossflow system as explained in chapter 7, section 7.2.3. Typically, a 28.27 cm^2 area of the membrane sample was kept in the crossflow system and compacted at 5 bar pressure for 30 minutes. Then, the PWP was evaluated at 4 bar pressure.

The salt removal percentage was evaluated using a feed solution containing 1000 ppm of Na_2SO_4 and NaCl. The heavy metal removal analysis was performed using a 10 ppm aqueous heavy metal salt solution of $Pb(NO_3)_2$ and $Cd(NO_3)_2$. The salt concentration in permeate was determined using a conductivity meter (Systronics) and the heavy metal ion concentration was identified using inductively coupled plasma-optical emission spectrometry (ICP-OES, Optima 7300DV, PerkinElmer). The salt rejection and heavy metal ion removal, R, was calculated as explained in chapter 7, section 7.2.3.

8.2.2 Synthesis of P(MBAAm-co-SVBS)@L-Cys nanoparticles

The P(MBAAm-co-SVBS) nanoparticles were synthesized through the DPP method (Ibrahim *et al*. 2017). Briefly, in a 250 mL round-bottom flasks, the monomers, SVBS (0.17 g, 0.82 mmol) and MBAAm (1.0 g, 6.48 mmol) and initiator AIBN (0.0225 g, 0.13 mmol) were dissolved in 100 mL of acetonitrile; then the flask was connected to a dean-stark. The

mixture was degassed for 20 minutes by bubbling with nitrogen (commercial grade). The temperature of the mixture was increased slowly to achieve a reflux condition. The temperature was maintained between 100 and 110 ^{o}C using an oil bath. After distilling 40 mL of acetonitrile over a period of one hour, the reaction mixture was cooled down to room temperature and further stirred for one hour at room temperature. The reaction mixture was transferred into centrifuge tubes and nanoparticles were isolated by centrifugation. The unreacted monomers and oligomers were removed by repeating the centrifugation three times. The isolated nanoparticles were dried in an oven at 50 ^{o}C for 12 hours.

L-Cys were covalently attached to the P(MBAAm-co-SVBS) nanoparticles to induce the zwitterionic property, following a previously reported process (Liu *et al*. 2016). Briefly, 0.9 g of P(MBAAm-co-SVBS) nanoparticles were dispersed in ethanol/water (2:3 v/v) mixture in a round-bottom flask. To this mixture, 0.5 g of L-Cys and 0.045 g of AIBN were added. The solution was bubbled with nitrogen (commercial grade) for 20 minutes to remove the dissolved oxygen. This solution was heated to 80 ^{o}C and stirred for 24 hours in an oil bath, followed by cooling to room temperature and further stirring for one hour. The zwitterionic nanoparticles were isolated by centrifugation. The schematic representation of the synthetic scheme for the P(MBAAm-co-SVBS)@L-Cys zwitterionic nanoparticles is shown in scheme 8.1A.

8.2.3 Fabrication of zwitterionic thin film nanocomposite (Z-TFN) and thin film composite (TFC) membranes

To integrate zwitterionic nanoparticles, P(MBAAm-co-SVBS)@L-Cys, into the active layer of TFN membranes, thin-film composite membranes fabricated through dispersing the nanoparticles in the precursor solution, used for interfacial polymerization. The interfacial polymerization was performed on macroporous supports. The macroporous polysulfone (PSF) membrane was fabricated and used them as the support layer. For the preparation of PSF support, a method reported in the literature was adopted (Misdan *et al*. 2013). For all thin-film composite (TFC) and Z-TFN membranes, the PA active layer was synthesized through interfacial polymerization. The processing parameters were adopted from the previous report on NF membrane fabrication (Lai *et al*. 2016). Briefly, the Z-TFN membranes were prepared as follows: an aqueous solution of 2.0 % (w/v) PIP in DI water was made by dissolving 0.4 g of PIP in 20 mL of DI water, at room temperature. Organic

solutions containing TMC and P(MBAAm-co-SVBS)@L-Cys nanoparticles were prepared by adding 0.15 % (w/v) TMC and different concentration of P(MBAAm-co-SVBS)@L-Cys nanoparticles (0.025 %, 0.05 % and 0.1 % (w/v) in 20 ml cyclohexane; the solutions were sonicated in an ultrasonic cleaning bath (SPECTRALAB UCB) for 30 minutes.

To form the PA layer, the aqueous solution was poured on the surface of the PSF substrate; the substrate was kept in the horizontal position for two minutes to allow for the infiltration of the aqueous solution into the substrate. Then, the excess solution was removed by a rubber roller. Subsequently, the organic solution was dispensed on the PIP-infiltrated PSF substrates and the solution was drained off after 10 seconds. The as-prepared Z-TFN membrane was rinsed with DI water and kept in an oven at 60 ^{o}C for eight minutes. For preparing control TFN membranes, the same procedure was repeated without using any nanoparticle in the organic solution; the solution composition and concentration and the processing conditions were kept the same. The as-prepared TFN and Z-TFN membranes were stored in DI water for further use. The membranes were labeled as Z-TFN-1, Z-TFN-2 and Z-TFN-3 corresponding to the 0.025 %, 0.05 % and 0.1 % (w/v) concentration of the P(MBAAm-co-SVBS)@L-Cys nanoparticles in the organic solution, respectively. The schematic representation of Z-TFN membrane preparation is given in scheme 8.1B.

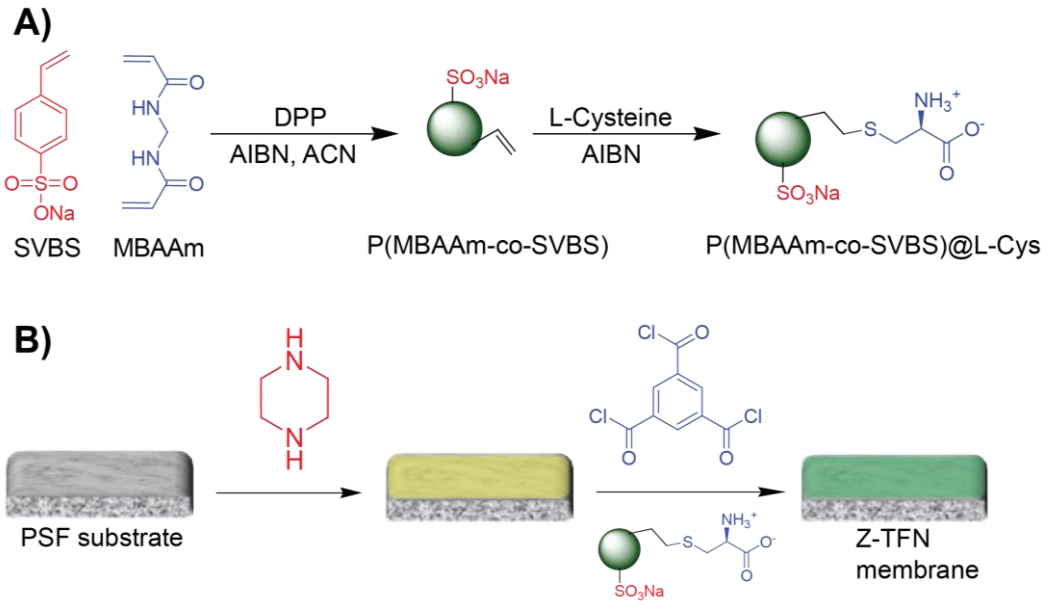

Scheme 8.1 A) Schematic representation of P(MBAAm-co-SVBS)@L-Cys zwitterionic nanoparticles synthesis (green sphere represents the nanoparticles) and B) Z-TFN membrane fabrication via interfacial polymerization

8.2.4 Characterization

The molecular weight cut-off (MWCO) and r_p were calculated by the solute rejection experiment using 0.2 g/L PEG (200-1000 Da) as explained in chapter 7, section 7.2.3. The experiments were performed at 4 bar differential pressure.

The antifouling properties of the membranes were assessed using 0.5 g/L BSA as the foulant. Initially, the membrane was stabilized with DI water for three hours at 4 bar and the pure water permeability (PWP, 'J_w') was noted. Then, the feed solution was replaced with the BSA solution; the filtration was performed at 4 bar in crossflow configuration and the permeate flux ('J_p') was measured. After the BSA fouling cycle, the membranes were cleaned with DI water by circulating DI water in crossflow mode. After the cleaning cycle, the water permeability was measured, noted as 'J_{w1}' and the flux recovery ratio (FRR) was calculated as explained in chapter 7, section 7.2.3.

8.3 RESULTS AND DISCUSSION

8.3.1 Characterization of P(MBAAm-co-SVBS)@L-Cys nanoparticles

Figure 8.1A presents the gas sorption-desorption isotherms for the nanoparticles; as shown, the nitrogen sorption represents a H2 type hysteresis loops which indicates the presence of ink-bottle-shaped pores according to the Brunauer-Deming-Deming-Teller (BDDT) classification (Li *et al*. 2017). The estimated specific surface area of the particles was ~370 m^2/g. The pore diameter and pore volume for the sample were estimated to be 3.37 nm and 0.52 cc/g, respectively. Thus, the pore size of the nanoparticles falls in the range of mesoporous (Bantawal *et al*. 2018). The BET surface area of the as-synthesized nanoparticles is relatively large when compared with the other mesoporous materials (Table 8.1).

Table 8.1 BET surface area comparison of as-synthesized nanoparticles along with literatures

Nanomaterial	BET surface area (m^2/g)	Pore volume (cc/g)	Ref.
ZrO_2	24.6	0.04	(Wang *et al*. 2005)
MesoporousAl_2O_3	312.0	0.36	(Labhsetwar *et al*. 2009)
HNTs	64.5	0.20	(Jin *et al*. 2015)
TiO_2 nanotubes	173.9	0.27	(Al-Maadeed 2016)
TiO_2 P25	56.0	0.25	(Subramaniam *et al*. 2017)
CNTs-OH	145.7	0.52	(Zheng *et al*. 2017)
P(MBAAm-co-SVBS)@L-Cys	**370.0**	**0.52**	**Present study**

Figure 8.1C shows the ATR-FTIR spectra of the precursor and nanoparticles. The peaks at 1058 cm^{-1} and 1132 cm^{-1} were ascribed to S=O symmetric and asymmetric stretching vibrations (Azari *et al*. 2013). Additionally, the C=O stretch (amide I) and N-H bending (amide II) in the P(MBAAm-co-SVBS) nanoparticles were observed at 1654 cm^{-1} and 1527 cm^{-1} (Ma *et al*. 2016). For P(MBAAm-co-SVBS)@L-Cys zwitterionic nanoparticles, a new salient peak appeared at 1583 cm^{-1}; which attributed to the carboxylate group of L-Cys. The shift in the wavenumber of the carboxylate stretch can be explained by the resonance effect and hydrogen bonding (Blom *et al*. 2007, Rijs *et al*. 2010, Silverstein *et al*. 2014). The surface charge of the P(MBAAm-co-SVBS)@L-Cys nanoparticles was measured to be ξ= -13.22 mV at pH 7.0; the negative charge was attributed to the presence of sulfonate functional groups.

Figure 8.1D shows the TEM image of the nanoparticles. The nanoparticles were spherical in shape with the particle size ranging between 20 and 40 nm. The ring-like selected area electron diffraction (SAED) pattern, shown in the inset of Figure 8.1D, implies that the as-synthesized nanoparticles are polycrystalline in nature. The SEM image of the sample on the conductive tape along with the representative EDX elemental mapping is shown in Figure 8.2E. The presence of sulfur signal confirms the successful attachment of the L-Cys to the P(MBAAm-co-SVBS) nanoparticles.

Figure 8.1F depicts the TGA curves of P(MBAAm-co-SVBS) and P(MBAAm-co-SVBS)@L-Cys nanoparticles. In P(MBAAm-co-SVBS) nanoparticles, the weight loss around 120 ^{o}C is attributed to the adsorbed water molecules. The second weight loss, observed in the temperature window of 264 to 500 ^{o}C attributed to the loss of stable oxygen functionalities (Pandey *et al*. 2014). For the P(MBAAm-co-SVBS)@L-Cys nanoparticles, an additional drop in the TGA thermogram can be observed, between 232 to 280 ^{o}C, which attributed to the degradation of the L-Cys groups.

To further evaluate the chemical composition of the nanoparticles, XPS measurement on the particles was performed. As shown in Figure 8.1G, the sulfur signal in the XPS signal confirms the presence of L-Cys in the sample. Figure 8.1H presents the C 1s spectra of the nanoparticles. This peak is deconvoluted into five peaks located at 284.61, 286.30, 287.42, 288.61 and 289.88, assigned to C-C, C-O/C-N, C=O, O-C=O and N-C=O, respectively (Tien *et al*. 2011, Das *et al*. 2012,). As shown in Figure 8.1I, the N 1s spectrum is deconvoluted into four peaks, centered at 399.44 eV, 401.49 eV, 402.19 eV and 403.89 assigned to amine (NH_2), amide (N-C=O), protonated amine (NH_3^+) and oxidized nitrogen ($N\text{-}O^-$), respectively (Tawil *et al*. 2013). The presence of NH_3^+ points to the zwitterionic nature of the nanoparticles.

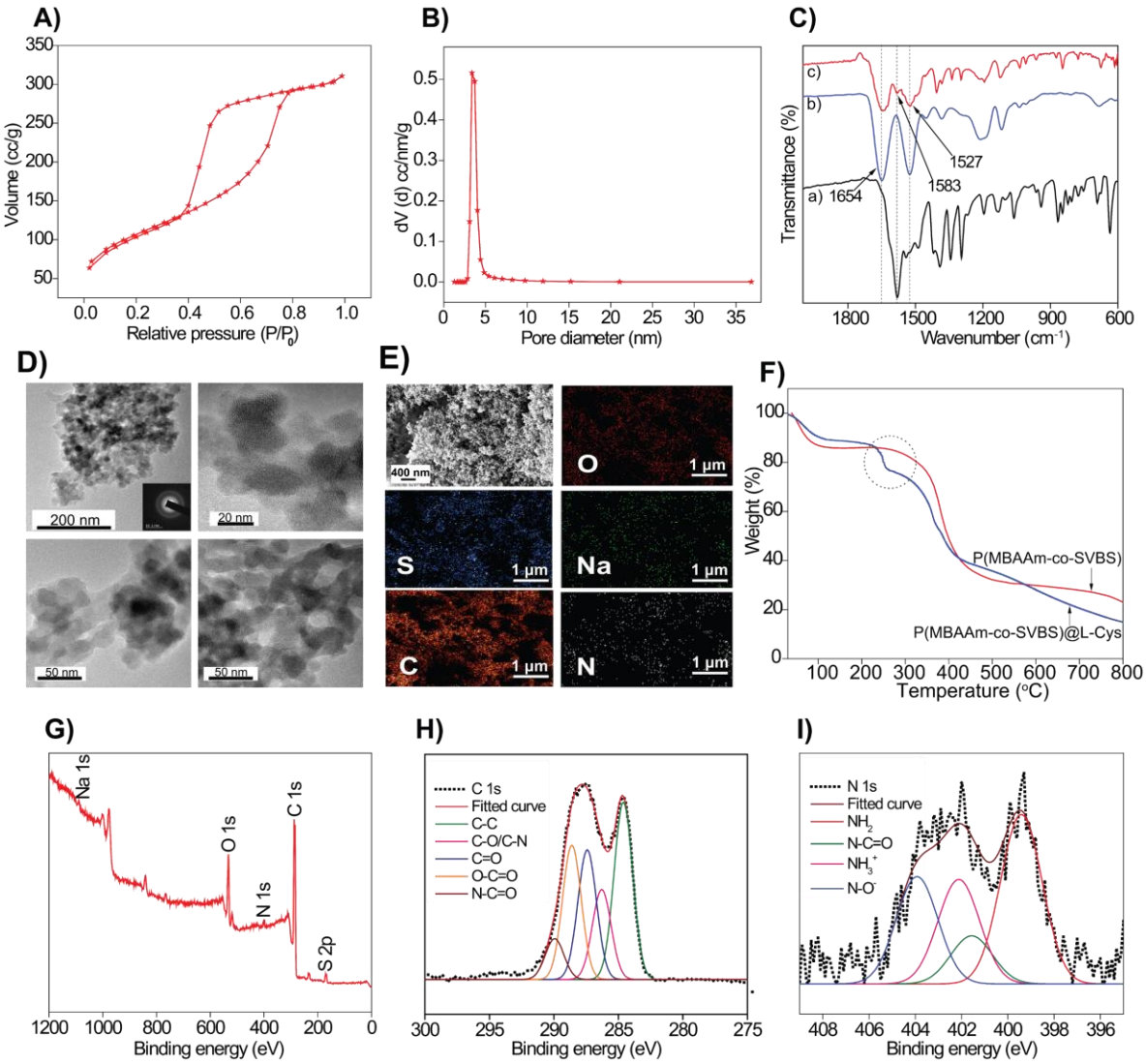

Figure 8.1 Nanoparticles characterization. A) and B) BET surface area and pore size distribution of P(MBAAm-co-SVBS)@L-Cys nanoparticles. C) ATR-FTIR spectra of a) Sodium 4-vinylbenzenesulfonate, b) P(MBAAm-co-SVBS) and c) P(MBAAm-co-SVBS)@L-Cys. D) TEM images (Inset: SAED pattern), E) EDX elemental mapping of P(MBAAm-co-SVBS)@L-Cys and F) TGA curve of P(MBAAm-co-SVBS) and P(MBAAm-co-SVBS)@L-Cys. G), H) and I) XPS survey and high resolution spectra of P(MBAAm-co-SVBS)@L-Cys

8.3.2 Characterization of Z-TFN and TFC membranes

To evaluate the structural properties and surface topography of the composite membranes SEM and AFM were used. Figure 8.2a-d' shows the structural properties of the cross-section of the membranes. Both the TFC and Z-TFN membranes exhibited a dense

PA layer, with a thickness of around 120 to 145 nm, supported on the spongy PSF substrates. Nonetheless, no significant change was observed between the TFC and Z-TFN. On the contrary, the AFM height images of different membranes, shown in Figure 8.2A-D, suggest that the roughness factor of the membranes was increased when organic precursor solution with a higher concentration of the nanoparticles was used to fabricate membranes. The roughness parameters including root-mean-square of the height deviations (R_q), maximum roughness (R_{max}) and average plane roughness (R_a) are tabulated in Table 8.2. The increased surface roughness of the Z-TFN membranes was attributed to the hydrophilic nature of nanoparticles. Upon bringing the organic phase in contact with the support PSF layer, soaked in aqueous piperazine solution, these hydrophilic nanoparticles migrate to the aqueous phase interface, resulting in the formation of membranes with different surface topography (Qu *et al*. 2010). Furthermore, the thickness of the formed polyamide layer is in the range of the nanoparticles dimension; hence, it is expected that the assembly of nanoparticles led to a rougher surface (Karan *et al*. 2015).

Table 8.2 AFM surface roughness parameters of TFC and Z-TFN membranes

Membrane	Roughness parameters		
	R_a (nm)	R_q (nm)	R_{max} (nm)
TFC	35.3	48.5	303.2
Z-TFN-1	46.2	72.6	412.4
Z-TFN-2	79.6	109.3	478.8
Z-TFN-3	102.5	135.4	521.3

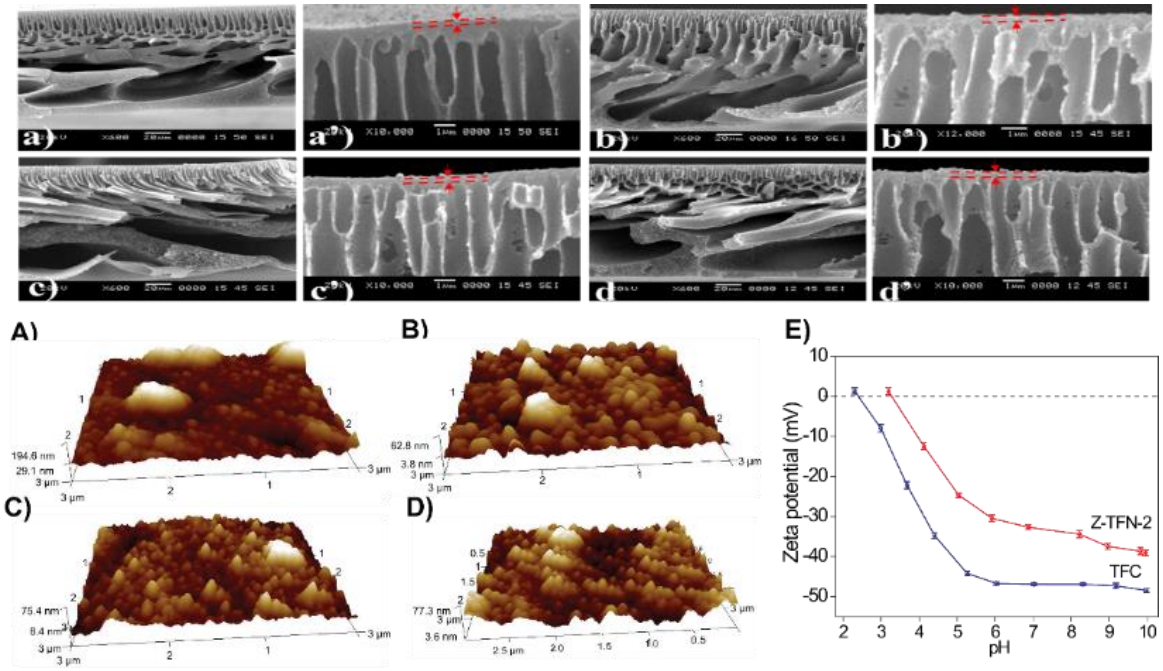

Figure 8.2 Membrane characterization. SEM cross-sectional images of a), a') TFC, b), b') Z-TFN-1, c), c') Z-TFN-2 and d), d') Z-TFN-3 and AFM 3D images of A) TFC, B) Z-TFN-1, C) Z-TFN-2 and D) Z-TFN-3 membranes and E) zeta potential (ξ) of TFC and Z-TFN-2 membranes

The zeta potential (ξ) of the membranes were measured to evaluate the surface charge of both TFC and Z-TFN membranes. The ξ of TFC and Z-TFN over a pH range of 2-10 and are shown in Figure 8.2E. The TFC membrane presented a negative charge in a wide range of pH with an isoelectric point (IEP) at pH 2.40; this characteristic is attributed to the presence of a hydrolyzed carboxylic acid group (–COOH) on the PA layer. For the Z-TFN-2 membrane, a shift in the IEP of the membranes toward higher pH values was noted. A plausible reason for this trend is the electrical neutrality of the zwitterionic particles present on the membrane surface, reducing the negative charge density of the nanocomposite membrane surface. Taken as a whole, the ξ analysis revealed that the as-synthesized nanocomposite membrane was negatively charged, owing to the presence of –COOH and $–SO_3Na$ groups.

To evaluate the membrane's transport properties, PEG rejection experiments were conducted. The MWCO of the Z-TFN-2 membrane was determined as 743 Da with a PEG Stokes radius (r_p) of 0.66 nm; these values suggest that these membranes can be categorized

as nanofiltration membranes (Ng *et al*. 2013). Further the PWP for different membranes was measured. The PWP of TFC, Z-TFN-1, Z-TFN-2 and Z-TFN-3 was found to be 6.2, 7.4, 11.4 and 13.1 L/m^2h bar, respectively. This trend indicates that increasing the concentration of the nanoparticle in the PA precursor solution results in an increase in the water permeability of the membranes. Nonetheless, the membranes prepared with nanoparticle concentration above 0.05 % (w/v) did not show satisfactory salt rejection and a trade-off between permeability and selectively was observed. Z-TFN-2 membrane was chosen for the remainder of our work as both the salt rejection and permeability were satisfactory.

Comparing the Z-TFN-2 with the TFC membranes, Z-TFN-2 membranes provide 1.8 times higher flux at the same salt rejection value when compared with the TFC membranes. The improved PWP was attributed to the increased surface roughness and the higher free volume created in the PA layer through the introduction of new interfacial domains between nanoparticles and polymers. This free volume can act as a water channel enhancing water permeability. Here, it was postulated that the formation of a large defect was hindered by a tight interaction between two organic phases, the zwitterionic nanoparticles and polyamide, hindering the phase segregation (Membranes 2013). In addition, it is expected that the zwitterionic nanoparticles on the PA layer, create a hydration layer on the membrane surface, which increases the interaction between water molecules and PA layer (Liu *et al*. 2017, Duong *et al*. 2018, He *et al*. 2018, Lee *et al*. 2018, Ma *et al*. 2018). This can be deduced from the increased contact angle of the Z-TFN membrane when compared with the TFC membrane.

The performance of the fabricated NF membranes was further evaluated using Na_2SO_4, $MgSO_4$, NaCl and $MgCl_2$ and heavy metals salts such as ($Pb(NO_3)_2$ and $Cd(NO_3)_2$) as the solute. As shown in Figures 9.3A, the TFC membrane rejection for Na_2SO_4, $MgSO_4$, NaCl and $MgCl_2$ were 97 %, 97.3 %, 14.3 % and 14.7 % respectively. After incorporating 0.05 % (w/v) of zwitterionic nanoparticles in the PA layer, no drastic change in the salt rejection was observed. However, the permeate flux was increased two-fold compared to the TFC membrane. The higher rejection of divalent ions was attributed to the increased charge density of SO_4^{2-} ions compared to Cl^- ions. Thus, SO_4^{2-} ions could exhibit better electrostatic repulsion against the negatively charged membrane surface (Donnan effect).

Simultaneously, while increasing the zwitterionic nanoparticles concentration of precursor solution from 0.05 % to 0.1 % (w/v), it was noted that the salt rejection properties of the fabricated membranes deteriorated. The reduced salt rejection was associated with the formation of defects within the PA layer, allowing the ions to pass through. A similar observation is reported in the literature for the nanocomposite membranes (Ma *et al*. 2012, Mollahosseini *et al*. 2013, Ghanbari *et al*. 2015, Zhu *et al*. 2017). Hence, here, the optimum concentration for the zwitterionic P(MBAAm-co-SVBS)@L-Cys nanoparticles was identified as 0.05 % (w/v). Figures 9.3B shows the permeability of membranes tested using salt solutions. Figure 8.3C shows the NF membrane performance in heavy metal ion removal. As shown, the Z-TFN-2 membrane exhibited the Pb^{2+} and Cd^{2+} ions removal of 99.48 % and 95.67 %. As noted earlier, the MWCO and r_p of the Z-TFN-2 membrane were 743 Da and 0.66 nm, respectively. The hydrated radii of Pb^{2+}, Cd^{2+} and NO_3^- are 0.401 nm, 0.426 nm and 0.335 nm (Nightingale *et al.* 1959).

Thus, the removal of these ions is not based on a size-exclusion mechanism. It was postulated that the removal efficiency of the membranes is due to Donnan exclusion. The IEP of the Z-TFN-2 membrane is 3.2; hence, at pH 5, where the separation test is performed, the electrostatic repulsion between the negatively charged membrane and NO_3^- ion. The principles of electroneutrality on the membrane surface mandate that the Pb^{2+} and Cd^{2+} ions be repelled. The observed phenomenon is well aligned with the reported literature (Mehiguene *et al*. 1999, Mehdipour *et al*. 2015). Table 8.3 presents the comparison of the NF membrane's performance with respect to heavy metal removal and desalination.

The antifouling ability of the as-synthesized TFC and Z-TFN-2 membranes was assessed by filtering a solution containing BSA (0.5 g/L) as foulant. As depicted in Figure 8.3D, the permeability of both TFC and the Z-TFN-2 membrane was reduced due to fouling. The Z-TFN-2 membrane exhibited a flux reduction of 25 % after 20 hours of continuous testing, whereas the TFC membrane demonstrated a flux reduction of 30 %. Thereafter, the membranes were simply cleaned with pure water and water permeabilities were measured again. The Z-TFN-2 membranes showed FRR of 83.1 % while the TFC membranes exhibited FRR of 71.5 %. The improved FRR was ascribed to the presence of zwitterionic P(MBAAm-co- SVBS)@L-Cys nanoparticles, which form a hydration layer on the membrane surface (Zhang *et al*. 2009, Fan *et al*. 2017). In addition, the Z-TFN-2

membrane is negatively charged (Figure 8.2E); hence, a larger electrostatic repulsion between the negatively charged membrane surface and BSA molecules is expected (Ang *et al*. 2007).

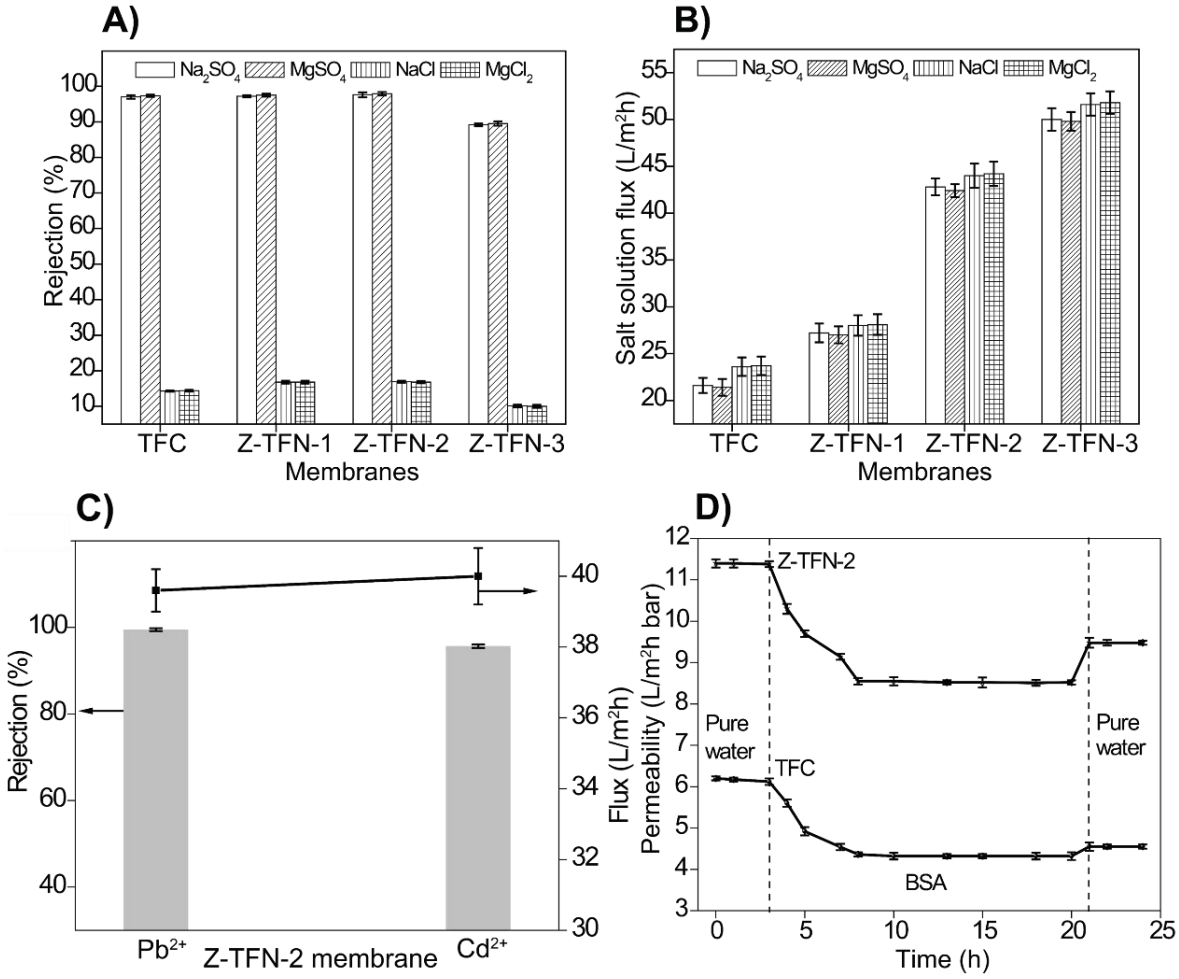

Figure 8.3 Membrane performance. A), B) Na_2SO_4, $MgSO_4$, $MgCl_2$, and NaCl rejection and flux of TFC and Z-TFN membranes, C) Pb^{2+} and Cd^{2+} removal and flux of Z-TFN-2 membrane at 4 bar and pH 5 and D)

Table 8.3 Comparison of heavy metal removal and desalination capacity of as-prepared NF membrane along with literatures

Membrane	Pressure (bar)	Salt rejection (%)	PWP (L/m^2h bar)	Heavy metal removal (%)	Ref.
TMC cross-linked Chitosan−PES	10	$MgCl_2$ = 96.3	3.45	Pb^{2+} = 93.00 Ni^{2+} = 96.30	(Zhang *et al.* 2014)
Matrimid/PEI/Nexar	10	$MgCl_2$ = 96.5 NaCl =71.2	2.4	Pb^{2+} = 99.80 Cd^{2+} = 98.20	(Thong *et al.* 2014)
HPEI modified GO&EDA framework	1	Na_2SO_4 ~ 40.0[a] NaCl ~59.0 [a]	5.01	Pb^{2+} = 95.70 Cd^{2+} = 90.50	(Zhang *et al.* 2015)
PEI-PEG conjugate modified Ag nanocomposite poly(PIP)	5	Na_2SO_4 ~ 85.0 [a] NaCl ~ 40 [a]	~ 8.00	Pb^{2+} = 99.80 Cd^{2+} = 90.30	(Bera *et al.* 2018)
HTFC-1	10	**Na_2SO_4 = 97.6** **NaCl =16.9**	7.0	**Pb^{2+} = 98.10** **Cd^{2+} = 96.30**	Chapter 7 Table 7.3
Z-TFN-2 membrane	**4**	**Na_2SO_4 = 97.6** **NaCl =16.9**	**11.4**	**Pb^{2+} = 99.48** **Cd^{2+} = 95.67**	**Present work**

[a]Assessed from published figures; PWP: Pure water permeability

8.4 CONCLUSIONS

In summary, the zwitterionic P(MBAAm-co-SVBS)@L-Cys nanoparticles incorporated into thin-film nanocomposite nanofiltration membranes enhanced the

performance of the membranes in removing heavy metals. The zwitterionic thin-film nanocomposite membranes exhibited improved pure water permeability when the nanoparticle concentration was increased. Above a certain concentration of nanoparticles in the membrane the permeability-selectivity trade-off sets in and the performance deteriorate. The compatibility between the organic nanoparticle and the polyamide allows for the tight integration of these nanoparticles within the polyamide films. A concentration of 0.05 % (w/v) of nanoparticles was noted as the optimum concentration of nanoparticles in the precursor solution and thin-film nanocomposite membranes with superior performance compared to that of thin-film composite membranes were fabricated. The zwitterionic and high surface area P(MBAAm-co-SVBS)@L-Cys nanoparticles improved the antifouling performances of the Z-TFN-2 membrane against organic fouling and the flux recovery ratio and flux reduction were 83.1 % and 25 % after 20 hours of filtration. Overall, the Z-TFN-2 membrane was suitable for desalination and heavy metal removal.

CHAPTER 9

SUMMARY AND CONCLUSIONS

Abstract: *This chapter bestows the brief summary of the whole research work and draws a short comparison between in-house fabricated membranes in terms of their properties and performance. It also confers the major conclusions drawn from the work.*

9.1 SUMMARY

- A total of thirty membranes (7 series) were fabricated with different types of additives.
- Among the thirty membranes, 22 membranes were ultrafiltration and 8 membranes were nanofiltration.
- Hydrophilic additives such as tannic acid modified halloysite nanotubes, zwitterionically modified Fe_3O_4 and graphene oxide (GO), zwitterionic polymer nanoparticles and functionalized poly(styrene-co-maleic anhydride) copolymer were used to improve the polysulfone membrane performances.
- Both hollow fiber and flat sheet membranes were prepared via the phase inversion method.
- All the membrane surface properties were characterized using SEM, AFM, zeta potential, contact angle and XPS analysis and the performances were evaluated by examining the surface porosity, water uptake, hydrophilicity, antifouling and solute rejection.
- Finally, the as-prepared membranes were exposed to the purification of wastewater containing heavy metal ions, dyes and humic acid respectively.

The following important results were obtained from the present research work.

1. HM-2 HF membrane fabricated with 2 wt% of tannic acid modified halloysite nanotubes demonstrated improved pure water permeability (PWP) of 46 L/m^2 h bar compared to the pristine membrane. Also exhibited rejection of > 99 % of RB 5 and > 97.5 % of RO 16 with the dye solution permeability of 43.5 L/m^2 h and 44 L/ m^2 h bar respectively.
2. ZM-3 nanocomposite HF membrane (MWCO 9242 Da) showed high pure water permeability of 56 L/ m^2 h bar and rejection of RB 5 (> 98 %) and RO 16 (> 80.7 %) with the dye permeability of 51 L/ m^2 h bar and 51.8 L/ m^2 h bar at a dye concentration of 100 ppm.
3. FM-2 HF membrane showed improved antifouling property with a flux recovery ratio (FRR) of 88.4 % and irreversible fouling of 11.9 %. The highest HA removal was

demonstrated by the FM-3 membrane. However, owing to the partial agglomeration of nanoparticles, the permeability of the FM-3 membrane was reduced when compared to the FM-2 membrane. In addition, the FM-2 membrane demonstrated high removal of reactive dyes (RB 5 >99 % and RO 16 >84 %).

4. TM-2 HF membrane with 0.25 wt% loading of nanomaterial exhibited high PWP (49.6 L/m^2 h bar) and reactive dyes such as RB-5 (99 %) and RO-16 (74 %) rejection with high salt permeability.
5. M-3 membrane with PSF/PAH blend ratio of 85:15 exhibited 91.5 % of Pb^{2+} and 72.3 % of Cd^{2+} ions removal with feed concentration of 10 mg/L. The results also revealed that the further increase of PAH amount beyond 20 % diminished the hydrophilicity, porosity and PWP.
6. HTFC-1 membrane demonstrated increased PWP of 7.0 L/m^2h bar, salt rejection (Na_2SO_4 - 97.0 %, $MgSO_4$ - 97.4 %, NaCl - 23.3 %), heavy metal rejection (Pb^{2+}- 98.1 %, Cd^{2+}- 96.3 %) and FRR (96.9 %) comparted to control membrane.
7. Z-TFN-2 membranes exhibited PWP of 11.4 L/m^2h bar and salt rejection value of 97.6 % and 16.9 %, for sodium sulfate and sodium chloride, respectively. The fabricated membranes demonstrated metal ion removal efficiencies of 99.48 % and 95.67 % for Pb^{2+} and Cd^{2+}, respectively.

The performance of all the prepared membranes in terms of PWP, contact angle and solute rejection are compared in Table 9.1.

Table 9.1 Series of prepared membranes

Membrane series	Membranes	Type of membrane	Type of modification
HM	HM-0, HM-1, HM-2 and HM-3	Ultrafiltration/Hollow fiber	Nanocomposite
ZM	ZM-0, ZM-1, ZM-2, ZM-3 and ZM-4	Ultrafiltration/Hollow fiber	Nanocomposite
FM	FM-0, FM-1, FM-2 and FM-3	Ultrafiltration/Hollow fiber	Nanocomposite
TM	TM-0, TM-1, TM-2 and TM-3	Ultrafiltration/Hollow fiber	Nanocomposite
M	M-0, M-1, M-2, M-3 and M-4	Ultrafiltration/Flat sheet	Blending
HTFC	Control, HTFC-1, HTFC-2 and HTFC-3	Nanofiltration/Flat sheet	Thin film coating
Z-TFN	TFC, Z-TFN-1, Z-TFN-2 and Z-TFN-3	Nanofiltration/Flat sheet	Thin film coating

The pure water permeability (PWP) of all the prepared hollow fiber and flat sheet UF membranes are compared in Figure 9.1A and B. As shown, the FM-2 hollow fiber UF membrane prepared with 1 wt% of PSBMA@Fe_3O_4 nanoparticles exhibited increased PWP compared to all the prepared hollow fiber membranes. The PM-2 flat sheet UF membrane with 1 wt% of ionic nanoparticles demonstrated the highest PWP. The improved PWP of the UF membranes was attributed to the increased porosity and hydrophilicity.

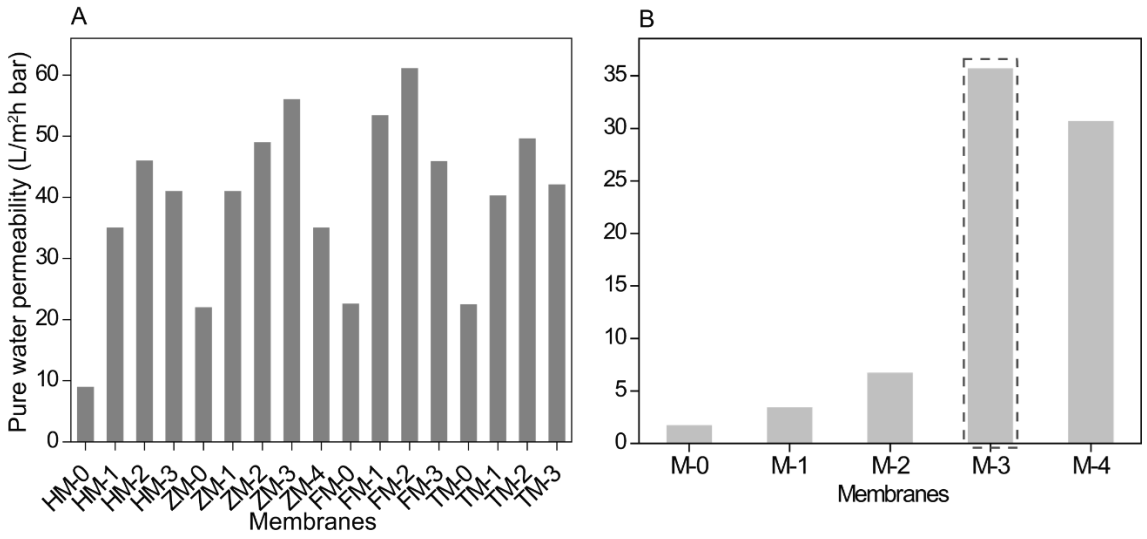

Figure 9.1 Comparison of pure water permeability of A) hollow fiber and B) flat sheet ultrafiltration membranes

The surface hydrophilicity of the membrane plays an important role in membrane properties such as permeability and antifouling performances. Figure 9.2A and B depict the comparison of the contact angle of both UF and NF membranes. Among the UF membranes prepared, the M-3 blend membrane fabricated with PSF: PAH ratio of 85:15 exhibited lowest contact angle. The results indicated that the blend UF membranes demonstrated improved hydrophilicity compared to nanocomposite UF membranes. The increased hydrophilicity was attributed to the presence of hydrophilic polymer. Whereas in nanocomposite UF membranes, as the concentration of hydrophilic nanoparticles is less in the membrane matrix, the surface hydrophilicity was not increased to a greater extent.

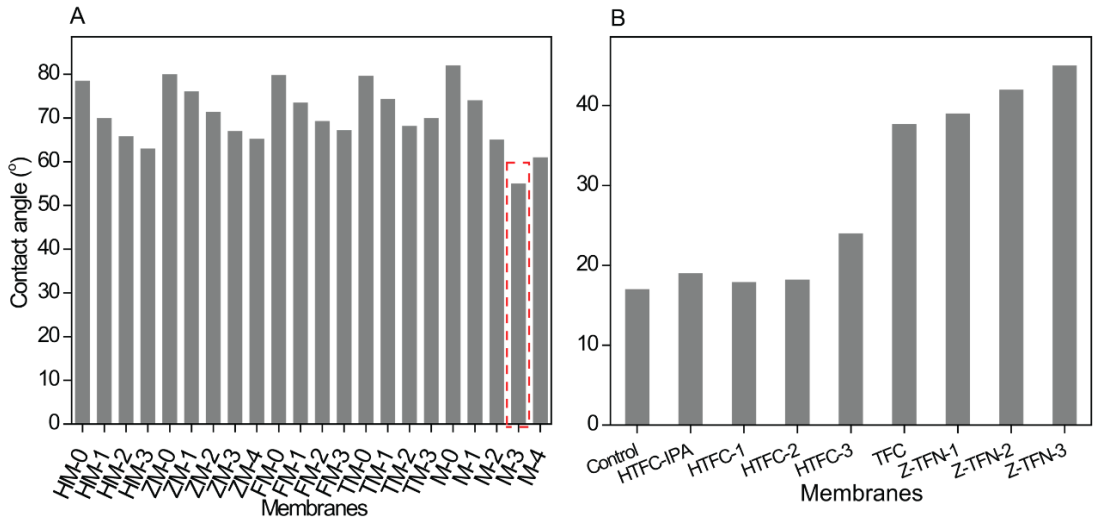

Figure 9.2 Comparison of contact angle of A) ultrafiltration and B) nanofiltration membranes

Figure 9.3A and B present the dye removal efficiency of hollow fiber UF membranes. As shown, all the hollow fiber UF membranes exhibited >99 % of rejection for Reactive black 5, whereas, for Reactive orange 16, the rejection was in the range of 74 to 90 %. The reduced rejection of Reactive orange 16 was attributed to the lower molecular weight of Reactive orange 16 dye molecules compared to Reactive black 5.

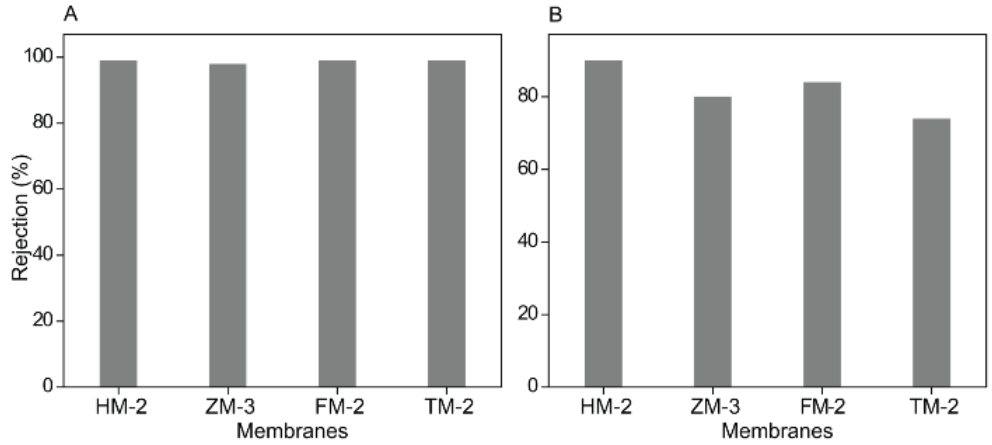

Figure 9.3 Comparison of A) Reactive black 5 and B) Reactive orange 16 removal of hollow fiber ultrafiltration membrane HM, ZM, FM and TM series

The PWP and Na_2SO_4 rejection of prepared TFC and TFN NF membranes were compared in Figure 9.4A and B. All the TFC and TFN NF membranes demonstrated >90 % rejection of Na_2SO_4. However, improved PWP was observed for the Z-TFN NF

membranes compared to TFC NF membranes. The improved PWP of Z-TFN membranes was ascribed to the formation of nanovoids in the polyamide layer.

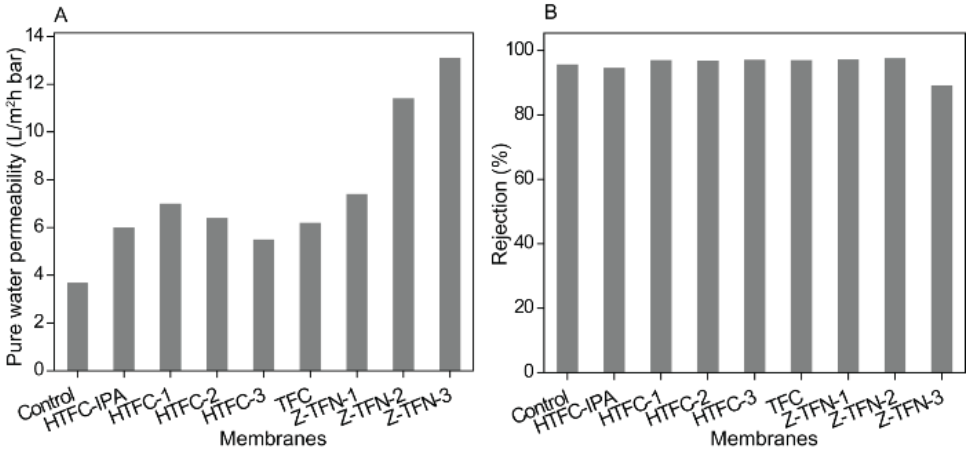

Figure 9.4 Comparison of A) pure water permeability and B) Na_2SO_4 rejection of HTFC and Z-TFN nanofiltration membrane series

9.2 CONCLUSIONS

The major conclusions of the present study are listed below.

1. The added tannic acid-functionalized HNTs, zwitterionic GO and Fe_3O_4, zwitterionic and ionic polymer nanoparticles improved hydrophilicity, porosity and antifouling performance of the PSF membrane.
2. The blending of hydrophilic polymer (PAH) with PSF exhibited a change in the morphology and increased membrane performances such as PWP, hydrophilicity and heavy metal removal.
3. The higher concentration of nanomaterials/hydrophilic polymer caused the deterioration of membrane performance due to the agglomeration or decreased hydrophilicity.
4. The increased surface charge played a vital role in increasing repulsion between membrane surface charge and dye molecules.
5. Incorporation of zwitterionic/ionic polymer nanoparticles resulted in the improved hydrophilicity and antifouling performance by forming a hydration layer on the membrane surface.
6. The IPA and EDA treatment for the polyamide layer could bring about change in the polyamide layer thickness and surface charge.

7. The addition of zwitterionic nanomaterials in the polyamide layer improved permeability by forming a nanovoid.

Present research work gives a glance of interminable opportunities within the resources of different modification techniques in developing membranes with specific properties that can be tuned based on targeted applications. As much more is to be explored, the future work will be devoted to further understanding of the effect of modification techniques on the morphology to property relationship of the membranes. Successively, the developed membranes will be tested for long-term performance, durability, the stability of polymer in adverse conditions and will be optimized for superior antifouling and antibiofouling property for water purification.

REFERENCES

Abbas, A., Al-Amer, A. M., Laoui, T., Al-Marri, M. J., Nasser, M. S., Khraisheh, M. and Atieh, M. A. (2016). "Heavy metal removal from aqueous solution by advanced carbon nanotubes: Critical review of adsorption applications." *Sep. Purif. Technol.*, 157, 141-161.

Abdullah, N., Gohari, R., Yusof, N., Ismail, A., Juhana, J., Lau, W. and Matsuura, T. (2016). "Polysulfone/hydrous ferric oxide ultrafiltration mixed matrix membrane: preparation, characterization and its adsorptive removal of lead (II) from aqueous solution." *Chem. Eng. J.*, 289, 28-37.

Abraham, J., Vasu, K. S., Williams, C. D., Gopinadhan, K., Su, Y., Cherian, C. T., Dix, J., Prestat, E., Haigh, S. J., Grigorieva, I. V., Carbone, P., Geim, A. K. and Nair, R. R. (2017). "Tunable sieving of ions using graphene oxide membranes." *Nat. Nanotechnol.*, 12, 546.

Achilli, A., Cath, T. Y. and Childress, A. E. (2009). "Power generation with pressure retarded osmosis: An experimental and theoretical investigation." *J. Membr. Sci.*, 343, (1), 42-52.

Ai, L., Zhang, C. and Chen, Z. (2011). "Removal of methylene blue from aqueous solution by a solvothermal-synthesized graphene/magnetite composite." *J. Hazard. Mater.*, 192, (3), 1515-1524.

Akbari, A., Desclaux, S., Rouch, J.-C. and Remigy, J.-C. (2007). "Application of nanofiltration hollow fibre membranes, developed by photografting, to treatment of anionic dye solutions." *J. Membr. Sci.*, 297, (1), 243-252.

Akbari, A., Aliyarizadeh, E., Mojallali Rostami, S. M. and Homayoonfal, M. (2016). "Novel sulfonated polyamide thin-film composite nanofiltration membranes with improved water flux and anti-fouling properties." *Desalination*, 377, 11-22.

Al-Amoudi, A. and Lovitt, R. W. (2007). "Fouling strategies and the cleaning system of NF membranes and factors affecting cleaning efficiency." *J. Membr. Sci.*, 303, (1-2), 4-28.

Al-Degs, Y. S., El-Barghouthi, M. I., El-Sheikh, A. H. and Walker, G. M. (2008). "Effect of solution pH, ionic strength, and temperature on adsorption behavior of reactive dyes on activated carbon." *Dyes Pigm.*, 77, (1), 16-23.

Al-Maadeed, M. A. S. (2016). "TiO 2 nanotubes and mesoporous silica as containers in self-healing epoxy coatings." *Sci. Rep.*, 6, 38812.

Al-Rashdi, B. A. M., Johnson, D. J. and Hilal, N. (2013). "Removal of heavy metal ions by nanofiltration." *Desalination*, 315, 2-17.

Alam, M. M., ALOthman, Z. A., Naushad, M. and Aouak, T. (2014). "Evaluation of heavy metal kinetics through pyridine based Th (IV) phosphate composite cation exchanger using particle diffusion controlled ion exchange phenomenon." *J. Ind. Eng. Chem*, 20, (2), 705-709.

Alhoshan, M., Alam, J., Dass, L. A. and Al-Homaidi, N. (2013). "Fabrication of Polysulfone/ZnO Membrane: Influence of ZnO Nanoparticles on Membrane Characteristics." *Advances in Polymer Technology*, 32, (4), 21369.

Ali, M. E., Wang, L., Wang, X. and Feng, X. (2016). "Thin film composite membranes embedded with graphene oxide for water desalination." *Desalination*, 386, 67-76.

Alsohaimi, I. H., Kumar, M., Algamdi, M. S., Khan, M. A., Nolan, K. and Lawler, J. (2017). "Antifouling hybrid ultrafiltration membranes with high selectivity fabricated from polysulfone and sulfonic acid functionalized TiO2 nanotubes." *Chemical Engineering Journal*, 316, 573-583.660-661

Ang, W. S. and Elimelech, M. (2007). "Protein (BSA) fouling of reverse osmosis membranes: Implications for wastewater reclamation." *J. Membr. Sci.*, 296, (1), 83-92.

Ayranci, E. and Duman, O. (2004). "Binding of lead ion to bovine serum albumin studied by ion selective electrode." *Protein and peptide letters*, 11, (4), 331-337.

Azari, S. and Zou, L. (2013). "Fouling resistant zwitterionic surface modification of reverse osmosis membranes using amino acid l-cysteine." *Desalination*, 324, 79-86.

Babu, K. and Dhamodharan, R. (2009). "Synthesis of polymer grafted magnetite nanoparticle with the highest grafting density via controlled radical polymerization." *Nanoscale Res. Lett.*, 4, (9), 1090.

Bai, F., Yang, X. and Huang, W. (2004). "Synthesis of narrow or monodisperse poly(divinylbenzene) microspheres by distillation-precipitation polymerization." *Macromolecules*, 37, (26), 9746-9752.

Bai, F., Yang, X. and Huang, W. (2004). "Synthesis of narrow or monodisperse poly (divinylbenzene) microspheres by distillation− precipitation polymerization." *Macromolecules*, 37, (26), 9746-9752.

Bai, L., Liu, Y., Ding, A., Ren, N., Li, G. and Liang, H. (2019). "Fabrication and characterization of thin-film composite (TFC) nanofiltration membranes incorporated with cellulose nanocrystals (CNCs) for enhanced desalination performance and dye removal." *Chem. Eng. J.*, 358, 1519-1528.

Baker, R. W. (2000)."*Membrane technology*. Pulisher name, Wiley Online Library Place.

Bandara, P. C., Perez, J. V. D., Nadres, E. T., Nannapaneni, R. G., Krakowiak, K. J. and Rodrigues, D. F. (2019). "Graphene Oxide Nanocomposite Hydrogel Beads for Removal of Selenium in Contaminated Water." *ACS Applied Polymer Materials*, 1, (10), 2668-2679.

Bano, S., Mahmood, A., Kim, S.-J. and Lee, K.-H. (2015). "Graphene oxide modified polyamide nanofiltration membrane with improved flux and antifouling properties." *J. Mater. Chem. A*, 3, (5), 2065-2071.

Bantawal, H., Shenoy, U. S. and Bhat, D. K. (2018). "Tuning the Photocatalytic Activity of SrTiO3 by Varying the Sr/Ti Ratio: Unusual Effect of Viscosity of the Synthesis Medium." *J. Phys. Chem. C*, 122, (34), 20027-20033.

Barakat, M. (2011). "New trends in removing heavy metals from industrial wastewater." *Arabian journal of chemistry*, 4, (4), 361-377.

Barnum, D. W. (1983). "Hydrolysis of cations. Formation constants and standard free energies of formation of hydroxy complexes." *Inorg. Chem.*, 22, (16), 2297-2305.

Basu, S. and Balakrishnan, M. (2017). "Polyamide thin film composite membranes containing ZIF-8 for the separation of pharmaceutical compounds from aqueous streams." *Sep. Purif. Technol.*,, 179, 118-125.

Baughman, G. L. and Weber, E. J. (1994). "Transformation of dyes and related compounds in anoxic sediment: kinetics and products." *Environ. Sci. Technol.*, 28, (2), 267-276.

Bechhold, H. (1908). "Durchlässigkeit von Ultrafiltern." *Zeitschrift für Physikalische Chemie*, 64, (1), 328-342.

Ben-Sasson, M., Lu, X., Nejati, S., Jaramillo, H. and Elimelech, M. (2016). "In situ surface functionalization of reverse osmosis membranes with biocidal copper nanoparticles." *Desalination*, 388, 1-8.

Bengani-Lutz, P., Converse, E., Cebe, P. and Asatekin, A. (2017). "Self-assembling zwitterionic copolymers as membrane selective layers with excellent fouling resistance: Effect of zwitterion chemistry." *ACS Appl. Mater. Interfaces*, 9, (24), 20859-20872.

Bera, A., Trivedi, J. S., Kumar, S. B., Chandel, A. K. S., Haldar, S. and Jewrajka, S. K. (2018). "Anti-organic fouling and anti-biofouling poly(piperazineamide) thin film nanocomposite membranes for low pressure removal of heavy metal ions." *J. Hazard. Mater.*, 343, 86-97.

Berg, P., Hagmeyer, G. and Gimbel, R. (1997). "Removal of pesticides and other micropollutants by nanofiltration." *Desalination*, 113, (2-3), 205-208.

Bes-Piá, A., Iborra-Clar, M., Iborra-Clar, A., Mendoza-Roca, J., Cuartas-Uribe, B. and Alcaina-Miranda, M. (2005). "Nanofiltration of textile industry wastewater using a physicochemical process as a pre-treatment." *Desalination*, 178, (1-3), 343-349.

Blom, M. N., Compagnon, I., Polfer, N. C., von Helden, G., Meijer, G., Suhai, S., Paizs, B. and Oomens, J. (2007). "Stepwise solvation of an amino acid: the appearance of zwitterionic structures." *J. Phy. Chem. A*, 111, (31), 7309-7316.

Bouranene, S., Fievet, P., Szymczyk, A., El-Hadi Samar, M. and Vidonne, A. (2008). "Influence of operating conditions on the rejection of cobalt and lead ions in aqueous solutions by a nanofiltration polyamide membrane." *J. Membr. Sci.*, 325, (1), 150-157.

Brant, J., Lecoanet, H., Hotze, M. and Wiesner, M. (2005). "Comparison of Electrokinetic Properties of Colloidal Fullerenes (n-C60) Formed Using Two Procedures." *Environ. Sci. Technol.*, 39, (17), 6343-6351.

Brostow, W. and Hagg Lobland, H. E. (2008). "Predicting wear from mechanical properties of thermoplastic polymers." *Polym. Eng. Sci.*, 48, (10), 1982-1985.

Buonomenna, M., Golemme, G., Jansen, J. and Choi, S.-H. (2011). "Asymmetric PEEKWC membranes for treatment of organic solvent solutions." *J. Membr. Sci.,*, 368, (1), 144-149.

Burkinshaw, S. and Kabambe, O. (2011). "Attempts to reduce water and chemical usage in the removal of bifunctional reactive dyes from cotton: part 2 bis (vinyl sulfone), aminochlorotriazine/vinyl sulfone and bis (aminochlorotriazine/vinyl sulfone) dyes." *Dyes Pigm.*, 88, (2), 220-229.

Butler, G. B. and Bunch, R. L. (1949). "Preparation and Polymerization of Unsaturated Quaternary Ammonium Compounds." *J. Am. Chem. Soc.*, 71, (9), 3120-3122.

Butler, G. B. and Ingley, F. L. (1951). "Preparation and Polymerization of Unsaturated Quaternary Ammonium Compounds. II. Halogenated Allyl Derivatives1,2." *J. Am. Chem. Soc.*, 73, (3), 895-896.

Cassagneau, T., Guérin, F. and Fendler, J. H. (2000). "Preparation and characterization of ultrathin films layer-by-layer self-assembled from graphite oxide nanoplatelets and polymers." *Langmuir*, 16, (18), 7318-7324.

Cassano, A., Molinari, R., Romano, M. and Drioli, E. (2001). "Treatment of aqueous effluents of the leather industry by membrane processes: a review." *J. Membr. Sci.*, 181, (1), 111-126.

Cath, T. Y., Childress, A. E. and Elimelech, M. (2006). "Forward osmosis: principles, applications, and recent developments." *J. Membr. Sci.*, 281, (1), 70-87.

Cavallaro, G., Lazzara, G., Milioto, S., Parisi, F. and Sanzillo, V. (2013). "Modified halloysite nanotubes: nanoarchitectures for enhancing the capture of oils from vapor and liquid phases." *ACS Appl. Mater. Interfaces*, 6, (1), 606-612.

Chai, P., Mahmoudi, E., Teow, Y. and Mohammad, A. (2017). "Preparation of novel polysulfone-Fe 3 O 4/GO mixed-matrix membrane for humic acid rejection." *J. Water Process Eng.*, 15, 83-88.

Chakrabarty, B., Ghoshal, A. and Purkait, M. (2010). "Cross-flow ultrafiltration of stable oil-in-water emulsion using polysulfone membranes." *Chem. Eng. J.*, 165, (2), 447-456.

Chang, Y., Shih, Y. J., Lai, C. J., Kung, H. H. and Jiang, S. (2013). "Blood-Inert Surfaces via Ion-Pair Anchoring of Zwitterionic Copolymer Brushes in Human Whole Blood." *Adv. Funct. Mater*, 23, (9), 1100-1110.

Chao, C., Liu, J., Wang, J., Zhang, Y., Zhang, B., Zhang, Y., Xiang, X. and Chen, R. (2013). "Surface modification of halloysite nanotubes with dopamine for enzyme immobilization." *ACS Appl. Mater. Interfaces*, 5, (21), 10559-10564.

Chavan, A. A., Li, H., Scarpellini, A., Marras, S., Manna, L., Athanassiou, A. and Fragouli, D. (2015). "Elastomeric nanocomposite foams for the removal of heavy metal ions from water." *ACS Appl. Mater. Interfaces*, 7, (27), 14778-14784.

Chen, G., Chai, X., Po-Lock, Y. and Mi, Y. (1997). "Treatment of textile desizing wastewater by pilot scale nanofiltration membrane separation." *J. Membr. Sci.*, 127, (1), 93-99.

Chen, M. H., Chiao, T. C. and Tseng, T. W. (1996). "Preparation of sulfonated polysulfone/polysulfone and aminated polysulfone/polysulfone blend membranes." *J. Appl. Polym. Sci.*, 61, (7), 1205-1209.

Chen, S. and Jiang, S. (2008). "An New Avenue to Nonfouling Materials." *Adv. Mater.*, 20, (2), 335-338.

Chen, S., Li, L., Zhao, C. and Zheng, J. (2010). "Surface hydration: principles and applications toward low-fouling/nonfouling biomaterials." *Polymer*, 51, (23), 5283-5293.

Chen, S., Zhu, J., Wu, X., Han, Q. and Wang, X. (2010). "Graphene oxide− MnO2 nanocomposites for supercapacitors." *ACS Nano*, 4, (5), 2822-2830.

Chenglin, Y., Yiqun, Y., Ye, Z., Na, L., Xiaoya, L., Jing, L. and Ming, J. (2012). "Self-assembly and emulsification of poly {[styrene-alt-maleic acid]-co-[styrene-alt-(N-3, 4-dihydroxyphenylethyl-maleamic acid)]}." *Langmuir*, 28, (25), 9211-9222.

Cheryan, M. (1998). "Ultrafiltration and Microfiltration Handbook, Technomic." *Lancaster, PA*, 116, 123.

Chethana, M., Sorokhaibam, L. G., Bhandari, V. M., Raja, S. and Ranade, V. V. (2016). "Green Approach to Dye Wastewater Treatment Using Biocoagulants." *ACS Sustain. Chem. Eng.*, 4, (5), 2495-2507.

Chiag, Y.-C., Chang, Y., Chen, W.-Y. and Ruaan, R.-c. (2011). "Biofouling resistance of ultrafiltration membranes controlled by surface self-assembled coating with PEGylated copolymers." *Langmuir,* 28, (2), 1399-1407.

Childress, A. E. and Elimelech, M. (2000). "Relating nanofiltration membrane performance to membrane charge (electrokinetic) characteristics." *Environ. Sci. Technol.*, 34, (17), 3710-3716.

Chung, T.-S., Qin, J.-J. and Gu, J. (2000). "Effect of shear rate within the spinneret on morphology, separation performance and mechanical properties of ultrafiltration polyethersulfone hollow fiber membranes." *Chem. Eng. Sci.*, 55, (6), 1077-1091.

Ciardelli, G. and Ranieri, N. (2001). "The treatment and reuse of wastewater in the textile industry by means of ozonation and electroflocculation." *Water Res.*, 35, (2), 567-572.

Cohen, E. (1899)."*Jacobus Henricus van't Hoff*. Pulisher name, W. Engelmann Place.

Corry, B. (2008). "Designing carbon nanotube membranes for efficient water desalination." *J. Phys. Chem. B.,* 112, (5), 1427-1434.

Daraei, P., Madaeni, S. S., Ghaemi, N., Salehi, E., Khadivi, M. A., Moradian, R. and Astinchap, B. (2012). "Novel polyethersulfone nanocomposite membrane prepared by PANI/Fe 3 O 4 nanoparticles with enhanced performance for Cu (II) removal from water." *J. Membr. Sci.*, 415, 250-259.

Das, S. K., Dickinson, C., Lafir, F., Brougham, D. F. and Marsili, E. (2012). "Synthesis, characterization and catalytic activity of gold nanoparticles biosynthesized with Rhizopus oryzae protein extract." *Green Chem.,* 14, (5), 1322-1334.

Demirbas, A. (2008). "Heavy metal adsorption onto agro-based waste materials: a review." *J. Hazard. Mater.*, 157, (2), 220-229.

DeRuiter, J., Swearingen, B. E., Wandrekar, V. and Mayfield, C. A. (1989). "Synthesis and in vitro aldose reductase inhibitory activity of compounds containing an N-acylglycine moiety." *J.Med.Chem,* 32, (5), 1033-1038.

De, S., Das, C., & DasGupta, S. (2009). Treatment of Tannery Effluents by Membrane Separation Technology. Nova Science Publishers.

Dervin, S., Dionysiou, D. D. and Pillai, S. C. (2016). "2D nanostructures for water purification: graphene and beyond." *Nanoscale,* 8, (33), 15115-15131.

Ding, X., Liu, Z., Li, X., Zhao, H., Hua, M. and Zhang, Y. (2016). "Synthesis and performance of a novel nanofiltration membrane with a crosslinked sulfonated polysulfone separation layer." *Desalin. Water Treat.,*, 57, (54), 25960-25971.

Donnan, F. G. (1911). "Theorie der Membrangleichgewichte und Membranpotentiale bei Vorhandensein von nicht dialysierenden Elektrolyten. Ein Beitrag zur physikalisch-chemischen Physiologie." *Berichte der Bunsengesellschaft für physikalische Chemie*, 17, (14), 572-581.

Du, Y., Zhang, C., Zhong, Q. Z., Yang, X., Wu, J. and Xu, Z. K. (2017). "Ultrathin alginate coatings as selective layers for nanofiltration membranes with high performance." *ChemSusChem*, 10, (13), 2788-2795.

Duan, J., Liu, R., Chen, T., Zhang, B. and Liu, J. (2012). "Halloysite nanotube-Fe 3 O 4 composite for removal of methyl violet from aqueous solutions." *Desalination*, 293, 46-52.

Duman, O. and Ayranci, E. (2010). "Attachment of benzo-crown ethers onto activated carbon cloth to enhance the removal of chromium, cobalt and nickel ions from aqueous solutions by adsorption." *J. Hazard. Mater.*, 176, (1), 231-238.

Dumée, L., Sears, K., Schü tz, J. r., Finn, N., Duke, M. and Gray, S. (2010). "Carbon nanotube based composite membranes for water desalination by membrane distillation." *Desalin. Water Treat.*,, 17, (1-3), 72-79.

Echaide-Górriz, C., Zapata, J. A., Etxeberría-Benavides, M., Téllez, C. and Coronas, J. (2020). "Polyamide/MOF bilayered thin film composite hollow fiber membranes with tuned MOF thickness for water nanofiltration." *Sep. Purif. Technol.*, 236, 116265.

Egerton, R. F. (2005)."*Physical principles of electron microscopy*. Pulisher name, Springer Place.

Elimelech, M. and Phillip, W. A. (2011). "The future of seawater desalination: energy, technology, and the environment." *science*, 333, (6043), 712-717.

Fan, L., Ma, Y., Su, Y., Zhang, R., Liu, Y., Zhang, Q. and Jiang, Z. (2015). "Green coating by coordination of tannic acid and iron ions for antioxidant nanofiltration membranes." *RSC Adv.*, 5, (130), 107777-107784.

Fan, L., Zhang, Q., Yang, Z., Zhang, R., Liu, Y.-n., He, M., Jiang, Z. and Su, Y. (2017). "Improving permeation and antifouling performance of polyamide nanofiltration membranes through the incorporation of arginine." *ACS Appl. Mater. Interfaces*, 9, (15), 13577-13586.

Fan, Z., Wang, Z., Duan, M., Wang, J. and Wang, S. (2008). "Preparation and characterization of polyaniline/polysulfone nanocomposite ultrafiltration membrane." *J. Membr. Sci.*, 310, (1-2), 402-408.

Fang, J. and Shen, P. K. (2006). "Quaternized poly(phthalazinon ether sulfone ketone) membrane for anion exchange membrane fuel cells." *J. Membr. Sci.*, 285, (1), 317-322.

Fang, J. and Deng, B. (2014). "Rejection and modeling of arsenate by nanofiltration: Contributions of convection, diffusion and electromigration to arsenic transport." *J. Membr. Sci.*, 453, 42-51.

Fang, X., Li, J., Li, X., Pan, S., Zhang, X., Sun, X., Shen, J., Han, W. and Wang, L. (2017). "Internal pore decoration with polydopamine nanoparticle on polymeric ultrafiltration membrane for enhanced heavy metal removal." *Chem. Eng. J.*, 314, 38-49.

Feng, L., Zhang, Z., Mai, Z., Ma, Y., Liu, B., Jiang, L. and Zhu, D. (2004). "A super-hydrophobic and super-oleophilic coating mesh film for the separation of oil and water." *Angew. Chem. Int. Ed.*, 43, (15), 2012-2014.

Fersi, C., Gzara, L. and Dhahbi, M. (2005). "Treatment of textile effluents by membrane technologies." *Desalination*, 185, (1-3), 399-409.

Fick, A. (1855). "Ueber diffusion." *Annalen der Physik*, 170, (1), 59-86.

Forgacs, E., Cserhati, T. and Oros, G. (2004). "Removal of synthetic dyes from wastewaters: a review." *Environ. Int.*, 30, (7), 953-971.

Fu, F. and Wang, Q. (2011). "Removal of heavy metal ions from wastewaters: a review." *J. Environ. Manage*, 92, (3), 407-418.

Fu, W., Pei, T., Mao, Y., Li, G., Zhao, Y. and Chen, L. (2019). "Highly hydrophilic poly(vinylidene fluoride) ultrafiltration membranes modified by poly(N-acryloyl glycinamide) hydrogel based on multi-hydrogen bond self-assembly for reducing protein fouling." *J. Membr. Sci.*, 572, 453-463.

Galvin, C. J., Dimitriou, M. D., Satija, S. K. and Genzer, J. (2014). "Swelling of polyelectrolyte and polyzwitterion brushes by humid vapors." *J. Am. Chem. Soc.*, 136, (36), 12737-12745.

Ganesh, B., Isloor, A. M. and Ismail, A. F. (2013). "Enhanced hydrophilicity and salt rejection study of graphene oxide-polysulfone mixed matrix membrane." *Desalination*, 313, 199-207.

Geckeler, K. E. and Volchek, K. (1996). "Removal of hazardous substances from water using ultrafiltration in conjunction with soluble polymers." *Environ. Sci. Technol.*, 30, (3), 725-734.

Geng, Z., Lin, Y., Yu, X., Shen, Q., Ma, L., Li, Z., Pan, N. and Wang, X. (2012). "Highly efficient dye adsorption and removal: a functional hybrid of reduced graphene oxide–Fe 3 O 4 nanoparticles as an easily regenerative adsorbent." *J. Mater. Chem.*, 22, (8), 3527-3535.

Ghanbari, M., Emadzadeh, D., Lau, W., Matsuura, T., Davoody, M. and Ismail, A. (2015). "Super hydrophilic TiO2/HNT nanocomposites as a new approach for fabrication of high performance thin film nanocomposite membranes for FO application." *Desalination*, 371, 104-114.

Gharabaghi, M., Irannajad, M. and Azadmehr, A. R. (2012). "Selective sulphide precipitation of heavy metals from acidic polymetallic aqueous solution by thioacetamide." *Ind. Eng. Chem. Res.*, 51, (2), 954-963.

Goh, K., Setiawan, L., Wei, L., Si, R., Fane, A. G., Wang, R. and Chen, Y. (2015). "Graphene oxide as effective selective barriers on a hollow fiber membrane for water treatment process." *J. Membr. Sci.*, 474, 244-253.

Gohari, R. J., Korminouri, F., Lau, W., Ismail, A., Matsuura, T., Chowdhury, M., Halakoo, E. and Gohari, M. J. (2015). "A novel super-hydrophilic PSf/HAO nanocomposite ultrafiltration membrane for efficient separation of oil/water emulsion." *Sep. Purif. Technol.*, 150, 13-20.

Gol, R. M., Bera, A., Banjo, S., Ganguly, B. and Jewrajka, S. K. (2014). "Effect of amine spacer of PEG on the properties, performance and antifouling behavior of poly(piperazineamide) thin film composite nanofiltration membranes prepared by in situ PEGylation approach." *J. Membr. Sci.*, 472, 154-166.

Gorgojo, P., Jimenez-Solomon, M. F. and Livingston, A. G. (2014). "Polyamide thin film composite membranes on cross-linked polyimide supports: Improvement of RO performance via activating solvent." *Desalination*, 344, 181-188.

Gottenbos, B., van der Mei, H. C., Klatter, F., Nieuwenhuis, P. and Busscher, H. J. (2002). "In vitro and in vivo antimicrobial activity of covalently coupled quaternary ammonium silane coatings on silicone rubber." *Biomaterials*, 23, (6), 1417-1423.

Graham, T. (1866). "On the absorption and dialytic separation of gases by colloid septa." *Philosophical transactions of the Royal Society of London*, 156, 399-439.

Grainger, S. and El-Sayed, M. (2010). "Biologically responsive hybrid biomaterials." *Artech House, Boston, MA, USA*, 171-190.

Günister, E., İşçi, S., Öztekin, N., Erim, F. B., Ece, Ö. I. and Güngör, N. (2006). "Effect of cationic surfactant adsorption on the rheological and surface properties of bentonite dispersions." *J. Coll. Inter. Sci.*, 303, (1), 137-141.

Guo, Y.-S., Mi, Y.-F., Ji, Y.-L., An, Q.-F. and Gao, C.-J. (2019). "One-Step Surface Grafting Method for Preparing Zwitterionic Nanofiltation Membrane via In Situ Introduction of Initiator in Interfacial Polymerization." *ACS Appl. Poly. Mater.*, 1, (5), 1022-1033.

Hadidi, M. and Zydney, A. L. (2014). "Fouling behavior of zwitterionic membranes: Impact of electrostatic and hydrophobic interactions." *J. Membr. Sci.*, 452, 97-103.

Han, G., Liu, Y., Zhang, L., Kan, E., Zhang, S., Tang, J. and Tang, W. (2014). "MnO 2 nanorods intercalating graphene oxide/polyaniline ternary composites for robust high-performance supercapacitors." *Sci. Rep.*, 4, 4824.

Han, Y., Xu, Z. and Gao, C. (2013). "Ultrathin graphene nanofiltration membrane for water purification." *Adv. Funct. Mater*, 23, (29), 3693-3700.

Hanaor, D., Michelazzi, M., Leonelli, C. and Sorrell, C. C. (2012). "The effects of carboxylic acids on the aqueous dispersion and electrophoretic deposition of ZrO 2." *J. Eur. Ceram. Soc.*, 32, (1), 235-244.

He, G., Zhao, J., Hu, S., Li, L., Li, Z., Li, Y., Li, Z., Wu, H., Yang, X. and Jiang, Z. (2014). "Functionalized carbon nanotube via distillation precipitation polymerization and its application in Nafion-based composite membranes." *ACS Appl. Mater. Interfaces*, 6, (17), 15291-15301.

He, G., Chang, C., Xu, M., Hu, S., Li, L., Zhao, J., Li, Z., Li, Z., Yin, Y. and Gang, M. (2015). "Tunable nanochannels along graphene oxide/polymer core–shell nanosheets to enhance proton conductivity." *Adv. Funct. Mater*, 25, (48), 7502-7511.

He, S., Zhang, F., Cheng, S. and Wang, W. (2016). "Synthesis of Sodium Acrylate and Acrylamide Copolymer/GO Hydrogels and Their Effective Adsorption for Pb2+ and Cd2+." *ACS. Sustain. Chem. Eng.*, 4, (7), 3948-3959.

He, Y., Hower, J., Chen, S., Bernards, M. T., Chang, Y. and Jiang, S. (2008). "Molecular simulation studies of protein interactions with zwitterionic phosphorylcholine self-assembled monolayers in the presence of water." *Langmuir*, 24, (18), 10358-10364.

He, Y., Liu, J., Han, G. and Chung, T.-S. (2018). "Novel thin-film composite nanofiltration membranes consisting of a zwitterionic co-polymer for selenium and arsenic removal." *J. Membr. Sci.*, 555, 299-306.

Hebbar, R. S., Isloor, A. M. and Ismail, A. (2014). "Preparation and evaluation of heavy metal rejection properties of polyetherimide/porous activated bentonite clay nanocomposite membrane." *RSC Advances*, 4, (88), 47240-47248.

Hebbar, R. S., Isloor, A. M., Ismail, A., Shilton, S. J., Obaid, A. and Fun, H.-K. (2015). "Probing the morphology and anti-organic fouling behaviour of a polyetherimide membrane modified with hydrophilic organic acids as additives." *New J. Chem.*, 39, (8), 6141-6150.

Hebbar, R. S., Isloor, A. M., Ananda, K. and Ismail, A. (2016). "Fabrication of polydopamine functionalized halloysite nanotube/polyetherimide membranes for heavy metal removal." *J. Mater. Chem. A*, 4, (3), 764-774.

Hebbar, R. S., Isloor, A. M., Ananda, K., Abdullah, M. S. and Ismail, A. (2017). "Fabrication of a novel hollow fiber membrane decorated with functionalized Fe 2 O 3 nanoparticles: towards sustainable water treatment and biofouling control." *New J. Chem.*, 41, (10), 4197-4211.

Hebbar, R. S., Isloor, A. M., Prabhu, B., Inamuddin, Asiri, A. M. and Ismail, A. F. (2018). "Removal of metal ions and humic acids through polyetherimide membrane with grafted bentonite clay." *Sci. Rep.*, 8, (1), 4665.

Hegazy, M. A., Abdallah, M., Awad, M. K. and Rezk, M. (2014). "Three novel di-quaternary ammonium salts as corrosion inhibitors for API X65 steel pipeline in acidic solution. Part I: Experimental results." *Corros. Sci.*, 81, 54-64.

Helin, H., Na, L., Linlin, W., Zhong, H., Guangxia, W., Zonghuan, Y., Xiangwei, L. and Lianyi, T. (2008). "Anti-fouling ultrafiltration membrane prepared from polysulfone-graft-methyl acrylate copolymers by UV-induced grafting method." *J. Environ. Sci*, 20, (5), 565-570.

Ho, W. W. and Sirkar, K. (1992). "Membrane Handbook Van Nostrand-Reinhold." *New York*,
Hoek, E. M. and Elimelech, M. (2003). "Cake-enhanced concentration polarization: a new fouling mechanism for salt-rejecting membranes." *Environ. Sci. Technol.*, 37, (24), 5581-5588.

Holmlin, R. E., Chen, X., Chapman, R. G., Takayama, S. and Whitesides, G. M. (2001). "Zwitterionic SAMs that resist nonspecific adsorption of protein from aqueous buffer." *Langmuir*, 17, (9), 2841-2850.

Hong, S. and Elimelech, M. (1997). "Chemical and physical aspects of natural organic matter (NOM) fouling of nanofiltration membranes." *J. Membr. Sci.*, 132, (2), 159-181.

Hu, M. and Mi, B. (2013). "Enabling graphene oxide nanosheets as water separation membranes." *Environmental Science and Technology*, 47, (8), 3715-3723.

Huang, H., Song, Z., Wei, N., Shi, L., Mao, Y., Ying, Y., Sun, L., Xu, Z. and Peng, X. (2013). "Ultrafast viscous water flow through nanostrand-channelled graphene oxide membranes." *Nat. Commun.*, 4, 2979.

Huang, T., Zhang, L., Chen, H. and Gao, C. (2015). "Sol–gel fabrication of a non-laminated graphene oxide membrane for oil/water separation." *J. Mater. Chem. A*, 3, (38), 19517-19524.

Hummer, G., Rasaiah, J. C. and Noworyta, J. P. (2001). "Water conduction through the hydrophobic channel of a carbon nanotube." *Nature*, 414, (6860), 188-190.

Humplik, T., Lee, J., O'hern, S., Fellman, B., Baig, M., Hassan, S., Atieh, M., Rahman, F., Laoui, T. and Karnik, R. (2011). "Nanostructured materials for water desalination." *Nanotechnology*, 22, (29), 292001.

Hurwitz, G., Guillen, G. R. and Hoek, E. M. (2010). "Probing polyamide membrane surface charge, zeta potential, wettability, and hydrophilicity with contact angle measurements." *J. Membr. Sci.*, 349, (1), 349-357.

Hwang, L.-L., Tseng, H.-H. and Chen, J.-C. (2011). "Fabrication of polyphenylsulfone/polyetherimide blend membranes for ultrafiltration applications: The effects of blending ratio on membrane properties and humic acid removal performance." *J. Membr. Sci.*, 384, (1), 72-81.

Hwang, S. K., Park, T. J., Kim, K. L., Cho, S. M., Jeong, B. J. and Park, C. (2014). "Organic one-transistor-type nonvolatile memory gated with thin ionic liquid-polymer film for low voltage operation." *ACS Appl. Mater. Interfaces*, 6, (22), 20179-20187.

Ibrahim, G. P. S., Isloor, A. M., Inamuddin, Asiri, A. M., Ismail, N., Ismail, A. F. and Ashraf, G. M. (2017). "Novel, one-step synthesis of zwitterionic polymer nanoparticles via distillation-precipitation polymerization and its application for dye removal membrane." *Sci. Rep.*, 7, (1), 15889.

Ibrahim, G. P. S., Isloor, A. M., Moslehyani, A. and Ismail, A. F. (2017). "Bio-inspired, fouling resistant, tannic acid functionalized halloysite nanotube reinforced polysulfone loose nanofiltration hollow fiber membranes for efficient dye and salt separation." *J. Water Process Eng.*, 20, 138-148.

Ibrahim, G. P. S., Isloor, A. M., Moslehyani, A. and Ismail, A. F. (2017). "Bio-inspired, fouling resistant, tannic acid functionalized halloysite nanotube reinforced polysulfone loose nanofiltration hollow fiber membranes for efficient dye and salt separation." *J. Water Process Eng.*, 20, (Supplement C), 138-148.

Ibrahim, G. P. S., Isloor, A. M., Yuliwati, E. and Ismail, A. F. (2019)."*Chapter 2 - Carbon-based nanocomposite membranes for water and wastewater purification*. Elsevier, Page 23-44.

Ibrahim, G. S., Isloor, A. M., Al Ahmed, A. and Lakshmi, B. (2016). "Fabrication and Characterization of Polysulfone-Zeolite ZSM-5 Mixed Matrix Membrane for Heavy Metal Ion Removal Application." *J. Appl. Mem. Sci. Tech.*, 18, (1), 25-37.

Ibrahim, G. S., Isloor, A. M., Asiri, A. M., Ismail, A., Kumar, R. and Ahamed, M. I. (2018). "Performance intensification of the polysulfone ultrafiltration membrane by blending with copolymer encompassing novel derivative of poly (styrene-co-maleic anhydride) for heavy metal removal from wastewater." *Chem. Eng. J.*, 353, 425-435.

Ibrahima, G. S., Isloora, A. M. and Farnoodb, R. (2019). "Fundamentals and basics of reverse osmosis." *Current Trends and Future Developments on (Bio-) Membranes: Reverse and Forward Osmosis: Principles, Applications, Advances*, 141.

Idris, A., Zain, N. M. and Noordin, M. (2007). "Synthesis, characterization and performance of asymmetric polyethersulfone (PES) ultrafiltration membranes with polyethylene glycol of different molecular weights as additives." *Desalination*, 207, (1-3), 324-339.

Ismail, A. F. (2013). "Polysulfone-chitosan blend ultrafiltration membranes: preparation, characterization, permeation and antifouling properties." *RSC Adv.*, 3, (21), 7855-7861.

Jain, P., Hung, H.-C., Lin, X., Ma, J., Zhang, P., Sun, F., Wu, K. and Jiang, S. (2017). "Poly(ectoine) Hydrogels Resist Nonspecific Protein Adsorption." *Langmuir*, 33, (42), 11264-11269.

Jang, J. and Lee, W. (1994). "Polyetherimide-modified high performance epoxy resin." *Polymer journal*, 26, (5), 513-525.

Janson, J.-C. (2012)."*Protein purification: principles, high resolution methods, and applications*. Pulisher name, John Wiley & Sons Place.

Jeong, B.-H., Hoek, E. M., Yan, Y., Subramani, A., Huang, X., Hurwitz, G., Ghosh, A. K. and Jawor, A. (2007). "Interfacial polymerization of thin film nanocomposites: a new concept for reverse osmosis membranes." *J. Membr. Sci.*, 294, (1), 1-7.

Ji, J., Dickson, J., Childs, R. and McCarry, B. (2000). "Mathematical model for the formation of thin-film composite membranes by interfacial polymerization: porous and dense films." *Macromolecules*, 33, (2), 624-633.

Ji, Y.-L., An, Q.-F., Zhao, Q., Sun, W.-D., Lee, K.-R., Chen, H.-L. and Gao, C.-J. (2012). "Novel composite nanofiltration membranes containing zwitterions with high permeate flux and improved anti-fouling performance." *J. Membr. Sci.*, 390, 243-253.

Ji, Y., An, Q., Zhao, Q., Chen, H. and Gao, C. (2011). "Preparation of novel positively charged copolymer membranes for nanofiltration." *J. Membr. Sci.*, 376, (1), 254-265.

Jia, T.-Z., Lu, J.-P., Cheng, X.-Y., Xia, Q.-C., Cao, X.-L., Wang, Y., Xing, W. and Sun, S.-P. (2019). "Surface enriched sulfonated polyarylene ether benzonitrile (SPEB) that enhances heavy metal removal from polyacrylonitrile (PAN) thin-film composite nanofiltration membranes." *J. Membr. Sci.*, 580, 214-223.

Jian, P., Yahui, H., Yang, W. and Linlin, L. (2006). "Preparation of polysulfone–Fe 3 O 4 composite ultrafiltration membrane and its behavior in magnetic field." *J. Membr. Sci.*, 284, (1), 9-16.

Jiang, J.-H., Zhu, L.-P., Zhang, H.-T., Zhu, B.-K. and Xu, Y.-Y. (2014). "Improved hydrodynamic permeability and antifouling properties of poly (vinylidene fluoride) membranes using polydopamine nanoparticles as additives." *J. Membr. Sci.*, 457, 73-81.

Jiang, M., Ye, K., Deng, J., Lin, J., Ye, W., Zhao, S. and Van der Bruggen, B. (2018). "Conventional ultrafiltration as effective strategy for dye/salt fractionation in textile wastewater treatment." *Environ. Sci. Technol.*, 52, (18), 10698-10708.

Jiang, S. and Cao, Z. (2010). "Ultralow-fouling, functionalizable, and hydrolyzable zwitterionic materials and their derivatives for biological applications." *Adv. Mater.*, 22, (9), 920-932.

Jiang, S. and Cao, Z. (2010). "Ultralow-fouling, functionalizable, and hydrolyzable zwitterionic materials and their derivatives for biological applications." *Adv. Mater.*, 22, (9), 920-932.

Jimbo, T., Higa, M., Minoura, N. and Tanioka, A. (1998). "Surface characterization of poly (acrylonitrile) membranes graft-polymerized with ionic monomers as revealed by ζ potential measurement." *Macromolecules*, 31, (4), 1277-1284.

Jin, J., Fu, L., Yang, H. and Ouyang, J. (2015). "Carbon hybridized halloysite nanotubes for high-performance hydrogen storage capacities." *Sci. Rep.*, 5, 12429.

Jin, X., Shan, J., Wang, C., Wei, J. and Tang, C. Y. (2012). "Rejection of pharmaceuticals by forward osmosis membranes." *J. Hazard. Mater.*, 227, 55-61.

Jiraratananon, R., Sungpet, A. and Luangsowan, P. (2000). "Performance evaluation of nanofiltration membranes for treatment of effluents containing reactive dye and salt." *Desalination*, 130, (2), 177-183.

Jones, E. R., Semsarilar, M., Blanazs, A. and Armes, S. P. (2012). "Efficient synthesis of amine-functional diblock copolymer nanoparticles via RAFT dispersion polymerization of benzyl methacrylate in alcoholic media." *Macromolecules*, 45, (12), 5091-5098.

Joo, M., Shin, J., Kim, J., You, J. B., Yoo, Y., Kwak, M. J., Oh, M. S. and Im, S. G. (2017). "One-step synthesis of cross-linked ionic polymer thin films in vapor phase and its application to an oil/water separation membrane." *J. Am. Chem. Soc.*, 139, (6), 2329-2337.

Joo, Y., Sim, J. H., Jeon, Y., Lee, S. U. and Sohn, D. (2013). "Opening and blocking the inner-pores of halloysite." *Chem. Commun.*, 49, (40), 4519-4521.

Joseph Elford, W. (1931). "A new series of graded collodion membranes suitable for general bacteriological use, especially in filterable virus studies." *The Journal of Pathology*, 34, (4), 505-521.

Joseph, S., Mashl, R. J., Jakobsson, E. and Aluru, N. (2003). "Electrolytic transport in modified carbon nanotubes." *Nano Lett.*, 3, (10), 1399-1403.

Joshi, M., Mukherjee, A. and Thakur, B. (2001). "Development of a new styrene copolymer membrane for recycling of polyester fibre dyeing effluent." *J. Membr. Sci.*, 189, (1), 23-40.

Junxia, Y., Mi, T., Xiaomei, S. and Buhai, L. (2007). "Poly (methacrylic acid) modified biomass for enhancement adsorption of Pb2+, Cd2+ and Cu2+." *J. Chem. Technol. Biotechnol.*, 82, (6), 558-565.

Kaiya, Y., Itoh, Y., Fujita, K. and Takizawa, S. (1996). "Study on fouling materials in the membrane treatment process for potable water." *Desalination*, 106, (1), 71-77.

Kalaiselvi, G., Maheswari, P., Mohan, D. and Balasubramanian, S. (2015). "Synthesis and characterization of poly 3-methyl 2-vinyl pyridinium nitrate incorporated polyvinylidine fluoride ultrafiltration membrane for metal ion removal." *Sep. Purif. Technol.*, 143, 105-114.

Kaleekkal, N. J., Radhakrishnan, R., Sunil, V., Kamalanathan, G., Sengupta, A. and Wickramasinghe, R. (2018). "Performance evaluation of novel nanostructured modified mesoporous silica/polyetherimide composite membranes for the treatment of oil/water emulsion." *Sep. Purif. Technol.*, 103, (1), 81-87.
Kan, L., Xu, Z. and Gao, C. (2010). "General avenue to individually dispersed graphene oxide-based two-dimensional molecular brushes by free radical polymerization." *Macromolecules*, 44, (3), 444-452.

Kan, L., Xu, Z. and Gao, C. (2011). "General avenue to individually dispersed graphene oxide-based two-dimensional molecular brushes by free radical polymerization." *Macromolecules*, 44, (3), 444-452.

Kang, G.-d. and Cao, Y.-m. (2012). "Development of antifouling reverse osmosis membranes for water treatment: a review." *Water research*, 46, (3), 584-600.

Kankara, R. S., S. Arockiaraj, and K. Prabhu. (2016). "Environmental sensitivity mapping and risk assessment for oil spill along the Chennai Coast in India." *Marine pollution bulletin*, 106, no. 1-2: 95-103.

Karan, S., Jiang, Z. and Livingston, A. G. (2015). "Sub–10 nm polyamide nanofilms with ultrafast solvent transport for molecular separation." *Science*, 348, (6241), 1347-1351.

Keating IV, J. J., Imbrogno, J. and Belfort, G. (2016). "Polymer brushes for membrane separations: a review." *ACS Appl. Mater. Interfaces*, 8, (42), 28383-28399.

Kedem, O. and Katchalsky, A. (1961). "A physical interpretation of the phenomenological coefficients of membrane permeability." *J. gen. phys.*, 45, (1), 143-179.

Kim, H. J., Lim, M.-Y., Jung, K. H., Kim, D.-G. and Lee, J.-C. (2015). "High-performance reverse osmosis nanocomposite membranes containing the mixture of carbon nanotubes and graphene oxides." *J. Mater. Chem. A*, 3, (13), 6798-6809.

Kim, K., Lee, K., Cho, K. and Park, C. (2002). "Surface modification of polysulfone ultrafiltration membrane by oxygen plasma treatment." *J. Membr. Sci.*, 199, (1), 135-145.

Kim, K., Kim, H., Lim, J. H. and Lee, S. J. (2016). "Development of a Desalination Membrane Bioinspired by Mangrove Roots for Spontaneous Filtration of Sodium Ions." *ACS nano*, 10, (12), 11428-11433.

Kim, S. H., Kwak, S.-Y. and Suzuki, T. (2005). "Positron annihilation spectroscopic evidence to demonstrate the flux-enhancement mechanism in morphology-controlled thin-film-composite (TFC) membrane." *Environ. Sci. Technol.*, 39, (6), 1764-1770.

Kitano, H., Imai, M., Sudo, K. and Ide, M. (2002). "Hydrogen-bonded network structure of water in aqueous solution of sulfobetaine polymers." *J. Phys. Chem. B*, 106, (43), 11391-11396.

Kolff, W., Berk, H., WELLE, N. M., Ley, A., Dijk, E. and Noordwijk, J. (1944). "The artificial kidney: a dialyser with a great area." *Acta Medica Scandinavica*, 117, (2), 121-134.

Kotov, N. A., Dékány, I. and Fendler, J. H. (1996). "Ultrathin graphite oxide–polyelectrolyte composites prepared by self-assembly: Transition between conductive and non-conductive states." *Adv. Mater.*, 8, (8), 637-641.

Koyuncu, I. (2002). "Reactive dye removal in dye/salt mixtures by nanofiltration membranes containing vinylsulphone dyes: effects of feed concentration and cross flow velocity." *Desalination*, 143, (3), 243-253.

Koyuncu, I. and Topacik, D. (2003). "Effects of operating conditions on the salt rejection of nanofiltration membranes in reactive dye/salt mixtures." *Sep. Purif. Technol.*, 33, (3), 283-294.

Koyuncu, I., Topacik, D. and Wiesner, M. R. (2004). "Factors influencing flux decline during nanofiltration of solutions containing dyes and salts." *Water Res.*, 38, (2), 432-440.

Krishnan, S., Ayothi, R., Hexemer, A., Finlay, J. A., Sohn, K. E., Perry, R., Ober, C. K., Kramer, E. J., Callow, M. E. and Callow, J. A. (2006). "Anti-biofouling properties of comblike block copolymers with amphiphilic side chains." *Langmuir*, 22, (11), 5075-5086.

Krishnan, S., Weinman, C. J. and Ober, C. K. (2008). "Advances in polymers for anti-biofouling surfaces." *J. Mater. Chem.*, 18, (29), 3405-3413.

Kumar, M. and Ulbricht, M. (2013). "Novel antifouling positively charged hybrid ultrafiltration membranes for protein separation based on blends of carboxylated carbon nanotubes and aminated poly (arylene ether sulfone)." *J. Membr. Sci.*, 448, 62-73.

Kumar, M., Gholamvand, Z., Morrissey, A., Nolan, K., Ulbricht, M. and Lawler, J. (2016). "Preparation and characterization of low fouling novel hybrid ultrafiltration membranes based on the blends of GO− TiO 2 nanocomposite and polysulfone for humic acid removal." *J. Membr. Sci.*, 506, 38-49.

Kumar, R., Ismail, A. F., Kassim, M. A. and Isloor, A. M. (2013). "Modification of PSf/PIAM membrane for improved desalination applications using Chitosan coagulation media." *Desalination*, 317, 108-115.

Kumar, R., Isloor, A. M. and Ismail, A. (2014). "Preparation and evaluation of heavy metal rejection properties of polysulfone/chitosan, polysulfone/N-succinyl chitosan and polysulfone/N-propylphosphonyl chitosan blend ultrafiltration membranes." *Desalination*, 350, 102-108.

Kumar, S., Isloor, A. M., Kumar, G. M. and Asiri, A. M. (2019). "nanohydroxyapatite Reinforced chitosan composite Hydrogel with tunable Mechanical and Biological properties for cartilage Regeneration." *Sci. Rep.*, 9, (1), 1-13.

Kuzmenko, D., Arkhangelsky, E., Belfer, S., Freger, V. and Gitis, V. (2005). "Chemical cleaning of UF membranes fouled by BSA." *Desalination*, 179, (1), 323-333.

Kwei, T. (1984). "The effect of hydrogen bonding on the glass transition temperatures of polymer mixtures." *Poly. Sci. C: Poly. Lett.*, 22, (6), 307-313.

Kwon, Y. N., Tang, C. Y. and Leckie, J. O. (2008). "Change of chemical composition and hydrogen bonding behavior due to chlorination of crosslinked polyamide membranes." *J. Appl. Polym. Sci.*, 108, (4), 2061-2066.

Labhsetwar, N., Doggali, P., Chankapure, P., Valechha, D., Lokhande, S., Watanabe, A., Rayalu, S., Haneda, H. and Mitsuhashi, T. (2009). "La 3.5 Ru 4.0 O 13 Perovskite type Catalyst for Carbon Monoxide and Hydrocarbon Oxidation." *Topics in Catalysis*, 52, (13-20), 1909.

Lai, G., Lau, W., Goh, P., Ismail, A., Yusof, N. and Tan, Y. (2016). "Graphene oxide incorporated thin film nanocomposite nanofiltration membrane for enhanced salt removal performance." *Desalination*, 387, 14-24.

Lai, G., Lau, W., Gray, S., Matsuura, T., Gohari, R. J., Subramanian, M., Lai, S., Ong, C., Ismail, A. and Emazadah, D. (2016). "A practical approach to synthesize polyamide thin film nanocomposite (TFN) membranes with improved separation properties for water/wastewater treatment." *J. Mater. Chem. A*, 4, (11), 4134-4144.

Lai, G., Yusob, M., Lau, W., Gohari, R. J., Emadzadeh, D., Ismail, A., Goh, P., Isloor, A. and Arzhandi, M. R.-D. (2017). "Novel mixed matrix membranes incorporated with dual-nanofillers for enhanced oil-water separation." *Sep. Purif. Technol.*, 178, 113-121.

Lai, G. S., Lau, W. J., Goh, P. S., Ismail, A. F., Tan, Y. H., Chong, C. Y., Krause-Rehberg, R. and Awad, S. (2018). "Tailor-made thin film nanocomposite membrane incorporated with graphene oxide using novel interfacial polymerization technique for enhanced water separation." *Chem. Eng. J.*, 344, 524-534.

Laine, J.-M., Hagstrom, J. P., Clark, M. M. and Mallevialle, J. (1989). "Effects of ultrafiltration membrane composition." *J. Am. Water Works Assoc.*, 61-67.

Lau, W., Gray, S., Matsuura, T., Emadzadeh, D., Chen, J. P. and Ismail, A. (2015). "A review on polyamide thin film nanocomposite (TFN) membranes: history, applications, challenges and approaches." *Water Res.*, 80, 306-324.

Lee, H., Dellatore, S. M., Miller, W. M. and Messersmith, P. B. (2007). "Mussel-inspired surface chemistry for multifunctional coatings." S*cience*, 318, (5849), 426-430.

Lee, J.-W., Choi, S.-P., Thiruvenkatachari, R., Shim, W.-G. and Moon, H. (2006). "Evaluation of the performance of adsorption and coagulation processes for the maximum removal of reactive dyes." *Dyes Pigm.*, 69, (3), 196-203.

Lei, L., Zhang, Q., Shi, S. and Zhu, S. (2017). "Highly porous poly (high internal phase emulsion) membranes with "open-cell" structure and CO2-switchable wettability used for controlled oil/water separation." *Langmuir*, 33, (43), 11936-11944.

Leng, C., Huang, H., Zhang, K., Hung, H.-C., Xu, Y., Li, Y., Jiang, S. and Chen, Z. (2018). "Effect of Surface Hydration on Antifouling Properties of Mixed Charged Polymers." *Langmuir*, 7, (22), 6538-45.

Levis, S. and Deasy, P. (2002). "Characterisation of halloysite for use as a microtubular drug delivery system." *Inter. J. Pharmaceut.*, 243, (1), 125-134.

Li, B., Zhou, F., Huang, K., Wang, Y., Mei, S., Zhou, Y. and Jing, T. (2016). "Highly efficient removal of lead and cadmium during wastewater irrigation using a polyethylenimine-grafted gelatin sponge." *Sci. Rep.*, 6, 33573.

Li, D., Müller, M. B., Gilje, S., Kaner, R. B. and Wallace, G. G. (2008). "Processable aqueous dispersions of graphene nanosheets." *Nat. Nanotechnol.*, 3, (2), 101-105.

Li, T., Jiang, Z., Xu, C., Liu, B., Liu, G., Wang, P., Li, X., Chen, W., Ning, C. and Wang, Z. (2017). "Effect of pore structure on shale oil accumulation in the lower third member of the Shahejie formation, Zhanhua Sag, eastern China: Evidence from gas adsorption and nuclear magnetic resonance." *Marine and Petroleum Geology*, 88, 932-949.

Li, Y., Su, Y., Zhao, X., He, X., Zhang, R., Zhao, J., Fan, X. and Jiang, Z. (2014). "Antifouling, high-flux nanofiltration membranes enabled by dual functional polydopamine." *ACS Appl. Mater. Interfaces*, 6, (8), 5548-5557.

Li, Y., Song, Y., Zhang, X., Wu, X., Wang, F. and Wang, Z. (2015). "Programmable Polymer Memory Device Based on Hydrophilic Polythiophene and Poly (ionic liquid) Electrolyte." *Macromol. Chem. Phys.*, 216, (1), 113-121.

Liao, Y., Farrell, T. P., Guillen, G. R., Li, M., Temple, J. A., Li, X.-G., Hoek, E. M. and Kaner, R. B. (2014). "Highly dispersible polypyrrole nanospheres for advanced nanocomposite ultrafiltration membranes." *Mater. Horiz.*, 1, (1), 58-64.

Lin, J., Tang, C. Y., Ye, W., Sun, S.-P., Hamdan, S. H., Volodin, A., Van Haesendonck, C., Sotto, A., Luis, P. and Van der Bruggen, B. (2015). "Unraveling flux behavior of superhydrophilic loose nanofiltration membranes during textile wastewater treatment." *J. Membr. Sci.*, 493, 690-702.

Lin, J., Ye, W., Zeng, H., Yang, H., Shen, J., Darvishmanesh, S., Luis, P., Sotto, A. and Van der Bruggen, B. (2015). "Fractionation of direct dyes and salts in aqueous solution using loose nanofiltration membranes." *J. Membr. Sci.*, 477, 183-193.

Lin, J., Ye, W., Baltaru, M.-C., Tang, Y. P., Bernstein, N. J., Gao, P., Balta, S., Vlad, M., Volodin, A. and Sotto, A. (2016). "Tight ultrafiltration membranes for enhanced separation of dyes and Na2SO4 during textile wastewater treatment." *J. Membr. Sci.*, 514, 217-228.

Lin, J., Ye, W., Baltaru, M.-C., Tang, Y. P., Bernstein, N. J., Gao, P., Balta, S., Vlad, M., Volodin, A. and Sotto, A. (2016). "Tight ultrafiltration membranes for enhanced separation of dyes and Na 2 SO 4 during textile wastewater treatment." *J. Membr. Sci.*, 514, 217-228.

Lin, J., Liang, H., Jia, H., Chen, S., Guo, J., Qi, J., Qu, C., Cao, J., Fei, W. and Feng, J. (2017). "In situ encapsulated Fe 3 O 4 nanosheet arrays with graphene layers as an anode for high-performance asymmetric supercapacitors." *J. Mater. Chem. A*, 5, (47), 24594-24601.

Lin, S. H. and Peng, C. F. (1994). "Treatment of textile wastewater by electrochemical method." *Water Res.*, 28, (2), 277-282.

Lin, Y., Jin, J. and Song, M. (2011). "Preparation and characterisation of covalent polymer functionalized graphene oxide." *J. Mater. Chem.*, 21, (10), 3455-3461.

Liu, C., Lee, J., Ma, J. and Elimelech, M. (2017). "Antifouling thin-film composite membranes by controlled architecture of zwitterionic polymer brush layer." *Environ. Sci. Technol.*, 51, (4), 2161-2169.

Liu, C., Mao, H., Zheng, J. and Zhang, S. (2017). "In situ surface crosslinked tight ultrafiltration membrane prepared by one-step chemical reaction-involved phase inversion process between activated PAEK-COOH and PEI." *J. Membr. Sci.*, (538), 58-67.

Liu, C., Mao, H., Zheng, J. and Zhang, S. (2017). "Tight ultrafiltration membrane: Preparation and characterization of thermally resistant carboxylated cardo poly (arylene ether ketone) s (PAEK-COOH) tight ultrafiltration membrane for dye removal." *J. Membr. Sci.*, 530, 1-10.

Liu, C., Mao, H., Zheng, J. and Zhang, S. (2017). "In situ surface crosslinked tight ultrafiltration membrane prepared by one-step chemical reaction-involved phase inversion process between activated PAEK-COOH and PEI." *J. Membr. Sci.*, 538, 58-67.

Liu, F., Chung, S., Oh, G. and Seo, T. S. (2012). "Three-dimensional graphene oxide nanostructure for fast and efficient water-soluble dye removal." *ACS Appl. Mater. Interfaces*, 4, (2), 922-927.

Liu, G., Yang, X. and Wang, Y. (2007). "Preparation of monodisperse hydrophilic polymer microspheres with N, N′-methylenediacrylamide as crosslinker by distillation precipitation polymerization." *Poly. Inter.*, 56, (7), 905-913.

Liu, J., Tang, J. and Gooding, J. J. (2012). "Strategies for chemical modification of graphene and applications of chemically modified graphene." *J. Mater. Chem.*, 22, (25), 12435-12452.

Liu, J., Chen, J. and Huang, L. (2015). "Heavy metal removal from MSS fly ash by thermal and chlorination treatments." *Sci. Rep.*, 5, 17270.

Liu, J., Yang, K., Qu, Y., Li, S., Wu, Q., Liang, Z., Zhang, L. and Zhang, Y. (2015). "An efficient approach to prepare boronate core–shell polymer nanoparticles for glycoprotein recognition via combined distillation precipitation polymerization and RAFT media precipitation polymerization." *Chem. Commun.*, 51, (18), 3896-3898.

Liu, J. (2016). "Interfacing zwitterionic liposomes with inorganic nanomaterials: surface forces, membrane integrity, and applications." *Langmuir*, 32, (18), 4393-4404.

Liu, J., Yang, K., Shao, W., Li, S., Wu, Q., Zhang, S., Qu, Y., Zhang, L. and Zhang, Y. (2016). "Synthesis of zwitterionic polymer particles via combined distillation precipitation polymerization and click chemistry for highly efficient enrichment of glycopeptide." *ACS Appl. Mater. Interfaces*, 8, (34), 22018-22024.

Liu, K., Li, H., Wang, Y., Gou, X. and Duan, Y. (2015). "Adsorption and removal of rhodamine B from aqueous solution by tannic acid functionalized graphene." *Colloid Surface A*, 477, 35-41.

Liu, R., Zhang, B., Mei, D., Zhang, H. and Liu, J. (2011). "Adsorption of methyl violet from aqueous solution by halloysite nanotubes." *Desalination*, 268, (1), 111-116.

Liu, S., Zeng, T. H., Hofmann, M., Burcombe, E., Wei, J., Jiang, R., Kong, J. and Chen, Y. (2011). "Antibacterial activity of graphite, graphite oxide, graphene oxide, and reduced graphene oxide: membrane and oxidative stress." *ACS Nano*, 5, (9), 6971-6980.

Liu, S. Q., Yang, C., Huang, Y., Ding, X., Li, Y., Fan, W. M., Hedrick, J. L. and Yang, Y. Y. (2012). "Antimicrobial and antifouling hydrogels formed in situ from polycarbonate and poly (ethylene glycol) via Michael addition." *Adv. Mater.*, 24, (48), 6484-6489.

Liu, T.-Y., Yuan, H.-G., Li, Q., Tang, Y.-H., Zhang, Q., Qian, W., Van der Bruggen, B. and Wang, X. (2015). "Ion-responsive channels of zwitterion-carbon nanotube membrane for rapid water permeation and ultrahigh mono-/multivalent ion selectivity." *ACS Nano*, 9, (7), 7488-7496.

Liu, Y., Yue, X., Zhang, S., Ren, J., Yang, L., Wang, Q. and Wang, G. (2012). "Synthesis of sulfonated polyphenylsulfone as candidates for antifouling ultrafiltration membrane." *Sep. Purif. Technol.*, 98, 298-307.

Liu, Y. L., Chang, Y., Chang, Y. H. and Shih, Y. J. (2010). "Preparation of amphiphilic polymer-functionalized carbon nanotubes for low-protein-adsorption surfaces and protein-resistant membranes." *ACS Appl. Mater. Interfaces*, 2, (12), 3642-3647.

Loeb, S. and Sourirajan, S. (1962)."*Sea water demineralization by means of an osmotic membrane,* Chapter 9, pp 117-132, *ACS Publications*,

Lowe, A. B. and McCormick, C. L. (2002). "Synthesis and solution properties of zwitterionic polymers." *Chem. Rev.*, 102, (11), 4177-4190.

Lowell, S., Shields, J. E., Thomas, M. A. and Thommes, M. (2012)."*Characterization of porous solids and powders: surface area, pore size and density*. Pulisher name, Springer Science & Business Media Place.

Luo, J. and Wan, Y. (2011). "Effect of highly concentrated salt on retention of organic solutes by nanofiltration polymeric membranes." *J. Membr. Sci.*, 372, (1), 145-153.

Lv, Y., Yu, L., Huang, H., Feng, Y., Chen, D. and Xie, X. (2012). "Application of the soluble salt-assisted route to scalable synthesis of ZnO nanopowder with repeated photocatalytic activity." *Nanotechnology*, 23, (6), 065402.

Ma, N., Wei, J., Liao, R. and Tang, C. Y. (2012). "Zeolite-polyamide thin film nanocomposite membranes: towards enhanced performance for forward osmosis." *J. Membr. Sci.*, 405, 149-157.

Ma, R., Ji, Y.-L., Weng, X.-D., An, Q.-F. and Gao, C.-J. (2016). "High-flux and fouling-resistant reverse osmosis membrane prepared with incorporating zwitterionic amine monomers via interfacial polymerization." *Desalination*, 381, 100-110.

Machida, M., Mochimaru, T. and Tatsumoto, H. (2006). "Lead (II) adsorption onto the graphene layer of carbonaceous materials in aqueous solution." *Carbon*, 44, (13), 2681-2688.

Majumdar, P., Lee, E., Gubbins, N., Stafslien, S. J., Daniels, J., Thorson, C. J. and Chisholm, B. J. (2009). "Synthesis and antimicrobial activity of quaternary ammonium-functionalized POSS (Q-POSS) and polysiloxane coatings containing Q-POSS." *Polymer*, 50, (5), 1124-1133.

Manawi, Y., Kochkodan, V., Hussein, M. A., Khaleel, M. A., Khraisheh, M. and Hilal, N. (2016). "Can carbon-based nanomaterials revolutionize membrane fabrication for water treatment and desalination?" *Desalination*, 391, 69-88.

Mansourpanah, Y. and Momeni Habili, E. (2013). "Preparation and modification of thin film PA membranes with improved antifouling property using acrylic acid and UV irradiation." *J. Membr. Sci.*, 430, 158-166.

Mansourpanah, Y., Shahebrahimi, H. and Kolvari, E. (2015). "PEG-modified GO nanosheets, a desired additive to increase the rejection and antifouling characteristics of polyamide thin layer membranes." *Chem. Eng. Res. Des.*, 104, 530-540.

Marcano, D. C., Kosynkin, D. V., Berlin, J. M., Sinitskii, A., Sun, Z., Slesarev, A., Alemany, L. B., Lu, W. and Tour, J. M. (2010). "Improved synthesis of graphene oxide." *ACS Nano*, 4, (8), 4806-4814.

Marcucci, M., Ciardelli, G., Matteucci, A., Ranieri, L. and Russo, M. (2002). "Experimental campaigns on textile wastewater for reuse by means of different membrane processes." *Desalination*, 149, (1-3), 137-143.

Marcus, Y. (1988). "Ionic radii in aqueous solutions." *Chem. Rev.*, 88, (8), 1475-1498.

Marcus, Y. (1991). "Thermodynamics of solvation of ions. Part 5.—Gibbs free energy of hydration at 298.15 K." *Journal of the Chemical Society, Faraday Transactions*, 87, (18), 2995-2999.

Mariano, A. J., Kourafalou, V. H., Srinivasan, A., Kang, H., Halliwell, G. R., Ryan, E. H., & Roffer, M. (2011). On the modeling of the 2010 Gulf of Mexico oil spill. *Dynamics of Atmospheres and Oceans*, 52, (1-2), 322-340.

Mariën, H., Bellings, L., Hermans, S. and Vankelecom, I. F. J. (2016). "Sustainable Process for the Preparation of High-Performance Thin-Film Composite Membranes using Ionic Liquids as the Reaction Medium." *ChemSusChem*, 9, (10), 1101-1111.

Matsuyama, H., Maki, T., Teramoto, M. and Kobayashi, K. (2003). "Effect of PVP additive on porous polysulfone membrane formation by immersion precipitation method." *Sep. Sci. Technol.*, 38, (14), 3449-3458.

Matthiasson, E. and Sivik, B. (1980). "Concentration polarization and fouling." *Desalination*, 35, 59-103.

Mauter, M. S., Wang, Y., Okemgbo, K. C., Osuji, C. O., Giannelis, E. P. and Elimelech, M. (2011). "Antifouling ultrafiltration membranes via post-fabrication grafting of biocidal nanomaterials." *ACS Appl. Mater. Interfaces*, 3, (8), 2861-2868.

Mbareck, C., Nguyen, Q. T., Alaoui, O. T. and Barillier, D. (2009). "Elaboration, characterization and application of polysulfone and polyacrylic acid blends as ultrafiltration membranes for removal of some heavy metals from water." *J. Hazard. Mater.*, 171, (1), 93-101.

McBain, J. and Kistler, S. (1931). "Ultrafiltration as a test for colloidal constituents in aqueous and non-aqueous systems." *J. of Physical Chemistry*, 35, (1), 130-136.

McCloskey, B. D., Park, H. B., Ju, H., Rowe, B. W., Miller, D. J., Chun, B. J., Kin, K. and Freeman, B. D. (2010). "Influence of polydopamine deposition conditions on pure water flux and foulant adhesion resistance of reverse osmosis, ultrafiltration, and microfiltration membranes." *Polymer*, 51, (15), 3472-3485.

McCloskey, B. D., Park, H. B., Ju, H., Rowe, B. W., Miller, D. J. and Freeman, B. D. (2012). "A bioinspired fouling-resistant surface modification for water purification membranes." *J. Membr. Sci.*, 413, 82-90.

McKelvey, S. A. and Koros, W. J. (1996). "Phase separation, vitrification, and the manifestation of macrovoids in polymeric asymmetric membranes." *J. Membr. Sci.*, 112, (1), 29-39.

McMaster, L. and Ahmann, F. F. (1928). "Action of thionyl chloride on organic acids." *J. Am. Chem. Soc.*, 50, (1), 145-149.

McVerry, B. T., Temple, J. A., Huang, X., Marsh, K. L., Hoek, E. M. and Kaner, R. B. (2013). "Fabrication of low-fouling ultrafiltration membranes using a hydrophilic, self-doping polyaniline additive." *Chem Mater.*, 25, (18), 3597-3602.

Mehdipour, S., Vatanpour, V. and Kariminia, H.-R. (2015). "Influence of ion interaction on lead removal by a polyamide nanofiltration membrane." *Desalination*, 362, 84-92.

Mehiguene, K., Garba, Y., Taha, S., Gondrexon, N. and Dorange, G. (1999). "Influence of operating conditions on the retention of copper and cadmium in aqueous solutions by nanofiltration: experimental results and modelling." *Sep. Purif. Technol.*, 15, (2), 181-187.

Membranes, H. F. T. F. N. (2013). "Based on Metal-Organic Frameworks for Organic Solvent Nanofiltration Sorribas, Sara; Gorgojo, Patricia; Tellez, Carlos; Coronas, Joaquin; Livingston, Andrew G." *J. Am. Chem. Soc.*, 135, (40), 15201-15208.

Meng, L., Fu, C. and Lu, Q. (2009). "Advanced technology for functionalization of carbon nanotubes." *Prog. Nat. Sci-Mater.*, 19, (7), 801-810.

Merle, G., Wessling, M. and Nijmeijer, K. (2011). "Anion exchange membranes for alkaline fuel cells: A review." *J. Membr. Sci.*, 377, (1-2), 1-35.

Mi, F.-L., Wu, Y.-B., Shyu, S.-S., Chao, A.-C., Lai, J.-Y. and Su, C.-C. (2003). "Asymmetric chitosan membranes prepared by dry/wet phase separation: a new type of wound dressing for controlled antibacterial release." *J. Membr. Sci.*, 212, (1), 237-254.

Mi, L., Giarmarco, M. M., Shao, Q. and Jiang, S. (2012). "Divalent cation-mediated polysaccharide interactions with zwitterionic surfaces." *Biomaterials*, 33, (7), 2001-2006.

Mi, L. and Jiang, S. (2014). "Integrated antimicrobial and nonfouling zwitterionic polymers." *Angew. Chem. Int. Ed.*, 53, (7), 1746-1754.

Misdan, N., Lau, W., Ismail, A. and Matsuura, T. (2013). "Formation of thin film composite nanofiltration membrane: effect of polysulfone substrate characteristics." *Desalination*, 329, 9-18.

Miyoshi, H. (1999). "Donnan dialysis with ion-exchange membranes. III. Diffusion coefficients using ions of different valence." *Sep. Sci. Technol.*, 34, (2), 231-241.

Mohammad, A. W., Teow, Y., Ang, W., Chung, Y., Oatley-Radcliffe, D. and Hilal, N. (2015). "Nanofiltration membranes review: Recent advances and future prospects." *Desalination*, 356, 226-254.

Mohammadi Ghaleni, M., Al Balushi, A., Kaviani, S., Tavakoli, E., Bavarian, M. and Nejati, S. (2018). "Fabrication of Janus Membranes for Desalination of Oil-Contaminated Saline Water." *ACS Appl. Mater. Interfaces*, 10, (51), 44871-44879.

Moideen K, I., Isloor, A. M., Garudachari, B. and Ismail, A. (2016). "The effect of glycine betaine additive on the PPSU/PSF ultrafiltration membrane performance." *Desalin. Water Treat.*, 1-11.

Moideen K, I., Isloor, A. M., Garudachari, B. and Ismail, A. (2016). "The effect of glycine betaine additive on the PPSU/PSF ultrafiltration membrane performance." *Desalin. Water Treat.*, 57, (52), 24788-24798.

Moideen K, I., Isloor, A. M., Ismail, A., Obaid, A. and Fun, H.-K. (2016). "Fabrication and characterization of new PSF/PPSU UF blend membrane for heavy metal rejection." *Desalin. Water Treat.*, 57, (42), 19810-19819.

Mollahosseini, A. and Rahimpour, A. (2013). "A new concept in polymeric thin-film composite nanofiltration membranes with antibacterial properties." *Biofouling*, 29, (5), 537-548.

Mondal, M., Dutta, M. and De, S. (2017). "A novel ultrafiltration grade nickel iron oxide doped hollow fiber mixed matrix membrane: Spinning, characterization and application in heavy metal removal." *Sep. Purif. Technol.*, 188, 155-166.

Mondal, S., Ouni, H., Dhahbi, M. and De, S. (2012). "Kinetic modeling for dye removal using polyelectrolyte enhanced ultrafiltration." *J. Hazard Mater.*, 229, 381-389.

Mondini, S., Leonzino, M., Drago, C., Ferretti, A. M., Usseglio, S., Maggioni, D., Tornese, P., Chini, B. and Ponti, A. (2015). "Zwitterion-Coated Iron Oxide Nanoparticles: Surface Chemistry and Intracellular Uptake by Hepatocarcinoma (HepG2) Cells." *Langmuir*, 31, (26), 7381-7390.

Mukherjee, M. and De, S. (2015). "Reduction of microbial contamination from drinking water using an iron oxide nanoparticle-impregnated ultrafiltration mixed matrix membrane: preparation, characterization and antimicrobial properties." *Environ. Sci. Water Res. Technol.*, 1, (2), 204-217.

Mukherjee, M., Panda, S. R. and De, S. (2017). "Adhesion resistant chitosan coated iron oxide polyacrylonitrile mixed matrix membrane for disinfection of surface water." *J. Chem. Technol. Biotechnol.*, 92, (2), 408-419.

Mulder, J. (2012)."*Basic principles of membrane technology*. Pulisher name, Springer Science & Business Media Place.

Munari, S., Bottino, A., Capannelli, G., Moretti, P. and Bon, P. P. (1988). "Preparation and characterization of polysulfone-polyvinylpyrrolidone based membranes." *Desalination*, 70, (1-3), 265-275.

Nabe, A., Staude, E. and Belfort, G. (1997). "Surface modification of polysulfone ultrafiltration membranes and fouling by BSA solutions." *J. Membr. Sci.*, 133, (1), 57-72.

Nayak, M. C., Isloor, A. M., Moslehyani, A. and Ismail, A. F. (2017). "Preparation and characterization of PPSU membranes with BiOCl nanowafers loaded on activated charcoal for oil in water separation." *J. Taiwan Inst. Chem. Eng.*, 77, 293-301.

Nernst, W. (1888). "Zur kinetik der in lösung befindlichen körper." *Z. phys. Chem*, 2, (9), 613-679.

Ng, L. Y., Mohammad, A. W., Leo, C. P. and Hilal, N. (2013). "Polymeric membranes incorporated with metal/metal oxide nanoparticles: a comprehensive review." *Desalination*, 308, 15-33.

Nguyen, T. C., Loganathan, P., Nguyen, T. V., Vigneswaran, S., Kandasamy, J. and Naidu, R. (2015). "Simultaneous adsorption of Cd, Cr, Cu, Pb, and Zn by an iron-coated Australian zeolite in batch and fixed-bed column studies." *Chem. Eng. J.*, 270, 393-404.

Nightingale Jr, E. (1959). "Phenomenological theory of ion solvation. Effective radii of hydrated ions." *J. Phys. Chem.*, 63, (9), 1381-1387.

Nishimura, S., Kohgo, O., Kurita, K. and Kuzuhara, H. (1991). "Chemospecific manipulations of a rigid polysaccharide: syntheses of novel chitosan derivatives with excellent solubility in common organic solvents by regioselective chemical modifications." *Macromolecules*, 24, (17), 4745-4748.

Nollet, J.-A. (1752). "Recherches sur les Causes du Bouillonnement des Liquides." *Histoire de l'Academie Royale des Sciences, Paris Annee*, 1748, (57), 1752.

Nunes, S. P. and Peinemann, K.-V. (2001)."*Membrane technology*. Pulisher name, Wiley Online Library Place.

Ong, C., Goh, P., Lau, W., Misdan, N. and Ismail, A. (2016). "Nanomaterials for biofouling and scaling mitigation of thin film composite membrane: A review." *Desalination*, 393, 2-15.

Ong, C. S., Goh, P., Lau, W., Misdan, N. and Ismail, A. F. (2016). "Nanomaterials for biofouling and scaling mitigation of thin film composite membrane: A review." *Desalination*, 393, 2-15.

Ong, Y. K., Li, F. Y., Sun, S.-P., Zhao, B.-W., Liang, C.-Z. and Chung, T.-S. (2014). "Nanofiltration hollow fiber membranes for textile wastewater treatment: Lab-scale and pilot-scale studies." *Chem. Eng. Sci.*, 114, 51-57.

Owoseni, O., Nyankson, E., Zhang, Y., Adams, S. J., He, J., McPherson, G. L., Bose, A., Gupta, R. B. and John, V. T. (2014). "Release of surfactant cargo from interfacially-active halloysite clay nanotubes for oil spill remediation." *Langmuir,* 30, (45), 13533-13541.

Pal, A., Das, D., Sarkar, A. K., Ghorai, S., Das, R. and Pal, S. (2015). "Synthesis of glycogen and poly (acrylic acid)-based graft copolymers via ATRP and its application for selective removal of Pb 2+ ions from aqueous solution." *Eur. Polym. J.*, 66, 33-46.

Pala, A. and Tokat, E. (2002). "Color removal from cotton textile industry wastewater in an activated sludge system with various additives." *Water Res.*, 36, (11), 2920-2925.

Pan, L., Wang, H., Wu, C., Liao, C. and Li, L. (2015). "Tannic-Acid-Coated Polypropylene Membrane as a Separator for Lithium-Ion Batteries." *ACS Appl. Mater. Interfaces*, 7, (29), 16003-16010.

Panda, S. R., Mukherjee, M. and De, S. (2015). "Preparation, characterization and humic acid removal capacity of chitosan coated iron-oxide-polyacrylonitrile mixed matrix membrane." *J. Water Process Eng.*, 6, 93-104.

Pandey, R. P., Thakur, A. K. and Shahi, V. K. (2014). "Sulfonated polyimide/acid-functionalized graphene oxide composite polymer electrolyte membranes with improved proton conductivity and water-retention properties." *ACS Appl. Mater. Interfaces*, 6, (19), 16993-17002.

Parvez, M., Salam, M., Haraguchi, N. and Itsuno, S. (2012). "Synthesis of chiral ionic polymers containing quaternary ammonium sulfonate structure and their catalytic activity in asymmetric alkylation." *J. Chin. Chem. Soc.*, 59, (7), 815-821.

Peeva, L. and Livingston, A. (2019)."*Nanofiltration in the Pharmaceutical and Biopharmaceutical Technology*. Elsevier, 97-121.

Pereira, V. R., Isloor, A. M., Bhat, U. K. and Ismail, A. (2014). "Preparation and antifouling properties of PVDF ultrafiltration membranes with polyaniline (PANI) nanofibers and hydrolysed PSMA (H-PSMA) as additives." *Desalination,* 351, 220-227.

Pereira, V. R., Isloor, A. M., Al Ahmed, A. and Ismail, A. (2015). "Preparation, characterization and the effect of PANI coated TiO 2 nanocomposites on the performance of polysulfone ultrafiltration membranes." *New J. Chem.*, 39, (1), 703-712.

Pereira, V. R., Isloor, A. M., Zulhairun, A., Subramaniam, M., Lau, W. and Ismail, A. (2016). "Preparation of polysulfone-based PANI–TiO 2 nanocomposite hollow fiber membranes for industrial dye rejection applications." *RSc Adv.*, 6, (102), 99764-99773.

Peters, C. J., Young, R. J. and Perry, R. (1980). "Factors influencing the formation of haloforms in the chlorination of humic materials." *Environ. Sci. Technol.*, 14, (11), 1391-1395.

Petersen, R. J. (1993). "Composite reverse osmosis and nanofiltration membranes." *J. Membr. Sci.*, 83, (1), 81-150.

Petrinić, I., Andersen, N. P. R., Šostar-Turk, S. and Le Marechal, A. M. (2007). "The removal of reactive dye printing compounds using nanofiltration." *Dyes Pigm.*, 74, (3), 512-518.

Phillip, W. A., Yong, J. S. and Elimelech, M. (2010). "Reverse draw solute permeation in forward osmosis: modeling and experiments." *Environ. Sci. Technol.*, 44, (13), 5170-5176.

Prime, K. L. and Whitesides, G. M. (1993). "Adsorption of proteins onto surfaces containing end-attached oligo (ethylene oxide): a model system using self-assembled monolayers." *J. Am. Chem. Soc.*, 115, (23), 10714-10721.

Purkait, M., DasGupta, S. and De, S. (2004). "Removal of dye from wastewater using micellar-enhanced ultrafiltration and recovery of surfactant." *Sep. Purif. Technol.*, 37, (1), 81-92.

Purkait, M. K., & Singh, R. (2018). Membrane Technology in Separation Science. CRC Press.

Qi, Y., Zhu, L., Shen, X., Sotto, A., Gao, C. and Shen, J. (2019). "Polythyleneimine-modified original positive charged nanofiltration membrane: Removal of heavy metal ions and dyes." *Sep. Purif. Technol.*, 222, 117-124.

Qiu, W. and Zheng, Y. (2009). "Removal of lead, copper, nickel, cobalt, and zinc from water by a cancrinite-type zeolite synthesized from fly ash." *Chem. Eng. J.*, 145, (3), 483-488.

Qu, P., Tang, H., Gao, Y., Zhang, L. and Wang, S. (2010). "Polyethersulfone composite membrane blended with cellulose fibrils." *BioResources*, 5, (4), 2323-2336.

Qu, Y., Liu, J., Yang, K., Liang, Z., Zhang, L. and Zhang, Y. (2012). "Boronic acid functionalized core–shell polymer nanoparticles prepared by distillation precipitation polymerization for glycopeptide enrichment." *Chem. Eur. J.*, 18, (29), 9056-9062.

Quintanilla, V. A. Y. (2010)."*Rejection of emerging organic contaminants by nanofiltration and reverse osmosis membranes: effects of fouling, modelling and water reuse*. Pulisher name, CRC Press/Balkema Place.

Rafatullah, M., Sulaiman, O., Hashim, R. and Ahmad, A. (2010). "Adsorption of methylene blue on low-cost adsorbents: a review." *J. Hazard. Mater.*, 177, (1), 70-80.

Rana, D. and Matsuura, T. (2010). "Surface Modifications for Antifouling Membranes." *Chem. Rev.*, 110, (4), 2448-2471.

Rechendorff, K., Hovgaard, M. B., Foss, M., Zhdanov, V. and Besenbacher, F. (2006). "Enhancement of protein adsorption induced by surface roughness." *Langmuir*, 22, (26), 10885-10888.

Reid, C. and Breton, E. (1959). "Water and ion flow across cellulosic membranes." *J. Appl. Polym. Sci.*, 1, (2), 133-143.

Reinsch, V. E., Greenberg, A. R., Kelley, S. S., Peterson, R. and Bond, L. J. (2000). "A new technique for the simultaneous, real-time measurement of membrane compaction and performance during exposure to high-pressure gas." *J. Membr. Sci.*, 171, (2), 217-228.

Rijs, A. M., Ohanessian, G., Oomens, J., Meijer, G., Von Helden, G. and Compagnon, I. (2010). "Internal proton transfer leading to stable zwitterionic structures in a neutral isolated peptide." *Angew. Chem. Int. Ed.*, 49, (13), 2332-2335.

Riley, R., Lonsdale, H., Lyons, C. and Merten, U. (1967). "Preparation of ultrathin reverse osmosis membranes and the attainment of theoretical salt rejection." *J. Appl. Poly. Sci.*, 11, (11), 2143-2158.

Rohani, M. M. and Zydney, A. L. (2012). "Protein transport through zwitterionic ultrafiltration membranes." *J. Membr. Sci.*, 397, 1-8.

Romack, T., Maury, E. and DeSimone, J. M. (1995). "Precipitation polymerization of acrylic acid in supercritical carbon dioxide." *Macromolecules*, 28, (4), 912-915.

Rosberg, R. (1997). "Ultrafiltration (new technology), a viable cost-saving pretreatment for reverse osmosis and nanofiltration—a new approach to reduce costs." *Desalination*, 110, (1), 107-113.

Russell, V. A., Evans, C. C., Li, W. and Ward, M. D. (1997). "Nanoporous molecular sandwiches: pillared two-dimensional hydrogen-bonded networks with adjustable porosity." *Science*, 276, (5312), 575-579.

Safarpour, M., Vatanpour, V., Khataee, A. and Esmaeili, M. (2015). "Development of a novel high flux and fouling-resistant thin film composite nanofiltration membrane by embedding reduced graphene oxide/TiO2." *Sep. Purif. Technol.*, 154, 96-107.

Saikaew, W., Mattaraj, S. and Jiraratananon, R. (2010). "Nanofiltration performance of lead solutions: effects of solution pH and ionic strength." *Water Sci. Techol.: Water Supply*, 10, (2), 193-200.

Sajitha, C. J., Mahendran, R. and Mohan, D. (2002). "Studies on cellulose acetate-carboxylated polysulfone blend ultrafiltration membranes - Part I." *Eur. Polym. J.*,, 38, (12), 2507-2511.

Salimi, E., Ghaee, A. and Ismail, A. F. (2016). "Performance and antifouling enhancement of polyethersulfone hollow fiber membranes incorporated with highly hydrophilic hydroxyapatite nanoparticles." *RSc Adv.*, 6, (50), 44480-44488.

Salleh, M. A. M., Mahmoud, D. K., Karim, W. A. W. A. and Idris, A. (2011). "Cationic and anionic dye adsorption by agricultural solid wastes: A comprehensive review." *Desalination*, 280, (1), 1-13.

Santosh, V., Gopinath, J., Babu, P. V., Sainath, A. V. S. and Reddy, A. V. R. (2018). "Acetyl-d-glucopyranoside functionalized carbon nanotubes for the development of high performance ultrafiltration membranes." *Sep. Purif. Technol.*, 191, 134-143.

Sawada, I., Fachrul, R., Ito, T., Ohmukai, Y., Maruyama, T. and Matsuyama, H. (2012). "Development of a hydrophilic polymer membrane containing silver nanoparticles with both organic antifouling and antibacterial properties." *J. Membr. Sci.*, 387, 1-6.

Schaep, J., Van der Bruggen, B., Vandecasteele, C. and Wilms, D. (1998). "Influence of ion size and charge in nanofiltration." *Sep. Purif. Technol.*, 14, (1), 155-162.

Schlenoff, J. B. (2014). "Zwitteration: coating surfaces with zwitterionic functionality to reduce nonspecific adsorption." *Langmuir*, 30, (32), 9625-9636.

Schweinsberg, D. P. and Ashworth, V. (1988). "The inhibition of the corrosion of pure iron in 0.5 M sulphuric acid by n-alkyl quaternary ammonium iodides." *Corros. Sci.*, 28, (6), 539-545.

Semsarilar, M., Ladmiral, V., Blanazs, A. and Armes, S. (2011). "Anionic polyelectrolyte-stabilized nanoparticles via RAFT aqueous dispersion polymerization." *Langmuir*, 28, (1), 914-922.

Service, R. F. (2006). "Desalination freshens up." *Science (New York, NY)*, 313, (5790), 1088.

Shalev, T., Gopin, A., Bauer, M., Stark, R. W. and Rahimipour, S. (2012). "Non-leaching antimicrobial surfaces through polydopamine bio-inspired coating of quaternary ammonium salts or an ultrashort antimicrobial lipopeptide." *J. Mater. Chem.*, 22, (5), 2026-2032.

Shang, H., Liu, J., Zheng, Y. and Wang, L. (2009). "Synthesis, characterization, and flocculation properties of poly (acrylamide-methacryloxyethyltrimethyl ammonium chloride-methacryloxypropyltrimethoxy silane)." *J. Appl. Polym. Sci.*, 111, (3), 1594-1599.

Shannon, M. A., Bohn, P. W., Elimelech, M., Georgiadis, J. G., Marinas, B. J. and Mayes, A. M. (2008). "Science and technology for water purification in the coming decades." *Nature*, 452, (7185), 301-310.

Shannon, M. A., Bohn, P. W., Elimelech, M., Georgiadis, J. G., Mariñas, B. J. and Mayes, A. M. (2008). "Science and technology for water purification in the coming decades." *Nature*, 452, (7185), 301-310.

Shao, Q. and Jiang, S. (2015). "Molecular understanding and design of zwitterionic materials." *Adv. Mater.*, 27, (1), 15-26.

Sharma, N. and Purkait, M. (2016). "Enantiomeric and racemic effect of tartaric acid on polysulfone membrane during crystal violet dye removal by MEUF process." *J. Water Process Eng.*, 10, 104-112.

Shen, J., Hu, Y., Qin, C. and Ye, M. (2008). "Layer-by-layer self-assembly of multiwalled carbon nanotube polyelectrolytes prepared by in situ radical polymerization." *Langmuir*, 24, (8), 3993-3997.

Shen, J., Hu, Y., Li, C., Qin, C., Shi, M. and Ye, M. (2009). "Layer-by-layer self-assembly of graphene nanoplatelets." *Langmuir*, 25, (11), 6122-6128.

Shen, J., Hu, Y., Shi, M., Lu, X., Qin, C., Li, C. and Ye, M. (2009). "Fast and facile preparation of graphene oxide and reduced graphene oxide nanoplatelets." *Chem. Mater.*, 21, (15), 3514-3520.

Shen, L., Cheng, C., Yu, X., Yang, Y., Wang, X., Zhu, M. and Hsiao, B. S. (2016). "Low pressure UV-cured CS-PEO-PTEGDMA/PAN thin film nanofibrous composite nanofiltration membranes for anionic dye separation." *J. Mater. Chem. A*, 4, (40), 15575-15588.

Shenvi, S., Ismail, A. and Isloor, A. M. (2014). "Enhanced permeation performance of cellulose acetate ultrafiltration membranes by incorporation of sulfonated poly (1, 4-phenylene ether ether sulfone) and poly (styrene-co-maleic anhydride)." *Ind. Eng. Chem. Res.*, 53, (35), 13820-13827.

Shenvi, S. S., Isloor, A. M., Ismail, A. F., Shilton, S. J. and Al Ahmed, A. (2015). "Humic acid based biopolymeric membrane for effective removal of methylene blue and rhodamine B." *Ind. Eng. Chem. Res.*, 54, (18), 4965-4975.

Shi, B., Li, G., Wang, D., Feng, C. and Tang, H. (2007). "Removal of direct dyes by coagulation: The performance of preformed polymeric aluminum species." *J. Hazad. Mater.*, 143, (1), 567-574.

Sileika, T. S., Barrett, D. G., Zhang, R., Lau, K. H. A. and Messersmith, P. B. (2013). "Colorless Multifunctional Coatings Inspired by Polyphenols Found in Tea, Chocolate, and Wine." *Angew. Chem. Int. Ed.*, 52, (41), 10766-10770.

Silverstein, R. M., Webster, F. X., Kiemle, D. J. and Bryce, D. L. (2014)."*Spectrometric identification of organic compounds*. Pulisher name, John wiley & sons Place.

Sinha, A. K., Pradhan, M. and Pal, T. (2013). "Morphological evolution of two-dimensional MnO2 nanosheets and their shape transformation to one-dimensional ultralong MnO_2 nanowires for robust catalytic activity." *J. Phys. Chem. C*, 117, (45), 23976-23986.

So, M., Eirich, F., Strathmann, H. and Baker, R. (1973). "Preparation of asymmetric loeb-sourirajan membranes." *J. Poly. Sci. Part C: Poly. Lett.*, 11, (3), 201-205.

Song, H., Shao, J., He, Y., Hou, J. and Chao, W. (2011). "Natural organic matter removal and flux decline with charged ultrafiltration and nanofiltration membranes." *J. Membr. Sci.*, 376, (1), 179-187.

Song, Y. Q., Sheng, J., Wei, M. and Yuan, X. B. (2000). "Surface modification of polysulfone membranes by lowtemperature plasma-graft poly(ethylene glycol) onto polysulfone membranes." *J. Appl. Poly. Sci.*, 78, (5), 979-985.

Sosnowski, S., Gadzinowski, M. and Slomkowski, S. (1996). "Poly (l, l-lactide) microspheres by ring-opening polymerization." *Macromolecules*, 29, (13), 4556-4564.

Sounthararajah, D., Loganathan, P., Kandasamy, J. and Vigneswaran, S. (2015). "Adsorptive removal of heavy metals from water using sodium titanate nanofibres loaded onto GAC in fixed-bed columns." *J. Hazard. Mater.*, 287, 306-316.

Spiegler, K. (1958). "Transport processes in ionic membranes." *Transactions of the Faraday Society*, 54, 1408-1428.

Srivastava, N. K. and Majumder, C. B. (2008). "Novel biofiltration methods for the treatment of heavy metals from industrial wastewater." *J. Hazard. Mater.*, 151, (1), 1-8.

Stanicki, D., Boutry, S., Laurent, S., Wacheul, L., Nicolas, E., Crombez, D., Vander Elst, L., Lafontaine, D. L. and Muller, R. N. (2014). "Carboxy-silane coated iron oxide nanoparticles: a convenient platform for cellular and small animal imaging." *J. Mater. Chem. B*, 2, (4), 387-397.

Stankovich, S., Dikin, D. A., Piner, R. D., Kohlhaas, K. A., Kleinhammes, A., Jia, Y., Wu, Y., Nguyen, S. T. and Ruoff, R. S. (2007). "Synthesis of graphene-based nanosheets via chemical reduction of exfoliated graphite oxide." *Carbon*, 45, (7), 1558-1565.

Staverman, A. (1952). "Non-equilibrium thermodynamics of membrane processes." *Transactions of the Faraday Society*, 48, 176-185.

Subramaniam, M., Goh, P., Lau, W., Tan, Y., Ng, B. and Ismail, A. (2017). "Hydrophilic hollow fiber PVDF ultrafiltration membrane incorporated with titanate nanotubes for decolourization of aerobically-treated palm oil mill effluent." *Chem. Eng. J.*, 316, 101-110.

Suksaroj, C., Heran, M., Allegre, C. and Persin, F. (2005). "Treatment of textile plant effluent by nanofiltration and/or reverse osmosis for water reuse." *Desalination*, 178, (1-3), 333-341.

Sun, J., Zhou, S., Hou, P., Yang, Y., Weng, J., Li, X. and Li, M. (2007). "Synthesis and characterization of biocompatible Fe3O4 nanoparticles." *J. Biomed. Mater. Res. B*, 80, (2), 333-341.

Sun, S. P., Hatton, T. A., Chan, S. Y. and Chung, T.-S. (2012). "Novel thin-film composite nanofiltration hollow fiber membranes with double repulsion for effective removal of emerging organic matters from water." *J. Membr. Sci.*, 401, 152-162.

Sun, W., Liu, J., Chu, H. and Dong, B. (2013). "Pretreatment and membrane hydrophilic modification to reduce membrane fouling." *Membranes*, 3, (3), 226-241.

Sundaram, H. S., Cho, Y., Dimitriou, M. D., Finlay, J. A., Cone, G., Williams, S., Handlin, D., Gatto, J., Callow, M. E. and Callow, J. A. (2011). "Fluorinated amphiphilic polymers and their blends for fouling-release applications: the benefits of a triblock copolymer surface." *ACS Appl. Mater. Interfaces*, 3, (9), 3366-3374.

Sundarrajan, S. and Ramakrishna, S. (2007). "Fabrication of nanocomposite membranes from nanofibers and nanoparticles for protection against chemical warfare stimulants." *J. Mater. Sci.*, 42, (20), 8400-8407.

Sunkara, V. and Cho, Y.-K. (2013). "Aminosilane layers on the plasma activated thermoplastics: Influence of solvent on its structure and morphology." *J. Colloid Interf. Sci.*, 411, 122-128.

Susanto, H. and Ulbricht, M. (2007). "Photografted thin polymer hydrogel layers on PES ultrafiltration membranes: characterization, stability, and influence on separation performance." *Langmuir*, 23, (14), 7818-7830.

Tang, C. and Chen, V. (2002). "Nanofiltration of textile wastewater for water reuse." *Desalination*, 143, (1), 11-20.

Tang, C., Ye, S. and Liu, H. (2007). "Electrospinning of poly (styrene-co-maleic anhydride)(SMA) and water-swelling behavior of crosslinked/hydrolyzed SMA hydrogel nanofibers." *Polymer*, 48, (15), 4482-4491.

Tang, C., Amin, D., Messersmith, P. B., Anthony, J. E. and Prud'homme, R. K. (2015). "Polymer directed self-assembly of pH-responsive antioxidant nanoparticles." *Langmuir*, 31, (12), 3612-3620.

Tang, C. Y. and Leckie, J. O. (2007). "Membrane Independent Limiting Flux for RO and NF Membranes Fouled by Humic Acid." *Environ. Sci. Technol.*, 41, (13), 4767-4773.

Tang, C. Y., Chong, T. and Fane, A. G. (2011). "Colloidal interactions and fouling of NF and RO membranes: a review." *Adv. Colloid Interface Sci.*, 164, (1), 126-143.

Tang, S.-H., Domino, M. Y., Venault, A., Lin, H.-T., Hsieh, C., Higuchi, A., Chinnathambi, A., Alharbi, S. A., Tayo, L. L. and Chang, Y. (2018). "Bio-inert Control of Zwitterionic Poly (ethylene terephtalate) Fibrous Membranes." *Langmuir*, 35, (5), 1727-1739.

Tang, Y. P., Chan, J. X., Chung, T. S., Weber, M., Staudt, C. and Maletzko, C. (2015). "Simultaneously covalent and ionic bridging towards antifouling of GO-imbedded nanocomposite hollow fiber membranes." *J. Mater. Chem. A*, 3, (19), 10573-10584.

Tang, Y. P., Yuwen, S., Chung, T. S., Weber, M., Staudt, C. and Maletzko, C. (2016). "Synthesis of hyperbranched polymers towards efficient boron reclamation via a hybrid ultrafiltration process." *J. Membr. Sci.*, 510, 112-121.

Tawil, N., Sacher, E., Boulais, E., Mandeville, R. and Meunier, M. (2013). "X-ray photoelectron spectroscopic and transmission electron microscopic characterizations of bacteriophage–nanoparticle complexes for pathogen detection." *J. Phys. Chem. C*, 117, (40), 20656-20665.

Thomas, J. A. and McGaughey, A. J. (2008). "Reassessing fast water transport through carbon nanotubes." *Nano Lett.*, 8, (9), 2788-2793.

Thong, Z., Han, G., Cui, Y., Gao, J., Chung, T.-S., Chan, S. Y. and Wei, S. (2014). "Novel nanofiltration membranes consisting of a sulfonated pentablock copolymer rejection layer for heavy metal removal." *Environ. Sci. Technol.*, 48, (23), 13880-13887.

Thorén, K., Meding, B., Nordlinder, R. and Belin, L. (1986). "Contact dermatitis and asthma from reactive dyes." *Contact dermatitis*, 15, (3), 186-186.

Tien, H.-W., Huang, Y.-L., Yang, S.-Y., Wang, J.-Y. and Ma, C.-C. M. (2011). "The production of graphene nanosheets decorated with silver nanoparticles for use in transparent, conductive films." *Carbon*, 49, (5), 1550-1560.

Tratnyek, P. G., Elovitz, M. S. and Colverson, P. (1994). "Photoeffects of textile dye wastewaters: sensitization of singlet oxygen formation, oxidation of phenols and toxicity to bacteria." *Environ. Toxicol. Chem.*, 13, (1), 27-33.

Traube, M. (1867). "Physiologie und wissenschaftliche Medizin." *Arch. An. Physiol*, 87.

Tremblay, A. Y., Tam, C. M. and Guiver, M. D. (1992). "Variations in the pore size of charged and noncharged hydrophilic polysulfone membranes." *Indust. Eng. Chem. Res.*, 31, (3), 834-838.

Trivedi, J. S., Bhalani, D. V., Bhadu, G. R. and Jewrajka, S. K. (2018). "Multifunctional amines enable the formation of polyamide nanofilm composite ultrafiltration and nanofiltration membranes with modulated charge and performance." *J. Mater. Chem. A*, 6, (41), 20242-20253.

Uchida, E., Uyama, Y. and Ikada, Y. (1994). "Zeta potential of polycation layers grafted onto a film surface." *Langmuir*, 10, (4), 1193-1198.

Ulbricht, M., Riedel, M. and Marx, U. (1996). "Novel photochemical surface functionalization of polysulfone ultrafiltration membranes for covalent immobilization of biomolecules." *J. Membr. Sci.*, 120, (2), 239-259.

Ulbricht, M. (2006). "Advanced functional polymer membranes." *Polymer*, 47, (7), 2217-2262.

Jiang, Shaoyi; Cao, Zhiqiang, (2010). "Hydrolyzable Zwitterionic Materials and Their Derivatives for Biological Applications." *Adv. Mater.,*, 22, (9), 920-932.

Van der Bruggen, B., Schaep, J., Wilms, D. and Vandecasteele, C. (1999). "Influence of molecular size, polarity and charge on the retention of organic molecules by nanofiltration." *J. Membr. Sci.*, 156, (1), 29-41.

Van der Bruggen, B., Daems, B., Wilms, D. and Vandecasteele, C. (2001). "Mechanisms of retention and flux decline for the nanofiltration of dye baths from the textile industry." *Sep. Purif. Technol.*, 22, 519-528.

Van der Bruggen, B., Vandecasteele, C., Van Gestel, T., Doyen, W. and Leysen, R. (2003). "A review of pressure-driven membrane processes in wastewater treatment and drinking water production." *Environmental progress*, 22, (1), 46-56.

Van der Bruggen, B., Cornelis, G., Vandecasteele, C. and Devreese, I. (2005). "Fouling of nanofiltration and ultrafiltration membranes applied for wastewater regeneration in the textile industry." *Desalination*, 175, (1), 111-119.

Vardon, D. R., Sharma, B., Scott, J., Yu, G., Wang, Z., Schideman, L., Zhang, Y. and Strathmann, T. J. (2011). "Chemical properties of biocrude oil from the hydrothermal liquefaction of Spirulina algae, swine manure, and digested anaerobic sludge." *Bioresource technology*, 102, (17), 8295-8303.

Vatanpour, V., Madaeni, S. S., Rajabi, L., Zinadini, S. and Derakhshan, A. A. (2012). "Boehmite nanoparticles as a new nanofiller for preparation of antifouling mixed matrix membranes." *J. Membr. Sci.*, 401-402, 132-143.

Venault, A., Huang, W.-Y., Hsiao, S.-W., Chinnathambi, A., Alharbi, S. A., Chen, H., Zheng, J. and Chang, Y. (2016). "Zwitterionic modifications for enhancing the antifouling properties of poly (vinylidene fluoride) membranes." *Langmuir*, 32, (16), 4113-4124.

Vlyssides, A., Papaioannou, D., Loizidoy, M., Karlis, P. and Zorpas, A. (2000). "Testing an electrochemical method for treatment of textile dye wastewater." *Waste Manage.*, 20, (7), 569-574.

Vrijenhoek, E. M., Hong, S. and Elimelech, M. (2001). "Influence of membrane surface properties on initial rate of colloidal fouling of reverse osmosis and nanofiltration membranes." *J. Membr. Sci.*, 188, (1), 115-128.

Wan Azelee, I., Goh, P. S., Lau, W. J., Ismail, A. F., Rezaei-DashtArzhandi, M., Wong, K. C. and Subramaniam, M. N. (2017). "Enhanced desalination of polyamide thin film nanocomposite incorporated with acid treated multiwalled carbon nanotube-titania nanotube hybrid." *Desalination*, 409, 163-170.

Wang, F., Li, F.-L., Xu, M.-M., Yu, H., Zhang, J.-G., Xia, H.-T. and Lang, J.-P. (2015). "Facile synthesis of a Ag(i)-doped coordination polymer with enhanced catalytic performance in the photodegradation of azo dyes in water." *J. Mater. Chem. A*, 3, (11), 5908-5916.

Wang, H., Wang, M., Zhao, N., Wei, W. and Sun, Y. (2005). "CaO–ZrO 2 solid solution: a highly stable catalyst for the synthesis of dimethyl carbonate from propylene carbonate and methanol." *Catalysis letters*, 105, (3-4), 253-257.

Wang, J.-T., Wang, L., Ji, X., Liu, L. and Zhao, H. (2017). "Synthesis of Zwitterionic Diblock Copolymers with Cleavable Biotin Groups at the Junction Points and Fabrication of Bioconjugates by Biotin–Streptavidin Coupling." *Macromolecules*, 50, (6), 2284-2295.

Wang, J., Gao, X., Wang, J., Wei, Y., Li, Z. and Gao, C. (2015). "O-(Carboxymethyl)-chitosan nanofiltration membrane surface functionalized with graphene oxide nanosheets for enhanced desalting properties." *ACS Appl. Mater. Interfaces*, 7, (7), 4381-4389.

Wang, J., Wang, Y., Zhang, Y., Uliana, A., Zhu, J., Liu, J. and Van der Bruggen, B. (2016). "Zeolitic imidazolate framework/graphene oxide hybrid nanosheets functionalized thin film nanocomposite membrane for enhanced antimicrobial performance." *ACS Appl. Mater. Interfaces*, 8, (38), 25508-25519.

Wang, J., Zhang, Y., Zhu, J., Hou, J., Liu, J. and Van der Bruggen, B. (2016). "Zwitterionic functionalized layered double hydroxides nanosheets for a novel charged mosaic membrane with high salt permeability." *J. Membr. Sci.*, 510, 27-37.

Wang, K. Y., Matsuura, T., Chung, T.-S. and Guo, W. F. (2004). "The effects of flow angle and shear rate within the spinneret on the separation performance of poly (ethersulfone)(PES) ultrafiltration hollow fiber membranes." *J. Membr. Sci.*, 240, (1), 67-79.

Wang, W., Lu, Y., Luo, M., Zhao, Q., Wang, Y., Liu, Q., Li, M. and Wang, D. (2016). "Zwitterionic-polymer-functionalized poly (vinyl alcohol-co-ethylene) nanofiber membrane for resistance to the adsorption of bacteria and protein." *J. Appl. Polym. Sci.*, 133, (44), 102-106.

Wang, X. S., Zhou, Y., Jiang, Y. and Sun, C. (2008). "The removal of basic dyes from aqueous solutions using agricultural by-products." *J. Hazard. Mater.*, 157, (2), 374-385.

Wang, Y., Chen, J., Lu, L. and Lin, Z. (2013). "Reversible switch between bulk MgCO3· 3H2O and Mg (OH) 2 micro/nanorods induces continuous selective preconcentration of anionic dyes." *ACS Appl. Mater. Interfaces*, 5, (16), 7698-7703.

Wang, Y., Zhu, J., Dong, G., Zhang, Y., Guo, N. and Liu, J. (2015). "Sulfonated halloysite nanotubes/polyethersulfone nanocomposite membrane for efficient dye purification." *Sep. Purif. Technol.*, 150, 243-251.

Wang, Z., Wang, Z., Lin, S., Jin, H., Gao, S., Zhu, Y. and Jin, J. (2018). "Nanoparticle-templated nanofiltration membranes for ultrahigh performance desalination." *Nat. Commun.*, 9, (1), 2004.

Weber, E. J. and Adams, R. L. (1995). "Chemical-and sediment-mediated reduction of the azo dye disperse blue 79." *Environ. Sci. Technol.*, 29, (5), 1163-1170.

Wei, Q. and Haag, R. (2015). "Universal polymer coatings and their representative biomedical applications." *Mater. Horiz.*, 2, (6), 567-577.

Wenzel, R. N. (1949). "Surface roughness and contact angle." *J. Phys. Chem.*, 53, (9), 1466-1467.

Werber, J. R., Osuji, C. O. and Elimelech, M. (2016). "Materials for next-generation desalination and water purification membranes." *Nat. Rev. Mater.*, 1, 16018.

Wu, J., Wang, J., Li, H., Du, Y., Huang, K. and Liu, B. (2013). "Designed synthesis of hematite-based nanosorbents for dye removal." *J. Mater. Chem. A*, 1, (34), 9837-9847.

Xiang, T., Wang, R., Zhao, W.-F., Sun, S.-D. and Zhao, C.-S. (2014). "Covalent deposition of zwitterionic polymer and citric acid by click chemistry-enabled layer-by-layer assembly for improving the blood compatibility of polysulfone membrane." *Langmuir*, 30, (18), 5115-5125.

Xiao, W., Lin, J., Li, M., Ma, Y., Chen, Y., Zhang, C., Li, D. and Gu, H. (2012). "Prolonged in vivo circulation time by zwitterionic modification of magnetite nanoparticles for blood pool contrast agents." *Contrast Media Mol. I.*, 7, (3), 320-327.

Xie, M. and Xu, Y. (2011). "Partial desalination and concentration of glyphosate liquor by nanofiltration." *J. Hazard. Material*, 186, (1), 960-964.

Xie, M., Nghiem, L. D., Price, W. E. and Elimelech, M. (2012). "Comparison of the removal of hydrophobic trace organic contaminants by forward osmosis and reverse osmosis." *Water Res.*, 46, (8), 2683-2692.

Xing, L., Guo, N., Zhang, Y., Zhang, H. and Liu, J. (2015). "A negatively charged loose nanofiltration membrane by blending with poly (sodium 4-styrene sulfonate) grafted SiO 2 via SI-ATRP for dye purification." *Sep. Purif. Technol.*, 146, 50-59.

Xu, C., Wang, X. and Zhu, J. (2008). "Graphene−Metal Particle Nanocomposites." *J. Phys. Chem. C*, 112, (50), 19841-19845.

Xu, L. Q., Pranantyo, D., Neoh, K.-G., Kang, E.-T. and Fu, G. D. (2016). "Thiol Reactive Maleimido-Containing Tannic Acid for the Bioinspired Surface Anchoring and Post-Functionalization of Antifouling Coatings." *ACS Sustain. Chem. Eng.*, 4, (8), 4264-4272.

Xu, Y., Lebrun, R. E., Gallo, P.-J. and Blond, P. (1999). "Treatment of textile dye plant effluent by nanofiltration membrane." *Sep. Sci. Technol.*, 34, (13), 2501-2519.

Xuan, F. and Liu, J. (2009). "Preparation, characterization and application of zwitterionic polymers and membranes: current developments and perspective." *Polym. Int.*, 58, (12), 1350-1361.

Xue, J., Jiao, Z., Bi, R., Zhang, R., You, X., Wang, F., Zhou, L., Su, Y. and Jiang, Z. (2019). "Chlorine-resistant polyester thin film composite nanofiltration membranes prepared with β-cyclodextrin." *J. Membr. Sci.*, 584, 282-289.

Xue, S.-M., Xu, Z.-L., Tang, Y.-J. and Ji, C.-H. (2016). "Polypiperazine-amide nanofiltration membrane modified by different functionalized multiwalled carbon nanotubes (MWCNTs)." *ACS Appl. Mater. Interfaces*, 8, (29), 19135-19144.

Yang, K., Berg, M. M., Zhao, C. and Ye, L. (2009). "One-pot synthesis of hydrophilic molecularly imprinted nanoparticles." *Macromolecules*, 42, (22), 8739-8746.

Yang, R., Xu, J., Ozaydin-Ince, G., Wong, S. Y. and Gleason, K. K. (2011). "Surface-tethered zwitterionic ultrathin antifouling coatings on reverse osmosis membranes by initiated chemical vapor deposition." *Chem. Mater.*, 23, (5), 1263-1272.

Yang, X., Wan, Y., Zheng, Y., He, F., Yu, Z., Huang, J., Wang, H., Ok, Y. S., Jiang, Y. and Gao, B. (2019). "Surface functional groups of carbon-based adsorbents and their roles in the removal of heavy metals from aqueous solutions: A critical review." *Chem. Eng. J.*, 366, 608-621.

Yang, Y.-F., Wan, L.-S. and Xu, Z.-K. (2009). "Surface hydrophilization for polypropylene microporous membranes: a facile interfacial crosslinking approach." *J. Membr. Sci.*, 326, (2), 372-381.

Yang, Y., Miao, L., Hu, J., Liu, G., Tu, Y., Lin, S., Liu, F., Li, F., Wu, Y. and Zhang, G. (2014). "Hydrophilization of polysulfone membranes using a binary graft copolymer." *J. Mater. Chem. A*, 2, (27), 10410-10423.

Yang, Z., Huang, X., Ma, X.-h., Zhou, Z.-w., Guo, H., Yao, Z., Feng, S.-P. and Tang, C. Y. (2019). "Fabrication of a novel and green thin-film composite membrane containing nanovoids for water purification." *J. Membr. Sci.*, 570-571, 314-321.

Ye, C.-C., An, Q.-F., Wu, J.-K., Zhao, F.-Y., Zheng, P.-Y. and Wang, N.-X. (2019). "Nanofiltration membranes consisting of quaternized polyelectrolyte complex nanoparticles for heavy metal removal." *Chem. Eng. J.*, 359, 994-1005.

Ye, G., Lee, J., Perreault, F. o. and Elimelech, M. (2015). "Controlled architecture of dual-functional block copolymer brushes on thin-film composite membranes for integrated “defending” and “attacking” strategies against biofouling." *ACS Appl. Mater. Interfaces*, 7, (41), 23069-23079.

Yi, Z., Zhu, L. P., Xu, Y. Y., Zhao, Y. F., Ma, X. T. and Zhu, B. K. (2010). "Polysulfone-based amphiphilic polymer for hydrophilicity and fouling-resistant modification of polyethersulfone membranes." *J. Membr. Sci.*,, 365, (1-2), 25-33.

Yin, J. and Zhou, J. (2015). "Novel polyethersulfone hybrid ultrafiltration membrane prepared with SiO2-g-(PDMAEMA-co-PDMAPS) and its antifouling performances in oil-in-water emulsion application." *Desalination*, 365, 46-56.

Yoon, H., Na, S.-H., Choi, J.-Y., Latthe, S. S., Swihart, M. T., Al-Deyab, S. S. and Yoon, S. S. (2014). "Gravity-driven hybrid membrane for oleophobic–superhydrophilic oil–water separation and water purification by graphene." *Langmuir*, 30, (39), 11761-11769.

Yu, H., Cao, Y., Kang, G., Liu, J., Li, M. and Yuan, Q. (2009). "Enhancing antifouling property of polysulfone ultrafiltration membrane by grafting zwitterionic copolymer via UV-initiated polymerization." *J. Membr. Sci.*, 342, (1), 6-13.

Yu, L., Zhang, Y., Zhang, B., Liu, J., Zhang, H. and Song, C. (2013). "Preparation and characterization of HPEI-GO/PES ultrafiltration membrane with antifouling and antibacterial properties." *J. Membr. Sci.*, 447, 452-462.

Yu, L., Zhang, Y., Wang, Y., Zhang, H. and Liu, J. (2015). "High flux, positively charged loose nanofiltration membrane by blending with poly (ionic liquid) brushes grafted silica spheres." *J. Hazard. Mater.*, 287, 373-383.

Yu, L., Wang, H., Zhang, Y., Zhang, B. and Liu, J. (2016). "Recent advances in halloysite nanotube derived composites for water treatment." *Environ. Sci.: Nano*, 3, (1), 28-44.

Yu, S., Gao, C., Su, H. and Liu, M. (2001). "Nanofiltration used for desalination and concentration in dye production." *Desalination*, 140, (1), 97-100.

Yu, S., Liu, M., Ma, M., Qi, M., Lü, Z. and Gao, C. (2010). "Impacts of membrane properties on reactive dye removal from dye/salt mixtures by asymmetric cellulose acetate and composite polyamide nanofiltration membranes." *J. Membr. Sci.*, 350, (1-2), 83-91.

Yuan, J. and Antonietti, M. (2011). "Poly (ionic liquid) latexes prepared by dispersion polymerization of ionic liquid monomers." *Macromolecules*, 44, (4), 744-750.

Yuan, J. and Antonietti, M. (2011). "Poly(ionic liquid)s: Polymers expanding classical property profiles." *Polymer*, 52, (7), 1469-1482.

Yuan, J., Soll, S., Drechsler, M., Müller, A. H. and Antonietti, M. (2011). "Self-assembly of poly (ionic liquid) s: polymerization, mesostructure formation, and directional alignment in one step." *J. Am. Chem. Soc.*, 133, (44), 17556-17559.

Yurekli, Y. (2016). "Removal of heavy metals in wastewater by using zeolite nano-particles impregnated polysulfone membranes." *J. Hazard. Mater.*, 309, 53-64.

Zambare, R. S., Dhopte, K. B., Patwardhan, A. V. and Nemade, P. R. (2017). "Polyamine functionalized graphene oxide polysulfone mixed matrix membranes with improved hydrophilicity and anti-fouling properties." *Desalination*, 403, 24-35.

Zeng, G., He, Y., Zhan, Y., Zhang, L., Shi, H. and Yu, Z. (2016). "Preparation of a novel poly (vinylidene fluoride) ultrafiltration membrane by incorporation of 3-aminopropyltriethoxysilane-grafted halloysite nanotubes for oil/water separation." *Ind. Eng. Chem. Res.*, 55, (6), 1760-1767.

Zhang, G., Jiang, J., Zhang, Q., Gao, F., Zhan, X. and Chen, F. (2016). "Ultralow Oil-Fouling Heterogeneous Poly (ether sulfone) Ultrafiltration Membrane via Blending with Novel Amphiphilic Fluorinated Gradient Copolymers." *Langmuir*, 32, (5), 1380-1388.

Zhang, J., Zhang, Y., Chen, Y., Du, L., Zhang, B., Zhang, H., Liu, J. and Wang, K. (2012). "Preparation and characterization of novel polyethersulfone hybrid ultrafiltration membranes bending with modified halloysite nanotubes loaded with silver nanoparticles." *Ind. Eng. Chem. Res.*, 51, (7), 3081-3090.

Zhang, L., Xue, H., Gao, C., Carr, L., Wang, J., Chu, B. and Jiang, S. (2010). "Imaging and cell targeting characteristics of magnetic nanoparticles modified by a functionalizable zwitterionic polymer with adhesive 3,4-dihydroxyphenyl-l-alanine linkages." *Biomaterials*, 31, (25), 6582-6588.

Zhang, R., Liu, Y., He, M., Su, Y., Zhao, X., Elimelech, M. and Jiang, Z. (2016). "Antifouling membranes for sustainable water purification: strategies and mechanisms." *Chem. Soc. Rev.*, 45, (21), 5888-5924.

Zhang, S., Peh, M. H., Thong, Z. and Chung, T.-S. (2014). "Thin film interfacial cross-linking approach to fabricate a chitosan rejecting layer over poly (ether sulfone) support for heavy metal removal." *Ind. Eng. Chem. Res.*, 54, (1), 472-479.

Zhang, X., Wang, J., He, X., Chen, L. and Zhang, Y. (2015). "Tailor-made boronic acid functionalized magnetic nanoparticles with a tunable polymer shell-assisted for the selective enrichment of glycoproteins/glycopeptides." *ACS Appl. Mater. Interfaces*, 7, (44), 24576-24584.

Zhang, X., Lv, Y., Yang, H. C., Du, Y. and Xu, Z. K. (2016). "Polyphenol coating as an interlayer for thin-film composite membranes with enhanced nanofiltration performance." *ACS Appl. Mater. Interfaces*, 8, (47), 32512-32519.

Zhang, X., Ren, P.-F., Yang, H.-C., Wan, L.-S. and Xu, Z.-K. (2016). "Co-deposition of tannic acid and diethlyenetriamine for surface hydrophilization of hydrophobic polymer membranes." *Appl. Surf. Sci.*, 360, 291-297.

Zhang, Y., Su, Y., Peng, J., Zhao, X., Liu, J., Zhao, J. and Jiang, Z. (2013). "Composite nanofiltration membranes prepared by interfacial polymerization with natural material tannic acid and trimesoyl chloride." *J. Membr. Sci.*, 429, 235-242.

Zhang, Y., Zhang, S. and Chung, T.-S. (2015). "Nanometric graphene oxide framework membranes with enhanced heavy metal removal via nanofiltration." *Environ. Sci. Technol.*, 49, (16), 10235-10242.

Zhang, Z., Chao, T., Chen, S. and Jiang, S. (2006). "Superlow fouling sulfobetaine and carboxybetaine polymers on glass slides." *Langmuir*, 22, (24), 10072-10077.

Zhang, Z., Finlay, J. A., Wang, L., Gao, Y., Callow, J. A., Callow, M. E. and Jiang, S. (2009). "Polysulfobetaine-grafted surfaces as environmentally benign ultralow fouling marine coatings." *Langmuir*, 25, (23), 13516-13521.

Zhang, Z., Kang, G., Yu, H., Jin, Y. and Cao, Y. (2019). "Fabrication of a highly permeable composite nanofiltration membrane via interfacial polymerization by adding a novel acyl chloride monomer with an anhydride group." *J. Membr. Sci.*, 570-571, 403-409.

Zhao, C., Xue, J., Ran, F. and Sun, S. (2013). "Modification of polyethersulfone membranes–a review of methods." *Prog. Mater. Sci.*, 58, (1), 76-150.

Zhao, H., Qiu, S., Wu, L., Zhang, L., Chen, H. and Gao, C. (2014). "Improving the performance of polyamide reverse osmosis membrane by incorporation of modified multi-walled carbon nanotubes." *J. Membr. Sci.*, 450, 249-256.

Zhao, J., Zhu, Y., He, G., Xing, R., Pan, F., Jiang, Z., Zhang, P., Cao, X. and Wang, B. (2016). "Incorporating zwitterionic graphene oxides into sodium alginate membrane for efficient water/alcohol separation." *ACS Appl. Mater. Interfaces*, 8, (3), 2097-2103.

Zhao, S., Wang, Z., Wei, X., Zhao, B., Wang, J., Yang, S. and Wang, S. (2012). "Performance improvement of polysulfone ultrafiltration membrane using well-dispersed polyaniline–poly (vinylpyrrolidone) nanocomposite as the additive." *Ind. Eng. Chem. Res.*, 51, (12), 4661-4672.

Zhao, W., Su, Y., Li, C., Shi, Q., Ning, X. and Jiang, Z. (2008). "Fabrication of antifouling polyethersulfone ultrafiltration membranes using Pluronic F127 as both surface modifier and pore-forming agent." *J. Membr. Sci.*, 318, (1-2), 405-412.

Zhao, X., Su, Y., Dai, H., Li, Y., Zhang, R. and Jiang, Z. (2015). "Coordination-enabled synergistic surface segregation for fabrication of multi-defense mechanism membranes." *J. Mater. Chem. A*, 3, (7), 3325-3331.

Zhao, X., Su, Y., Liu, Y., Li, Y. and Jiang, Z. (2016). "Free-standing graphene oxide-palygorskite nanohybrid membrane for oil/water separation." *ACS Appl. Mater. Interfaces*, 8, (12), 8247-8256.

Zhao, Y.-H., Wee, K.-H. and Bai, R. (2010). "Highly hydrophilic and low-protein-fouling polypropylene membrane prepared by surface modification with sulfobetaine-based zwitterionic polymer through a combined surface polymerization method." *J. Membr. Sci.*, 362, (1), 326-333.

Zhao, Y., Abdullayev, E., Vasiliev, A. and Lvov, Y. (2013). "Halloysite nanotubule clay for efficient water purification." *J. Colloid Interf. Sci.*, 406, 121-129.

Zheng, J., Li, M., Yao, Y., Zhang, X. and Wang, L. (2017). "Zwitterionic carbon nanotube assisted thin-film nanocomposite membranes with excellent efficiency for separation of mono/divalent ions from brackish water." *J. Mater. Chem. A*, 5, (26), 13730-13739.

Zheng, X. and Liu, J. (2006). "Dyeing and printing wastewater treatment using a membrane bioreactor with a gravity drain." *Desalination*, 190, (1), 277-286.

Zheng, Y., Yao, G., Cheng, Q., Yu, S., Liu, M. and Gao, C. (2013). "Positively charged thin-film composite hollow fiber nanofiltration membrane for the removal of cationic dyes through submerged filtration." *Desalination*, 328, 42-50.

Zhenxin, Z. and Matsuura, T. (1991). "Discussions on the formation mechanism of surface pores in reverse osmosis, ultrafiltration, and microfiltration membranes prepared by phase inversion process." *J. Coll. Inter. Sci.*, 147, (2), 307-315.

Zhu, J., Guo, N., Zhang, Y., Yu, L. and Liu, J. (2014). "Preparation and characterization of negatively charged PES nanofiltration membrane by blending with halloysite nanotubes grafted with poly (sodium 4-styrenesulfonate) via surface-initiated ATRP." *J. Membr. Sci.*, 465, 91-99.

Zhu, J., Tian, M., Zhang, Y., Zhang, H. and Liu, J. (2015). "Fabrication of a novel "loose" nanofiltration membrane by facile blending with Chitosan–Montmorillonite nanosheets for dyes purification." *Chem. Eng. J.*, 265, 184-193.

Zhu, J., Zhang, Y., Tian, M. and Liu, J. (2015). "Fabrication of a mixed matrix membrane with in situ synthesized quaternized polyethylenimine nanoparticles for dye purification and reuse." *ACS. Sustain. Chem. Eng.*, 3, (4), 690-701.

Zhu, J., Tian, M., Hou, J., Wang, J., Lin, J., Zhang, Y., Liu, J. and Van der Bruggen, B. (2016). "Surface zwitterionic functionalized graphene oxide for a novel loose nanofiltration membrane." *J. Mater. Chem. A*, 4, (5), 1980-1990.

Zhu, J., Uliana, A., Wang, J., Yuan, S., Li, J., Tian, M., Simoens, K., Volodin, A., Lin, J., Bernaerts, K., Zhang, Y. and Van der Bruggen, B. (2016). "Elevated salt transport of antimicrobial loose nanofiltration membranes enabled by copper nanoparticles via fast bioinspired deposition." *J. Mater. Chem. A*, 4, (34), 13211-13222.

Zhu, J., Qin, L., Uliana, A., Hou, J., Wang, J., Zhang, Y., Li, X., Yuan, S., Li, J. and Tian, M. (2017). "Elevated performance of thin film nanocomposite membranes enabled by modified hydrophilic MOFs for nanofiltration." *ACS Appl. Mater. Interfaces*, 9, (2), 1975-1986.

Zhu, J., Yuan, S., Uliana, A., Hou, J., Li, J., Li, X., Tian, M., Chen, Y., Volodin, A. and der Bruggen, B. V. (2018). "High-flux thin film composite membranes for nanofiltration mediated by a rapid co-deposition of polydopamine/piperazine." *J. Membr. Sci.*, 554, 97-108.

Zhu, L.-P., Zhang, X.-X., Xu, L., Du, C.-H., Zhu, B.-K. and Xu, Y.-Y. (2007). "Improved protein-adsorption resistance of polyethersulfone membranes via surface segregation of ultrahigh molecular weight poly (styrene-alt-maleic anhydride)." *Colloid. Surface B.*, 57, (2), 189-197.

Zhu, L.-P., Yi, Z., Liu, F., Wei, X.-Z., Zhu, B.-K. and Xu, Y.-Y. (2008). "Amphiphilic graft copolymers based on ultrahigh molecular weight poly (styrene-alt-maleic anhydride) with poly (ethylene glycol) side chains for surface modification of polyethersulfone membranes." *Eur. Polym. J.*, 44, (6), 1907-1914.

Zhu, W.-P., Sun, S.-P., Gao, J., Fu, F.-J. and Chung, T.-S. (2014). "Dual-layer polybenzimidazole/polyethersulfone (PBI/PES) nanofiltration (NF) hollow fiber membranes for heavy metals removal from wastewater." *J. Membr. Sci.*, 456, 117-127.

Zhu, X., Cheng, X., Xing, J., Wang, T., Xu, D., Bai, L., Luo, X., Wang, W., Li, G. and Liang, H. (2020). "In-situ covalently bonded supramolecular-based protective layer for improving chlorine resistance of thin-film composite nanofiltration membranes." *Desalination*, 474, 114197.

Zhu, Y., Xie, W., Zhang, F., Xing, T. and Jin, J. (2017). "Superhydrophilic In-Situ-Cross-Linked Zwitterionic Polyelectrolyte/PVDF-Blend Membrane for Highly Efficient Oil/Water Emulsion Separation." *ACS Appl. Mater. Interfaces*, 9, (11), 9603-9613.

Zinadini, S., Zinatizadeh, A. A., Rahimi, M., Vatanpour, V. and Zangeneh, H. (2014). "Preparation of a novel antifouling mixed matrix PES membrane by embedding graphene oxide nanoplates." *J. Membr. Sci.*, 453, 292-301.

Zsigmondy, R. and Bachmann, W. (1918). "Ueber neue filter." *Zeitschrift für anorganische und allgemeine Chemie*, 103, (1), 119-128.

LIST OF PUBLICATIONS

List of papers

1. **Ibrahim, G. P. S**., Isloor, A. M., Moslehyani, A. and Ismail, A. F. (2017). "Bio-inspired, fouling resistant, tannic acid functionalized halloysite nanotube reinforced polysulfone loose nanofiltration hollow fiber membranes for efficient dye and salt separation." **Journal of Water Process Engineering**, 20, 138-148.

2. **Ibrahim, G. P. S**., Isloor, A. M., Inamuddin., A.M. Asiri, Norafiqah., Ismail, A. F., and Ashraf, G.M. (2017). "Novel, one-step synthesis of zwitterionic polymer nanoparticles via distillation-precipitation polymerization and its application for dye removal membrane." **Scientific Reports**., 7, (1), 15889 (**Nature publication**).

3. **Ibrahim, G. P. S**., Isloor, A. M., Inamuddin, Asiri, A. M., Ismail, A. F., Kumar, R. and Ahamed, M. I. (2018). "Performance intensification of the polysulfone ultrafiltration membrane by blending with copolymer encompassing novel derivative of poly(styrene-co-maleic anhydride) for heavy metal removal from wastewater." **Chemical Engineering Journal**, 353, 425-435.

4. **Ibrahim, G. P. S**., A. M. Isloor, Inamuddin, A. M. Asiri & R. Farnood. (2020). "Tuning the surface properties of Fe_3O_4 by zwitterionic sulfobetaine: Application to antifouling and dye removal membrane" **International Journal of Environmental Science and Technology,** 1-14.

5. **Ibrahim, G. P. S**., Isloor, A.M., A. F. Ismail and Ramin Farnood. (2020). "One-step synthesis of novel zwitterionic graphene oxide nanohybrid: Application to polysulfone tight ultrafiltration hollow fiber membrane." **Scientific Reports**, 10, 6880 (**Nature publication**).

6. **Ibrahim, G. P. S**., Isloor, A.M., Mona Bavarian and Siamak Nejati. (2020). "Integration of zwitterionic polymer nanoparticles in interfacial polymerization for ion separation" **ACS Applied Polymer Materials**, 2, (4), 1508-1517.

7. **Ibrahim, G. P. S**., Isloor, A.M., Mona Bavarian and Siamak Nejati., "Poly(homopiperazine-amide) thin film composites for nanofiltration of heavy metal ions" *Communicated to ACS Omega-Under Review*.

List of book chapters

1. **Ibrahim, G. P. S**, A.M. Isloor, E. Yuliati, A.F. Ismail. (2019). Carbon-based nanocomposite membranes for water and wastewater purification, in: Advanced Nanomaterials for Membrane Synthesis and its Applications, **Elsevier**, 23-44.
2. **Ibrahim, G. P. S**, A.M. Isloor, E. Yuliwati. (2019). A Review: Desalination by Forward Osmosis: Current Trends and Future Developments on (Bio-) Membranes, **Elsevier,** 199-214.
3. **Ibrahim, G. P. S**., Isloor, A.M. and Farnood, R. (2019). Fundamentals and basics of reverse osmosis. Current Trends and Future Developments on (Bio-) Membranes: Reverse and Forward Osmosis: Principles, Applications, Advances, **Elsevier**, 141-163.
4. **Ibrahim, G. P. S**., Isloor, A.M. and Farnood, R. (2019). Reverse osmosis pretreatment techniques, fouling and control strategies. Current Trends and Future Developments on (Bio-) Membranes: Reverse and Forward Osmosis: Principles, Applications, Advances, **Elsevier**, 165-186.
5. **Ibrahim, G. P. S**., Isloor, A.M. and Farnood, R. (2020). Role of Hollow Fiber Contactors Based Technology in Fermentation and Enzymatic Transformation and in Chiral Separations, **CRC Press**- In press.
6. **Ibrahim, G. P. S** and Isloor, A.M. and B. Lakshmi. (2020). Synthetic Polymer based Membrane for Dyes and Pigments Removal, in: Synthetic Polymeric Membranes for Advanced Water Treatment, Gas Separation, and Energy Sustainability **Elsevier**, 39-52.

LIST OF CONFERENCES ATTENDED

1. Presented poster presentation on a research paper titled, "Fabrication and characterization of polysulfone-zeolite mixed matrix membrane for heavy metal ion removal application". International conference on Recent Advances in Material and Chemical Sciences, Department of chemistry, Bundelkhand University, Jhansi, March 2-5, 2016.
2. Presented poster presentation on a research paper titled, "Synthesis and characterization of novel Poly[styrene-alt-(N-4-benzoylglycine-maleamic acid)], cumene terminated-blend-Polysulfone ultrafiltration membranes for heavy metal removal." International conference on Advanced Polymers for Science and Technology, VIT University, Vellore, October 24-26, 2016 (**Best poster award**).
3. Presented oral presentation on a research paper titled, "Tannic acid functionalized halloysite nanotube reinforced PSF loose nanofiltration HF membranes for dye removal." National Conference on Advances in Materials Research Ramaiah University, Bangalore, 18-19 August 2017.
4. Presented poster presentation on a research paper titled, "Novel, one-step synthesis of zwitterionic polymer nanoparticles via distillation-precipitation polymerization and its application for dye removal membrane". International Conference on Systems and Processes in Physics, Chemistry and Biology (ICSPPCB), Assam University, March 1-3, 2018 (**Best poster award**).

BIODATA

G P SYED IBRAHIM

Phone: +91 9442858491, Email: gpsyed@gmail.com

WORK EXPERIENCE		
Company/Institute Name	**Position**	**Year**
Orchid Chemicals and Pharmaceuticals Ltd (R & D center), Chennai, India.	Research Executive • To design a non-infringing route and synthesis of desired Active Pharmaceutical Ingredient. • Optimization of the reaction conditions, developing the process and transferring the process to commercial plant scale level.	2009-2013 (**4 years**)
SeQuent Scientific Ltd (R & D center), Mangalore, India.	Scientist • To design a non-infringing route and synthesis of desired Active Pharmaceutical Ingredient. • Optimization of the reaction conditions, developing the process and transferring the process to commercial plant scale level.	2013-2016 (**2.5 years**)

EDUCATION		
Degree	**University**	**Year**
Bachelor of Science in Chemistry (*University 7th rank*)	Alagappa University, Karikudi, India.	2007
Master of Science in Chemistry (*University 10th rank*)	Bharathidasan University, Trichy, India.	2009
Ph.D.	National Institute of Technology Karnataka, India.	2015 to 2020

Patents

1. **WO 2011/ 145019** (Improved process for Diphenylpropylamine derivatives)
2. **IN323444** (Improved process for Diphenylpropylamine derivatives)
3. **IN326804** (A method for synthesizing d-perosamine)

Papers

1. **G.P.S. Ibrahim**., Isloor, A. M.; Inamuddin; Asiri, A. M.; Ismail, N.; Ismail, A. F.; Ashraf, G. M., (2017). Novel, one-step synthesis of zwitterionic polymer nanoparticles via distillation-precipitation polymerization and its application for dye removal membrane. **Scientific Reports,** 7 (1), 15889 (**Nature publication**).
2. **G.P.S. Ibrahim**., Isloor, A. M.; Moslehyani, A.; Ismail, A. F., (2017). Bio-inspired, fouling resistant, tannic acid-functionalized halloysite nanotube-reinforced polysulfone loose nanofiltration hollow fiber membranes for efficient dye and salt separation. **Journal of Water Process Engineering**, 20, 138-148.
3. **G.P.S. Ibrahim**., Isloor, A. M., Asiri, A. M., Ismail, A. F., Kumar, R., & Ahamed, M. I. (2018). Performance intensification of the polysulfone ultrafiltration membrane by blending with copolymer encompassing novel derivative of poly (styrene-co-maleic anhydride) for heavy metal removal from wastewater. **Chemical Engineering Journal**, 353, 425-435.
4. M. Kumar, A.M. Isloor, T. Somasekhara Rao, **G.P.S. Ibrahim**, Inamuddin, N. Ismail, A.F. Ismail, A.M. Asiri. (2019). Fabrication of polyphenylsulfone/cellulose acetate and polyphenylsulfone/cellulose acetate phthalate ultrafiltration hollow fiber membranes for the removal of arsenic from drinking water, **International Journal of Biological Macromolecules**, 129, 715-727.
5. M. Kumar, A.M. Isloor, T. Somasekhara Rao, **G.P.S. Ibrahim**, Inamuddin, N. Ismail, A.F. Ismail, A.M. Asiri. (2020). Fabrication, characterization and rejection properties of different dyes and proteins from aqueous solution by PPSU/CA and PPSA/CAP hollow fiber membranes, **Environmental Chemistry Letters,** 18, 881–887.
6. **Ibrahim, G. P. S**., Isloor, A.M., A. F. Ismail and Ramin Farnood. (2020). “One-step synthesis of novel zwitterionic graphene oxide nanohybrid: Application to

polysulfone tight ultrafiltration hollow fiber membrane" **Scientific Reports**, 10, 6880 (**Nature publication**).

7. **Ibrahim, G. P. S**., Isloor, A.M., Mona Bavarian and Siamak Nejati. (2020). "Integration of Zwitterionic Polymer Nanoparticles in Interfacial Polymerization for Ion Separation" **ACS Applied Polymer Materials**, 2, 4, 1508-1517.

8. **Ibrahim, G. P. S**., Isloor, A. M., Inamuddin, Asiri, A. M., Ismail A. F., "Tuning the surface properties of Fe_3O_4 by zwitterionic sulfobetaine: Application to antifouling and dye removal membrane" **International Journal of Environmental Science and Technology,** DOI: 10.1007/s13762-020-02730-z.

Book chapters

1. **Ibrahim, G. P. S**, A.M. Isloor, E. Yuliwati, A.F. Ismail, Carbon-based nanocomposite membranes for water and wastewater purification, in: Advanced Nanomaterials for Membrane Synthesis and its Applications, **Elsevier**, 2019, 23-44.
2. **Ibrahim, G. P. S**, A.M. Isloor, E. Yuliwati, A Review: Desalination by Forward Osmosis, in: Current Trends and Future Developments on (Bio-) Membranes, **Elsevier**, 2019, 199-214.
3. **Ibrahim, G. P. S**., Isloor, A.M. and Farnoodb, R. Fundamentals and basics of reverse osmosis. Current Trends and Future Developments on (Bio-) Membranes: Reverse and Forward Osmosis: Principles, Applications, Advances, **Elsevier**, 2019, 141-163.
4. **Ibrahim, G. P. S**., Isloor, A.M. and Farnoodb, R., Reverse osmosis pretreatment techniques, fouling and control strategies. Current Trends and Future Developments on (Bio-) Membranes: Reverse and Forward Osmosis: Principles, Applications, Advances, **Elsevier**, 2019, 165-186.
5. **Ibrahim, G. P. S**., Isloor, A.M. and Farnoodb, R., Role of Hollow Fiber Contactors Based Technology in Fermentation and Enzymatic Transformation and in Chiral Separations, **CRC Press,** In press**.**
6. **Ibrahim, G. P. S** and Isloor, A.M, Synthetic Polymer based Membrane for Dyes and Pigments Removal, **Elsevier,** 2020, 39-52.

Merits/Awards/Achievement

1. Secured prestigious Water Advanced Research Innovation Internship for six months at the University of Nebraska, USA, which is supported by Indo-US Science and Technology Forum (IUSSTF), Department of Science and Technology, India and University of Nebraska.
2. Visiting Ph.D. student to the University of Toronto, Canada under the supervision of Prof. Ramin Farnood.
3. Visiting Ph.D. student to University Technology Malaysia (UTM), Malaysia under the supervision of Prof. Ahmad Fauzi Ismail.
4. Best poster award obtained in International conference held in Vellore Institute of Technology, Vellore, India.
5. Best poster award obtained in International conference held in Assam University, Silchar, India.
6. Summer Research Project on Borane Mediated Asymmetric reduction of alpha tetralone under the supervision of Prof. D. Basavaiah, University of Hyderabad, India.

RESEARCH INTEREST

1. Design and synthesize of novel surface-functionalized nanomaterials
2. Design and synthesize of novel membranes for water purification.
3. Design and synthesize of functional polymers